Variation in soil microbiomes associated with kauri trees threatened by dieback disease

Zoe King

A research component submitted to Auckland University of Technology in fulfilment of the requirements for the degree of Doctor of Philosophy (PhD)

2026

School of Science

Abstract

Forest ecosystems are increasingly threatened by climate change, land-use pressures, and emerging pathogens, highlighting the need to understand how different ecosystem components mediate and respond to such disturbances. Soil microbial communities are central to nutrient cycling, plant growth, and disease suppression, yet their interactions with soil-borne pathogens in natural forest systems remain poorly understood. This thesis addresses this gap using *Agathis australis* (kauri), a foundation tree species endemic to New Zealand currently threatened by the soil-borne oomycete *Phytophthora agathidicida* (causal agent of kauri dieback), as a case study. The work investigated how pathogen presence, tree health, spatial location, and edaphic gradients relate to forest soil microbial community composition and functional potential.

Soils were collected around the basal trunk of 96 kauri trees comprising healthy, declining, and dead canopy states across three sites and six plots in the Waitākere Ranges, Auckland, New Zealand. By combining amplicon sequencing, shotgun metagenomics, loop-mediated isothermal amplification (LAMP), and measurements of soil physicochemical properties, this framework provided a comprehensive view of the soil microbiome across tree health and environmental gradients.

Results showed that soil microbial communities were strongly structured by spatial and edaphic variation. Soil carbon, nitrogen, C:N ratios, pH, and moisture consistently emerged as dominant drivers of both bacterial and fungal communities. Pathogen presence, confirmed by LAMP, and tree health status were only weakly related. Nevertheless, specific bacterial and fungal taxa were significantly more abundant in pathogen-detected soils, including taxa previously linked with disease suppression. Soils beneath declining trees contained significantly greater abundance of taxa associated with later stages of litter decomposition, suggesting links between canopy decline, litter accumulation, and microbial community structure. While bacterial communities were relatively stable across all health states, fungal communities were more strongly related to tree decline. Functional profiles derived from shotgun metagenomics revealed that broad metabolic capacities were conserved across health states, consistent with functional redundancy. However, fine-scale shifts in some gene families and pathways indicated that microbial communities could reorganise their functions under changing conditions, with possible implications for decomposition and nutrient cycling.

This work demonstrates the complementarity and value of combining multiple molecular approaches to assess different components of the microbial community. It also suggests that soil microbial communities in kauri forests are influenced by strong environmental and spatial filtering, with pathogen and host decline potentially contributing secondary, but small, influences. By providing one of the first comprehensive metagenomic baselines for kauri soil microbial communities under threat of dieback, this thesis contributes to understanding how pathogen presence, tree health decline, and microbial communities interact in a natural forest system. Together, these insights advance ecological understanding of how a biotic disturbance shapes soil microbiomes in natural forest ecosystems and informs long-term monitoring and future research on kauri dieback. Building our understanding of the long-term consequences of forest decline due to death of kauri, and by extension, other foundation tree species worldwide, will depend on recognising the resilience and sensitivity of soil microbial communities within their complex environmental contexts.

Table of Contents

Abstract ..... **i**
List of Figures ..... **vi**
List of Tables ..... **xiii**
Attestation of Authorship ..... **xiv**
Co-authorship Contributions ..... **xv**
Acknowledgments ..... **xvii**
Chapter 1 ..... **1**
1.1 Introduction 2
1.2 Literature review 2
1.2.1 Kauri 2
1.2.2 Kauri dieback 7
1.2.3 *Phytophthora agathidicida* biology 10
1.2.4 Disease detection 12
1.2.5 *Phytophthora agathidicida* ecology 17
1.2.6 Disease monitoring in the Waitākere Ranges 19
1.2.7 Disease management 21
1.2.8 Mātauranga Māori 24
1.2.9 Belowground microbial ecology and kauri dieback 26
1.2.10 Methods for investigating forest soil microbial communities 35
1.3 Research gaps and thesis aims 37
Chapter 2 ..... **39**
Abstract 41
2.1 Introduction 42
2.2 Experimental Procedures 44
2.2.1 Field sampling 44
2.2.2 Soil DNA extraction, amplicon and shotgun metagenome sequencing 45
2.2.3 *Phytophthora* detection 46
2.2.4 Bioinformatics 47
2.2.5 Statistical analysis 49
2.3 Results 51
2.3.1 Detection of *P. agathidicida* 51
2.3.2 Microbial community taxonomic composition 52
2.3.3 Microbial community diversity 55
2.3.4 Functional potential of bacterial communities 56
2.3.5 Concordance between amplicon and shotgun metagenome datasets 57
2.4 Discussion 59
2.4.1 Summary of key findings 59

2.4.2 *Phytophthora agathidicida* detection across different methods 59
2.4.3 Impacts of *P. agathidicida* presence on microbial community composition 61
2.4.4 Functional shifts in the microbial community 61
2.4.5 Alignment between shotgun metagenome and amplicon-derived profiles 62
2.5 Conclusion 63
Chapter 3 65
Abstract 67
3.1 Introduction 68
3.2 Methods 70
3.2.1 Field sampling 70
3.2.2 Soil DNA extraction, PCR and amplicon sequencing 70
3.2.3 Bioinformatics 72
3.2.4 Environmental variables 72
3.2.5 Statistical analyses 73
3.3 Results 75
3.3.1 General characteristics of bacterial and fungal communities 75
3.3.2 Spatial variation in community structure was highest at the tree-level scale 76
3.3.3 ASV abundance and fungal diversity, but not bacterial diversity or composition, was associated with tree health status 77
3.3.4 Soil physicochemical properties were associated with bacterial and fungal community composition 83
3.4 Discussion 83
3.4.1 Microbial community structure across spatial scales 84
3.4.2 Tree health status and microbial community structure 85
3.4.3 Association with environmental variables 86
3.4.4 Implications and considerations for future research 87
3.5 Conclusion 87
Chapter 4 88
Abstract 90
4.1 Introduction 91
4.2 Methods 93
4.2.1 Field sampling 93
4.2.2 Soil DNA extraction and metagenome shotgun sequencing 94
4.2.3 Quality control 94
4.2.4 Contig assembly, gene prediction, and gene annotation 95
4.2.5 Soil physicochemical characteristics 95
4.2.6 Statistical analysis 96
4.3 Results 98
4.3.1 Shotgun metagenome dataset overview 98
4.3.2 Soil physicochemical properties vary across sites and plots but not tree health 98
4.3.3 Gene composition reflects spatial structuring across sites and plots 99

4.3.4 Gene presence, diversity, and composition across tree health groups 102
4.3.5 Differential abundance analysis 104
4.4 Discussion 108
4.4.1 Summary of key findings 108
4.4.2 Spatial and environmental structuring of functional potential 108
4.4.3 Tree health effects on microbial functional potential 109
4.4.4 Functional processes and gene families associated with soil properties and tree health 110
4.5 Conclusion 112
Chapter 5 113
5.1 Synthesis of findings 115
5.1.1 Weak direct, and stronger indirect, effects of *P. agathidicida* on soil microbial communities 115
5.1.2 Redundancy at broad scales, reorganisation at finer scales 116
5.1.3 Environmental filtering as the dominant structuring force 117
5.1.4 Complementary molecular approaches for ecological insight and monitoring 118
5.2 Novelty of the research 118
5.3 Limitations and future research directions 119
5.4 Concluding remarks 120
References 122
Appendix A 162
A.1 Supplementary figures 162
A.2 Supplementary tables 172
A.3 Supplementary files 172
Appendix B 173
B.1 Supplementary figures 173
B.2 Supplementary tables 183
Appendix C 187
C.1 Supplementary figures 187
C.2 Supplementary tables 197
C.3 Supplementary files 201

List of Figures

Figure 1.1: Tāne Mahuta, the largest living kauri tree located in the Waipoua Forest of Northland Region, New Zealand. 3

Figure 1.2: Kauri forest in the Waitākere Ranges showing a range of kauri health states. Mature kauri tree with a healthy canopy (red arrow), kauri with a declining canopy (yellow arrow), a fallen dead kauri (pink arrow). 4

Figure 1.3: Symptoms of kauri dieback: (A) basal bleeding, (B) crown thinning, (C) yellowing leaves, all leading to eventual (D) tree death. 9

Figure 2.1: (A) Bacterial and (B) fungal genera showing differential abundance between soil samples where *Phytophthora agathidicida* was detected and not detected. Genera with a positive log fold change (natural log) show increased abundance in soils without *P. agathidicida* detected and genera with a negative log fold change (natural log) show increased abundance in soils with *P. agathidicida* detected. All genera identified passed ANCOM-BC2 sensitivity scoring. LFC = log fold change. 55

Figure 2.2: Procrustes analysis comparing community composition profiles of (A) bacterial genera, (B) fungal genera, and (C) KEGG Orthologs (KO) derived from amplicon (gold) and shotgun metagenome (purple) sequencing. Arrows connect matching samples, with arrow length indicating the degree of dissimilarity between the two datasets for that sample (longer arrows = greater discordance). For each rotation, the M^2 statistic and associated *P*-value are shown, where M^2 represents the proportion of variance unexplained by the Procrustes fit (lower values indicate better agreement between datasets). 58

Figure 3.1: The amount of variation in (A) bacterial and (B) fungal community diversity across three spatial scales: site-level (*n* = 3), plot-level (*n* = 6), and tree-level (*n* = 96) determined by variation partitioning analysis using db-RDA on the Euclidean distance matrix of Shannon indices. This figure is based on the intermediate taxa dataset (taxa in ≥1% and ≤90% of samples). Samples were rarefied to an even depth (775 and 596 reads for bacteria and fungi, respectively). 77

Figure 3.2: The representativeness of (A) bacterial and (B) fungal phyla detected in samples grouped by tree health status (dead: *n* = 20, healthy: *n* = 84, defoliated: bacterial dataset *n* = 276, fungal dataset *n* = 265). This figure is based on the intermediate taxa dataset (taxa in ≥1% and ≤90% of samples). 79

Figure 3.3: Robust Aitchison principal component analysis of (A) bacterial and (B) fungal community composition of the tree-scale robust Aitchison distance matrices of different tree health status groups, cardinal samples were combined per tree and ASV counts were averaged (dead: *n* = 5, healthy: *n* = 21, defoliated: *n* = 70). This figure is based on the intermediate taxa dataset (taxa in ≥1% and ≤90% of samples). Black borders indicate plot number, presence of black border = plot 1, no black border = plot 2. Larger shapes represent centroids of the sites. Large crosses indicate centroids of tree health status communities. Environmental variables were overlaid as vectors calculated using the *envfit* function via the vegan R package onto the ordination and only factors that were significantly correlated ($P < 0.05$) with ordination axes were included. Physicochemical data of soils were generated by (Mohini 2024). 81

Figure 3.4: (A) Bacterial and (B) fungal ASVs, grouped at the phylum level, passing ANCOM-BC2 sensitivity scoring, showing the greatest differential abundance (|log fold change| > 1) between tree scale samples collected around healthy and unhealthy (combined defoliated and dead samples) trees. This analysis is based on the full dataset after ASVs present in less than 10% of samples were removed. Green data points indicate an increase in the abundance of ASVs in soils surrounding

healthy trees, and red data points indicate an increase in the abundance of ASVs in soils surrounding unhealthy trees (defoliated and dead trees). All differentially abundant ASVs may be viewed in Figure B5..... 82

Figure 3.5: The amount of variation in (A) bacterial and (B) fungal community composition that could be explained by physicochemical properties (pH, total carbon, total nitrogen, total hydrogen, carbon to nitrogen (C:N) ratio, electrical conductivity, bulk density, and water holding capacity), site and plot, and elevation. Values less than 0 are not shown. This figure is based on the intermediate taxa dataset (taxa in ≥1% and ≤90% of samples). 83

Figure 4.1: Soil physicochemical variation across kauri tree health states and locations. (A) Principal component analysis (PCA) of Euclidean distances of soil physicochemical properties of kauri trees of different health status (dead: *n* = 5, healthy: *n* = 21, defoliated: *n* = 69) across different sites (Cascades, Piha, Huia) and plots. Black borders indicate plot number, presence of black border = plot 1, no black border = plot 2. Larger shapes represent centroids of the sites. Large crosses indicate centroids of tree health status communities. (B) Boxplots of soil physicochemical properties that showed significant differences ($P < 0.05$) between tree health states in univariate analyses; other measured properties were not significant and can be viewed in Figure C2; Appendix C. Physicochemical data of soils were generated by Mohini (2024). 99

Figure 4.2: Drivers of variation in microbial functional gene composition annotated by the eggNOG database. (A) Variation partitioning analysis showing the proportion of variance in gene composition explained by physicochemical properties (pH, total carbon, total nitrogen, total hydrogen, carbon to nitrogen (C:N) ratio, electrical conductivity, bulk density, and water holding capacity), site and plot, and tree health (healthy and unhealthy). Values less than 0 are not shown. (B) Constrained ordination (db-RDA) of Bray-Curtis dissimilarities based on TPM-normalised gene abundance, constrained by site and nested plot (formula: site/plot) to account for spatial structure. Black borders indicate plot number, presence of black border = plot 1, no black border = plot 2. Overlaid vectors show significant soil physicochemical variables identified via the *envfit* function from the vegan R package that were significantly correlated (P <0.05) with ordination axes. Physicochemical data of soils were generated by Mohini (2024). 101

Figure 4.3: Gene diversity and composition of eggNOG annotated genes across kauri tree health states (healthy *n* = 21, defoliated *n* = 69, and dead *n* = 5). (A) Venn diagrams showing shared vs health-state-specific genes. (B) Box plots show gene diversity (richness; calculated as the number of annotated genes detected per sample). Each box represents the interquartile range of the data (IQR; 25th and 75th percentiles), whiskers show the largest and smallest values 1.5x the IQR and median values are represented by the bar within each box. (C) Gene composition differences visualised by Principal Coordinates Analysis of Bray-Curtis dissimilarities from TPM-normalised gene abundances. Black borders indicate plot number, presence of black border = plot 1, no black border = plot 2. Similar results were obtained for NCyc and CAZy annotations, which can be viewed in Figure C5 and Figure C6; Appendix C. 103

Figure 4.4: Differential abundance of eggNOG-annotated genes between soils from around healthy (*n* = 21) and unhealthy (*n* = 74) kauri trees. (A) Volcano plot shows the effect size (coefficient) and significance of predicted genes identified as differentially abundant by MaAsLin2. Negative coefficients indicate enrichments in soils around healthy kauri trees, while positive coefficients indicate enrichments in soils from around unhealthy kauri trees. (B) Bar plots depict the mean effect size ± standard error of the significantly differentially abundant genes with effect sizes > 0.4 and < -1, grouped by COG annotation. Error bars indicate the standard error of the mean effect size, calculated across genes sharing the same annotation; annotations represented by a single gene have no error bars. Bars are coloured by COG category, C = energy production and conversion, E = amino

acid transport and metabolism, G = carbohydrate transport and metabolism, H = coenzyme metabolism, J = translation, ribosomal structure and biogenesis, K = transcription, L = DNA replication, recombination and repair, M = cell wall/membrane/envelope biogenesis, O = posttranslational modification, protein turnover, chaperones, S = function unknown. A full table of significantly differentially abundant genes and their eggNOG annotation is provided in Appendix C3 Supplementary File 2. 105

Figure 4.5: Differential abundance of NCyc-annotated genes between soils from around healthy (*n* = 21) and unhealthy (*n* = 74) kauri trees. (A) Volcano plot shows the effect size (coefficient) and significance of predicted genes identified as differentially abundant by MaAsLin2. Negative coefficients indicate enrichments in soils around healthy kauri trees, while positive coefficients indicate enrichments in soils from around unhealthy kauri trees. (B) Bar plots depict the mean effect size ± standard error of the differentially abundant genes, grouped by NCyc gene annotation and coloured by their pathway association. Error bars indicate the standard error of the mean effect size, calculated across genes sharing the same annotation; annotations represented by a single gene have no error bars. 106

Figure 4.6: Differential abundance of CAZy-annotated genes between soils from around healthy (*n* = 21) and unhealthy (*n* = 74) kauri trees. (A) Volcano plot shows the effect size (coefficient) and significance of predicted genes identified as differentially abundant by MaAsLin2. Negative coefficients indicate enrichments in soils around healthy kauri trees, while positive coefficients indicate enrichments in soils from around unhealthy kauri trees. (B) Bar plots depict the mean effect size ± standard error of the significantly differentially abundant genes with an |effect size| > 0.15, grouped by their CAZy gene annotation and coloured by their associated enzyme class. Error bars indicate the standard error of the mean effect size, calculated across genes sharing the same annotation; annotations represented by a single gene have no error bars. A full table of significantly differentially abundant genes and their CAZy annotation is provided in Appendix C3 Supplementary File 2. 107

Figure 5.1: Conceptual diagram of the kauri forest system showing the multiple interacting components that shape tree health and soil microbial communities. The central kauri tree is placed within the wider ecological network that includes aboveground drivers such as sunlight, rainfall, wildlife, and other vegetation, and belowground processes involving soil physicochemical properties (purple (carbon) and green (nitrogen) circles), roots, microbes, and pathogens. Arrows represent flows of resources, influences, and interactions: Trees contribute (1) litter and (2) root exudates to soils. Soil microbes (3) support plant growth, can (4) influence pathogen dynamics, and (5) recycle nutrients while interacting with soil physicochemical properties that filter community composition and function. The pathogen (*P. agathidicida*) infects (6) tree roots, reducing tree health and contributing to canopy decline. (7) Wildlife, (8) climate, and (9) surrounding vegetation also shape both tree health and soil processes. The red coloured arrows represent the key interactions explored in this thesis, grey arrows indicate broader system drivers that are acknowledged but not directly studied, and blue arrows represent the influence of soil physicochemical properties which provide an essential backdrop for interpreting the tree-pathogen-microbe interactions. 115

Figure A1: Map of the three sampling sites (Cascades, Piha, Huia) in the North Island, New Zealand, that each contain two plots (*n* = 6) where 16 kauri trees, per plot, were selected for soil sampling (*n* = 96). 162

Figure A2: Rarefaction curves showing observed microbial richness in amplicon and shotgun metagenome datasets. Figures A and B show rarefaction curves for (A) bacterial and (C) fungal ASVs from amplicon sequencing, while figures B and D show rarefaction curves for (B) bacterial and (D) fungal species identified from shotgun metagenome data. Each curve represents an individual soil

samples collected from around kauri trees, coloured by *P. agathidicida* (PA) detection status based on LAMP analysis. The dotted line indicates the minimum sequencing depth to with each dataset was rarefied to. 163

Figure A3: Canopy healthy scores of kauri trees across sites (Cascades, Huia, and Piha, within the Waitākere Ranges, Auckland, New Zealand), with point size proportional to the number of trees at each site-score combination. Each point is displayed as a pie chart showing the proportion of trees testing positive or negative for *P. agathidicida* by LAMP analysis. 164

Figure A4: Read count of *P. agathidicida*-associated DNA per sample against detection status inferred by LAMP analysis (detected *n* = 39, not detected *n* = 21). Boxes represent the interquartile range of the data (25th and 75th percentiles), whiskers show the largest and smallest values 1.5x the IQR and median values are represented by the bar within each box..... 164

Figure A5: Heatmap of the relative abundance of the top bacterial phyla (>1% MRA), and genera (>0.5% MRA) identified using amplicon and shotgun metagenomic sequencing. Detection of *P. agathidicida* was determined by LAMP analysis (detected *n* = 37 (amplicon), 39 (shotgun), or not detected (*n* = 21)). The heatmap uses NMDS ordination to order the samples (columns) arranging them based on their similarity in microbial community composition as captured by the first ordination axis. 165

Figure A6: Heatmap of the relative abundance of the top fungal phyla (>1% MRA), and genera (>0.5% MRA) identified using amplicon and shotgun metagenomic sequencing. Detection of *P. agathidicida* was determined by LAMP analysis (detected *n* = 38 (amplicon), 39 (shotgun), or not detected *n* = 19 (amplicon), 21 (shotgun)). The heatmap uses NMDS ordination to order the samples (columns) arranging them based on their similarity in microbial community composition as captured by the first ordination axis. 166

Figure A7: Principal Coordinates Analysis (PCoA) of (A and B) bacterial and (C and D) fungal genus-level community composition of Bray-Curtis distance matrices from amplicon and shotgun metagenome datasets. Samples were normalised by cumulative-sum scaling. Points are coloured based on LAMP detection of *P. agathidicida* (Bacterial dataset: detected *n* = 37 (amplicon), 39 (shotgun) and not detected *n* = 21 (amplicon and shotgun). Fungal dataset: detected *n* = 38 (amplicon), 39 (shotgun), or not detected *n* = 19 (amplicon), 21 (shotgun). 167

Figure A8: Measures of (A and B) bacterial and (C and D) fungal taxonomic alpha diversity at the genus level estimated by Shannon diversity and observed richness from amplicon and shotgun metagenome datasets. Samples are grouped based on the LAMP detection of *P. agathidicida* (Bacterial dataset: detected *n* = 37 (amplicon), 39 (shotgun) and not detected *n* = 21 (amplicon and shotgun). Fungal dataset: detected *n* = 38 (amplicon), 39 (shotgun), or not detected *n* = 19 (amplicon), 21 (shotgun)). Samples were rarefied to an even depth (Reads per sample: amplicon 16S: 15,420, amplicon ITS: 4,192, shotgun bacteria: 9,963,524, shotgun fungi: 42,440). Boxes represent the interquartile range of the data (25th and 75th percentiles), whiskers show the largest and smallest values 1.5x the IQR and median values are represented by the bar within each box. 168

Figure A9: Heatmaps showing the relative abundance of KOs identified through shotgun metagenome sequencing and eggNOG annotation, grouped by KEGG functional classifications and LAMP detection of *P. agathidicida* (detected *n* = 39, not detected *n* = 21). (A) KOs grouped according to KEGG BRITE hierarchies at level 2 and level 3, (B) KOs grouped by KEGG pathway levels 1 and level 2. Samples are clustered based on default Euclidian clustering from the ComplexHeatmap R package. Pathways associated with Organismal systems and Human disease were removed from the dataset. 169

Figure A10: Heatmaps showing the relative abundance of KOs identified through functional inference by PICRUSt2 of ASVs from amplicon sequencing, grouped by KEGG functional classifications and LAMP detection of *P. agathidicida* (detected *n* = 37, not detected *n* = 21). (A) KOs grouped according to KEGG BRITE hierarchies at level 2 and level 3, (B) KOs grouped by KEGG pathway levels 1 and level 2. Samples are clustered based on default Euclidian clustering from the ComplexHeatmap R package. Pathways associated with Organismal systems and Human disease were removed from the dataset. 170

Figure A11: Boxplots showing estimated alpha diversity of microbial functional potential based on KO profiles from (A) amplicon sequencing (via PICRUSt2) and (B) shotgun metagenome sequencing (via eggNOG annotation). Samples were grouped by LAMP detection of *P. agathidicida* (detected *n* = 37 (amplicon), 39 (shotgun), not detected *n* = 21 (amplicon), 21 (shotgun)). Boxes represent the interquartile range of the data (25th and 75th percentiles), whiskers show the largest and smallest values 1.5x the IQR and median values are represented by the bar within each box. 171

Figure A12: Principal Coordinates Analysis (PCoA) of amplicon-based inference (PICRUSt2) and shotgun metagenome sequencing (eggNOG annotation) of KOs based on Bray-Curtis distance matrices. Samples were normalised by CSS. Points are coloured based on LAMP detection of *P. agathidicida* (detected *n* = 37 (amplicon), 39 (shotgun), not detected *n* = 21 (amplicon), 21 (shotgun)). 171

Figure A13: Venn diagram showing the overlap of KOs identified from shotgun metagenome sequencing (eggNOG annotation) and amplicon-based functional inference (PICRUSt2). 172

Figure B1: Relative abundances of genera identified in (A) bacterial and (B) fungal mock microbial community controls. The theoretical sample provides the expected abundances of taxa within the ZymoBIOMICS Microbial Community DNA standard (mock community DNA standard)..... 173

Figure B2: The amount of variation in (A) bacterial and (B) fungal community diversity across three spatial scales: site-level (*n* = 3), plot-level (*n* = 6), and tree-level (*n* = 96) determined by variation partitioning analysis using db-RDA on the Euclidean distance matrix of observed richness counts. This figure is based on the full taxa dataset..... 174

Figure B3: Stacked bar plots of relative abundance. Proportional relative abundance of bacterial (A) phyla and (B) genera and fungal (C) phyla and (D) genera from soil surrounding kauri trees of three health status groupings. This figure is based on the intermediate taxa dataset. Samples within respective health status groupings were collapsed together. Un-collapsed relative abundance data of phyla (dead: *n* = 20, healthy: *n* = 84, defoliated: bacterial dataset *n* = 276, fungal dataset: *n* = 265) can be viewed in Figure B10. 175

Figure B4: Measures of (A) bacterial and (B) fungal alpha diversity estimated by Shannon diversity and observed richness between tree health status groups (healthy: *n* = 84, unhealthy (defoliated and dead trees): bacterial dataset *n* = 296, fungal dataset: *n* = 285). This figure is based on the intermediate taxa dataset (9,331 bacteria ASVs, 3,733 fungal ASVs). Samples were rarefied to an even depth (775 and 596 reads for bacteria and fungi, respectively). Boxes represent the interquartile range of the data (25th and 75th percentiles), whiskers show the largest and smallest values 1.5x the IQR and median values are represented by the bar within each box. Coloured points represent cardinal point samples. 176

Figure B5: Log fold change of differential abundance. (A) Bacterial and (B) fungal ASVs, grouped at the phylum level, passing ANCOM-BC2 sensitivity scoring, showing differential abundance between tree scale samples collected around healthy and unhealthy (combined defoliated and dead samples) trees. This analysis is based on the full dataset. Green data points indicate an increase in the

abundance of ASVs in soils surrounding healthy trees, and red data points indicate an increase in the abundance of ASVs in soils surrounding unhealthy tree. 177

Figure B6: Measures of (A) bacterial and (B) fungal alpha diversity estimated by Shannon diversity and observed richness between tree health status groups (healthy: *n* = 84, dead: *n* = 20, defoliated: bacterial dataset *n* = 276, fungal dataset: *n* = 265). This figure is based on the full taxa dataset. Samples were rarefied to an even depth (1499 and 997 reads for bacteria and fungi, respectively). Boxes represent the interquartile range of the data (25th and 75th percentiles), whiskers show the largest and smallest values 1.5x the IQR and median values are represented by the bar within each box. Coloured points represent cardinal point samples. 178

Figure B7: The representativeness of (A) bacterial and (B) fungal phyla detected in samples grouped by tree health status (dead: *n* = 20, healthy: *n* = 84, defoliated: bacterial dataset *n* = 276, fungal dataset *n* = 265). This figure is based on the full taxa dataset. 179

Figure B8: Robust Aitchison principal component analysis of (A) bacterial and (B) fungal community composition of Robust Aitchison distance matrices of different tree health status groups, cardinal samples were combined per tree and ASV counts were averaged (dead: *n* = 5, healthy: *n* = 21, defoliated: *n* = 70). This figure is based on the full taxa dataset. Black borders indicate plot number, presence of black border = plot 1, no black border = plot 2. 180

Figure B9: (A) Bacterial and (B) fungal ASVs shared amongst tree health status groupings. This figure is based on the intermediate taxa dataset. 181

Figure B10: Relative abundance of (A) bacterial and (B) fungal phyla surrounding kauri trees of three health status groupings (dead: *n* = 20, healthy: *n* = 84, defoliated: bacterial dataset *n* = 276, fungal dataset: *n* = 265). This figure is based on the intermediate taxa dataset. 182

Figure C1: Study area and representative images of kauri forest. (A) Map of the Waitākere Ranges in the Auckland region of the North Island, New Zealand (inset), showing the three study sites where soils samples were collected. Each site contained two plots, and 16 trees per plot were sampled. (B) Kauri forest within the Waitākere Ranges, showing a mature healthy kauri canopy (red arrow), declining kauri canopy (yellow arrow), and a fallen dead kauri (pink arrow). (C) Regenerating stand of young kauri trees. (D) Mature kauri tree representing the intact forest canopy structure. 188

Figure C2: Boxplots showing the distribution of soil physicochemical properties across healthy (*n* = 21) and unhealthy (*n* = 74) kauri tree groups. Each panel represents one physicochemical property, with differences between groups tested using the Wilcoxon rank-sum test. Asterisks (*) indicate statistically significant differences ($P < 0.05$). Each box represents the interquartile range of the data (25th and 75th percentiles), whiskers show the largest and smallest values 1.5x the IQR and median values are represented by the bar within each box. Physicochemical data of soils were generated by Mohini (2024). 189

Figure C3: Drivers of variation in microbial functional gene composition annotated by the NCyc database. (A) Variation partitioning analysis showing the proportion of variance in gene composition explained by physicochemical properties (pH, total carbon, total nitrogen, total hydrogen, carbon to nitrogen (C:N) ratio, electrical conductivity, bulk density, and water holding capacity), site and plot, and tree health (healthy and unhealthy). Values less than 0 are not shown. (B) Constrained ordination (db-RDA) of Bray-Curtis dissimilarities based on TPM-normalised gene abundance, constrained by site and nested plot (formula: site/plot) to account for spatial structure. Black borders indicate plot number, presence of black border = plot 1, no black border = plot 2. Overlaid vectors show significant soil physicochemical variables identified via the *envfit* function from the vegan R package that were significantly correlated ($P < 0.05$) with ordination axes. Physicochemical data of soils were generated by Mohini (2024). 190

Figure C4: Drivers of variation in microbial functional gene composition annotated by the CAZy database. (A) Variation partitioning analysis showing the proportion of variance in gene composition explained by physicochemical properties (pH, total carbon, total nitrogen, total hydrogen, carbon to nitrogen (C:N) ratio, electrical conductivity, bulk density, and water holding capacity), site and plot, and tree health (healthy and unhealthy). Values less than 0 are not shown. (B) Constrained ordination (db-RDA) of Bray-Curtis dissimilarities based on TPM-normalised gene abundance, constrained by site and nested plot (formula: site/plot) to account for spatial structure. Black borders indicate plot number, presence of black border = plot 1, no black border = plot 2. Overlaid vectors show significant soil physicochemical variables identified via the *envfit* function from the vegan R package that were significantly correlated (P <0.05) with ordination axes. Physicochemical data of soils were generated by Mohini (2024). 191

Figure C5: Gene diversity and composition of NCyc annotated genes across kauri tree health states (healthy n = 21, defoliated n = 69, and dead n = 5). (A) Venn diagrams showing shared vs health-state-specific genes. (B) Box plots show gene diversity (richness; calculated as the number of annotated genes detected per sample). Each box represents the interquartile range of the data (IQR; 25th and 75th percentiles), whiskers show the largest and smallest values 1.5x the IQR and median values are represented by the bar within each box. (C) Gene composition differences visualised using PCoA of Bray-Curtis dissimilarities from TPM-normalised gene abundances. Black borders indicate plot number, presence of black border = plot 1, no black border = plot 2. 192

Figure C6: Gene diversity and composition of CAZy annotated genes across kauri tree health states (healthy n = 21, defoliated n = 69, and dead n = 5). (A) Venn diagrams showing shared vs health-state-specific genes. (B) Box plots show gene diversity (richness; calculated as the number of annotated genes detected per sample). Each box represents the interquartile range of the data (IQR; 25th and 75th percentiles), whiskers show the largest and smallest values 1.5x the IQR and median values are represented by the bar within each box. (C) Gene composition differences visualised using PCoA of Bray-Curtis dissimilarities from TPM-normalised gene abundances. Black borders indicate plot number, presence of black border = plot 1, no black border = plot 2. 193

Figure C7: Heatmap of functional gene composition based on eggNOG annotations. For each gene, TPM counts were first normalised within samples (per-column normalisation), and then scaled so that values summed to 1 across all samples (per-row normalisation). Colours represent the relative distribution of each gene across samples. Columns represent individual samples, ordered and grouped by canopy score, while rows are organised by higher-level COG functional groupings. The heatmap was generated using ComplexHeatmap v. 2.21.2 (Gu 2022). 194

Figure C8: Heatmap of functional gene composition based on NCyc annotations. For each gene, TPM counts were first normalised within samples (per-column normalisation), and then scaled so that values summed to 1 across all samples (per-row normalisation). Colours represent the relative distribution of each gene across samples. Columns represent individual samples, ordered and grouped by canopy score, while rows are organised by the pathway the genes are involved in. The heatmap was generated using ComplexHeatmap v. 2.21.2 (Gu 2022). 195

Figure C9: Heatmap of functional gene composition based on CAZy annotations. For each gene, TPM counts were first normalised within samples (per-column normalisation) before grouping by CAZy enzyme family. Counts per family were then scaled so that values summed to 1 across all samples (per-row normalisation). Colours represent the relative distribution of each enzyme family across samples. Columns represent individual samples, ordered and grouped by canopy score. The heatmap was generated using ComplexHeatmap v. 2.21.2 (Gu 2022). 196

List of Tables

Table 3.1: Nested PERMANOVA results summary for spatial scale variation amongst sites (*n* = 3), plots (*n* = 6), trees (*n* = 96) of robust Aitchison dissimilarity matrices for bacterial and fungal intermediate datasets (taxa in ≥1% and ≤90% of samples). Permutations were restricted within plots and sites. R^2 values represent the amount of variation in the community structure explained by different spatial scales. 76

Table A1: Amplicon samples with <1000 reads that were removed prior to statistical analyses. .. 172

Table B1: Samples with <1000 reads, removed during quality control of amplicon data. 183

Table B2: Allocation of ASVs and sequences across the three different subcommunities of the dataset. Percentage value is representative of the full dataset. 184

Table B3: Environmental variables associated with soil bacterial and fungal community composition. Factors that were significantly correlated with ordination axes are denoted by *, where $P \leq 0.05$ is *, $P \leq 0.01$ is **, and $P \leq 0.001$ is ***. 185

Table B4: Environmental variables of sites (mean ± standard deviation). 186

Table C1: Pairwise PERMANOVA results comparing soil physicochemical properties between sites and between plots within sites. Analyses were based on Euclidean distance matrices generated from standardised soil variables. Pairwise comparisons between plots were nested within sites to account for the hierarchical sampling design. *P*-values were adjusted using Holm correction..... 197

Table C2: Pairwise PERMANOVA results comparing gene composition between sites and between plots within sites. Analyses were based on Bray-Curtis distance matrices generated from TPM normalised gene coverage. Pairwise comparisons between plots were nested within sites to account for the hierarchical sampling design. *P*-values were adjusted using Holm correction..... 198

Table C3: Results of *envfit* analysis showing correlations between soil physicochemical properties and microbial functional potential across three functional annotation datasets (eggNOG, NCyc, and CAZy). 200

Table C4: PERMOANOVA results testing differences in gene composition between healthy (*n* = 21) and unhealthy (*n* = 74) kauri trees based on Bray-Curtis dissimilarities. Analyses were conducted separately for the three functional gene annotation databases (eggNOG, NCyc, and CAZy). Gene composition was derived from TPM normalised gene abundance profiles. 201

Attestation of Authorship

I hereby declare that this submission is my own work and that, to the best of my knowledge and belief, it contains no material previously published or written by another person (except where explicitly defined in the acknowledgements), nor used artificial intelligence tools or generative artificial intelligence tools (unless it is clearly stated, and referenced, along with the purpose of use), nor material which to a substantial extent has been submitted for the award of any other degree or diploma of a university or other institution of higher learning.

Zoe King

Date: 03-10-2025

Co-authorship Contributions

STUDENT AND SUPERVISOR APPROVALS

By signing you are confirming that the co-author contributions stated in the table(s) below are accurate.

Student Name	Zoe King	**Signature**		**Date**	03-10-2025
Supervisor Name	Donnabella Lacap-Bugler	**Signature**		**Date**	03-10-2025

Chapter Number:	2
Manuscript Title:	Comparative amplicon and shotgun metagenome profiling of soil microbial communities in kauri forests affected by *Phytophthora agathidicida*
Publication Status:	**Submitted for Publication**
Reference if published:	

AUTHOR SURNAME: (order as per manuscript)	CONTRIBUTION (May copy from the guidelines above)
King	Conceptualisation, acquisition of research data, analysis or interpretation of research data, drafting
Buckley	Conceptualisation, contribution of knowledge, critically revising
Lear	Conceptualisation, contribution of knowledge, critically revising
Seale	Contribution of knowledge, critically revising
Lee	Contribution of knowledge, critically revising
Schwendenmann	Contribution of knowledge, critically revising
Lacap-Bugler	Conceptualisation, contribution of knowledge, critically revising

Chapter Number:	3
Manuscript Title:	Spatial variation of soil microbial communities associated with dieback of a foundation tree species
Publication Status:	**Submitted for Publication**
Reference if published:	

AUTHOR SURNAME: (order as per manuscript)	CONTRIBUTION (May copy from the guidelines above)
King	Conceptualisation, acquisition of research data, analysis or interpretation of research data, drafting
Buckley	Conceptualisation, contribution of knowledge, critically revising
Lear	Conceptualisation, contribution of knowledge, critically revising
Seale	Contribution of knowledge, critically revising
Lee	Contribution of knowledge, critically revising
Lacap-Bugler	Conceptualisation, contribution of knowledge, critically revising

Chapter Number:	4
Manuscript Title:	Soil microbial functional potential in kauri forests is shaped by spatial and physicochemical gradients more than tree health decline
Publication Status:	**Unpublished/Ready for submission for Publication**
Reference if published:	

AUTHOR SURNAME: (order as per manuscript)	**CONTRIBUTION** (May copy from the guidelines above)
King	Conceptualisation, acquisition of research data, analysis or interpretation of research data, drafting
Buckley	Conceptualisation, contribution of knowledge, critically revising
Lear	Conceptualisation, contribution of knowledge, critically revising
Seale	Contribution of knowledge, critically revising
Lee	Contribution of knowledge, critically revising
Lacap-Bugler	Conceptualisation, contribution of knowledge, critically revising

Acknowledgments

The completion of this thesis reflects not only my work, but also the guidance, encouragement, and support of many people over the past few years, for which I am deeply grateful for.

First and foremost, this endeavour would not have been possible without the guidance and support from my supervisory team. I am especially indebted to my primary supervisor Professor Donnabella Lacap-Bugler, for accepting me into this project and for your continued enthusiasm and support throughout its duration. You have always been there to listen to my ideas and ramblings, and to help me stop spiralling when things became overwhelming. I am truly thankful for every opportunity you have given me.

My sincere thanks also go to Professor Hannah Buckley for your thoughtful guidance and support throughout all aspects of this project. I am extremely thankful for your steady presence and endless ideas and suggestions on how to navigate this challenging project. I am grateful to Professor Gavin Lear for your expertise and input throughout this project. Your attention to detail and endless suggestions have helped me turn my mountain of data into something I can finally make sense of.

I would also like to thank Dr Kevin Lee for your patient guidance with R and bioinformatics throughout this project. I have learned so much from you, and your willingness to answer my many questions (and to debug endless amounts of code) made a daunting task manageable. Finally, special thanks are due to Associate Professor Brent Seale, who has been part of my academic journey from my very first microbiology lab to this thesis. I am thankful for your ongoing support and for helping me keep sight of the big picture whenever I became lost in the details.

I gratefully acknowledge the financial support from Ngā Rākau Taketake (NRT), which provided a stipend, fees, and research costs for this project. To Professor Luitgard Schwendenmann and the wider NRT group, thank you all for providing a space to collaborate about all things kauri. Additionally, I extend my deepest thanks to Te Kawerau ā Maki for granting us access to the Waitākere Ranges to collect the samples for this research.

Thank you to the AUT staff and technicians, especially Tim Lawrence for all his support in the lab. Sincere thanks go to Dini and the team at NeSI for providing access to the HPC, as well as for the consultations and continued support in managing and analysing the mountain of data generated in this project. I acknowledge that ChatGPT was used for technical purposes in debugging R and python

code and structuring analyses. Additionally, it was used to help refine and polish my writing for clarity, flow, and conciseness. To Dr Jieyun Wu, thank you for your time and support in analysing the shotgun metagenome data.

Many thanks to all members of the Microbiology Research Group for your feedback and support throughout this journey. To friends old, new, and even those lost along the way, thank you for the encouragement and perspective you provided through different stages of this journey. My heartfelt thanks to Praveenth for your steadfast support, I am grateful to have had a friend like you by my side since the beginning of this journey. To Rozanne and Amber, thank you for sustaining me during the final stretch, providing a space to vent my (many) frustrations, and always finding the right words of encouragement to keep me going.

I am endlessly grateful to Jean and Tim, whose steady support has carried me through many years of study. Your patience, understanding, and reassurance have allowed me to fully invest myself into this project. To my other family members, thank you all for your interest, encouragement, and providing a much-needed outlet during difficult moments throughout all stages of this project. A special mention goes to Ronnie, my cat, for being the best late-night study buddy, always stealing my foot stool, and knowing when a cuddle was needed the most.

Finally, to my Amber, I express every thanks I have for your unwavering and endless support. You have been through every high and low of this journey with me and encouraged me to keep going when I really wanted to stop. I am forever grateful for the endless love, support, understanding, and laughs you have given me over the duration of this project, thank you.

Chapter 1

General Introduction and Literature Review

1.1 Introduction

Forest ecosystems are increasingly subjected to a range of biotic and abiotic threats, including climate change, land-use change, exposure to pollutants, pests, and pathogens (Balla et al. 2021; Kurz et al. 2008; Pascual et al. 2022; Saatchi et al. 2021; Smith et al. 2016). These pressures threaten forest biodiversity, resilience, and health, making it important to understand and monitor the underlying ecological processes that support forest stability. A key aspect of these processes is the role of the soil microbial community, which can contribute both positive and negative effects towards plant communities (Hackl et al. 2005; Stewart et al. 2021; Yu et al. 2022). The interactions between the soil microbial community, plant pathogens, and trees are complex and can directly affect the tree's health and survival (Garrastatxu et al. 2024; Ruiz Gómez et al. 2019). The shifts in microbial community composition and function, and how they may be influenced or influence the spread and expression of the pathogen and the tree's health, are not well understood. One of New Zealand's foundation native tree species, kauri (*Agathis australis*), is threatened by the dieback causing soil-borne oomycete *Phytophthora agathidicida*. This presents a compelling case study to explore and understand the complex interactions of the soil microbial community and the directionality of their influence on the pathogen and the tree (Beever et al. 2009; Gadgil 1974; Weir et al. 2015). This thesis explores the role and influence of the soil microbial communities associated with kauri trees threatened by dieback disease to deepen our understanding of the interactions between pathogen, tree, and soil microbial communities.

1.2 Literature review

1.2.1 Kauri

Agathis australis (D. Don) Lindl. ex Loudon, commonly known as kauri, is an endemic tree found in the northern 'third' of New Zealand (Ecroyd 1982). Kauri (Figure 1.1) belongs to the Araucariaceae, an ancient family of evergreen, coniferous trees consisting of three extant genera, *Agathis*, *Aracaria*, and *Wollemia* (Jones et al. 1995; Stockey 1982). During the Jurassic and Cretaceous periods, the Araucariaceae family was globally distributed; however, towards the end of the Cretaceous period, the trees became extinct from the northern hemisphere and are now primarily found in the Southern Hemisphere, except for a few *Agathis* species located in Malesia (Singh 2006; Stockey 1982; 1994). The *Agathis* genus is natively found within Australasia and Southeast Asia, and kauri are the southernmost and only indigenous member of the Araucariaceae in New Zealand (Ecroyd 1982; Whitmore 1977). They can grow north of 38 degrees south (°S) and

on offshore islands around the North Island of New Zealand; in subtropical or warm temperate forests, and have a natural southern limit near Hauturu, Waikato (Ecroyd 1982; Whitmore 1977).

Figure 1.1: Tāne Mahuta, the largest living kauri tree located in the Waipoua Forest of Northland Region, New Zealand.

1.2.1.1 Morphological features of kauri

1.2.1.1.1 Tree growth

Three distinct stages characterise the growth of kauri. Young or juvenile trees have a typical conifer form with a tapering trunk, a narrow conical crown, and exhibit monopodial growth, with whorls of long, slender branches along the entire trunk (Halkett and Sale 1986; Orwin 2004; Wilson et al. 1998). When kauri reach around 30 to 50 years old, they shed their lower branches through abscission and continue to grow until they reach above the forest canopy (Orwin 2004; Wilson et al. 1998). This is described as the 'ricker' stage of growth, named after the naval masts and spars these kauri were commonly used for (Orwin 2004). After breaking through the forest canopy (Figure 1.2), kauri begin to fully mature, with adult branches forming to support their spreading crowns and increasing their girth to create a large symmetrical trunk or column (Figure 1.1) (Orwin 2004; Wilson

et al. 1998). The process of maturation can take hundreds of years, however, the pay-off situates kauri as the largest timber tree by volume in the world (Orwin 2004). The final height and size of kauri are dependent on the site and conditions of growth, and age can vary greatly between trees of similar diameters (Orwin 2004).

Figure 1.2: Kauri forest in the Waitākere Ranges showing a range of kauri health states. Mature kauri tree with a healthy canopy (red arrow), kauri with a declining canopy (yellow arrow), a fallen dead kauri (pink arrow).

1.2.1.2 Root systems

As well as their above-ground appearance maturing as the tree grows, kauri roots also develop and change as the tree ages. Young kauri possess an established tap root system, accompanied by lateral and fine feeder roots that disperse throughout the litter and humus layer of the forest floor (Ecroyd 1982). As kauri mature, they lose their tap root system and instead develop deep peg roots, as well as developing lateral and feeder roots beyond the width of the crown (Steward and Beveridge 2010). This extensive lateral root system in mature trees helps kauri remain windfirm. Generally, kauri remain windfirm unless senescence or root rot sets in. The feeding roots of kauri possess small nodules that contain arbuscular mycorrhizal endophytes (Ecroyd 1982; Padamsee et al. 2016; Steward and Beveridge 2010). Kauri roots are also known to graft to each other, allowing nutrients and water to be exchanged with their neighbours, as well as pathogen transmission (Bader and Leuzinger 2019).

1.2.1.3 Reproductive structures

Kauri trees are monoecious, bearing both male and female reproductive organs. Their reproduction cycle is similar to other temperate pines, lasting around 19–20 months (Owens et al. 1997). Male cones or strobili are around 8–12 mm long and have a finger-like shape (Owens et al. 1995). These cones produce pollen and are usually found on branches above female cones, but are occasionally located on the same branch (Bergin and Steward 2004). Female cones are globose and around 5–7.5 cm in diameter when ripe and house the seeds of kauri (Bergin and Steward 2004). Viable seed is produced when kauri are between 25–40 years old (Halkett and Sale 1986). Fertilisation of the female cones, via pollen shedding in male cones, occurs before the female cones break open and the seeds are released which are dispersed through gravity and wind due to their small wings (Owens et al. 1997; Owens et al. 1995). Seeds do not usually travel far, with most seeds landing within 50 m of the parent tree (Enright et al. 1999). However, it has been suggested that seeds can travel up to 1.5 km (Ecroyd 1982).

1.2.1.4 Socio-cultural significance of kauri

1.2.1.4.1 Cultural significance

Woven into the traditions, legends, and cultural beliefs of the Indigenous Māori people, kauri hold immense importance. They are considered taonga (treasure) and the health of kauri is said to represent the health of the forest and the people (Orwin 2004). A significant whakataukī (proverb) spoken by local iwi Māori is "*Ko te kauri ko au, Ko te au ko kauri - I am the kauri, the kauri is me"*, demonstrating the significance kauri have in Māori culture (Lambert et al. 2018). The largest remaining living kauri in New Zealand forests is known locally as Tāne Mahuta ('Lord/God of the Forest'; Figure 1.1), standing 51.2 m tall, with a trunk girth of 13.77 m (Department of Conservation n.d). This significant tree is pivotal to the creation of life in Māori culture and is therefore of primary importance.

Early Māori settlers used kauri for many different purposes. The gum was widely used to start fires, as torches for fishing, as insecticide in kumara farms, as chewing gum, and even the soot from burning the gum was used in tattooing (Halkett and Sale 1986). The wood itself was also occasionally used to make canoes, carved from a tree in one piece (Irwin et al. 2017).

1.2.1.4.2 Economic significance

The economic significance of kauri was initially linked with the quality and volume of timber produced from mature trees, as well as the gum either buried in the ground or actively bled from

living trees (Orwin 2004; Sale 1978). Nowadays, furniture and other wooden items made from kauri are only permitted when using swamp kauri; kauri that has been preserved for centuries in anoxic bog environments, primarily in northern New Zealand (Lorrey et al. 2018; Steward and Beveridge 2010). Swamp kauri is also valuable to scientists for reconstructing demographic and climatic chronologies using dendrochronology (Lorrey et al. 2018).

Since the implementation of forest protection, eliminating extensive kauri logging, the economic focus of kauri has switched to the tourism trade. Northland has implemented a cultural tourism projects to celebrate and honour these significant trees (New Zealand Herald 2005). Tāne Mahuta is a significant tourist attraction in Northland, with an estimated 152,000 visitors a year (White 2019). The change in New Zealand's economic focus to include tourism has allowed kauri to regenerate and thrive while also reaping the economic benefits of these trees.

1.2.1.4.3 Ecological significance

Kauri are not always the dominant species of the forests they inhabit in terms of density. However, in terms of basal area and importance for surrounding systems, they are considered the most dominant (Ahmed and Ogden 1991). Kauri usually co-exist with other coniferous and angiosperm canopy species (Ahmed and Ogden 1991). As a foundation species of these forests, premature loss of kauri is likely to have consequential effects on plant community composition (Beever et al. 2009; Wyse et al. 2014). Mature kauri often supports epiphyte communities in their crowns and certain fungal species that are restricted to kauri alone (McKenzie et al. 2002; Wyse and Burns 2011; Wyse et al. 2014). Furthermore, mature kauri accumulates and stores large amounts of carbon, with kauri forests ranked as one of the most carbon-dense ecosystems globally (Macinnis-Ng et al. 2017; Silvester and Orchard 1999). The large amounts of both woody debris and leaf litter that accumulate on the forest floor surrounding kauri influence the soil processes beneath their canopies (Jongkind et al. 2007; Wyse 2012). The woody debris and leaf litter are rich in nitrogen and are slow to decompose, with accumulation of this litter contributing to the acidic and podsolised soils that are observed in kauri forests (Jongkind et al. 2007; Verkaik et al. 2007; Wyse 2012). Premature loss of this foundation species could drastically alter the dynamics of kauri forests by changing these unique habitats, removing certain species assemblages, and reducing the carbon uptake and storage by this ecosystem (Macinnis-Ng et al. 2017; Wyse et al. 2014).

1.2.1.5 History

Before European settlement in New Zealand in the 19th century, kauri forests dominated much of the country's northern third, with an estimated coverage of 1 to 1.5 million hectares (Sale 1978). Over 80 years, kauri were extensively logged for exportation due to their soft, straight-grain wood, which was comparatively durable and resistant to decay (Orwin 2004; Sale 1978; Steward and Beveridge 2010). Kauri gum was also exported in great quantities during the 19th century (Orwin 2004; Sale 1978). Currently, approximately 7,500 hectares of original kauri forest remain, less than 0.5 % of their original coverage, sparsely scattered across their former geographic range (Steward and Beveridge 2010).

Throughout the nineteenth century, kauri timber and gum were one of the largest and most stable export industries in New Zealand. Kauri wood was used to build ships, buildings, and furniture for both domestic and overseas markets. However, due to the intense demand and high prices of kauri timber, logging proceeded at a pace that pushed kauri to near extinction by the early twentieth century. Forests were also deliberately burned to open land for pastoral farming and to clear scrub for gum-mining. These fires could become out of control, with areas ablaze for weeks, destroying extensive forest areas and mature kauri. Together, commercial exploitation and settler land conversion accelerated the loss of kauri across its range (Orwin 2004; Sale 1978).

Today, logging and burning of kauri forests are prohibited under the 1973 Kauri Management Policy (Halkett 1983; Sale 1978). Additionally, regeneration programmes have established roughly 60,000 hectares of secondary forest and scrubland that contain kauri (Orwin 2004; Steward and Beveridge 2010). Despite this progress, both remnant and regenerated stands face a persistent biological threat known as kauri dieback.

1.2.2 Kauri dieback

Kauri dieback is a severe disease that imposes a rapidly increasing biological threat to kauri of all ages. Symptoms of kauri dieback were first identified on Great Barrier Island in 1972 (Gadgil 1974). The causative pathogen was identified as the soil-borne oomycete, *Phytophthora agathidicida*, causing root and collar rot (Beever et al. 2009; Gadgil 1974; Weir et al. 2015). Since first identifying kauri dieback on Great Barrier Island in 1972, and in mainland New Zealand in 2006, *P. agathidicida* has been identified throughout most of kauri's geographic range (Bradshaw et al. 2020). A recent report shows no evidence of *P. agathidicida* in the Hūnua Ranges, Auckland (Froud et al. 2025) and long-term monitoring of the Waitākere Ranges shows that *P. agathidicida* is limited

to the edges of the forest and is not widespread in the park interior (Froud et al. 2022). However, the increased prevalence of kauri dieback throughout most of kauri's geographic range has caused kauri to become listed as a threatened species (de Lange et al. 2018).

Several criteria have been proposed to define terms associated with cases of kauri dieback. Firstly, kauri dieback is defined as an infectious **disease** that is caused by the **pathogen** *P. agathidicida* (Froud 2020). The term "disease" is defined as the visible symptoms observed on a host that are related to one or more specific disorders caused by a pathogen. The "pathogen" is defined as the microorganism that infects and disrupts the host's physiology, causing the disease symptoms. Although the **disease** and **pathogen** are usually linked, the pathogen may be present in absence of the disease, and the disease may be present in the absence of the specific pathogen as symptoms may be caused by other biotic or abiotic factors (Froud 2020).

1.2.2.1 Infection and symptoms

Phytophthora agathidicida can affect kauri of any age or size, with above-ground symptoms developing during the chronic phase of disease and exhibiting varying lengths of infection from visible symptoms to tree death (Figure 1.2) (Beever and Bellgard 2010; Bellgard et al. 2016a; Waipara et al. 2013). When kauri are initially infected with *P. agathidicida*, the pathogen is generally localised to the fine root systems of the trees (Bellgard et al. 2013). As infection progresses, the pathogen moves towards the larger, woody roots before entering the cambium and collar of the tree where 'cankers' may form (Bellgard et al. 2013). Infection within the cork cambium can lead to gummosis or bleedings on the collar of the trees (Figure 1.3A) (Beever and Bellgard 2010; Bellgard et al. 2013). Chronic infection of *P. agathidicida* will eventually lead to a declining crown (Figure 1.3B) and chlorosis of leaves (Figure 1.3C) due to deterioration of the vascular systems (Beever and Bellgard 2010; Bellgard et al. 2013). Ultimately, prolonged infection of *P. agathidicida* will lead to the death of kauri (Figure 1.3D) (Beever and Bellgard 2010; Bellgard et al. 2013; Horner and Hough 2014; Waipara et al. 2013). Disease extent is defined based on a five-point classification system of the canopy health and colour where 1 = healthy, 2 = some foliar thinning, 3 = some branch dieback, 4 = severe shoot dieback, and 5 = dead (Bellgard et al. 2013; Hill et al. 2017). Additional half-point classifications are sometimes included to help differentiate later stages of infection (Froud et al. 2022; Horner et al. 2019a). Symptomatic trees have been defined by Bellgard et al. (2013) and Froud et al. (2022) as trees with basal bleeds and a canopy health scores above 3.

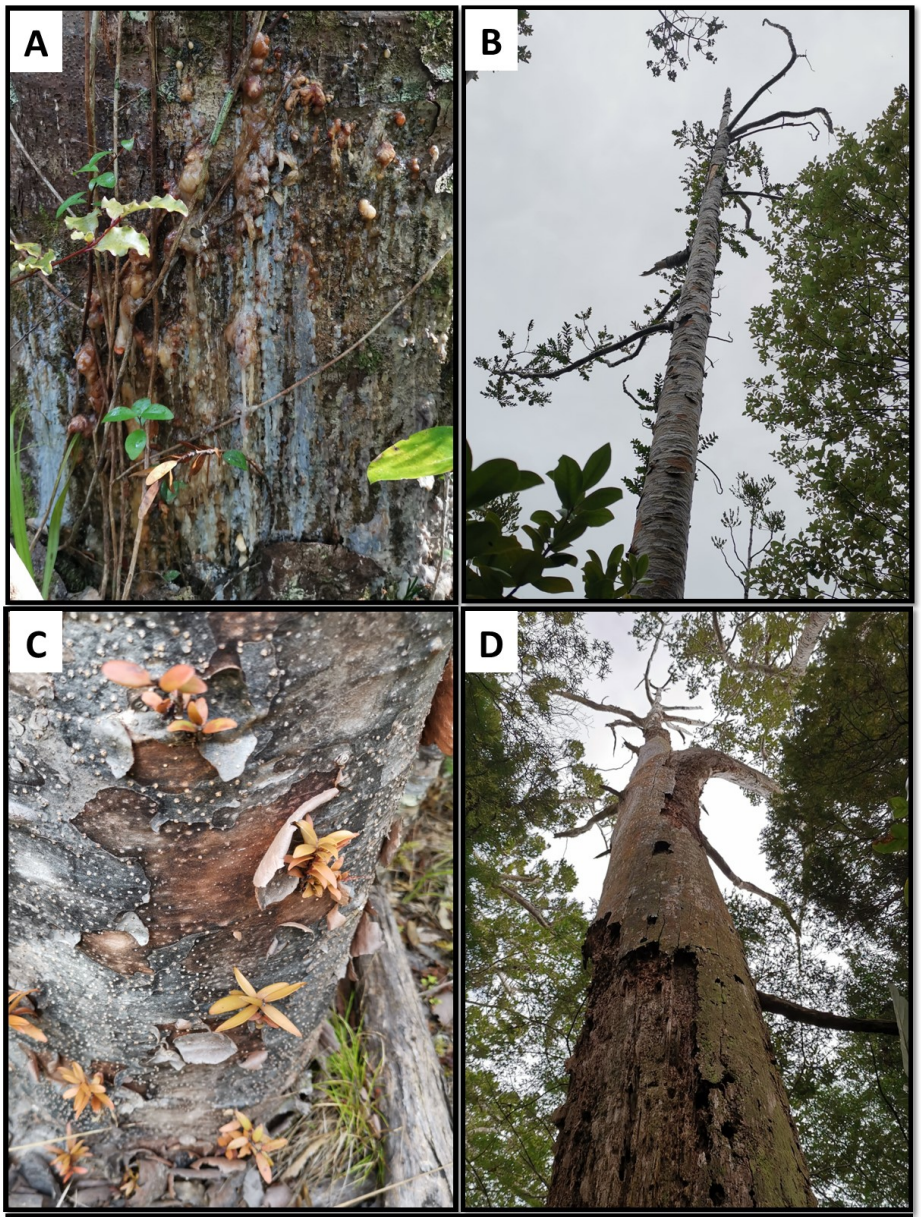

Figure 1.3: Symptoms of kauri dieback: (A) basal bleeding, (B) crown thinning, (C) yellowing leaves, all leading to eventual (D) tree death.

1.2.2.2 *Phytophthora* and kauri dieback in New Zealand

Phytophthora agathidicida was first discovered on Great Barrier Island in the 1970s (Gadgil 1974). Reports of dead young kauri trees and rickers, trees with yellowing leaves and depleting crowns, and the presence of cankers with severe gum bleeding led to an investigation and discovery of the cause of these symptoms (Gadgil 1974). Microorganisms were isolated from soil samples around these ill trees and *Phytophthora* was identified. The *Phytophthora* was initially incorrectly identified as *P. heveae* (Gadgil 1974).

In 2006, reports of unhealthy and dying kauri in the Waitākere Ranges (mainland New Zealand) were made by the public (Beever et al. 2009). This prompted an investigation which

observed kauri with similar symptoms as those seen on Great Barrier Island in 1972. The organism isolated from bleeding lesions of infected trees was analysed using molecular based methods to determine the taxonomy and phylogeny of the isolate (Beever et al. 2009; Cooke et al. 2000). This led to the temporary reclassification of the causative agent from *P. heveae* to *Phytophthora* 'taxon Agathis' (PTA), due to differences in the organisms Internal Transcribed Spacers (ITS) region (Beever et al. 2009). In 2015, PTA was officially reclassified as *P. agathidicida*, based on host specificity, morphology, and genetic differences (Weir et al. 2015). Since 2008, this organism has been classed as an Unwanted Organism in New Zealand under the Biosecurity Act 1993 (Waipara et al. 2013).

The origin or introduction of *P. agathidicida* into New Zealand is not well understood. One hypothesis for its origin is from the East Asia/Pacific region due to its genetic similarity to other members of its phylogenetic clade which consists primarily of isolates from East Asia and the Pacific Islands (Weir et al. 2015). There are three main suggestions for its introduction into New Zealand: (1) introduction in the 1940s from imported forestry and planting equipment (Beachman 2017), (2) introduction with the arrival of many European settlers between 1845 and 1940s (Hackwell and Bertram 1999), and (3) *P. agathidicida* has been present in New Zealand for several hundred to several thousand years (Winkworth et al. 2021).

1.2.3 *Phytophthora agathidicida* biology

1.2.3.1 Oomycetes and the *Phytophthora* genus

Oomycetes are a fungus-like eukaryotic microorganism belonging to the Stramenopile clade within the eukaryotic tree of life (Beakes et al. 2012). Morphologically, oomycetes differ from fungi due to their cell wall composition with oomycete cell walls consisting of cellulosic compounds and glycan, and fungal cell walls comprising of chitin (Mélida et al. 2013).

Oomycetes, and the *Phytophthora* genus in particular, are known for their pathogenicity towards many woody dicotyledonous plants, herbaceous plants and shrubs, and many important food crops and forest vegetation (Akrofi et al. 2003; Ho 2018; Weir et al. 2015). Of most notoriety is the Irish potato famine from 1845 to 1852, started by the potato crop failure caused by *P. infestans* (Yoshida et al. 2013). Wide infection of potato by this pathogen, leading to potato late blight, caused devastation throughout Europe and death by starvation of around 1 million people (Turner 2005), highlighting the devastation *Phytophthora* can have on plant species and humanity.

The genus *Phytophthora* currently comprises of 200 recognised species, divided into ten clades, of which *P. agathidicida* belongs to Clade 5 (Brasier et al. 2022; Kroon et al. 2012; Weir et al. 2015; Yang et al. 2017). *Phytophthora* have been isolated across the world (Gómez-Alpizar et al. 2007; Yang et al. 2017). However, all species within clade five have been isolated from Pacific and East Asian regions, suggesting a potential geographic link between these species (Weir et al. 2015; Yang et al. 2017).

1.2.3.2 Lifecycle and morphology

The different characteristics of propagules by *P. agathidicida* each have their own advantages for completing the pathogen's lifecycle and perpetuation of infection. The lifecycle of *P. agathidicida* is similar to that of other *Phytophthora* species, being able to reproduce asexually and, sexually, via a homothallic (self-fertile) system in which a single isolate can produce oospores in culture without a mating partner (Weir et al. 2015). From the production of spores to the hyphal colonisation of plant root systems, *P. agathidicida* is an efficient plant pathogen able to survive, disperse, and infect using a variety of propagules.

The sexual reproduction of *P. agathidicida* form oospores (long-term survival spores) that almost completely fill its oogonium (surrounding sac), with an average spore width of 27.7 µm and average sac width of 31.9 µm (Weir et al. 2015). Oospores are important for the long-term survival of *Phytophthora* species in soils or plant tissues (Babadoost and Pavon 2013; Crone et al. 2013; Fernández-Pavía et al. 2004). Although the survival of *P. agathidicida* oospores has not been tested in a natural environment, soils stored at 10 °C for 4–6 years still yielded viable *P. agathidicida*, indicating the long term viability of the pathogen even in the absence of a suitable host (Horner and Hough 2015). One notable difference between *P. agathidicida* and many other *Phytophthora* species is the lack of chlamydospores (thick-walled resting spores) within its life cycle instead relying on oospore production for long-term survival (Weir et al. 2015).

Phytophthora agathidicida is able to move to a new host through the formation of zoospores, which are only produced under favourable conditions. These spores are short-lived with a mobile lifespan of approximately 17 hours in sterile water under laboratory conditions; the lifespan of these spores in their natural environment is yet to be determined (Lawrence et al. 2017). Zoospores are produced in the sporangia which are derived from the germination of oospores to form sporangiophores (Weir et al. 2015). Approximately 20-30 zoospores within each sporangium may be released to find a new, suitable host (Bradshaw et al. 2020). Due to the presence of flagella,

zoospores are able to move through thin films of water towards new host roots via chemotaxis (Tyler 2002). The exact signals causing chemotaxis in *P. agathidicida* zoospores is unknown; however, it has been suggested that root exudate, released from the fine root system of kauri specifically attract *P. agathidicida* (Bradshaw et al. 2020).

Once the zoospores find a suitable site, they drop their flagella and begin to encyst (Bellgard et al. 2016a). Development of a cell wall occurs within five days of initial contact of the zoospore with the root material. The encysted cells germinate to produce hyphae which then spread across the root surface and penetrate into the roots (Bellgard et al. 2016a). The hyphae are aseptate and simple in structure (Weir et al. 2015). Penetration into the roots by hyphae can cause lignitubers (hyphae encased by lignin) to form around some of the hyphae, as well as stromata-like structures of aggregated hyphae (Bellgard et al. 2016a). These structures are formed to stop or restrict infection. It has been suggested by Jung et al. (2013), that hyphae surrounded by these lignotubers may remain viable due to protection from drought conditions and microbial decomposition. However, this hypothesis requires more research before a conclusion can be drawn.

Phytophthora are hemibiotrophic; they maintain an initial biotrophic phase which is asymptomatic for the host, followed by a necrotic phase where symptoms are exhibited, and this eventually leads to plant death (Bellgard et al. 2013; Lee and Rose 2010). Hyphal protrusion into the fine root systems, followed by establishing haustoria (a specialised structure used to absorb water and nutrients from the host), signals the beginning of the biotrophic phase of infection, allowing the pathogen to begin feeding off the plants nutrients (Bellgard et al. 2013). Prolonged hyphal colonization of the root system of kauri by *P. agathidicida* begins to rot both the fine feeder roots as well as the larger structural roots, indicating the start of the necrotic infection stage (Bellgard et al. 2016b). Extensive root rot due to chronic infection with *P. agathidicida*, hinders the ability of the tree to uptake nutrients and water leading to observations of above ground symptoms (Bellgard et al. 2016b). The latency in infection onset makes chronic infection hard to identify based on the presence or absence of symptoms alone.

1.2.4 Disease detection

With no known cure for kauri dieback, management and containment of the disease are the primary focus to ensure the disease does not spread into unaffected areas. Management of the disease is primarily coordinated by the Kauri Dieback Programme (KDP). The KDP is a collaborative partnership of central and local government established in 2009 (Kauri Dieback Programme n.d.).

Collaborative partners include the Ministry of Primary Industries (MPI), the Department of Conservation (DOC), tangata whenua (people of the land), and four councils that are within kauri's natural range: Northland Regional Council, Auckland council, Waikato Regional Council, and Bay of Plenty Regional Council (Kauri Dieback Programme n.d.). The programme aims to collaboratively manage and protect kauri through both scientific research and mātauranga Māori (Māori knowledge) (Kauri Dieback Programme n.d.).

1.2.4.1 *Phytophthora agathidicida* detection

Pathogen identification is an important step in disease management. It can be used to confirm the absence of *P. agathidicida* in areas thought to be disease free or to confirm presence in areas with symptomatic kauri. *Phytophthora agathidicida* may be identified from soil samples collected from around the tree or from plant material such as from bleeding lesions on the trunk of the tree.

Soil sampling is currently the standard method for isolating and identifying *P. agathidicida* in kauri forest systems. There are two methods in practice for collecting soil samples around a tree of interest with the aim of encompassing the trees rhizosphere (Beever and Bellgard 2010). Firstly, an eight-point collection method was proposed, comprising of four cardinal points taken at both 1 and 2 m from the trunk of interest (Beever and Bellgard 2010; Dick and Bellgard 2010). This sampling method collects soil from both close to the trunk, as well as at the drip line of the canopy. The second method only includes four cardinal point samples within 1 m of the trunk and eliminates the four drip line samples (Hill et al. 2017). Woody debris and leaf litter are removed from the sample area before the sample is collected from a surface depth between 10 to 15 cm; with the small kauri feeder roots included in collection where possible (Dick and Bellgard 2010; Hill et al. 2017). *Phytophthora* are not ordinarily detected beyond a surface layer depth of 20 cm using a soil baiting bioassay method, thus soil sample collection is primarily restricted to the first 10 to 15 cm of soil (Bellgard et al. 2013).

Once collected, soil samples may undergo a baiting bioassay, molecular identification, or a combination of both methods to identify *P. agathidicida*. *Phytophthora* species have commonly been detected and isolated from soil samples using soil baiting bioassays (Cooke et al. 2007; Erwin and Ribeiro 1996). These bioassays predominantly use plant material as baits to attract *Phytophthora* zoospores from a flooded soil sample. This bioassay method was first optimised for *P. agathidicida* in 2010 (Beever and Bellgard 2010). The optimised method starts with a pre-treatment phase

involving the air drying of samples for two days before a moist incubation for four days where zoospore formation is stimulated. The soil is then flooded with reverse osmosis water, and the bait of choice is placed on the waters' surface before incubating for two days. The baits are then placed onto P_5ARPH-CMA selective agar (Jeffers and Martin 1986) and any *Phytophthora*-like growth is subcultured onto both V8 juice agar (Tuite 1969) and potato dextrose agar (PDA). Identification of *Phytophthora* is obtained via observation of colony growth via microscopy or via DNA sequencing of the ITS1 region or the cytochrome c oxidase subunit 1 (Abad et al. 2023; Singh et al. 2017). This optimised baiting process takes approximately 14 days and requires some specialised skills to identify *Phytophthora* species via morphology alone.

The choice of bait depends on both the species of *Phytophthora* being identified as well as the host plant (Erwin and Ribeiro 1996). Examples of baits used for other *Phytophthora* species include fruits such as apple, pear, and citrus fruits; as well as pine needles and lupin seedlings or radicles (Erwin and Ribeiro 1996; Hargreaves and Duncan 1978). Many different baits have been evaluated for their consistency at detecting *P. agathidicida* from soil samples. Currently, lupin radicles (*Lupinus angustifolius*) and Himalayan cedar (*Cedrus deodara*) are considered the most consistent baits; with kauri leaves being one of the least effective (Beever and Bellgard 2010).

The soil baiting bioassay exploits the pathogenicity of the *Phytophthora* and will show that the organism is present in the sample, as well as able to cause infection (Erwin and Ribeiro 1996). However, the method also relies on breaking the dormancy of oospores to induce zoospore formation that are then chemotactically attracted to a nutrient source such as the bait of choice (Burgess et al. 2021; Cahill and Hardham 1994). Failure to stimulate oospores into sporangia and zoospore production leads to a false negative result (Bellgard et al. 2013). Breaking the dormancy of *P. agathidicida* oospores still provides a challenge for researchers to overcome (Froud 2020). Another limitation of the soil baiting method involves low inoculum levels of the pathogen. When infection of a kauri tree is at an advanced stage and the destruction of the fine root system is extensive, the *P. agathidicida* inoculum in soil samples can be reduced to low or even undetectable levels (Beever and Bellgard 2010).

Lesion sampling is a method that may be used to detect *Phytophthora* directly from the kauri tree (Beever and Bellgard 2010). When gummosis is present on the lower trunk of a kauri tree, a 5 – 10 cm^2 sample of necrotic tissue and outer cambium may be removed and placed onto *Phytophthora* selective agar P_5ARPH-CMA (Beever and Bellgard 2010; Waipara et al. 2013). Similar

to the baiting bioassay, any *Phytophthora* like growth is then subcultured onto V8 juice agar and PDA for morphological identification. *Phytophthora agathidicida* is primarily isolated from just below the outer bark into the cork cambium region, with isolation success reducing from the secondary phloem (Beever and Bellgard 2010). Sampling further into the tree into the vascular cambium is not desirable as it can cause long term harm to the tree and is a potential entry point for infections by other organisms; additionally *P. agathidicida* has not been isolated from this trunk region (Beever and Bellgard 2010).

Lateral flow devices (LFDs) are used as a way to identify *Phytophthora* from lesion samples in the field (Beever and Bellgard 2010). A small sample of plant tissue may be added to a vial with a buffer and ball bearings before vigorously shaking the sample to release the antigen of interest. The reagent is then placed onto a test strip, and a colour change reaction will occur indicating the presence or absence of *Phytophthora*. This method has been recommended as a complementary diagnostic tool to the direct isolation of *P. agathidicida* from lesion samples (Waipara et al. 2013).

Similar to the LFD method, an enzyme linked immunosorbent assay (ELISA) has been developed for the rapid detection of *P. agathidicida* (Beever and Bellgard 2010). However, current use of this method for detecting *P. agathidicida* is limited as the assay can cross-react with other microbial species and the resin from kauri trees may also interfere with the assay (Scott et al. 2015 in Froud (2020)).

Although tissue and lesion sampling is considered faster than isolating the pathogen from soil, the method has been considered culturally unpopular amongst some private landowners (Waipara et al. 2013). The method was perceived as invasive and increased the risk of spreading and acquiring the infection. Furthermore, lesion sampling can only be used on trees exhibiting symptoms of kauri dieback (basal bleeding) for confirmation of the pathogen; the method is unable to be completed on trees with no bleedings. Due to these reasons, lesion sampling is not currently used for the routine testing of kauri trees for *P. agathidicida*.

With direct isolation and antibody-based tests struggling to meet the demands of pathogen detection, molecular based methods have been explored. Quantitative real-time PCR (qPCR), loop-mediated isothermal amplification (LAMP), and metabarcoding are the main molecular based methods currently being adopted.

A qPCR method was first developed in 2013 based on TaqMan chemistry with the aim of creating a rapid and specific detection of *P. agathidicida* from soil (Than et al. 2013). The primers and probe of this assay were designed around the ITS region, which showed the highest variability between target and non-target species. Specificity testing of the qPCR method showed no cross-reactivity when tested against 26 other *Phytophthora* species (Than et al. 2013). It is important to note that the primers and probe may also attach to *Phytophthora katsurae* and *Phytophthora novaeguineae*. However, these species have not been isolated in New Zealand and are not considered as an important source of cross-reactivity. Sensitivity testing of the method ranges from 5.21 to 20 femtograms (fg) of *P. agathidicida* from soil samples (Singh et al. 2017; Than et al. 2013).

Advantages of the qPCR method include the shortened time of the assay and the detection of dormant *P. agathidicida* oospores, both limitations of the soil bioassay method. However, only using the qPCR assay will not determine if the pathogen is viable and able to infect kauri trees. For these reasons, a combination approach of both a soil baiting bioassay and qPCR is suggested for the detection and viability testing of *P. agathidicida* from soil samples (Singh et al. 2017).

Another molecular-based method based on a LAMP assay has been developed for the detection of *P. agathidicida*, targeting the mitochondrial apocytochrome b (*cod*) coding sequence (Winkworth et al. 2020). The assay relies on a hybrid approach with traditional soil baiting bioassays. The soil samples are baited but instead of culturing the baits, the DNA is extracted, and a LAMP assay is performed on the extraction. This hybrid method reduces the time and cost of detection compared to using the traditional baiting method, as well as being more sensitive. Detection limits of this assay from pure culture are 1 fg of total DNA, which is similar to the Than et al. (2013) qPCR method, with a detection limit of 2 fg from pure culture. Compared to the soil baiting bioassay, Winkworth et al. (2020) evaluated that the LAMP assay detected *P. agathidicida* at a higher frequency, with four times more samples testing positive using the hybrid LAMP approach. The LAMP assay offers several advantages over traditional soil-baiting: it is faster, cheaper, and requires less specialist expertise. Additionally, as LAMP-based detection occurs after an enrichment and cultivation step, the assay identifies viable *P. agathidicida*, whereas qPCR applied directly to soil may also detect residual DNA from dead cells.

Other methods for detecting *P. agathidicida* include metabolite profiling and the use of scent detection dogs. The pilot study of scent detector dogs was presented in 2016 and highlighted the ability of the Labrador dog named ‘Paddy’ to distinguish *P. agathidicida* from *P. cinnamomi*, and

P. multivora, that were inoculated onto oat grains (Bassett and Auckland Council Biosecurity 2016). Sensitivity of this detection method increased from 87% of positively identified samples in Paddy's first attempt to 100% in his second attempt. However, advancement into more complex samples was cancelled due to Paddy's loss of interest, likely due to the restricted conditions the training was conducted in to comply with permit restrictions. Although, Paddy was unable to advance with the detection of *P. agathidicida*, two new dogs have since been trained, 'Pip' and 'Mawhai' (Bell 2021). These two dogs began training in 2020 with the aim of detecting *P. agathidicida* on goods, footwear, and equipment, and to monitor compliance of boot cleaning stations. A fatty acid methyl ester (FAME) profile of *P. agathidicida* has also been defined to aid in the identification of *P. agathidicida*. This analysis takes less than a day and two fatty acids were identified that have the potential to be *Phytophthora* specific biomarkers (Lacey et al. 2021). Although this method still requires further testing, it provides a promising technique for fast detection of *P. agathidicida* in soil samples.

1.2.5 *Phytophthora agathidicida* ecology

1.2.5.1 Dispersal

The wide geographic distribution of *P. agathidicida* infections indicates that its dispersal cannot be explained by zoospore movement alone and must involve additional, independent vectors. The spread of this pathogen is not completely defined yet; however, significant known vectors include footwear via human traffic and through animal movements, by disrupting the fine root systems and surrounding soil where hyphae and oospores have colonised (Hill et al. 2017; Lewis et al. 2019; Sanson 2016). Many recreational walks around New Zealand are situated in or around kauri forests; the use and maintenance of these sites are the biggest known vector of *P. agathidicida* due to the transfer of contaminated soil usually on the underside of footwear (Sanson 2016). Wild pigs have also been suggested as a potential minor vector of this pathogen (Krull et al. 2013). Wild or feral pigs are known to rummage under kauri inadvertently getting potentially contaminated soil on their snouts and trotters which they may then transfer to other kauri trees (Krull et al. 2013). Ingestion of fine roots that carry *P. agathidicida* by pigs has also been suggested as a vector pathway but more investigation is required to confirm this (Bassett et al. 2017). The final vector suspected with *P. agathidicida* dispersal is water. Zoospore motility through water as well as rainfall and waterlogging moving infected soil downhill from infected areas towards non-infected areas is suspected to be involved in pathogen dispersal (Singh et al. 2017). Water mediated dispersal of other *Phytophthora* species has been determined (Ghimire et al. 2011; Loyd et al. 2014).

So far, two studies have focused on the natural spread rate of *P. agathidicida*. An intensive study in the Waitākere Ranges showed that *P. agathidicida* had a natural spread of 3.41 m ± 0.52 m between 2007 and 2013, equating to an estimated average of 0.57 m per year (Bellgard et al. 2013; Froud 2020). This value is well below the estimated value by Beever et al. (2009) of 3 m per year based on a study site of Great Barrier Island. The limited studies around the natural spread of *P. agathidicida* are insufficient to extrapolate the true natural spread of this pathogen, however, they suggest that the spread is highly variable, maybe site specific, and inked to other biotic and abiotic factors (Froud 2020).

1.2.5.2 Hosts and reservoirs

The host range of *P. agathidicidia* is not well understood and has primarily been explored in laboratory settings against other plant species that may be present in or adjacent to kauri forests, e.g. pasture and plantation land uses. Inoculating young native, non-kauri plant species through infected soil showed that rimu (*Dacrydium cupressinum*), māmāngi (*Coprosma arborea*), rewarewa (*Knightia excelsa*), manuka (*Leptospermum scoparium*), pōhutukawa (*Metrosideros excelsa*), kanuka (*Kunzea ericoides*), pigeonwood (*Hedycarya arborea*), korokia (*Corokia buddleioides*), tawa (*Beilschmiedia tawa*), and taraire (*Beilschmiedia taraire*) could become infected by *P. agathidicida* (Bellgard et al. 2013). The exotic plant species white clover (*Trifolium repens*), Caucasian clover (*T. ambiguum*), perennial ryegrass (*Lolium perenne*), annual ryegrass (*L. multiflorum*) and pine (*Pinus radiata*) have also shown susceptibility towards *P. agathidicida* in the laboratory (Lewis 2018). Additionally, *P. agathidicida* mycelial mats that were incubated in soils collected from pine plantations showed increased production of oospores compared to kauri forest soils from the Waipoua forest (Lewis et al. 2019). However, *P. agathidicida* has not been isolated directly from pine plantation soils.

1.2.5.3 Other pathogens and dieback symptoms

It is important to note that common symptoms associated with kauri dieback may not always be attributed to infection by *P. agathidicida*. There are many other biotic and abiotic factors that may interfere with the normal functions of kauri (Beever and Bellgard 2010). As well as being associated with *P. agathidicida* infection, yellowing of leaves is also associated with root rot caused by *P. cinnamomi* (Podger and Newhook 1971) and nitrogen deficiency (Silvester 2000); the thinning canopy is a natural part of kauri growth as the mature canopy develops and may be exacerbated by drought conditions (Ahmed and Ogden 1987; Beever and Bellgard 2010); and gummosis can also be attributed to mechanical injury to the trunk or the presence of other wood-rotting organisms such

as Basidiomycota (Beever and Bellgard 2010). Other *Phytophthora* species such as *P. cinnamomi*, *P. multivora*, and *P. cryptogea* have also been isolated from soil surrounding kauri with dieback symptoms (Hunter et al. 2024; Waipara et al. 2013). Although symptoms associated with kauri dieback may also be caused by other factors, the causal agent of kauri dieback is defined as *P. agathidicida* (Bellgard et al. 2013; Gadgil 1974). Many questions still remain on the epidemiology of this pathogen and other contributing factors that may increase the risk of a tree becoming infected and symptomatic (Froud 2020).

1.2.5.4 Disease distribution

Surveillance monitoring efforts are an important component of managing kauri dieback as they are used to understand the distribution and spread of the disease. Both aerial surveillance and ground-based surveys are used to locate symptomatic trees, which are then sampled and tested for the presence of *P. agathidicida* (Froud et al. 2022). There was also a passive surveillance programme, initiated by the Auckland Regional Council between 2008-2013, which utilised public reports of diseased trees to be further investigated (Waipara et al. 2013).

Ground-based sampling or ground truthing initially focused on priority areas with high conservation status or areas with culturally significant or iconic trees (Jamieson et al. 2014). However, this method is not an efficient way of surveying kauri's natural range, especially for off-track areas where some trees are inaccessible, and it can take a large amount of time to cover large land areas (Jamieson et al. 2014). Care must also be taken to reduce the spread of the pathogen when ground surveying. Due to the limitations of ground-based surveys, aerial surveillance and remote sensing technology have been used to monitor and detect symptomatic kauri (Jamieson et al. 2014; Meiforth et al. 2019). These methods are a more time- and cost-effective way of surveying large areas than ground-based methods.

1.2.6 Disease monitoring in the Waitākere Ranges

The Waitākere Ranges (Te Wao Nui ā Tiriwa) is a regional park covering more than 16,000 hectares of native forest. During the 19th century, the Waitākere Ranges was subject to extensive logging of native timbers, land clearing for farming and settlement, gum mining, and gum bleeding (Froud et al. 2022). Due to the large amounts of deforestation that occurred in this area, only small areas of original, mature kauri forests remain, with regenerated kauri forests appearing in once felled areas (Froud et al. 2022). Currently, the Waitākere Ranges contains one of the largest remaining kauri forests in Auckland, as well as being the most heavily kauri dieback-infected area (Hill et al. 2017).

Surveillance of kauri dieback throughout the Waitākere Ranges has utilised both ground-based and aerial-based methods to assess and monitor the health of kauri along both the visitor track network of the park and off-track areas (Hill et al. 2017; Jamieson et al. 2014). The first surveillance efforts employed in this area highlighted an increase in the distribution of *P. agathidicida* throughout kauri forest fragment areas in the Waitākere Ranges between 2011 and 2016 (Hill et al. 2017). These surveys showed that the proportion of kauri forest area within the Waitākere Ranges with confirmed dieback symptoms more than doubled (from 7.9% to 18.95%), along with an increase in kauri forest area suspected to be infected (from 2.7% to 4.65%) (Hill et al. 2017). Due to the increase in confirmed and suspected cases of kauri dieback in the Waitākere Ranges, a rāhui (customary prohibition) was placed over this area in 2017 by Te Kawerau ā Maki, the mana whenua of Waitākere, to prevent and control human access to the park until risks of spreading the disease were controlled (Te Kawerau ā Maki 2017).

A third major survey of the Waitākere Ranges was conducted in 2021 utilising an epidemiological approach (Froud et al. 2022). Initial stages of the monitoring programme included forest-level monitoring of the kauri population using remote sensing, followed by ground-based surveys, and finally, soil sampling. Through remote sensing, kauri trees >15 m tall within the forest canopy were detected. Of the 68,420 trees identified, 2,140 were randomly selected for ground-based surveillance and a further subset of 761 trees were selected for soil-based analysis to detect *P. agathidicida*. Using a soil baiting bioassay, *P. agathidicida* was identified in 76 out of the 761 soil samples, for a pathogen prevalence of 10%. Sampled trees were four times more likely to be symptomatic if *P. agathidicida* was isolated from their surrounding soil (Froud et al. 2022). The distribution of positive sample sites was restricted to localised areas, primarily around the northern (Cascades area), central-western (Piha area), and southern (Huia area) peripheries of the Waitākere Ranges, which is consistent with previous surveys (Froud et al. 2022; Hill et al. 2017). Detectable *P. agathidicida* were absent from central areas of the Ranges.

From ground-based surveys assessing symptomology of the trees, 413 trees (out of 2,140) were classified as symptomatic (with the symptoms assessed being bleeding basal lesions, lesions on the roots, canopy thinning, yellowing of foliage, and tree death) (Froud et al. 2022). These symptomatic kauri trees were not localised to the peripheral areas of the Waitākere Ranges, instead they were identified throughout the entire surveyed region. However, the most symptomatic areas were clustered around the northern (Cascades area), central-western (Piha area), and southern (Huia area) peripheries. Although *P. agathidicida* was not detected in the central areas of the ranges

based on soil sampling bioassays, many trees were classified as symptomatic. This was not unexpected as many of the symptoms related to kauri dieback are also caused by other biotic or abiotic factors, such as other *Phytophthora* species or drought (Froud et al. 2022).

1.2.7 Disease management

Controlling kauri dieback relies on strategies that both limit its spread and lessens its impacts. Management strategies include phosphite treatment, oospore control, and hygiene practices.

1.2.7.1 Phosphite treatment

Management of the disease at the tree level involves the application of a phosphorous acid (phosphite) treatment to an infected tree. This method was first developed in 2011 through *in vitro* trials with three *Phytophthora* species: *P. agathidicida*, *P. cactorum*, and *P. cinnamomi* (Horner and Hough 2011). These isolates were subcultured onto V8 agar with varying concentrations of phosphite added (0, 5, 15, 40, 100, and 250 µg/mL). Mycelial growth was inhibited in all *Phytophthora* species by the added phosphite. The success of the *in vitro* trials led to the glasshouse trials (Horner and Hough 2013). These trials tested two-year-old kauri seedlings artificially inoculated with *P. agathidicida*, either through contaminated soil or through direct inoculation into the trunk. Phosphite treatment was applied to the seedlings either before or after inoculation and through several different application methods: foliar spray, trunk injection, or soil drenching. Foliar, root, and lesion symptoms were monitored and measured to assess the efficacy of the phosphite treatment and application method on the kauri seedlings. Although some phytotoxic symptoms were noted on trees treated via injection, this was found to be the most effective application method for suppressing *P. agathidicida* activity within the kauri seedlings, with 100% of soil-infected kauri seedlings, and 67% of trunk-infected seedlings surviving. With the promising outlook of phosphite treatment, administered via injection, from these greenhouse trials, field testing with ricker trees was undertaken.

Field trials of phosphite treatment were first conducted in 2012 in four kauri stands across Auckland and Northland; two naturally regenerating stands, and two plantation stands (Horner et al. 2015). Two different treatments were administered in 20 cm intervals around ricker-aged trees: a high-dose treatment of a 20 mL 20% phosphite injection and a low-dose 20 mL injection of 7% phosphite. Initially, treatment seemed to reduce the advancement of basal lesions, and visual assessments of canopy colour noted some crowns becoming greener after treatment, suggesting the phosphite treatment may help restore diseased kauri back to health. However, some trees

injected with the high dose treatment showed signs of phytotoxicity, and it was suggested that this dose of phosphite was increasing the decline of heavily diseased trees. An updated assessment of these trials showed that there were still no active lesions present on most treated trees, and for some, canopies had started to regenerate, compared to untreated trees, where lesions remained active (Horner et al. 2024). However, for some trees that showed signs of phytotoxicity after initial high-dose treatment, the treatment seems to have accelerated the trees' mortality.

The development of field trials to include larger, mature kauri was completed in 2016 (Horner and Arnet 2020). These trials were conducted in three mature kauri stands, two in Northland, and one in the Waitākere Ranges, Auckland. Forty-two diseased trees across these three locations were injected with a lower dose of phosphite treatment than the rickers were in 2012, 4%. There were three treatments within this trial, a control (no injection), and a 20 mL injection of 4% phosphite treatment in either 40 or 80 cm intervals around the tree trunk. Tree health and lesion expansion was measured every six months; and treatments were reapplied in 2018 and 2019 mid-way between the initial injection points. The lower dose treatment on larger trees showed an absence of phytotoxic symptoms (as noted in the ricker trials). However, a single application of this treatment was not able to suppress lesion activity. After a second application of this low dose treatment, a reduction in lesion activity was noted; however, complete healing of lesions was still not achieved. The results of this trial indicated that further work is required in the treatment of these larger trees, focussing on higher doses of the phosphite treatment for complete lesion treatment (Horner et al. 2024).

Due to previous observations of phytotoxic symptoms after injection of high dose phosphite treatments (7.5% and 20%), research focused on reducing this methods phytotoxic effects, as well as assessing the efficacy of trunk spray application of phosphite (Horner et al. 2017). Trials began in 2016 across three sites, one in Huia (Waitākere Ranges, Auckland), and two in Northland. Seventy-two trees were included in the trial that were aged in the advanced ricker and mature stage of growth, all showing symptoms of kauri dieback. Treatments included a high dose 20 mL injection of 7.5% phosphite injected every 20 cm around the trunk, two low dose 20 mL injections of 4% phosphite injected either every 20 cm or every 40 cm around the trunk, and two 10% trunk sprays, one with bark penetrant and one without, applied in the lower 2 m of the trunk. Injected treatments resulted in the healing of most basal lesions after initial treatment, whereas the trunk spray required more frequent applications to achieve similar results (Horner et al. 2024).

1.2.7.2 Biological control

With the limitations of chemical treatments for kauri dieback, other mechanisms of treatment and control of *P. agathidicida* have been explored, including the use of biological control agents. These alternative treatments control pest animals or pathogens using the natural mechanisms of other organisms (Flint and Dreistadt 1998). The use of endophytes to suppress the growth of *P. agathidicida* have recently been explored as a natural strategy to aid the treatment of kauri dieback (Byers et al. 2021a; Lawrence et al. 2024). Endophytes are microorganisms that inhabit plant tissues and pose no harm to the host plant (Schulz and Boyle 2006). Laboratory based studies identified five fungal endophyte isolates, originally isolated from kauri root samples, that suppress the growth of *P. agathidicida* in dual culture assays (Lawrence et al. 2024). Of the isolates, *Coprinellus micaceus* and *Ilyonectria mors-panacisi* inhibited *P. agathidicida* growth the most, as well as suppressing zoospore formation of the oomycete (Lawrence et al. 2024). Although further work needs to be conducted, this research highlights an interesting natural treatment to control kauri dieback.

1.2.7.3 Hygiene Treatments

In 2015, the Kauri Dieback Recreation Project team was established through DOC to minimise the spread of kauri dieback via the use of public walking tracks on public conservation land (Aley and MacDonald 2018). The project has four main approaches to help reduce the spread of kauri dieback in these public areas: (1) upgrading tracks, (2) track closure, (3) addition of hygiene/cleaning stations, and (4) behaviour change strategies. Since the project began, the entire 735 km DOC managed track network has been surveyed and all kauri trees within 1.5 m of a track have been mapped (Department of Conservation 2019). From these surveys, 186 tracks were identified as needing upgrades or closure to help manage the spread of kauri dieback.

An important aspect of managing the spread of this disease is to reduce the amount of contaminated soil that is transported from infected to uninfected areas via footwear. To manage this spread in public areas DOC have created an optimised walk-through cleaning station to increase compliance of the public in removing soil from the underside of their shoes and disinfecting them before entering and exiting kauri forest areas (Aley and MacDonald 2018). These cleaning stations contain brushes and water spray to remove all visible soil from shoes before using a treadle that sprays sterigene onto the shoes when the user stands on it to sterilise the shoes. The mud and soil that is washed off the shoes is collected under the stations and removed to a secure, contained

landfill as this waste can contain *Phytophthora* species that are still viable, even after one year (Pau'uvale et al. 2011).

1.2.7.4 Oospore control

Oospores are the long-term survival spores produced by many *Phytophthora* species (Erwin and Ribeiro 1996). These spores can remain dormant for many years until conditions are favourable for them to germinate. Disinfectants and biocides that are effective treatments against other propagules of *P. agathidicida*, are not effective against oospores (Bellgard et al. 2010). Deactivating these spores to avoid further spread of the pathogen is a crucial part of disease management. Treatment methods were first considered in 2013 with high Trigene concentrations, exposure to sea water, fumigation with metam sodium, exposure to high and low pH levels, and time/temperature combinations tested for their efficacy in reducing the viability of oospores both in solution and soil (Dick and Kimberley 2013). The results of this study suggested heat treatment as the most effective and practical method for deactivation of *P. agathidicida* oospores in contaminated soils. The soil must be wet and then heated to 60 – 70 °C and held for four hours to completely kill all oospores. A high alkali pH treatment was also shown to be a highly effective treatment. Exposure of *P. agathidicida* spores to a pH level of 9 or 10 for 24 hours reduced the viability of oospores below any other treatment tested; and exposure for 48 hours led to no viable oospores.

1.2.8 Mātauranga Māori

1.2.8.1 Cultural Health Indicators

Mātauranga Māori is used in unison with conventional scientific practices to help combat and control kauri dieback through the use of indigenous knowledge, innovations, and practices. Monitoring approaches utilise a holistic view to assess the ngahere (bush/forest) of kauri ecosystem as a whole (Shortland 2011). A number of species that live on or near kauri, or species that are known to be vulnerable to environmental changes, that are known for their value as cultural health indicators have been chosen to help assess and monitor the health of kauri (Shortland 2011). This work has been developed over several phases. An initial literature review to collate and review both national and international examples of cultural health indicators (Shortland 2011). A second phase of developing a flexible framework to act as a guide for monitoring, collecting, and analysis data and information from kauri ngahere (Chetham and Shortland 2013). A third phase consisting of a pilot programme to test, evaluate, and confirm the cultural health indicators selected and methodology were suitable for monitoring kauri ngahere health (Shortland 2017a).

The monitoring framework is designed to be flexible with encouragement for mana whenua (authority over the land) to have a wānanga (to meet and discuss) to refine the tohu (indicators), atua (gods) domains, and elements they wish to monitor (Chetham and Shortland 2013). Atua domains include: The Realm of Tāne Mahuta, Papatūānuku, Tangaroa, Tāwhirimātea, Tamanuiterā, and Tūmatauenga. Each of these atua domains encompasses a different aspect of the ngahere used to assess and monitor all aspects of the kauri ngahere (Chetham and Shortland 2013). Briefly, Tāne Mahuta captures the core concept of whakapapa (genealogy/decent) and is the central focus of monitoring as it encapsulates the health of the kauri ngahere through monitoring approximately 90 species living in and around kauri. Monitoring this realm includes the assessment of different elements of the tohu species, including their bodily health and integrity (tinana oranga) and the abundance of the species at different life stages (whanaungatanga). Papatūānuku, the earth mother, allows information about how tohu species access and utilise the earth to grow, including leaf litter and pukahukahu mounds (dead wood), greenery, soil, and rock. The atua of the seas, rivers and lakes, Tangaroa, encourages the monitoring of tohu species availability to water and moisture for growth. Tāwhirimātea, the atua of wind and air, and Tamanuiterā, the atua that embodies the sun, are assessed on the availability of these elements to indicator species and kauri. Finally, Tūmatauenga, the atua of war and tāngata (people), is used to monitor human influence at the sites. This includes, walking trails, hunting, tourisms, and any adjacent commercial forestry and farming. Assessment of these realms encompass many different aspects of the kauri ngahere, helping to create a holistic view of the ecosystem as a whole (Chetham and Shortland 2013).

An overall measurement of kauri ngahere health may also be assessed through mauri (life force/vital essence). Ngahere health is based on four different classifications: ngahereora (pristine state), ngaheremaori (good health), ngaherekino (poor health), or ngaheremate (dead or dying). The classification is decided by the kaitiaki (monitor) and is a way of providing a baseline status for the health of the monitored site (Chetham and Shortland 2013).

1.2.8.2 Rongoā (Māori medicines)

As well as assessing cultural health indicators, mātauranga Māori, encompasses rongoā (traditional māori medicines), used to help improve the health of kauri ngahere through a holistic spiritual approach (Shortland 2017b). The holistic response comprises of three components: (1) to boost the immunity of the forest/trees, (2) to carry out remedial and physical interventions on at risk and diseased trees, and (3) to perform spiritual interventions.

Initial explorations into what rongoā would be best for helping kauri ngahere included a range of different components. Spiritual remedies aim to increase the personal and intimate strength of the bond between the ngahere and tangata whenua (Shortland 2017b). These include, a rāhui (restricted access), the burying of mauri stones (collected from special places) within the rāhui area, conducting a global karakia to invite the world to join Aotearoa in prayer, other aroha, karakia, or waiata to open chakra and let the forest respond to the vibrations; and finally, noho wahangu and whakarongo, a traditional mediation in the forest to listen and align to the cellular frequency of the forest (Shortland 2017b).

To boost the immunity of kauri trees, high grade whale oil has been suggested due to the close relationship of kauri and paraoa, the sperm whale (Shortland 2017b). This method is an indigenous innovation applied weekly directly onto the kauri tree. Another remedy from the ocean includes using dried or mulched seaweed applied to the soil surrounding kauri and reapplied to threated trees at six monthly intervals, used due to the deep connection between the forest and the sea (Shortland 2017b). Ash from wood, whale, or plant may also be used for disease resistance, with direct application to all kauri in proximity of diseased kauri (Shortland 2017b).

Physical and remedial interventions include aeration of the soil by forking or core plugging compacted soils surrounding all kauri near diseased kauri (Shortland 2017b). This practice aims to release moisture and encourage natural process to ‘decongest’ the soil, which should be completed every six months. Native bio-control sprays, such as Manuka, have also been suggested to combat zoospores. Field visit observations by forest health practitioners have noted the low number and diversity of seedlings growing in some forest. Therefore, it has been recommended that intervention is needed and planting of new seedlings from existing flora is needed.

Assessment of the efficacy of these pilot studies towards the ongoing health of kauri trees under threat of dieback disease is still ongoing. However, it is an important step in the inclusion of a rongoā Māori programme to help manage kauri dieback (Shortland 2017b).

1.2.9 Belowground microbial ecology and kauri dieback

1.2.9.1 Soil

Soil is an extremely complex system that appears at the intersection of the four major subsystems of Earth; the lithosphere, hydrosphere, biosphere, and atmosphere (Brevik et al. 2015). These environments consist of a range of biotic entities including, bacteria, fungi, archaea, protists,

oomycetes, animals, and plant roots; as well as abiotic factors, such as water, air, organic matter, and minerals. Uniting together, these components are constantly interacting and exerting a direct effect on above ground ecosystem functions (Bardgett and van der Putten 2014). The biodiversity present in soil systems actively contributes to nutrient cycling, water storage and purification, physical support for plant, animal, and human infrastructure, and providing habitats and niches for thousands of species (Brevik et al. 2015; Dominati et al. 2010).

1.2.9.2 Soil microbial communities

An intrinsic component of soil ecosystems is the microbial community. This large biological entity consists of bacteria, fungi, viruses, protists, and archaea; which are highly diverse due to the heterogeneity of soil environments (O'Brien et al. 2016; Roesch et al. 2007; Whitman et al. 1998). Soil is considered one of the greatest sources of biodiversity on Earth, with an estimation that one gram of soil could contain around 10^9 bacterial cells comprising of 6,000 to 50,000 different species (Curtis et al. 2002; Trevors 2009; Tringe et al. 2005). The high spatial and temporal variability exhibited by soil microbial communities reflects the different biotic and abiotic factors of soil environments (Islam et al. 2020). Across both large and small spatial scales soil environmental conditions vary, with climate, land-use, water availability, oxygen concentrations, and plant root systems all contributing to the multitude of niches available for soil microorganism to adapt to (Buscardo et al. 2024; Hermans et al. 2020; Maitra et al. 2024).

Together with the extensive diversity exhibited by soil microbial communities are the variety of roles these organisms play in ecosystem function. Microbial communities are an essential component of soil ecosystems and facilitate many biogeochemical cycles that are necessary for the growth and survival of plants and animals (van der Heijden et al. 2008). These cycles include the cycling of key elements through the breakdown and conversion of organic material into forms that may be utilised by other organisms (Falkowski et al. 2008). For example, nitrogen fixing bacteria and mycorrhizal fungi are crucial organisms involved in providing nitrogen and phosphorus, which are essential elements for plants to utilise (Cleveland et al. 1999; Hobbie and Hobbie 2006; van der Heijden et al. 2006). These communities are also able to produce and consume atmospheric gases, creating sources and sinks of greenhouse gases (Conrad 1996; Tarnocai et al. 2009; Zhao et al. 2019). As well as providing many positive effects on the surrounding ecosystem, the community may also contain pathogens, which may exhibit a negative effect on the performance of certain plant and animal dynamics (van der Heijden et al. 2008). The immense variation in diversity and function of

soil microbial communities highlights the important role these organisms play in both positively and negatively influencing the environment around them.

1.2.9.3 Drivers of soil microbial community diversity

Many studies have been conducted on soil microbial patterns across different spatiotemporal scales and have provided insights into the relationships between microbial communities and their surrounding environments (Islam et al. 2020; Lladó et al. 2018; Wei et al. 2022; Zhang et al. 2020). Although there is no single biotic or abiotic factor that can consistently predict the composition of a microbial community in a soil environment, several physicochemical properties have been identified as key indicators in certain environments.

For bacterial communities, pH can be a good predictor of diversity, especially at the phylum level (Geyer et al. 2014; Hermans et al. 2017; Lauber et al. 2009; Rousk et al. 2010). At both large scales (e.g. between continents) and small scales (e.g. <200 m), pH has been significantly correlated with differences in bacterial community composition (Lauber et al. 2009; Rousk et al. 2010). The strong correlation between pH and bacterial diversity have primarily been observed in soils with broader ranges of pH (e.g. 3.5-6.5), with narrower ranges (e.g. 6.2-8.9) exhibiting less correlation and higher diversity observed near neutral pH (Maestre et al. 2015; Rousk et al. 2010). Although pH can be a good predictor for bacterial diversity, the same patterns are not observed for fungal diversity (Rousk et al. 2010). This difference may be due to the optimal pH for growth required for bacterial and fungal taxa, with bacteria exhibiting a narrow pH range compared to the broad range exhibited by fungal species (Rousk et al. 2010). For fungal communities, at a global scale, precipitation had the strongest influence of community richness for most fungal groups based on taxonomy and functionality (Tedersoo et al. 2014). However, some fungal groups showed explicit preferences for specific soil characteristics such as pH, calcium, or phosphorus content (Tedersoo et al. 2014). For microbial biomass at the global scale, moisture availability and nitrogen content were equally important drivers (Serna-Chavez et al. 2013). Other large-scale factors that can influence microbial community compositions include soil type, land-use, and aboveground plant species (Hermans et al. 2017; Plassart et al. 2019; Urbanová et al. 2015).

1.2.9.4 Soil microbial communities and forest plant communities

Forests represent a large proportion of global land area and harbor a large proportion of the Earth's biodiversity (Crowther et al. 2015; Keenan et al. 2015). With the presence of large trees distinguishing forests from other land types such as agricultural, grasslands or wetlands, they also

provide a range of habitats for microorganisms to inhabit and facilitate a variety of interactions (Hardoim et al. 2015; Lladó et al. 2017; Urbanová et al. 2015). As the dominant primary producers in forests, trees exert great influence on other components of the ecosystem (Lladó et al. 2017). They are responsible for supplying the majority of carbon that enters the ecosystem through deposits of litter, deadwood and root activities (Hardoim et al. 2015; Phillips et al. 2011). Within the forest ecosystem soil microbial communities in particular exhibit symbiosis with the surrounding vegetation, providing commensal, mutualistic, and parasitic relationships (Bonfante and Anca 2009; Rajala et al. 2013; Terhonen et al. 2019).

Drivers of soil microbial communities in forest ecosystems are much the same as in other soil environments, with factors such as pH, soil nutrients, and climatic conditions playing an important role in determining the composition of the microbial community (Högberg et al. 2007; Shen et al. 2013). Additionally, vegetation is a major driver in defining microbial composition in forest ecosystems. Litter deposits directly influence the soil microbial community by providing organic matter for microorganisms to breakdown (Glassman et al. 2018). Litter originating from different plant species can show associations with specific microbial communities that are efficient at breaking down that specific litter, particularly for fungal communities (Palozzi and Lindo 2018; Veen et al. 2021). The inhabiting tree species of a forest may also have a direct influence on the residing microbial communities (Urbanová et al. 2015). Tree species composition is more directly associated with fungal than bacterial communities, where some fungal species show preference towards specific tree species (Urbanová et al. 2015). For bacterial communities, the tree effect is partially influenced by litter and soil chemistry, mediated by the effect of trees on the soil chemistry through litter deposits (Lladó et al. 2018; Urbanová et al. 2015).

Microbes play an important role in supporting forest trees through beneficial interactions in the rhizosphere, the narrow zone around plant roots (Yu et al. 2022). The rhizosphere is considered a microbial hotspot with beneficial bacteria and fungi facilitating and enhancing interactions between the soil and plant, particularly with nutrient uptake (Finzi et al. 2015; Kuzyakov and Blagodatskaya 2015; Wang et al. 2023a). The rhizosphere microbiome is shaped by a range of factors, including the host plant genotype, root morphology, and root exudates (Sasse et al. 2018).

A key component of the rhizosphere are mycorrhizal fungi. These fungi are commonly associated with plant root systems, establishing a mutualistic relationship where the fungi are able to utilise photosynthates produced by the plant and in turn the fungi are able to facilitate the

efficient uptake of nutrients such as nitrogen and phosphorus from the soil to the plant (Leake et al. 2004; van der Heijden et al. 2015). With nearly all tree species forming a symbiotic relationship with either ectomycorrhizal fungi or arbuscular mycorrhizal fungi, these fungal networks are an important component of forest systems (Anthony et al. 2022; Averill et al. 2022).

Endophytic microbes, which inhabit plant tissues without causing disease, additionally contribute to tree health and resistance towards stressors (Griffin and Carson 2018). Endophytes generally exhibit a range of beneficial interactions with their host plants, from promoting plant growth through the production of secondary metabolites such as phytohormones (Compant et al. 2005), providing nutrients such as nitrogen and phosphorus (Carrell and Frank 2014; Santoyo et al. 2016), and competing with pathogens through various mechanisms including antagonistic metabolites (Khare et al. 2018), the latter of which has opened the avenue for their potential use as biological control agents (Bilański and Kowalski 2022; Rabiey et al. 2019). Together, these microbial interactions create a supportive environment that supports the growth and resilience of forest trees against environmental stressors.

With forest systems facing increasing abiotic pressures from rising issues such as climate change and anthropogenic pressures, these systems are being put under immense stress (Anderegg et al. 2020; Saatchi et al. 2021). Susceptibility towards biotic pressures is also noted with increasing incidents of insect and pathogen infections causing vast destruction in these forest ecosystems (Canelles et al. 2021; Waipara et al. 2013). With these increasing stressors on forest environments, it is important to understand the role of the soil microbial community, if it is affected by these stressors, and if it is providing positive, negative, or neutral effects to the surrounding plant communities.

1.2.9.5 Soil microbial communities and plant diseases

Soil microbial communities can influence the establishment, severity, and progression of plant diseases. The interactions between the soil microbial communities, plants, and pathogens are bidirectional and can occur through several mechanisms. In some systems, soils may develop suppressiveness, where certain taxa in the microbial community naturally inhibit pathogens and reduce disease incidence. Mechanisms of disease suppression include improving plant health, inducing plant defence systems, parasitism, antibiosis, predation, and competition for resources (Liu et al. 2021). Examples of disease suppressive soils include tomato plants affected by wilt disease where reduction in the abundance of Firmicutes in the rhizosphere was associated with increased

incidence of disease (Lee et al. 2020) and in banana plants where *Trichoderma* spp. were isolated from healthy plants and showed antagonistic effects towards the phytopathogenic fungi from the *Fusarium* genus (Win et al. 2021). In contrast, other shifts in the microbial composition can facilitate disease progression when pathogen-favourable taxa increase or beneficial microbes are lost (Ridout and Newcombe 2015).

Antagonistic interactions are an important mechanism in which microbes can influence plant disease. Many bacteria and fungi produce secondary metabolites such as antibiotics, lytic enzymes, or volatile compounds that inhibit pathogens. For example, *Bacillus subtilis* can inhibit *Fusarium* spp. via the production of plipastatin, a bioactive lipopeptide with antifungal properties (Kiesewalter et al. 2021), or the production of volatile organic compounds by *T. atroviride* that both inhibit the growth of *F. oxysporum* while also promoting plant health (Rao et al. 2022). In the rhizosphere, disease outcomes are influenced by microbial competition, plant-mediated recruitment, and induced plant defences. Beneficial taxa compete with pathogens for limited nutrients and physical spaces, restricting colonisation. For example, a non-toxigenic *Aspergillus flavus* strain outcompetes *Fusarium verticillioides* in the colonisation of maize (Reis et al. 2020), and *Pseudomonas aeruginosa* produces siderophores that in turn provide a competitive advantage for iron acquisition (Chemeltorit et al. 2017). Beyond these direct interactions, soil microbes can also trigger an induced systemic resistance (ISR) in plants whereby a plant exhibits enhanced resistance towards pathogens once triggered by biological or chemical inducers (Walters et al. 2013); genera such as *Trichoderma*, *Pseudomonas*, and *Bacillus* can induce ISR in plants affected by *Fusarium* (Choudhary et al. 2007; Galletti et al. 2020). Plants can actively shape these interactions by adjusting root exudates and volatile compounds over time to recruit or enrich antagonistic microbes to prevent or increase response to pathogen attack (Berendsen et al. 2018; Rolfe et al. 2019; Sasse et al. 2018; Schulz-Bohm et al. 2018; Wen et al. 2023; Yang et al. 2023).

Abiotic drivers are also an important component of these interactions by shaping microbial communities and pathogen performance. Recent studies have associated climate variables such as temperature and relative humidity with outbreaks of soil-borne diseases (Delgado-Baquerizo et al. 2020; Romero et al. 2022; Velásquez et al. 2018). However, more localised factors such as increased soil moisture content have been associated with increased instances of plant diseases such as tomato bacterial wilt (Jiang et al. 2021) and Verticillium wilt disease in cotton (Batista et al. 2024). Other abiotic factors such as pH and nutrient availability can influence the abundance, composition, and function of microbial communities, including taxa antagonistic to pathogens (Carrell et al. 2023;

Mascher et al. 2014; Morrison et al. 2016). Similarly, increased litterfall from declining trees alters the amounts and quality of soil organic matter, creating niches for opportunistic microbes and changing nutrient availability (Byers et al. 2020b; Gómez-Aparicio et al. 2022). These examples highlight how soil microbial diversity, community composition, and functional traits interact with environmental factors and can influence the suppressive and conducive environments for plant disease.

Although these mechanisms are well-documented in agricultural systems, forest-specific studies remain sparse and are largely focused on Northern Hemisphere systems. Nevertheless, these emerging studies show that the below-ground community composition can influence disease outcomes. In Mediterranean cork oak forests threated by *P. cinnamomi*, tree decline was associated with shifts in soil bacterial and fungal diversity and co-occurrence networks (Gómez-Aparicio et al. 2022). In conifers, endophytes can directly suppress pathogens; for example, *Penicillium goetzii* presence correlates with reduced severity of *Dothistroma* needle blight in pine (Ridout and Newcombe 2015), and *Phialocephala europaea* produces secondary metabolites antagonistic to *Phytophthora* spp. (Tellenbach et al. 2013). At the rhizosphere scale, microbial communities with increased abundance of certain taxa such as Phycisphaeraceae and Rokubacteria have been linked to reduced susceptibility towards fungal pathogens across several forest tree hosts (Yu et al. 2022).

Emerging forest studies report consistent associations between tree health status and soil microbial community composition. Tree health is often associated with fungal diversity more than bacterial diversity, with many ectomycorrhiza and fungal endophytes linked with tree resilience (Diez-Hermano et al. 2023; Garrastatxu et al. 2024). Declines in fungal diversity with worsening tree health are observed (Diez-Hermano et al. 2024; Guo et al. 2023); however, this is not always the case (Byers et al. 2020b; Gómez-Aparicio et al. 2022). In slowly progressing diseases, increased microbial diversity around unhealthy trees may reflect new niches created by greater litter inputs, dead root biomass, and decreases in rhizodeposits that opportunistic taxa are able to occupy (Byers et al. 2020b; Custer et al. 2020; Gómez-Aparicio et al. 2022; Yuste et al. 2012). How the functional potential of these communities may change in the face of these stressors is an understudied area, particularly in forest systems under threat from soil-borne pathogens. Although microbial taxa are highly diverse, the functional roles mediated by microbes appear to be limited to a distinct set of metabolic pathways (Louca et al. 2018). This functional redundancy has been observed in soils from across the globe and is proposed to promote resilience and stability of an ecosystem allowing for the loss of some redundant species (Chen et al. 2022b).

Despite the recent studies on the role of soil microbial communities in forests affected by tree decline by invasive pathogens, more research is required to unravel the complexities of these interactions. The lack of studies in Southern Hemisphere forests also presents a research gap in our understanding of these communities. The kauri forests of New Zealand, and the presence of the invasive plant pathogen *P. agathidicida* provide a suitable case study to explore how the soil microbiome, plant (kauri), and pathogen (*P. agathidicida*) are interacting and affecting each other.

1.2.9.6 Kauri forest soils

Although kauri dieback has been identified in mainland New Zealand since 2007, there is still limited knowledge on the soil microbial community surrounding this iconic species. As a foundation species, kauri exert a strong influence on the structure of the surrounding soil environment (Wyse et al. 2014). They play a significant role in influencing the soil processes beneath their canopies, with acidic, low fertility soils being a prominent feature (Wyse 2012; Wyse et al. 2014). The large accumulation of woody debris and leaf litter on the forest floor is slow to decompose and can lead to the formation of a mor humus layer that can be up to 3 m deep (Silvester and Orchard 1999; Steward and Beveridge 2010). Additionally, the high tannin content of kauri leaf litter contributes to the storage of large amounts of immobilised nitrogen (Verkaik et al. 2006). As well as being acidic, kauri soils are high in carbon, total nitrogen and NH_4-N but low in NO_3-N (Wyse et al. 2014). The soil environment around kauri trees offers a unique case to characterise and understand what microbes are inhabiting this area, what their potential functions are, and if these are influencing or are influenced by the declining health of the foundation tree species due to the presence of an invasive pathogen.

Previous studies on soil microbial communities around kauri trees affected by dieback are limited. Studies based in the Waipoua Forest, Northland, focused on amplicon sequencing and functional gene analysis around symptomatic and asymptomatic mature kauri to understand the bacterial and fungal communities in soils and comparing it to pine plantation (*Pinus radiata* D. Don) soils (Byers et al. 2020a; Byers et al. 2020b). These studies revealed significant differences in the microbial community structure of mature kauri forests and that of pine plantations (Byers et al. 2020a). Comparisons between soils around asymptomatic and symptomatic kauri revealed an increase in abundance of key microbes associated with disease suppression and promoting plant health in soils around asymptomatic trees (Byers et al. 2020b).

Other studies on the microbial communities associated with kauri have focused on the arbuscular mycorrhizal fungi (AMF) that colonise kauri roots (Morrison and English 1967; Padamsee et al. 2016), and endophytes that show antagonistic effects towards *P. agathidicida* (Lawrence et al. 2024). Most, but not all, nodules on kauri roots are colonised by AMF, with molecular identification techniques identifying these inhabitants within five different families of *Glomeromycota* (Padamsee et al. 2016). The colonised root nodules have shown increased uptake of phosphorus compared to uncolonised nodules, likely aiding in uptake for the host plant as well (Morrison and English 1967). Research into endophyte communities is focused on the identification of isolates that could be used as biological control agents to suppress the growth of *P. agathidicida* and be used as treatment for kauri dieback (Lawrence et al. 2024). Five endophytes, isolated from the roots of kauri, have demonstrated growth suppression of *P. agathidicida* (Lawrence et al. 2024). The *Coprinellus micaceus* and *Ilyonectria mors-panacis* endophytes have been shown to completely inhibit the growth and viability of *P. agathidicida* and are a promising natural alternative to phosphite treatments of kauri dieback.

Limited studies have been done to understand the functional potential of the soil microbial communities around kauri trees. Using Geochip 5S microarray technology for functional analysis, significant differences were observed between asymptomatic versus symptomatic kauri in some specific genes associated with C and N cycling, however, when grouping genes by their broader functional gene categories, an overall trend was not identified (Byers et al. 2020b). It was suggested that the differences in composition and gene abundance of C cycling genes between soils from asymptomatic and symptomatic kauri trees may be due to the increase in litter quantity and quality exhibited following tree dieback. Although differences in N cycling gene composition and abundance were noted between soils from asymptomatic and symptomatic trees, no conclusions were able to be drawn about how tree dieback may influence this microbial function (Byers et al. 2020b). One other study has explored the functional potential of the soil microbial communities around kauri trees, using Geochip 5S technology (Lawrence et al. 2023). However, this study only included four kauri trees and did not include any information on the symptoms or health of the trees.

These studies provide a good baseline of information about soil microbial communities associated with kauri trees. The limited studies on these soil microbial communities associated with the declining health of kauri begin to show the potential long-term impacts kauri dieback may have on the surrounding ecosystem of kauri forests. However, the published studies involving kauri affected by dieback disease have been limited to only 40 mature trees with 20 trees exhibiting only

late stages on infection (Byers et al. 2020b). There is still a gap in knowledge around the soil microbial communities surrounding dead trees, as well as trees across a larger range of health status and age. Additionally, deciphering the functional potential of soil microbial communities surrounding kauri and how it may shift with declining tree health remains an under-explored area. The Geochip approach used previously has provided a baseline of information of what the functional potential of these microbial communities may be, providing a broad overview of the changes in composition and abundance of genes related to carbon and nitrogen cycling. There is still a lack of knowledge around the full functional potential of the soil microbial communities surrounding kauri across a wide range of health stages, including dead trees.

1.2.10 Methods for investigating forest soil microbial communities

The diverse composition of soil microbial communities, especially in forest soils, poses one of the greatest challenges for determining the taxonomy and abundance of these communities (Woodcroft et al. 2025). Due to the large heterogeneity of soil microbial communities, methods employed to understand them have switched from traditional culture-based techniques towards metagenomic approaches utilising high-throughput sequencing technologies (Daniel 2005). Metagenomics was first described in 1998 and is characterised as the genomic analysis of a community of microorganisms by direct analysis of DNA, thereby without culturing-bias (Handelsman 2004; Handelsman et al. 1998; Riesenfeld et al. 2004). With only a small fraction (<1%) of the microorganisms present on Earth being culturable, using culture-based methods to understand the diversity of soil microbial communities will greatly underestimate the true diversity of these samples (Trevors 2009; Vartoukian et al. 2010). In contrast, applying a metagenomics approach to understand these communities produces a larger profile of the microbial community within this complex ecosystem (Daniel 2005). Many studies have utilised high-throughput sequencing approaches to decipher the taxonomic and functional profiles of soil microbial communities in forest ecosystems (Byers et al. 2020b; Gómez-Aparicio et al. 2022; Guo et al. 2023; Hartmann et al. 2013; Tremblay et al. 2018).

There are two main approaches for utilising high-throughput sequencing methods to understand soil microbial communities, amplicon sequencing and shotgun sequencing. The most common method is amplicon sequencing, where extracted DNA undergoes a targeted two-step PCR to amplify certain DNA regions/markers that are taxonomically informative and to add barcodes and adapters to each sample (de Muinck et al. 2017; Fukuda et al. 2016). Taxonomic markers commonly used in amplicon analysis are the 16S rRNA gene for prokaryotes and the ITS region for eukaryotes

(Liu et al. 2020b). The amplicons may then undergo sequencing often utilising Illumina short-read sequencing technologies such as MiSeq or HiSeq to produce read lengths of ~150 bp (Liu et al. 2020b). With the advancement in accuracy of third-generation sequencing technologies, such as PacBio and Oxford Nanopore, long-read sequencing is emerging as an additional high-throughput option that can sequence the full-length of the 16S rRNA gene (Callahan et al. 2019; Tedersoo et al. 2021). However, these methods remain costly, require larger amounts of input starting material, and are still limited in the comprehensive suite of computer tools needed for analysis (Callahan et al. 2019; Tedersoo et al. 2021). Once sequenced, the raw reads are processed to produce operational taxonomic units (OTUs) or amplicon sequence variants (ASVs) which are then aligned to a reference database to infer taxonomy, generally only reaching genus-level resolution (Callahan et al. 2017; Liu et al. 2020b). Although this method is comparatively cheap and allows the processing of a large number of samples, the PCR-based method introduces biases during amplification and has limitations including relying on reference databases to infer taxonomy (Fasolo et al. 2024). Overall, amplicon sequencing is a popular tool used in microbiome analysis to estimate the microbial community composition and diversity across different samples. In forest systems it has been applied to understand alterations of microbial communities around trees impacted by tree decline and to link these changes with physicochemical properties of the soil (Byers et al. 2020b; Gómez-Aparicio et al. 2022; Morales-Rodríguez et al. 2024; Pinho et al. 2020; Ruiz Gómez et al. 2019).

The shotgun sequencing approach is an untargeted approach that aims to sequence all DNA in a sample to provide both taxonomic and functional information of the microbial community (Bharti and Grimm 2021). Although it is a more expensive approach compared to amplicon sequencing it avoids PCR biases introduced in amplicon workflows and it can help elucidate the functional potential of the sample community as well as providing a higher resolution for taxonomic classification (Franzosa et al. 2015; Morgan and Huttenhower 2012). With the ability to sequence all DNA in a sample, the data produced is magnitudes larger than targeted amplicon datasets creating its own challenges for analysis (Huttenhower et al. 2012; Rausch et al. 2019). There are two main pathways available for analysing shotgun data (1) taxonomic and functional annotation against reference databases, and (2) the generation of metagenome assembled genomes (MAGs) (Bharti and Grimm 2021). For reference-based analyses, the limitations are the same as that from amplicon data, the lack of a comprehensive reference database to compare sequence reads to. With a severe lack of representative microbial genomes and lack of knowledge around their functional capabilities, this makes it a challenging task to link community structure and metabolic function (Anthony et al.

2024). Exploring the functional potential and diversity of microbial systems is complicated further by the horizontal gene transfer exhibited by prokaryotes that can increase their ability to colonise, adapt, and survive in different environmental niches (Maheshwari et al. 2017). However, as technology has progressed and assembly algorithms have improved, there has been an increased recovery of metagenome assembled genomes (MAGs) from shotgun datasets (Singleton et al. 2021). The generation of these MAGs allows us to link functional genes to specific organisms. Despite the challenges that are involved with shotgun metagenomics, many studies have used this approach to characterise and monitor the functional potential of microbes in soil environments, as well as construct MAGs from datasets (Akinola et al. 2021; Muñoz-Ramírez et al. 2024; Nelkner et al. 2019; Xu et al. 2018).

1.3 Research gaps and thesis aims

As the spread of *P. agathidicida* continues to threaten the longevity of New Zealand's kauri forests, the role of the soil microbial community in this system remains understudied. Exploring the interactions between the soil microbial community, pathogen, and a foundation tree species offers insight into the way these three components interact in forest systems under increasing environmental stress. Despite the increasing occurrence of soil-borne pathogen invasions, research gaps remain in understanding the complex interactions occurring in these devastating infections. In particular, there are a lack of studies focussing on Southern Hemisphere forest systems which can limit our ability to compare the response of the microbial community across different spatial and temporal contexts. Additionally, little is known about soil microbial communities around dead kauri trees and if the loss of this foundation tree species is affecting, or is affected by, the belowground community. To address these research gaps, this thesis combines amplicon and shotgun metagenomic approaches with targeted pathogen detection and soil physicochemical analyses to characterise the soil microbial community and functional potential, and to evaluate how these are shaped by tree health, spatial location, and edaphic conditions in kauri forests. The findings of this research are presented across three chapters detailed below.

1. **Pathogen presence and microbial communities (Chapter 2)**

   Chapter 2 examined whether the confirmed presence of *P. agathidicida* (via LAMP analysis), is associated with significant differences in soil microbial community structure and functional potential. I hypothesised that pathogen-detected soils would exhibit distinct taxonomic and functional profiles compared with pathogen-negative soils, consistent with ecological

restructuring of microbial assemblages. This research provides insights into the direct interactions between pathogens and soil microbial communities, while also highlighting how different molecular methods can be applied for pathogen detection and microbial community profiling.

2. Community composition of soil microbiomes under tree decline (Chapter 3)

Chapter 3 investigated how soil microbial diversity and taxonomic composition vary with host canopy health decline. Specifically, I tested the hypothesis that spatial scale, tree healthy status, and soil physicochemical properties were associated with significant variation in soil microbial community composition and diversity in kauri forest soils. Amplicon sequencing was used to assess indirect effects of tree health on microbial communities, alongside spatial structuring at the tree, plot, and site levels, and associations with soil physicochemical properties. This research improves our understanding of how host decline, spatial heterogeneity, and edaphic conditions shape the structure of belowground microbial communities.

3. Spatial and environmental drivers of microbial functional profiles (Chapter 4)

Chapter 4 explored microbial functional potential in relation to tree health, soil physicochemical properties, and spatial location using shotgun metagenomic sequencing. I hypothesised that the functional gene composition of soil prokaryotic communities varies spatially and is structured by soil physicochemical gradients and tree health status in kauri forest soils. By integrating functional gene profiles with environmental and spatial gradients at the plot and site levels, this research advances our knowledge of how microbial functional capacity is influenced by both biotic and abiotic factors in forest soils.

Chapter 2

Comparative amplicon and shotgun metagenome profiling of soil microbial communities in kauri forests affected by *Phytophthora agathidicida*

Author names

Zoe King [a], Hannah L. Buckley [a], Gavin Lear [b], Brent Seale [a], Kevin C. Lee [a], Luitgard Schwendenmann [c], Donnabella C. Lacap-Bugler [a]

Author affiliations

[a] School of Science, Auckland University of Technology, Auckland CBD, Auckland, 1010, New Zealand

[b] School of Biological Sciences, The University of Auckland, Auckland CBD, Auckland, 1010, New Zealand

[c] School of Environment, The University of Auckland, Auckland CBD, Auckland, 1010, New Zealand

Code availability

All code used in this chapter can be found in the following GitHub repository https://github.com/zoesking/kauri-soil-comparative

Abstract

Soil-borne pathogens can influence microbial communities and ecosystem function, making it important to understand their broader ecological impacts. We investigated interactions between *Phytophthora agathidicida* (the causal agent of kauri tree dieback) and soil microbial communities, while also comparing detection and community-profiling methods. Soils from 60 kauri trees across three sites in the Waitākere Ranges, New Zealand, were analysed using loop-mediated isothermal amplification (LAMP) for pathogen detection, and 16S rRNA gene/ITS region amplicon sequencing alongside shotgun metagenomics for community characterisation. LAMP detected *P. agathidicida* in 39/60 samples, while shotgun sequencing detected *P. agathidicida*-associated DNA at very low abundance across all samples. Microbial community structure and functional potential showed weak association with pathogen presence, though differential abundance testing identified several genera enriched in pathogen-detected soils, including taxa previously linked to disease suppression. Amplicon and shotgun profiles were broadly consistent at higher taxonomic and functional levels but diverged at finer resolution, reflecting differences in sensitivity and database coverage. Importantly, functional predictions from PICRUSt2 closely matched shotgun-derived profiles at broader scales, indicating its suitability as a cost-effective tool for broad-scale monitoring. These findings suggest limited direct pathogen effects on microbial communities and highlight how integrating molecular approaches provides complementary insights into soil microbiome-pathogen interactions.

Keywords: Kauri dieback, *Phytophthora agathidicida*, soil microbiome, shotgun metagenomics, amplicon sequencing, LAMP detection, pathogen-microbe interactions

2.1 Introduction

Phytophthora agathidicida, the causal pathogen of kauri dieback, is a soil-borne oomycete that poses a significant threat to *Agathis australis* (kauri), a culturally and ecologically significant foundation tree species in New Zealand (Beever et al. 2009; Ecroyd 1982; Weir et al. 2015). The lifecycle of *P. agathidicida* involves phases of both dormancy and infection, where it may survive in the soil for extended periods through the production of oospores (Bradshaw et al. 2020; Weir et al. 2015). Upon sensing root-derived chemical signals from kauri, the pathogen breaks its dormancy stage, producing motile zoospores that travel towards the roots and initiate infection (Bradshaw et al. 2020). Disease progression is characterised by root rot, a thinning canopy, and basal bleeding/gummosis on the trunk or lateral roots, which eventually leads to tree death (Beever and Bellgard 2010; Bellgard et al. 2016a; Waipara et al. 2013). Understanding how the presence of *P. agathidicida* influences the surrounding soil microbial community is important for assessing the wider ecosystem impacts of kauri dieback and loss of this foundation tree species. The partially free-living but primarily pathogenic lifecycle of *P. agathidicida* suggests that the pathogen may affect the soil microbiome through direct interactions or indirectly via host-mediated effects (Feng et al. 2024b; Reverchon et al. 2023; Tong et al. 2024).

Various methods are used to detect and monitor *P. agathidicida*, describe and quantify disease expression in trees, characterise the soil microbiome, and assess the functional potential of the microbial community. These include visual assessment of symptoms, soil baiting and culturing followed by morphological identification, and molecular-based techniques such as loop-mediated isothermal amplification (LAMP), amplicon sequencing, and shotgun metagenomic sequencing, respectively (Beever and Bellgard 2010; Byers et al. 2020b; Dick and Bellgard 2010; Hill et al. 2017; Sivaprakasam et al. 2024; Winkworth et al. 2020). Determining whether the outputs of these different approaches are similar will provide important context for interpreting results and support the methods and approaches used in subsequent studies.

Although *P. agathidicida* detection is an essential component of disease management, it remains challenging, despite recent advancements. Visual assessment of kauri dieback symptoms is widely used in field surveillance, but its sensitivity is limited (Froud et al. 2022). Aboveground symptoms can develop long after the pathogen first infects the roots, and even when visible, they may reflect other causes such as infection by other *Phytophthora* species (rather than *P. agathidicida*

specifically) or drought (Beever and Bellgard 2010; Froud et al. 2022; Hunter et al. 2024; Waipara et al. 2013).

A symptomatic tree is defined as having at least one of the following symptoms: some branch dieback, gummosis on the trunk base or lateral roots, colour change of leaves to yellow or copper-brown, or tree death (Bellgard et al. 2013; Froud et al. 2022). Although more specific than visual assessment, the enrichment, culturing, and morphological identification of *P. agathidicida* is laborious, expensive, and prone to generating false negative results due to uneven pathogen distribution and difficulties in breaking oospore dormancy (Bellgard et al. 2013). The inclusion of molecular-based methods with *P. agathidicida* enrichment, using tools such as LAMP assays (Winkworth et al. 2020), has improved sensitivity for pathogen detection, and metabarcoding techniques offer further resolution (Hunter et al. 2024); however, each method has its limitations in terms of cost, scalability, and context-dependence.

Limited studies have investigated how *P. agathidicida* impacts soil microbial communities surrounding kauri. Existing research has primarily focused on describing microbial community differences between symptomatic and asymptomatic trees, using amplicon-based profiling for bacterial (16S rRNA gene) and fungal (internal transcribed spacer gene (ITS) gene) communities (Byers et al. 2020a; Byers et al. 2021b), or exploring microbial functional potential through microarray methods such as GeoChip (Byers et al. 2020b; Lawrence et al. 2023). While these studies have provided initial insights into the microbial communities, none have explicitly examined how the soil microbial community structure or function may be impacted by the confirmed presence or absence of *P. agathidicida* in natural forest soils. Additionally, no studies have applied shotgun metagenomic sequencing to kauri forest soils impacted by kauri dieback, which could increase taxonomic and functional resolution compared to previous methods.

In the presence of a plant pathogen, soil microbial communities may be affected by both direct and indirect interactions. Direct interactions include microbial competition with *P. agathidicida* for nutrients or niche space and the production of antimicrobial compounds that suppress pathogen activity (Chen et al. 2018; Gu et al. 2020). Indirect interactions may arise through changes in plant physiology in response to infection, such as increased litterfall or gummosis, which alter nutrient input into the surrounding soil environment (Avila et al. 2016; Delgado-Baquerizo et al. 2016), or shifts in root exudation profiles to recruit specific microbial taxa, including those with biocontrol potential (Köhl et al. 2019; Wang et al. 2021a). These complex and bidirectional

interactions involve antagonistic and compensatory processes that directly affect plant health and disease expression. As infection progresses, these shifts may create new ecological niches that enable opportunistic organisms, such as saprotrophs or secondary pathogens, to proliferate and further disrupt the native microbial community (Byers et al. 2020b; Gómez-Aparicio et al. 2022; Jung et al. 2018).

This study compares the various methods used to detect and measure the relationship between the presence of *P. agathidicida* and the structure and function of kauri forest soil microbial communities. We ask: (1) How do the detection rates of *P. agathidicida* using LAMP, amplicon sequencing, and shotgun metagenomic sequencing compare? (2) How is the soil microbial community structure (diversity and composition) related to the confirmed presence of *P. agathidicida*, as assessed by amplicon and shotgun sequencing? (3) How is the potential soil microbial community function related to the confirmed presence of *P. agathidicida*? and (4) How do the functional and taxonomic profiles derived from shotgun metagenomic profiling align with those inferred from 16S rRNA gene amplicon sequencing? Investigating these questions will improve our understanding of how microbial community structure and function are related to the confirmed presence of a plant pathogen. Further, this study provides insights into the reliability, complementarity, and limitations of two high-throughput sequencing techniques in detecting microbial community signatures associated with plant pathogen presence.

2.2 Experimental Procedures

2.2.1 Field sampling

Samples were collected from the Waitākere Ranges (Te Wao Nui ā Tiriwa), a regional park containing one of the largest remaining kauri forests in Auckland, New Zealand. Three sites within the Waitākere Ranges were selected for sampling: the Cascades, Piha, and Huia (Figure A1; Appendix A) (*n* = 3 sites). Within each site were two permanent vegetation plots established between 2012 and 2021 (*n* = 6 plots). Each plot was 40 × 50 m, and all kauri trees with a minimum diameter at breast height of 2 cm were identified and tagged at the plot's establishment. Ten kauri trees were selected for soil sampling in each plot, consisting of four trees at the corner of each plot and six other kauri trees randomly selected from within the plot (*n* = 60). Following an established protocol for soil sampling (Hill et al. 2017), woody and leaf litter were removed to expose soil before a hand trowel was use to collect soil from four cardinal points around each tree, 1 m from the trunk to a depth of 10 cm. The cardinal point soil samples were pooled into one bag before being transferred

to a -20 °C freezer and stored until processing. Soil sampling was conducted by BioSense Limited (Auckland, New Zealand) in February and March of 2022. Canopy scores were recorded for all sampled trees using an established five-point scoring system (1 = good condition, 2 = some foliar thinning, 3 = some branch dieback, 4 = severe shoot dieback, and 5 = dead) following Horner et al. (2019b), with additional half-point increments included to provide greater differentiation, particularly in the later stages of infection (Froud et al. 2022).

2.2.2 Soil DNA extraction, amplicon and shotgun metagenome sequencing

DNA was extracted from the 60 soil samples using a DNeasy PowerSoil Pro Kit (Qiagen, Germany), following the manufacturer's instructions, using 0.25 g of soil for each sample. Negative controls using nuclease-free water were included in each batch of extractions (*n* = 14), and DNA concentration was determined fluorometrically using Qubit double-stranded DNA BR assay kit (Thermo Fisher Scientific, Massachusetts, USA).

For amplicon sequencing, samples with a DNA concentration over 200 ng/µL were diluted with an equal volume of nuclease-free water to reduce the amount of starting material in the PCR reaction. Extracted DNA was amplified using the prokaryotic 341F (TCGTCGGCAGCGTCAGATGTGTATAAGAGACAGCCTACGGGNGGCWGCAG) and 805R (GTCTCGTGGGCTCGGAGATGTGTATAAGAGACAGGACTACHVGGGTATCTAATCC) primers to target the V3-V4 region of the 16S rRNA gene (Stoeck et al. 2010). The ITS1 region of the fungal ITS region was amplified using the ITS1-F (TCGTCGGCAGCGTCAGATGTGTATAAGAGACAGCTTGGTCATTTAGAGGAAGTAA) (Gardes and Bruns 1993) and ITS2 (GTCTCGTGGGCTCGGAGATGTGTATAAGAGACAGGCTGCGTTCTTCATCGATGC) (White et al. 1990) primers. Target-specific sequences are underlined; the remaining primer sequence consists of Illumina adaptor sequences necessary for downstream analysis.

Each 25 µL reaction contained 6.25 µL of KAPA HiFi Hotstart ReadyMix (Kapa Biosystems, Wilmington, MA, USA) and 2 µL of template. For 16S rRNA gene amplification, 0.75 µL of each primer (10 µM) was included per reaction and for ITS region amplification 1 µL of each primer (10 µM) was included. Thermocycler conditions were the same for both primer sets. They were as follows: initial denaturation at 95 °C for 3 minutes, followed by 30 cycles of 98 °C for 20 seconds (denaturation), 63 °C for 15 seconds (annealing) and 72 °C for 15 seconds (extension), with a final extension at 72 °C for 1 min.

PCR products were purified using AMPure XP beads (Beckman Coulter, Auckland, NZ) following the manufacturer's instructions. Purified products were quantified using a Qubit double-stranded DNA HS assay kit (Thermo Fisher Scientific, MA, USA) and normalised to 1 ng/µL. Samples were indexed (Nextera XT DNA Library Prep kit; Illumina, CA, USA), pooled, and purified using AMPure XP beads (Beckman Coulter, Auckland, NZ) following the manufacturer's instructions. Libraries were pooled at 1 nM, validated using an Agilent 2100 expert High Sensitivity DNA Bioanalyzer assay (Agilent Technologies, CA, USA), and sequenced using an Illumina MiSeq Reagent Kit v3 (600-cycle) to produce 2 x 300 bp reads.

For shotgun metagenome sequencing, extracted DNA was normalised to 10 ng/µL before sending to Livestock Improvement Corporation (LIC; Hamilton, New Zealand) for library preparation and sequencing on an Illumina NovaSeq 6000 system using an S4 flow cell, producing sequence lengths of 2 x 150 bp. Two samples failed sequencing on the S4 flow cell and were re-sequenced using an SP 300 flow cell. The SP 300 flow cell produced over double the number of sequences per sample compared to the S4 flow cell. To maintain a similar number of sequences per sample, 60 million sequence reads from each set of forward and reverse reads were randomly subset from the raw re-sequenced samples using seqtk (https://github.com/lh3/seqtk).

2.2.3 *Phytophthora* detection

The detection of *P. agathidicida* in each of the 60 soil samples was assessed by an initial baiting enrichment assay following the protocol described by Struijk et al. (2024) before total DNA was extracted from the cedar needle baits and analysed using the LAMP assay described by Winkworth et al. (2020). This assay was performed by BioSense Limited (Auckland, New Zealand).

High-throughput sequencing data from amplicon and shotgun metagenomic sequencing were analysed for *P. agathidicida* DNA. For the amplicon dataset, amplicon sequence variants (ASVs) were inferred from ITS1 sequences using DADA2 v1.24.0 (Callahan et al. 2016). To explore whether *P. agathidicida* could be detected within this fungal community dataset, ASVs were compared against a custom reference database using BLASTn via BLAST v2.16 (Camacho et al. 2009). The reference database was constructed from ITS sequences from *P. agathidicida* isolates (GenBank accessions: JX122749.1, (Than et al. 2013), KP295308.1, KP295314.1, KP295312.1, and KP295311.1 (Weir et al. 2015)) using the *makeblastdb* (-dbtype nucl) function with default parameters. BLASTn searches were run with the following parameters: -evalue 1e-10 -word_size 24 -perc_identity 97 -qcov_hsp_perc 90 -dust no. Broader taxonomic classification of ASVs was performed using the UNITE

"all eukaryotes" database v8.3 (Abarenkov et al. 2023), which includes 140 reference sequences from the genus *Phytophthora* but no specific reference sequence for *P. agathidicida*. To evaluate primer coverage, an *in silico* analysis was also conducted to assess alignment of the ITS1-F and ITS2 primers to the *P. agathidicida* reference genome (strain 3770, chromosome 10; GenBank accession: CP106980.1; positions: 57,500-58,500) using BLASTn-short (BLAST v2.16) with the parameters -task blastn-short, -strand both, -word_size 7, and -evalue 1000.

A custom Kraken2 database was constructed for shotgun metagenomic analysis using all NCBI Taxonomy entries associated with "Oomycota", Taxonomy ID: 4762. Shotgun metagenomic reads were quality filtered, and human-associated reads were removed before taxonomic classification using Kraken v2.1.2 (Wood et al. 2019) against the custom oomycota database (described in more detail below). Read counts were refined using Bracken v2.7 (Lu et al. 2017) to estimate the abundance of *P. agathidicida*-associated DNA across samples. In this study, "*P. agathidicida*-associated DNA" refers to shotgun metagenomic reads classified as *P. agathidicida* by Kraken2 against the custom reference database. This terminology acknowledges that taxonomic assignments from short-read classification may include sequences from closely related taxa or extracellular DNA and therefore does not confirm the presence of viable *P. agathidicida* cells.

2.2.4 Bioinformatics

2.2.4.1 Amplicon data

Raw sequence reads underwent adapter removal using Cutadapt v4.4 (Martin 2011), with a minimum length threshold of 200 bp and 20 bp for the 16S and ITS reads, respectively; untrimmed reads were discarded. Amplicon sequence variants were generated using DADA2 implemented in R v4.4.0 (R Core Team 2021). Due to the poor quality of the reverse reads, only the forward reads were analysed (Pauvert et al. 2019; Ramakodi 2021). ASV taxonomy was inferred using the naïve Bayesian classifier method (Wang et al. 2007) against the SILVA database NR99 v138.1 (Quast et al. 2012) for 16S ASVs and the UNITE "all eukaryotes" database v8.3 (Abarenkov et al. 2023) for ITS ASVs. Non-bacterial and non-fungal ASVs were removed from the 16S and ITS datasets, respectively. Samples with <1000 reads were removed from the datasets, resulting in the loss of two samples from the 16S dataset and three samples from the ITS dataset (Table A1; Appendix A). Reads were decontaminated using the *isContaminant* function in the R 'decontam' package v1.24.0 using the prevalence method and a threshold value of 0.5 (Davis et al. 2018). Briefly, the prevalence method identifies contaminants by comparing the presence or absence of each ASV in true positive samples (soil) with

those in negative controls (nuclease-free water), with contaminants expected to occur more frequently in the control samples (Davis et al. 2018). Eleven bacterial ASVs (614 reads) and 19 fungal ASVs (2,939 reads) were identified as likely contaminants and removed from their respective datasets before further analysis. Taxon-by-sample abundance tables were created at the genus taxonomic level to allow for direct comparison with shotgun metagenome taxonomic classifications.

Functional inference of the bacterial communities was performed using Phylogenetic Investigation of Communities by Reconstruction of Unobserved States 2 (PICRUSt2) v2.6.1 (Douglas et al. 2020) to predict the functional capabilities and abundance of the identified communities based on marker gene sequences. Predicted functions were compared with those directly observed in the shotgun metagenome dataset to evaluate the accuracy of this approach. This assessment also provides a basis for considering the use of PICRUSt2 as a complementary, lower-cost method for functional monitoring in kauri forests. The 16S ASV dataset was filtered to remove ASVs present in less than 10% of samples before running PICRUSt2. The Nearest Sequenced Taxon Index (NSTI) score was used to assess the accuracy of the predictions, with any ASV with an NSTI score >2 removed from the analysis (Langille et al. 2013). The final predicted metagenome Kyoto Encyclopedia of Genes and Genomes (KEGG) Orthology (KO) abundance data were converted to relative abundances per sample.

2.2.4.2 Shotgun metagenome data

Raw and demultiplexed metagenome sequencing reads were quality checked using the FastQC (https://www.bioinformatics.babraham.ac.uk/projects/fastqc/) and MultiQC tools (Ewels et al. 2016). Reads were trimmed using the BBDuk script via BBTools v39.01 (Bushnell 2017) to remove adapters, poor quality sequences, and PhiX reads (qtrim=rl, trimq=25, k=25, hdist=1). Following trimming, non-target DNA was removed in several stages. Human DNA was removed using the BBMap script via BBTools using the masked human reference genome, hg19 (minid=0.95, maxindel=3, bwr=0.16, bw=12, quickmatch, fast, minhits=2, qtrim=rl, trimq=10, untrim). Non-target plant and animal DNA were removed using the KrakenTools v1.2 extract_kraken_reads.py (Lu et al. 2022) script against the inbuilt RefSeq database for plants, from Kraken v2.1.2 (Wood et al. 2019), and eight custom databases for animalia DNA built from NCBI taxonomies: annelida, arthropoda, chordata, mollusca, nematoda, platyhelminthes, tardigrada, and oomycota. Summary statistics of sample reads at each quality control stage were generated using SeqKit v2.4.0 (Shen et al. 2024), and the full dataset of read counts and quality metrics is available in Appendix A3 Supplementary File 1.

After quality control of the metagenome reads, samples were assembled individually using MEGAHIT v1.2.9 (Li et al. 2016) with standard parameters and a minimum contig length of 1000 bp. Prokaryotic gene prediction was performed using Prodigal v2.6.3 (Hyatt et al. 2010) using standard parameters. Predicted genes were clustered at 95% sequence identity using CD-HIT-EST v4.8.1 (Fu et al. 2012) (parameters: -aS 0.9, -G 0, -g 1, -d 0) to generate a non-redundant gene catalogue. Gene annotation was performed on the non-redundant gene catalogue using eggNOG-mapper v2.1.12 (Huerta-Cepas et al. 2019) with DIAMOND alignment (Buchfink et al. 2021) against the eggNOG database v5.0. Coverage information of genes was determined using Bowtie2 v2.4.5 (--minins 200, --maxins 800, --sensitive) (Langmead and Salzberg 2012) and CoverM v0.7.0 (contig, -m count) (Aroney et al. 2025). Raw gene counts were normalised by predicted gene length to account for differences in gene length.

To profile the taxonomic community of the shotgun metagenome reads, Kraken2 v2.1.2 (Wood et al. 2019) was used with the standard bacterial and fungal Kraken databases. Bracken v2.7 (Lu et al. 2017) was then used to generate the final abundance profiles of the metagenome sequences. Taxonomic lineage information was added to the profile using bit v1.9.21 (Lee 2022) and TaxonKit (Shen and Ren 2021).

To determine the functional potential of the soil bacterial communities, 10,866 unique KO numbers were extracted from the eggNOG annotation output. Database entries of these unique KOs were obtained from the KEGG database using kegg_pull v3.1.0 (Huckvale and Moseley 2023), which obtained information on 10,805 KOs. The KOs that did not have any information on KEGG are likely deprecated KOs. From the pulled entries, KEGG BRITE hierarchy information was extracted to understand the broad functional categories of genes. KEGG pathway information was extracted to understand the soil's bacterial communities' metabolic and nutrient cycling capabilities. KEGG pathways associated with “Organismal systems” and “Human disease” were removed from the dataset.

2.2.5 Statistical analysis

All statistical analyses used R v4.4.0 (R Core Team 2021). To explore the taxonomic composition of the microbial communities, relative abundance counts (number of reads) were calculated at both the phylum and genus levels using the ‘phyloseq’ package v1.48.0 (McMurdie and Holmes 2013). Filtering was conducted to retain phyla with a mean relative abundance (MRA) >1% across all samples and genera with a mean relative abundance >0.5%. The resulting subset of taxa

was used to visualise differences in microbial community composition at the phylum and genus levels across samples. Heatmaps were generated using the *plot_heatmap* function from the 'phyloseq' package with sample clustering based on Bray-Curtis dissimilarity and NMDS ordination of the community composition. Samples were grouped by their detection status of *P. agathidicida* as determined by LAMP results.

To identify genera with differential abundance between samples with and without *P. agathidicida* detection, differential abundance testing was performed using the *ancombc2* function from the 'ANCOMBC' package v2.6.0 (Lin and Peddada 2024). The analysis used default parameters, including sensitivity testing based on pseudo-count addition. In this step, each taxon's differential abundance status was tested for consistency when a pseudo-count was added to the data. Taxa that retained their significance status (*P*-value remaining significant or non-significant) were considered robust to the pseudo-count addition and passed the sensitivity testing. Only genera passing this sensitivity score filter were considered to be significantly differentially abundant.

Rarefaction curves were generated using the *amp_rarecurve* function from the 'ampvis2' package v2.8.9 (Andersen et al. 2018) for ASVs (amplicon) and species (shotgun metagenome) to assess the species diversity across samples of varying sequencing depths. Sample curves plateaued, indicating that sequencing depth was sufficient for alpha diversity analysis (Figure A2; Appendix A). Samples were rarefied using the *rarefy_even_depth* function from the 'phyloseq' package (Reads per sample: amplicon 16S: 15,420, amplicon ITS: 4,192, shotgun metagenome bacteria: 9,963,524, shotgun metagenome fungi: 42,440) before estimating alpha diversity at the genus level using observed richness and Shannon diversity index. The difference in diversity between the two detection groups was tested for significance using the Wilcoxon test.

To assess the beta diversity differences in the bacterial and fungal community composition between communities for both the amplicon and shotgun metagenome datasets, the raw counts of unique genera were first normalised using cumulative sum scaling (CSS) using the *cumNorm* function from the 'metagenomeSeq' package v1.46.0 (Paulson et al. 2013a; Paulson et al. 2013b) before creating a Bray-Curtis dissimilarity matrix using the *vegdist* function from 'vegan' v2.6.10 (Oksanen et al. 2020) and visualising using a principal coordinate analysis (PCoA). Significant differences between community composition were tested using permutational multivariate analysis of variance (PERMANOVA) using the *adonis2* function from the 'vegan' package. Procrustes rotation analysis was used to assess the congruence between the amplicon and metagenome ordinations for fungal

community composition and bacterial community and functional composition using the *procrustes* function of the 'vegan' package. Permutational significance tests were conducted using the *protest* function with 999 permutations. The goodness of fit of the Procrustes analysis is measured by the M^2 statistic, representing the sum of squared differences between corresponding points of the two configurations. A lower M^2 indicates a closer match between configurations, while higher values indicate greater dissimilarity.

To explore the functional potential of the microbial community, relative abundance counts of KOs grouped at BRITE hierarchy levels 1 and 2 and KEGG pathway levels 2 and 3 were visualised using the 'ComplexHeatmap' R package v2.21.2 (Gu 2022). Default hierarchical clustering was used to order rows and columns of the heatmaps. To assess the consistency of KOs detected between amplicon-based functional inference and shotgun metagenomic sequencing, we used the 'ggVennDiagram' package v1.5.2 (Gao et al. 2024). Differential abundance testing of KOs between detection status groups (detected vs not detected) was calculated using the *ancombc2* function from the 'ANCOMBC' package. Only KOs passing the sensitivity testing were considered differentially abundant. Alpha diversity was estimated on KO counts rarefied using the *rrarefy* function of the 'vegan' package to 11,507,418 reads per sample for the shotgun dataset and 21,404,604 predicted gene copies per sample for the amplicon dataset. Observed richness was calculated using the *specnumber* function of the 'vegan' package, and differences between detection groups were tested using the Wilcoxon test. Functional composition between samples was assessed using CSS normalised KO counts to generate a Bray-Curtis distance matrix using the *vegdist* function from 'vegan' before visualising using PCoA. Similarity between the shotgun metagenome and amplicon-inferred functional prediction ordinations was assessed using Procrustes rotation analysis via the *procrustes* function of the 'vegan' package; permutational significance tests were conducted using the *protest* function with 999 permutations.

2.3 Results

2.3.1 Detection of *P. agathidicida*

2.3.1.1 LAMP analysis

Phytophthora agathidicida was detected in 39 out of 60 soil samples using the LAMP assay (Figure A3; Appendix A). Detection of the pathogen did not align well with canopy scores, as some trees with low canopy scores (indicating healthy trees) still detected *P. agathidicida*. All 21 soil

samples where *P. agathidicida* was not detected were collected around trees with canopy scores of ≤ 3.5.

2.3.1.2 Amplicon sequencing

We explored whether *P. agathidicida* could be detected from the ITS1 amplicon dataset, which was primarily generated to characterise the wider fungal community. A BLASTn search of ASVs against reference *P. agathidicida* ITS sequences returned no matches, and taxonomic classification using the UNITE "all-eukaryotes" database v8.3 similarly did not identify any sequences belonging to the *Phytophthora* genus. Examination of the primer-template alignment showed that both ITS1-F and ITS2 primers only partially matched the *P. agathidicida* reference sequence, with the ITS1-F primer aligning to 13 of 22 bases (100% identity, E-value = 1.85×10^{-4}) within the 18S rRNA gene and the ITS2 primer aligning to 16 of 20 bases (100% identity; E-value = 2.80×10^{-6}) within the 5.8S rRNA gene. These mismatches, particularly for the ITS1-F primer, likely limited the ability of this primer set to amplify *P. agathidicida* ITS sequences.

2.3.1.3 Shotgun metagenome sequencing

Across all shotgun metagenome samples, the proportion of reads classified to *P. agathidicida* based on the entire reference genome was very low, with most samples containing less than 0.002% of total reads (Figure A4; Appendix A), indicating that *P. agathidicida* DNA is rare in these soils. One sample showed a notably higher number of *P. agathidicida*-associated reads, with 2,454 reads classified as *P. agathidicida* (0.006% of reads). This same sample also tested positive for *P. agathidicida* using LAMP analysis, potentially suggesting consistency between the two detection methods in this case. However, despite this isolate match, there was generally a poor alignment between the LAMP results and the shotgun metagenomic-based detection via Kraken2 and Bracken analysis (Figure A4; Appendix A). As well as identifying *P. agathidicida*-associated DNA in these samples, reads associated with 58 other *Phytophthora* species were also identified (data not shown).

2.3.2 Microbial community taxonomic composition

2.3.2.1 General characteristics of amplicon and shotgun metagenome datasets

The amplicon datasets obtained 2,415,068 bacterial reads and 1,108,149 fungal reads from the soil samples around kauri trees. The bacterial reads were classified into 19,020 ASVs, comprising 39 phyla, 253 families, and 447 genera. Fungal reads were classified into 7,654 ASVs, comprising 10 phyla, 226 families, and 450 genera.

For the shotgun datasets, 7,230,854,958 sequences were obtained after quality control. From these, 871,250,634 reads were classified as bacterial, and 4,065,980 reads were classified as fungal. Bacterial reads were classified into 49 phyla, 562 families, and 1,983 genera, and fungal reads into three phyla, 30 families, and 54 genera.

2.3.2.2 Soil microbial community composition

To investigate whether the presence of *P. agathidicida* is associated with microbial taxonomic composition, the relative abundance of bacterial phyla (>1% MRA) and genera (>0.5% MRA) between soils where *P. agathidicida* was detected and not detected (via LAMP analysis) using both amplicon and shotgun metagenome sequencing data was assessed. In the amplicon dataset, dominant phyla included Planctomycetota (35% MRA), Verrucomicrobiota (33% MRA), and Proteobacteria (13% MRA, also known as Pseudomonadota), which were dominant across both *P. agathidicida* detected and not detected soil samples (Figure A5A and B; Appendix A). In the shotgun metagenome dataset, samples predominantly comprised two phyla, Proteobacteria (57% MRA) and Actinobacteriota (34% MRA, also known as Actinomycetota), while other phyla were present at much lower relative abundances. These dominant phyla appear consistent across samples where *P. agathidicida* was detected and not detected. At the genus level, both amplicon and shotgun metagenome datasets show similar profiles across both detection groups (Figure A5C and D; Appendix A). However, different genera were identified between the different sequencing methods, with the shotgun metagenome dataset providing a greater resolution and detecting a wider array of low-abundance bacterial genera.

For the fungal dataset, relative abundance patterns at both the phylum and genus levels were broadly similar across *P. agathidicida* detection groups for both sequencing methods. Ascomycota was the dominant phylum in the amplicon data set (58% MRA, Figure A6A; Appendix A); however, some samples exhibited a relatively higher abundance of Basidiomycota, corresponding to a decrease in Ascomycota abundance in those cases. The amplicon dataset detected a range of fungal genera, generally at low relative abundance (Figure A6C; Appendix A). Among these, *Mortierella* consistently showed the highest relative abundance across most samples (27% MRA). For the shotgun metagenome dataset, only 0.06% of total sequences were taxonomically categorised by the Kraken2 fungal database, suggesting a potential annotation bias and underestimation of fungal communities, with only three phyla, 30 families, and 54 genera detected. However, Ascomycota was identified as the dominant phylum (90% MRA), consistent with the amplicon dataset (Figure A6B; Appendix A). The genera *Fusarium* (9% MRA), *Thermothielavioides* (9% MRA), and *Colletotrichum*

(8% MRA) were generally the most abundant across all samples in the shotgun metagenome dataset (Figure A6D; Appendix A).

Beta diversity analysis also showed no significant differences in microbial community composition between *P. agathidicida* detected and not detected soils. Visualisation using PCoA based on Bray-Curtis dissimilarity did not reveal any clear groupings by *P. agathidicida* detection status (Figure A7; Appendix A). This was supported by PERMANOVA results, which indicated no statistically significant variation between detection groups (P >0.05). However, PERMANOVA revealed significant differences in soil microbial community composition among sites (Cascades, Piha, and Huia; P <0.05), but further investigation was beyond the scope of this study and will be addressed in future work.

Differential abundance analysis of the amplicon dataset revealed several bacterial and fungal genera that varied significantly between soils where *P. agathidicida* was detected against those where they were not (Figure 2.1). Among bacteria, *Lacunisphaera* was less abundant in soils where *P. agathidicida* was undetected, whereas *FCPS473*, *Thermostilla*, *1921-2*, *Pseudaminobacter*, *Ruminiclostridium*, *Rhizobacter*, and *Hirschia* were more abundant. For fungi, *Hygrocybe* and *Hypholoma* were enriched in soils where *P. agathidicida* was not detected with 19 genera more abundant where the pathogen was present. In both bacterial and fungal communities, the differentially abundant taxa were of low relative abundance across individual samples (<1%). No differentially abundant genera were identified in the shotgun metagenome datasets for either bacteria or fungi.

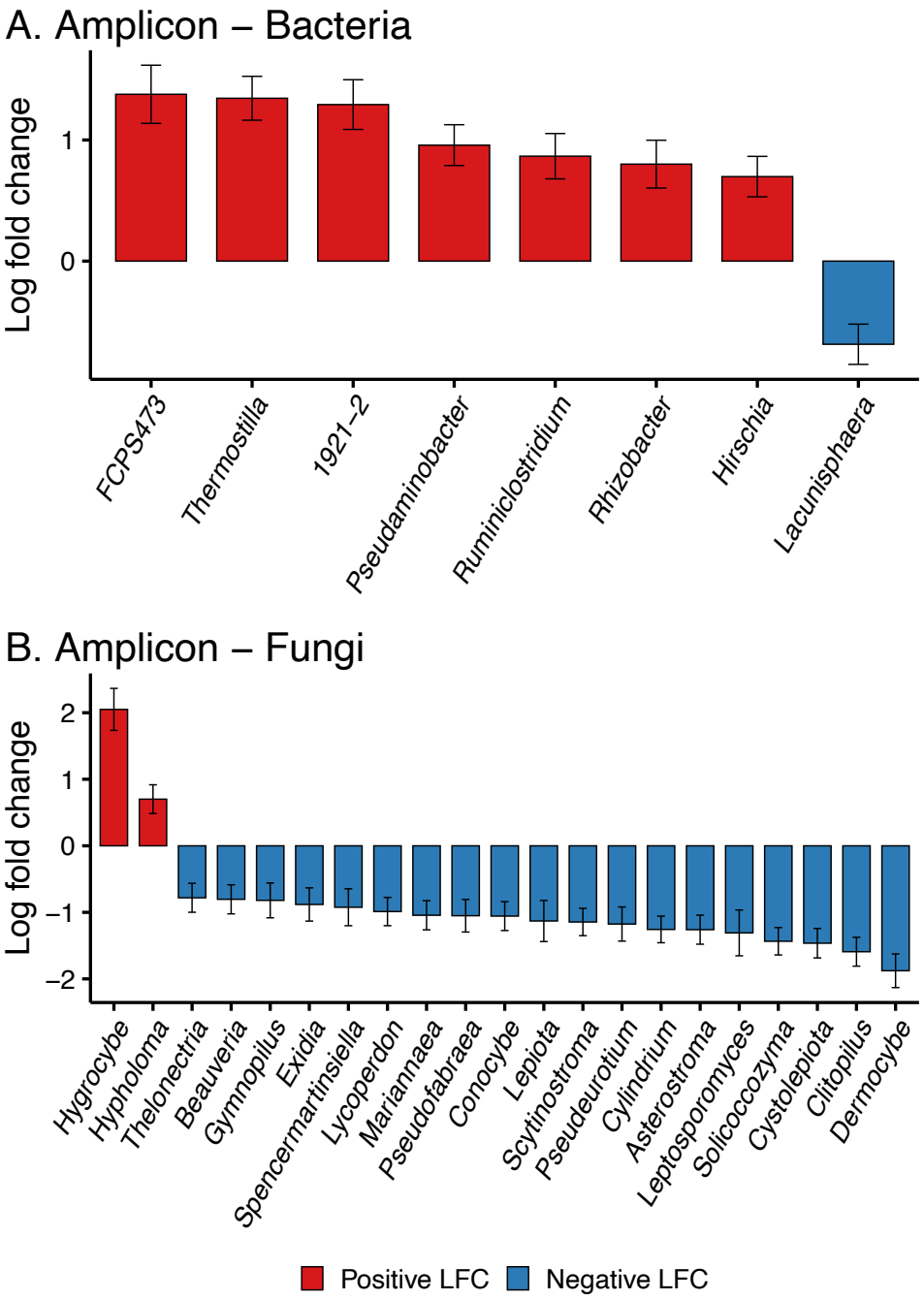

Figure 2.1: (A) Bacterial and (B) fungal genera showing differential abundance between soil samples where *Phytophthora agathidicida* was detected and not detected. Genera with a positive log fold change (natural log) show increased abundance in soils without *P. agathidicida* detected and genera with a negative log fold change (natural log) show increased abundance in soils with *P. agathidicida* detected. All genera identified passed ANCOM-BC2 sensitivity scoring. LFC = log fold change.

2.3.3 Microbial community diversity

There were no significant differences in alpha diversity estimates between samples with and without *P. agathidicida* detection. This was consistent across both observed richness and Shannon

diversity estimates (*P* >0.05) for bacterial and fungal genera, based on both amplicon and shotgun metagenome datasets (Figure A8; Appendix A).

Comparisons between the sequencing methods revealed some differences in richness estimates. Shotgun metagenome sequencing estimated a higher bacterial observed richness compared to amplicon sequencing. In contrast, fungal genera showed a higher observed richness in the amplicon dataset, with shotgun metagenome sequencing recovering relatively few fungal genera (Figure A8D; Appendix A), likely due to the reference database used for taxonomic classification.

2.3.4 Functional potential of bacterial communities

Functional potential of the bacterial communities was assessed by comparing KOs inferred by PICRUSt2 (from amplicon data) and genes predicted and annotated using Prodigal and eggNOG (from shotgun metagenome data). PICRUSt2 inferred 7,518 unique KOs from 2,183 ASVs (ASVs ≥ 10% sample prevalence), with an average NSTI value of 0.156, indicating a fair match between sequenced ASVs and the reference genomes. For the shotgun metagenome dataset, 8,519,250 genes were predicted; 30% of the predicted genes had an associated KO number, with 10,866 unique KOs identified across all samples.

The predicted KOs were grouped into higher-level functional categories using BRITE and KEGG pathway hierarchies. Despite differences in sequencing methodology and KO inference/prediction, the functional profiles generated from shotgun (Figure A9; Appendix A) and amplicon data (Figure A10; Appendix A) were relatively consistent. Across both datasets, the most abundant category was the BRITE level 3 category “Transporters”, a group of proteins involved in cellular import and export processes. Similarly, when KOs were grouped into KEGG pathways, both datasets revealed “Carbohydrate metabolism” and “Amino acid metabolism” as the most prominent functional pathways, highlighting the high potential microbial activity associated with nutrient cycling and organic matter processing.

Samples grouped based on LAMP-based detection of *P. agathidicida* showed no major differences in KO-level relative abundances between soils where *P. agathidicida* was detected and not detected. The consistent patterns of functional abundance across detection groups indicate that the presence of the pathogen may not be associated with large-scale shifts in functional potential detectable at broad KEGG category levels.

Differential abundance testing of individual KOs revealed no significantly differentially abundant KOs in the shotgun metagenome dataset when comparing samples where *P. agathidicida* was detected and not detected. In contrast, exploratory analysis of PICRUSt2-inferred KOs identified four putative differences; however, given the lack of support in the shotgun dataset, these should be interpreted cautiously.

While no significant differences in functional alpha diversity (based on observed richness) were observed between *P. agathidicida*-detected and not detected soils for either sequencing method (P >0.05, Figure A11; Appendix A), no clustering by *P. agathidicida* detection was observed using PCoA (Figure A12; Appendix A); PERMANOVA confirmed no significant differences (PICRUSt2: R^2 = 0.005, P = 0.83, n = 58; eggNOG: R^2 = 0.021, P = 0.271, n = 60) in KO composition between detection groups. PERMANOVA analysis indicated significant differences in the functional profiles of soil microbial communities across sites (P < 0.05); however, these patterns were not examined in detail here as they are beyond the scope of this study and will be addressed in future work.

2.3.5 Concordance between amplicon and shotgun metagenome datasets

Procrustes analysis was used to assess the similarity in variation among samples of bacterial and fungal genus-level community composition derived from amplicon and shotgun metagenome data (Figure 2.2A and B). For bacterial communities, a moderate alignment was observed (M^2 = 0.3124, P = 0.001), suggesting moderate agreement between sequencing methods despite differences in the taxa detected. For the fungal communities, the alignment between the sequencing methods was weaker (M^2 = 0.5664, P = 0.001) due to the higher M^2 value indicating greater dissimilarity between the amplicon and shotgun datasets. The Procrustes test used to compare community functional profiles between shotgun and amplicon-inferred KO predictions (Figure 2.2C) showed a moderate alignment between sequencing methods (M^2 = 0.333, P = 0.001).

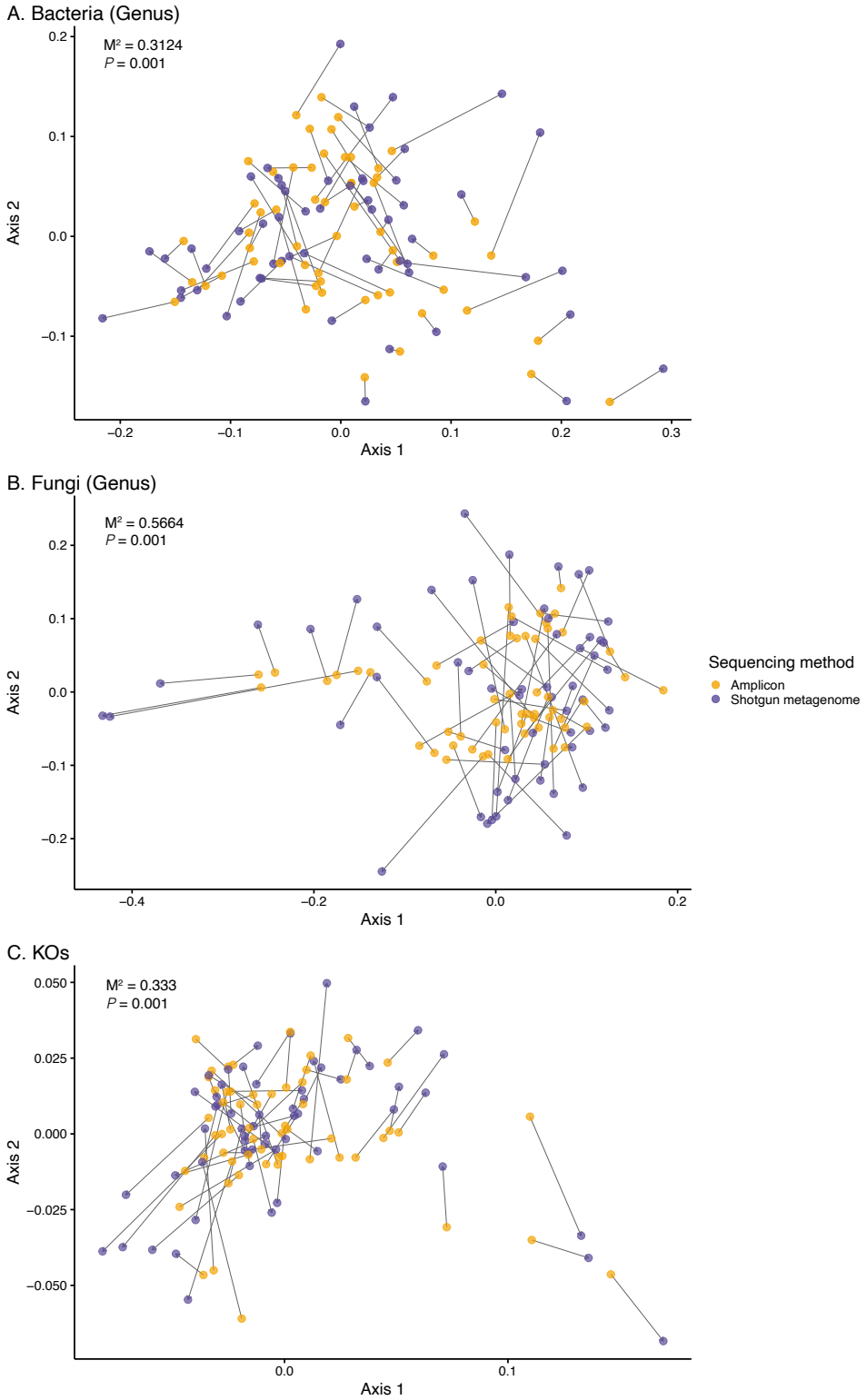

Figure 2.2: Procrustes analysis comparing community composition profiles of (A) bacterial genera, (B) fungal genera, and (C) KEGG Orthologs (KO) derived from amplicon (gold) and shotgun metagenome (purple) sequencing. Arrows connect matching samples, with arrow length indicating the degree of dissimilarity between the two datasets for that sample (longer arrows = greater discordance). For each rotation, the M^2 statistic and associated *P*-value are shown, where M^2 represents the proportion of variance unexplained by the Procrustes fit (lower values indicate better agreement between datasets).

Comparison of the KOs annotated by amplicon-based inference and shotgun metagenomic sequencing showed that 6,972 KOs were shared between both methods (Figure A13; Appendix A). The 546 KOs only identified in the amplicon-inferred dataset are likely false positives, as they were not detected through direct sequencing of the environmental DNA (shotgun metagenomics). Included in these is K06420, which was the only differentially abundant KO showing increased abundance in soils where *P. agathidicida* was not detected. The 3,833 KOs absent from the amplicon-based inference likely reflect false negatives and highlight the limitations of the PICRUSt2 method.

2.4 Discussion

2.4.1 Summary of key findings

Our study addressed four key questions to assess the methods used to detect and measure the relationship between the structure and function of soil microbial communities surrounding kauri and the presence of *P. agathidicida*. Firstly, in comparing detection methods, LAMP analysis provided both detection and viability information of the pathogen, whereas amplicon sequencing failed to detect any reads assigned to the *Phytophthora* genus. In contrast, shotgun metagenome sequencing detected *P. agathidicida*-associated DNA in all soil samples, although at low abundance. Secondly, observing the microbial community structure regarding taxonomic diversity and composition, we found that it was not substantially affected by *P. agathidicida* detection; however, several microbial taxa were differentially abundant between samples where the pathogen was detected and those where it was not. Similarly, analysis of community functional potential showed limited differentiation between samples with and without pathogen detection. Finally, shotgun metagenomic and amplicon sequencing approaches concord strongly in their broad-level taxonomic and functional profiles. Collectively, these findings suggest that while *P. agathidicida* may influence the abundance of specific microbial taxa, its detection is not strongly associated with shifts in the surrounding soil microbial community's core taxonomic or functional structure.

2.4.2 *Phytophthora agathidicida* detection across different methods

This study compared three methods for detecting *P. agathidicida* in soil samples collected around kauri trees: LAMP analysis combining traditional baiting techniques with rapid amplification, and two sequencing-based methods: amplicon sequencing of the ITS1 region and shotgun metagenomic sequencing. Together, these methods offer a range of sensitivity, specificity, and insight into pathogen detection and broader microbial context.

Amplicon sequencing of the ITS1 region failed to detect *P. agathidicida* or assign any ASVs to the Oomycota class, despite its detection being confirmed through shotgun metagenomics. This likely reflects both the low abundance of the pathogen in the soil and the taxonomic bias of ITS1 primers, which are optimised for capturing broad fungal diversity and, therefore, may not efficiently amplify oomycetes, especially in environments that are dominated by other fungal species (Sapkota and Nicolaisen 2015; Schoch et al. 2012). Previous studies have demonstrated greater success with *P. agathidicida* detection using more targeted PCR assays, such as nested PCR and more targeted primer sets for *Phytophthora* species or oomycete detection (Hunter et al. 2024; Legeay et al. 2019; Palmer et al. 2025). To reliably profile fungal and oomycete or *Phytophthora* communities using amplicon sequencing, primer sets must be specifically designed to capture both groups, or separate amplification steps should be undertaken for each target community.

Using shotgun metagenomics, *P. agathidicida*-associated DNA was detected in all samples, with little variation in read counts across the dataset, suggesting ubiquity of *P. agathidicida* DNA in all soils, albeit at a low abundance. In addition to detecting *P. agathidicida*-associated DNA, shotgun metagenomic sequencing identified reads classified as belonging to 58 other *Phytophthora* species, highlighting the broader taxonomic diversity this approach can capture to offer a more exhaustive overview of the oomycete community present in these soils. Previous research has also reported the co-occurrence of diverse *Phytophthora* species in kauri forests (Beever and Bellgard 2010; Hunter et al. 2024; Waipara et al. 2013). Although shotgun metagenomics was sensitive enough to capture the low abundance of *P. agathidicida* DNA in the samples, the viability of this pathogen is indistinguishable from non-viable DNA using this method, limiting its application for diagnosing active infections. This verifies the utility of LAMP-based detection and shows that the shotgun metagenome-based method is not a reliable indicator of LAMP-positive status for these samples but provides a more comprehensive view of the microbial community inhabiting the soil around kauri trees. Moreover, shotgun metagenomics enables simultaneous characterisation of fungal and oomycete communities, including *Phytophthora* species, without the primer biases in targeted amplicon approaches.

Despite their differing targets and sensitivities, all three methods offered complementary insights into detecting *P. agathidicida*. While LAMP provided reliable detection of viable *P. agathidicida*, and shotgun metagenomics indicated its widespread but low-abundance occurrence through *P. agathidicida*-associated DNA, these approaches suggest that while the pathogen is consistently detectable in these soils, it is often present at a low abundance, and in many cases may

be in a dormant or non-viable state. Although amplicon sequencing of the ITS1 region failed to detect *P. agathidicida* directly, likely due to primer bias and low DNA abundance, it still revealed broader community profiles consistent with shotgun metagenome data at higher taxonomic levels. This concordance between methods highlights the strengths and limitations of each method depending on the research goal, whether it be presence/absence, viability, or broader ecological context.

2.4.3 Impacts of *P. agathidicida* presence on microbial community composition

Although the overall microbial community composition and diversity were not significantly different between soil samples where *P. agathidicida* was detected and not detected, our results revealed a subtle, but significant shift in the abundance of specific microbial taxa that may be responding to the presence or absence of the pathogen. The differences in abundance of these taxa did not create large-scale shifts in the community composition. However, they may still reflect relevant responses to the presence or absence of the pathogen. The bacterial genera *Rhizobacter* and *Hirschia* were significantly higher in abundance in soils without *P. agathidicida* detection. These taxa have been previously associated with disease suppression and observed to be higher in soils around healthy plants (Ketehouli et al. 2024; Siegel-Hertz et al. 2018; Wright et al. 2022). *Rhizobacter* species, in particular, are recognised as plant growth-promoting bacteria and are also known to suppress the growth of pathogens by producing siderophores and secondary metabolites (Abbas et al. 2022).

Similarly, several of the fungal genera that had higher abundance in soils where *P. agathidicida* was detected have been linked with antagonistic activity towards plant pathogens. Members of the *Beauveria* genus, for example, are known to produce a wide array of enzymes and secondary metabolites and show antagonistic effects towards a range of phytopathogens, including *Phytophthora* species (Lozano-Tovar et al. 2017; Lozano-Tovar et al. 2013; Pachoute et al. 2024). The *Gymnopilus* genus has also previously been linked with disease suppression, showing antagonistic effects towards bacterial and fungal pathogens (Ranadive et al. 2013). Although these taxa did not drive large shifts in overall community structure, their differential abundance suggests potential direct or indirect interactions with *P. agathidicida*. It may reflect underlying microbial dynamics related to disease expression.

2.4.4 Functional shifts in the microbial community

Despite subtle differences in the taxonomic composition of microbial communities where *P. agathidicida* was detected and not detected, the predicted functional profiles of the soil microbial

communities remained relatively consistent. This consistency, especially at higher functional categorical levels, suggests the presence of functional redundancy within the microbial community. In such environments, multiple microbial taxa may carry out similar ecological functions, allowing the broader functional profile of the community to remain stable even when its taxonomic composition shifts (Li et al. 2021; Nannipieri et al. 2017). This redundancy may buffer the broad functions of a community against environmental disturbances, such as pathogen invasion, and supports the idea that soil microbial communities maintain key ecosystem processes through overlapping metabolic capacities (Chen et al. 2022a; Gao et al. 2021). Furthermore, it is possible that the presence of *P. agathidicida*, which likely comprises a relatively small proportion of total microbial biomass or exists in a metabolically inactive state, does not exert a strong effect to shift microbial community function at the scale captured by KEGG-level analyses. The localised microbial response to the pathogen may also be spatially restricted or masked by larger-scale variations in soil properties.

2.4.5 Alignment between shotgun metagenome and amplicon-derived profiles

While specific bacterial and fungal phyla were consistently identified in both amplicon and shotgun sequencing datasets, the genus-level profiles differed. These discrepancies likely reflect differences in detection sensitivity, sequencing depth, and database completeness between the two methods. The shotgun metagenome dataset, which had a much greater sequencing depth, revealed a broader diversity of bacterial genera and likely recovered more rare or low-abundance taxa (Brumfield et al. 2020; Madison et al. 2023). However, for fungal taxa, taxonomic resolution was limited. Although shotgun sequencing has the potential to detect a broader array of fungal diversity, this analysis was restricted by the limited reference database used (Kraken2), which included only 455 fungal species. Use of this database likely underestimated the true fungal diversity in the soil and emphasises the importance of database selection and the need for improved fungal reference databases to fully utilise shotgun metagenome data derived from diverse soil ecosystems (Avershina et al. 2025).

Despite differences in taxonomic composition between sequencing methods, the predicted functional profiles of the microbial communities remained relatively consistent. The PICRUSt2-inferred KOs and shotgun metagenome-derived annotations (via eggNOG) exhibit fundamental differences in their approaches to classifying genes and KOs. PICRUSt2 relies on phylogenetic inference from 16S rRNA gene sequences, whereas the shotgun metagenomic approach provides direct evidence of functional genes present in the community (Bharti and Grimm 2021; Douglas et

al. 2020). Despite these differences in approach, the overall patterns of microbial community function were largely consistent in this study. The consistency between these two methods, especially at higher levels of functional groupings, suggest that at least at the broad-scale, functional potential can be inferred from amplicon data, which is consistent with previous studies on soil environments (Toole et al. 2021). The accuracy of the PICRUSt2 predictions in this study was supported by a moderately low NSTI value, indicating a good alignment between observed ASVs and available reference genomes in the PICRUSt2 database (Douglas et al. 2020). However, the two methods had substantial differences in the total number of identified KOs. The large number of KOs uniquely identified by shotgun metagenome sequencing likely reflects the improved sensitivity and coverage of genes, especially for rare or uncharacterised functions.

These findings highlight both the strengths and limitations of each profiling method. Amplicon-based functional inference provided results that were largely consistent with shotgun sequencing at the level of broad functional categories, indicating that PICRUSt2 can be a reliable and cost-effective approach for monitoring microbial functional potential in kauri forest soils. This makes amplicon sequencing a practical choice for long-term or large-scale studies where resources are limited. In contrast, shotgun metagenomics, while more resource-intensive, offers additional advantages that cannot be obtain from amplicon sequencing. Beyond profiling community composition and function, shotgun data can be used to reconstruct metagenome-assembled genomes, enabling strain-level resolution and insights into novel or uncultured organisms. Importantly, shotgun sequencing also allows simultaneous identification of *P. agathidicida* alongside bacterial and fungal communities in a single dataset, providing an integrated view of the pathogen and its surrounding microbiome. Together, these results suggest that for many applications, particularly for broad-scale monitoring of microbial communities, amplicon sequencing with functional inference may be sufficient, while shotgun metagenome sequencing is best reserved for targeted studies where genome recovery or high-resolution community profiling are key objectives.

2.5 Conclusion

Overall, our study aimed to evaluate how different molecular-based tools compared in their ability to detect *P. agathidicida* and characterise the associated changes in soil microbial communities in soils surrounding kauri trees. We have provided a multifaceted view of how the presence of this plant pathogen may influence microbial diversity, composition, and function, while also evaluating the strengths and limitations of the methods used.

Our findings demonstrate that no single method provides a complete picture of pathogen detection or microbial community composition. Although *P. agathidicida* detection was associated with subtle changes in microbial community composition, our findings suggest that direct microbial responses to the pathogen presence may not be the dominant driver of community structure. Instead, indirect effects, such as declining tree health associated with canopy loss and gummosis may play a more substantial role in shaping the soil microbial community. Additionally, spatial variation and soil physicochemical properties require further investigation, as these broader environmental factors may influence how pathogen presence interacts with the soil microbial community structure and function. Future studies should integrate both amplicon and shotgun metagenome sequencing across finer spatial gradients and couple this with environmental data to help reveal the biotic and abiotic factors involved in shaping forest soil microbiomes to develop a deeper understanding of how kauri dieback influences and is influenced by the belowground microbial community.

Chapter 3

Spatial variation of soil microbial communities associated with dieback of a foundation tree species

Author names

Zoe King [a], Hannah L. Buckley [a], Gavin Lear [b], Brent Seale [a], Kevin C. Lee [a], Donnabella Lacap-Bugler [a]

Author affiliations

[a] School of Science, Auckland University of Technology, Auckland CBD, Auckland, 1010, New Zealand

[b] School of Biological Sciences, University of Auckland, Auckland CBD, Auckland, 1010, New Zealand

Code availability

All code used in this chapter can be found in the following GitHub repository https://github.com/zoesking/kauri-soil-amplicon

Abstract

Soil microbial communities vary immensely across both macro- and micro-spatial scales due to variations in biotic and abiotic conditions. Kauri (*Agathis australis*) forests in northern New Zealand are increasingly affected by the pathogen *Phytophthora agathidicida*, which causes tree dieback and death. To understand variation and interrelationships among soil microbial communities and kauri impacted by the pathogen, we collected four soil samples from around each of 96 kauri trees within three sites in the Waitākere Ranges, Auckland, each containing two plots of trees (40 × 50 m per plot). The physiochemistry of the soil samples were analysed, and the soil microbiome was characterised using 16S rRNA gene and ITS region metabarcoding. The composition of bacterial communities varied substantially around the smallest spatial scale (individual trees, $R^2 = 0.46$), with additional variation shared at the larger spatial scales of plots ($R^2 = 0.18$) and sites ($R^2 = 0.11$). Similar patterns were observed for the fungal data, tree-scale ($R^2 = 0.39$), plots ($R^2 = 0.09$), and sites ($R^2 = 0.32$). The overall diversity and composition of soil bacterial and fungal communities did not differ significantly among trees of different health status. However, certain bacterial and fungal taxa showed significant differential abundance around trees of varying health status. Soil physicochemical properties varied significantly between the three sites, explaining 36% of bacterial and 25% of fungal community composition. This study highlights the complex interactions among kauri trees, pathogens, the environment, and soil microbes, advancing our understanding of microbial responses to biotic and abiotic conditions.

Keywords: *Phytophthora agathidicida*, *Agathis australis*, soil microbial communities, spatial variation, Oomycetes, plant pathogen, plant-microbe interactions

3.1 Introduction

Soil microbial communities are a fundamental component of forest ecosystem processes, playing a crucial role in nutrient cycling, organic matter decomposition, disease suppression, and supporting plant growth (Baldrian 2017; Yu et al. 2022). These complex communities form intricate networks of interactions, with both large and small spatial scales playing different but essential roles in shaping community composition and function, due to associated spatial variation in biotic and abiotic conditions (Philippot et al. 2013). At larger spatial scales, factors such as climate, vegetation type, and soil type contribute to broadscale patterns of microbial diversity and composition across different regions (Constancias et al. 2015; van der Heijden et al. 2008). At smaller spatial scales, factors such as the quantity and quality of organic matter, plant root exudates, and localised soil physicochemical properties create fine-scale heterogeneity in soil microbial communities (Pantigoso et al. 2022; Vos et al. 2013). The interactions and effects of these different soil microbial community components on each other are understudied.

Forest ecosystems face growing pressures from land use change, climate change, invasive plant and animal species, and pathogens (Langmaier and Lapin 2020; Singh et al. 2023). Understanding how these stressors affect the dynamics of soil microbial communities at varying spatial scales is critical (Barati et al. 2023; Roy et al. 2014). The conifer, kauri (*Agathis australis*), endemic to New Zealand, is a canopy-forming foundation species that is threatened by the spread of *Phytophthora agathidicida*, a soil-borne oomycete responsible for kauri dieback disease (Gadgil 1974; Weir et al. 2015). The pathogen is now distributed across most of the kauri trees remaining geographic range (Beever et al. 2009; Bradshaw et al. 2020) and infects trees of all ages and sizes. *Phytophthora agathidicida* initially colonises the fine roots, causing root rot that compromises water and nutrient uptake, before spreading into the cambium and degrading vascular function, ultimately leading to chlorosis, gummosis, canopy loss, and death (Bellgard et al. 2016a; Bellgard et al. 2013; Waipara et al. 2013).

Kauri exert a strong influence on the soils beneath their canopies, creating unique physicochemical conditions and associated plant communities (Wyse et al. 2014). Their acidic, tannin-rich litter accumulates on the forest floor, storing large amounts of nitrogen and slowing decomposition (Steward and Beveridge 2010; Verkaik et al. 2006). Kauri forests are also among the most carbon-dense ecosystems globally (Keith et al. 2009; Macinnis-Ng and Schwendenmann 2015), and individual trees can achieve wood volumes exceeding 500 m^3 (The Gymnosperm Database n.d.).

These distinctive traits mean that shifts in kauri health could have cascading effects through altered nutrient inputs, soil processes, and microbial communities, providing an excellent case study for understanding how soil-borne pathogens and tree decline interact with soil microbial communities.

The few studies on soil microbial communities surrounding trees affected by soil-borne pathogens have focused mainly on Northern Hemisphere forests (Gómez-Aparicio et al. 2022; Pinho et al. 2020; Venice et al. 2021; Yu et al. 2022). This research gap is particularly evident in forests impacted by emerging pathogens, such as *P. agathidicida,* that not only affect the health and survival of kauri trees but are also likely to have direct and indirect effects on the composition and diversity of the surrounding soil microbial communities. Byers et al. (2020a), have provided the first insights into these dynamics. They showed that soils beneath kauri trees showed distinct microbial communities compared with exotic tree species (Byers et al. 2020a), and that differences in fungal and bacterial community composition occur between symptomatic and asymptomatic kauri (Byers et al. 2020b). Experimental seedling inoculations further demonstrated that bacterial communities responded more strongly than fungal communities to *P. agathidicida* infection (Byers et al. 2021b). Collectively, these findings suggest that disease progression is associated with shifts in the soil microbial communities, but understanding remains limited. The earlier work focused on a small number of mature tree, mostly in late stages of decline, and excluded dead trees (Byers et al. 2020b).

Our study aims to understand the spatial and environmental factors affecting soil microbial communities in kauri forests, focusing on variation associated with tree health status, i.e., kauri dieback disease caused by *P. agathidicida*. We ask: (1) What is the spatial variation in soil microbial community composition and diversity surrounding kauri trees among individual trees, plots, and sites? (2) Does microbial community composition and diversity in soil surrounding kauri trees differ significantly among trees of different health status? (3) Which soil physicochemical properties correlate with microbial composition and diversity in soils surrounding kauri trees of different tree health status? Investigating these questions will improve understanding of the complex interactions between soil microbial communities, kauri trees, and environmental conditions influenced by a major plant pathogen.

3.2 Methods

3.2.1 Field sampling

The Waitākere Ranges (Te Wao Nui ā Tiriwa), which contains one of the largest remaining kauri forests in Auckland, New Zealand, is a regional park covering more than 16,000 hectares of native forest (Froud et al. 2022). It is also the area most heavily infected with kauri dieback (Froud et al. 2022; Hill et al. 2017). Sampling was undertaken from June to August 2021 in three distinct sites within the park: The Cascades Stream area, Piha, and Huia (Figure A1; Appendix A) (*n* = 3 sites). Within each site, two 40 × 50 m permanent vegetation plots were established between 2012 and 2021 (*n* = 6 plots). Within each plot, all kauri trees with a diameter (at 1.3 m height) greater than 2 cm were tagged. Within each plot, four 10 × 50 m sub-plots were established (*n* = 24 sub-plots), and four kauri trees within each sub-plot were randomly selected for soil sampling (*n* = 96 trees). In one of the Cascades plots, one sub-plot only had three kauri trees present, so an additional tree was selected from a neighbouring sub-plot. Following an established protocol for soil sampling (Hill et al. 2017), a hand trowel was used to collect soil 1m from the trunk in four cardinal directions around each tree to a 10 cm depth (*n* = 384 samples) and placed into a sterile Whirl-Pack bag (Madison, WI, USA). Soil samples were transferred to and stored in a -20 °C freezer within a few hours until processing. Metadata related to the trees were also collected at the time of sampling. These include their diameter at breast height (DBH), the presence of gummosis and its activity (sticky = active, soft but not sticky = semi-active, hard = not active), and the canopy health. The condition of the canopy was scored using a five-point system described by Horner et al. (2019b): 1 = healthy, full canopy with no visible thinning, 2 = minor foliar thinning, 3 = some branch dieback, 4 = severe shoot dieback, and 5 = dead. Additional half-point increments were applied to capture intermediate stages of canopy decline as described by Froud et al. (2022). Based on the canopy scores, sampled trees were grouped into three categories: 1-2 “healthy” (*n* = 21), 2.5 – 4.5 “defoliated” (*n* = 70), and 5 “dead” (*n* = 5). Elevation of each tree was also recorded using an Emlid Reach RS+ GPS unit (Budapest, Hungary).

3.2.2 Soil DNA extraction, PCR and amplicon sequencing

DNA was extracted from the 384 soil samples [96 trees x 4 cardinal points = 384] using a DNeasy PowerSoil Pro Kit (Qiagen, Germany) following the manufacturer’s instructions, using 0.25 g of soil for each sample. Negative controls using nuclease-free water were included in each extraction batch (*n* = 14). DNA concentrations were determined fluorometrically using a Qubit double-stranded DNA BR assay kit (Thermo Fisher Scientific, Massachusetts, USA). Samples with a DNA concentration

over 200 ng/µL were diluted with an equal volume of nuclease-free water to reduce the amount of starting material in the PCR reaction.

Extracted DNA was amplified using the prokaryotic 341F (5'-TCGTCGGCAGCGTCAGATGTGTATAAGAGACAGCCTACGGGNGGCWGCAG-3') and 805R (5'-GTCTCGTGGGCTCGGAGATGTGTATAAGAGACAGGACTACHVGGGTATCTAATCC-3') primers to target the V3-V4 region of the 16S rRNA gene (Stoeck et al. 2010). The ITS1 region of the fungal internal transcribed spacer region (ITS) was amplified using the ITS1-F (5'-TCGTCGGCAGCGTCAGATGTGTATAAGAGACAGCTTGGTCATTTAGAGGAAGTAA-3') (Gardes and Bruns 1993) and ITS2 (5'-GTCTCGTGGGCTCGGAGATGTGTATAAGAGACAGGCTGCGTTCTTCATCGATGC-3') (White et al. 1990) primers. The target-specific sequences are underlined, with the remainder of the primer sequence comprising Illumina adaptor sequences required for downstream sequencing. Negative controls (nuclease free water) and a ZymoBIOMICS Microbial Community DNA Standard (mock community DNA standard; Zymo Research, California, USA) were included with each PCR run to assess contamination and sequencing bias (n = 5).

Each 25 µL reaction contained 6.25 µL of KAPA HiFi Hotstart ReadyMix (Kapa Biosystems, Wilmington, MA, USA) and 2 µL of template. For 16S rRNA gene amplification, 0.75 µL of each primer (10 µM) was included per reaction, and for ITS region amplification, 1 µL of each primer (10 µM) was included. Thermocycler conditions were the same for both primer sets. They were as follows: initial denaturation at 95 °C for 3 minutes, followed by 30 cycles of 98 °C for 20 seconds (denaturation), 63 °C for 15 seconds (annealing) and 72 °C for 15 seconds (extension), with a final extension at 72 °C for 1 minute.

PCR products were purified using AMPure XP beads (Beckman Coulter, CA, USA) following the manufacturer's instructions before being quantified using a Qubit double-stranded DNA HS assay kit (Thermo Fisher Scientific, MA, USA) and normalised to 1 ng/µL. Samples were then indexed (Nextera XT DNA Library Prep kit), pooled, and cleaned using AMPure XP beads (Beckman Coulter, CA, USA) following the manufacturer's instructions. Libraries were pooled at 1 nM, validated using an Agilent 2100 expert High Sensitivity DNA Bioanalyzer assay (Agilent Technologies, CA, USA), and sequenced using an Illumina MiSeq Reagent Kit v3 (600-cycle) to produce 2 x 300 bp reads.

3.2.3 Bioinformatics

The raw, demultiplexed sequence reads underwent primer and adapter removal using Cutadapt v4.4 (Martin 2011); untrimmed reads were also discarded. A minimum read length threshold was included to remove reads below 200 bp from the bacterial dataset, and 20 bp from the fungal dataset. The remaining reads were further processed using DADA2 v1.24.0 (Callahan et al. 2016) implemented in R v4.3.1 (R Core Team 2021) to generate amplicon sequence variants (ASVs). Due to the poor quality of the reverse reads for both amplicon regions, only the forward reads were analysed (Ramakodi 2021). The 16S reads were uniformly trimmed at 249 bp, and the pseudo-pooling method was used for sample inference for both datasets. Taxonomy was applied to the ASVs using a naive Bayesian classifier method (Wang et al. 2007) against the SILVA database NR99 v138.1 (Quast et al. 2012) for the 16S ASVs and the UNITE all eukaryotes database v8.3 (Abarenkov et al. 2023) for the ITS ASVs. Any ASVs not of bacterial origin were removed from the 16S dataset, including those from chloroplasts and mitochondria. Non-fungal ASVs were removed from the ITS dataset. Samples with <1000 reads were removed from the dataset. This resulted in the loss of four samples for the 16S dataset and 17 for the ITS dataset (Table B1; Appendix B).

Reads were decontaminated using the *isContaminant* function in the R 'decontam' package v1.24.0 using the prevalence method and a threshold value of 0.5 (Davis et al. 2018). This method identifies any sequences that are more prevalent in negative controls than true samples as contaminants. Fourteen bacterial ASVs (3,983 reads) and 33 fungal ASVs (48,316 reads) were identified as likely contaminants and removed from the respective datasets before additional downstream analysis. Mock community ASVs were classified to the genus level, and all eight of the expected bacterial genera, and the expected two fungal genera were identified in the sequenced mock community samples. Several other genera were also identified in both datasets; however, their relative abundance was below 1% in each mock sample (Figure B1; Appendix B). A possible source of this contamination is 'cross-talk' between indexing primers (Wright and Vetsigian 2016). Therefore, these ASVs were not removed from the full dataset. Overall, the relative abundance of the sequenced mock communities was not different from the community's theoretical composition (Figure B1; Appendix B).

3.2.4 Environmental variables

Approximately 200 g of soil from each of the four cardinal point samples was manually homogenised to create one soil sample per tree. These samples were processed to determine pH,

total carbon (%), total nitrogen (%), total hydrogen (%), carbon to nitrogen (C:N) ratio, electrical conductivity (µS/cm), bulk density (g/cm^3), soil moisture (%), and water holding capacity (%), as described in Manaaki Whenua Landcare Research (2021).

3.2.5 Statistical analyses

Statistical analysis and data visualisation were carried out using R v4.4.0 (R Core Team 2021). To assess the variability of microbial taxa which may be obscured by those in both extremes of their prevalence (i.e. present in almost all samples or those present in very few samples), the taxa were categorised into three groups: 'prevalent', 'intermediate', and 'rare' taxa based on their sample prevalence across all cardinal point samples. Prevalent taxa were defined as ASVs present in >90% of samples. Rare taxa were defined as ASVs present in <1% of samples. Intermediate taxa were defined as the remaining ASVs present in ≤90% and ≥1% of samples. All analyses were performed on the intermediate and full datasets, except for the differential abundance analysis which was only done on the full dataset.

The "robust Aitchison method" is a beta diversity metric that uses centred-log ratio transformation and matrix completion to handle the high compositional sparseness and non-normality of microbiome datasets (Martino et al. 2019). This method was applied to ASV tables via the *rpca* function in the 'gemelli' plugin v0.0.12 (Martino et al. 2019) in QIIME v2023.5 (Bolyen et al. 2019) to generate two pairwise distance matrices: (1) distances between all cardinal point samples (*n* = 384), henceforth referred to as the "cardinal point robust Aitchison distance matrix", and (2) distances between trees (*n* = 96), where the arithmetic mean read count of each ASV was computed for each tree (the average of the four cardinal point samples), referred to as the "tree-scale robust Aitchison distance matrix". These two matrices were used to quantify the variation in community composition at the cardinal point and tree scales and to visualise the compositional differences among cardinal points and among trees via Principal Component Analysis (PCA).

3.2.5.1 What is the spatial variation in soil microbial community composition and diversity surrounding kauri trees among individual trees, plots, and sites?

To determine the spatial variation in microbial community composition among cardinal point samples across all individual trees (tree-level), plots, and sites, permutational multivariate analysis of variance (PERMANOVA) was used on the cardinal point robust Aitchison distance matrix with a nested design to restrict permutations and account for the nested structure of the sampling design.

The PERMANOVA was implemented using the *adonis2* function in the R 'vegan' package v2.6.8 (Oksanen et al. 2020), and permutations were restricted using the 'permute' package v0.9.7.

For alpha diversity analysis, intermediate sequence reads were first rarefied to an even depth using the *rarefy_even_depth* function from the 'phyloseq' package v1.48.0 (McMurdie and Holmes 2013). Alpha diversity was then estimated using two indices, Shannon diversity and observed richness, using the *estimate_richness* function from the 'phyloseq' package. To determine the variation of diversity across spatial scales, the Shannon and observed richness indices were converted to pairwise distance matrices using Euclidean distances and used as input into variation partitioning analysis via distance-based redundancy analysis (db-RDA) using the *varpart* function from the 'vegan' package (Borcard et al. 1992).

3.2.5.2 Does microbial community composition and diversity in soil surrounding kauri trees differ significantly among trees of different health status?

Due to the low sample size of cardinal point samples around the five dead trees (*n* = 20 samples), these samples were combined with the defoliated samples to create the "unhealthy" group (bacteria: *n* = 296, fungi: *n* = 285); differences in samples in bacterial and fungal datasets is due to the removal of samples with <1000 reads (four samples from the bacterial dataset and 17 samples from the fungal dataset). Due to the lack of power, only the results for the two-level grouping (healthy, unhealthy) are presented where statistical significance testing was conducted. However, all analyses were repeated using the original tree health groups: healthy, defoliated, and dead.

To assess ASVs that were shared and unique amongst the health status groupings (dead, defoliated, and healthy), Venn diagrams were created using the *ggVennDiagram* function from the 'ggVennDiagram' package v1.5.3 (Gao et al. 2024).

A PERMANOVA was performed on the tree-scale robust Aitchison distance matrix to quantify the differences in community composition between healthy and unhealthy trees, using 999 permutations via the *adonis2* function of the 'vegan' package. Differences in community alpha diversity at the tree scale were tested with Wilcoxon tests on values from Shannon diversity and observed richness indices from the rarefied data.

Differential abundance analysis was conducted using only the full (all taxa) bacterial and fungal datasets using the *ancombc2* function from the 'ANCOMBC' package v2.6.0 (Lin and Peddada

2024). To aid in handling zero count taxa that are prevalent in microbiome data sets, the ANCOM-BC2 workflow applies several strategies. All structural zeroes are identified and undergo no further analysis. A prevalence-based filtration is implemented to remove taxa that are present in less than 10% of samples. Finally, the addition and assessment (sensitivity analysis) of a pseudo-count to taxa with remaining zeros. Pseudo-counts are assessed to determine whether the significant difference in the taxon's differential abundance changes in addition of the pseudo-count. If the *P*-value remains consistent (showing significance or non-significance) with tests excluding the zero counts, the taxon is considered not sensitive to the pseudo-count and passes the sensitivity testing. Only ASVs passing this sensitivity score filter were considered as differentially abundant.

3.2.5.3 Which soil physicochemical properties correlate with microbial composition and diversity in soils surrounding kauri trees of different tree health status?

To match the scale of the physicochemical measurements (one sample per tree), the tree-scale robust Aitchison distance matrix was used for the following analyses to make sure the microbial and environmental data were compared at the same minimum spatial scale. Variation partitioning analysis via db-RDA was conducted using the *varpart* function from the 'vegan' package to quantify the community composition variance explained by the soil physicochemical properties, elevation, and spatial scales site and plot. Before analysis, all soil physicochemical properties were standardised (method = 'standardise') using the *decostand* function from the 'vegan' package. The categorical variables site and plot were coded as a single dummy variable, e.g., Huia-plot-1. The spatial location of each tree was included as *x*-*y* coordinates in the NZ Transverse Mercator projection (metres). To understand the relationship of individual environmental variables with tree-scale community composition, the environmental variables were projected onto the tree-scale robust Aitchison PCA ordination via the *envfit* function from the vegan package using 999 permutations and only retaining environmental variables that were significantly correlated ($P < 0.05$).

3.3 Results

3.3.1 General characteristics of bacterial and fungal communities

A total of 15,690,282 bacterial and 7,014,423 fungal reads were retained after quality filtering and processing. These were classified into 52,759 bacterial ASVs consisting of 39 phyla, 302 families, and 620 genera, and 18,201 fungal ASVs comprising 14 phyla, 280 families, and 643 genera. The spread of ASVs across the three prevalence taxa groupings (prevalent, intermediate, and rare taxa) for both bacterial and fungal communities showed the highest number of ASVs in the rare taxa

groupings and the largest number of sequences in the intermediate taxa groupings (Table B2; Appendix B).

3.3.2 Spatial variation in community structure was highest at the tree-level scale

Spatial variation in both bacterial and fungal community composition was primarily at the scale of tree-level, i.e., differences among samples taken at the four cardinal points around the same tree, PERMANOVA R^2 = 0.46 and 0.39 for bacterial and fungal data, respectively; refer to 'Site:plot:tree' (Table 3.1). Variation among trees and among sites was much lower for bacterial and fungal communities (Table 3.1). Similarly, variation in Shannon's diversity index and observed richness for both bacteria and fungi were highest among samples taken around the same trees (db-RDA R^2, bacteria: 0.23, fungi: 0.25) and lower among trees within plots and among sites (Figure 3.1, Figure B2; Appendix B).

Table 3.1: Nested PERMANOVA results summary for spatial scale variation amongst sites (*n* = 3), plots (*n* = 6), trees (*n* = 96) of robust Aitchison dissimilarity matrices for bacterial and fungal intermediate datasets (taxa in ≥1% and ≤90% of samples). Permutations were restricted within plots and sites. R^2 values represent the amount of variation in the community structure explained by different spatial scales.

	Bacteria				
	Degrees of freedom	**Sum of Squares**	**R^2**	**pseudo-F**	***P*-value**
Site	2	85.2	0.11	60.5	< 0.001
Site:plot	3	144.2	0.18	68.3	< 0.001
Site:plot:tree	90	366.6	0.46	5.8	< 0.001
Residual	284	199.8	0.25		
	Fungi				
	Degrees of freedom	**Sum of Squares**	**R^2**	**pseudo-F**	***P*-value**
Site	2	263.7	0.32	233.9	< 0.001
Site:plot	3	73.6	0.09	43.5	< 0.001
Site:plot:tree	90	312.1	0.39	6.2	< 0.001
Residual	284	152.8	0.19		

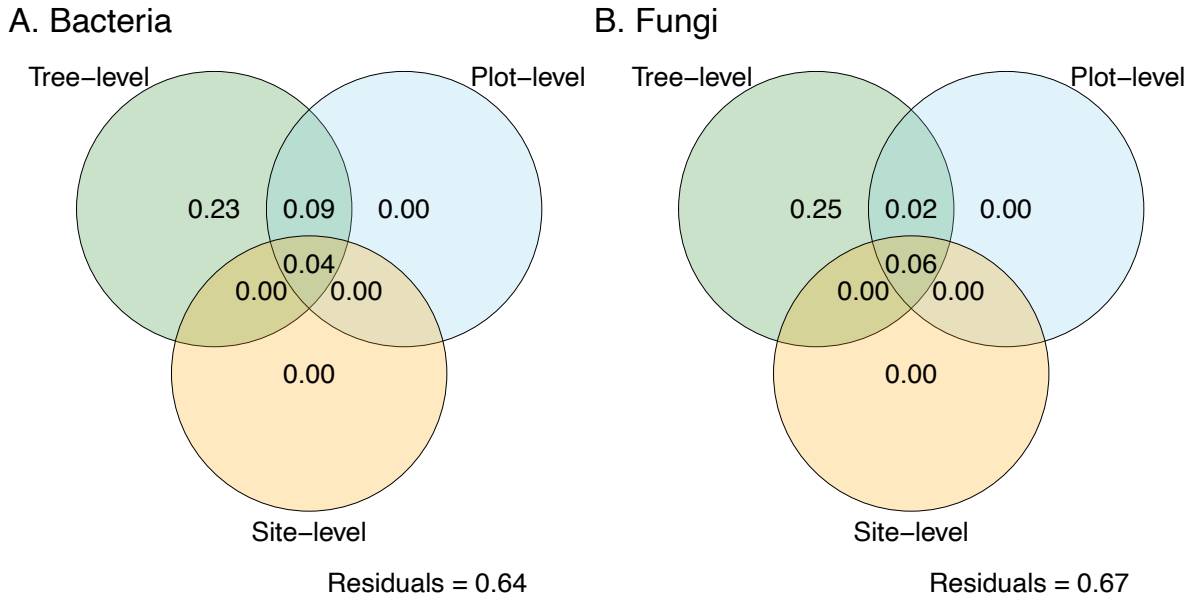

Figure 3.1: The amount of variation in (A) bacterial and (B) fungal community diversity across three spatial scales: site-level (*n* = 3), plot-level (*n* = 6), and tree-level (*n* = 96) determined by variation partitioning analysis using db-RDA on the Euclidean distance matrix of Shannon indices. This figure is based on the intermediate taxa dataset (taxa in ≥1% and ≤90% of samples). Samples were rarefied to an even depth (775 and 596 reads for bacteria and fungi, respectively).

3.3.3 ASV abundance and fungal diversity, but not bacterial diversity or composition, was associated with tree health status

Overall, the analyses of community structure (ASV composition and diversity) comparing the communities in soils associated with trees of different health status showed that (1) a subset of bacterial and fungal taxa were ubiquitous and highly abundant in soils, regardless of the health status of the associated tree (Figure 3.2 and Figure B3; Appendix B), (2) ASV composition and diversity did not differ significantly among soils near trees of different health status, with the exception of fungal diversity (Figure 3.3 and Figure B4; Appendix B), and (3) some bacterial and fungal taxa were significantly positively or negatively associated with trees of different health status (Figure B5; Appendix B). Results of the full dataset were broadly consistent with those from the intermediate dataset, with only minor shifts in the rank order of the most abundant phyla (Figure B6, Figure B7, and Figure B8; Appendix B).

3.3.3.1 Certain taxa were ubiquitous and highly abundant in soils, regardless of tree health status

Of the 9,331 bacterial and 3,733 fungal ASVs identified from soil samples collected around kauri trees, 38.95% of bacterial ASVs, and 31.97% of fungal ASVs were shared amongst soils around healthy, defoliated, and dead trees (Figure B9; Appendix B). Soil samples around defoliated trees contained the largest number of unique ASVs (13.65% bacterial, 16.64% fungal ASVs). Followed by

healthy trees, with only 30 unique bacterial ASVs (0.32%) and 26 fungal ASVs (0.7%). Only one unique bacterial ASV and two unique fungal ASVs were identified in soils around dead trees, noting that the number of samples collected from this category was small (*n* = 20).

The most abundant bacterial phylum, shared among trees of all health status groups, was Verrucomicrobiota, comprising ~37% of total reads in the soil samples around healthy, defoliated, and dead trees (Figure B3A; Appendix B). The next most abundant phyla shared across the health status groups were Planctomycetota (~30%) and Acidobacteriota (~10%). At the genus level, the two most abundant bacterial taxa shared among all health status groups, were *Candidatus Udaeobacter* (~30%) and *Candidatus Xiphinematobacter* (~3%, Figure B3B; Appendix B). For the fungal community, the most abundant phyla were Ascomycota (~70%) and to a lesser degree, Basidiomycota (~20%), and Mortierellomycota (~8%, Figure B3C; Appendix B). Fungal genera shared among soil samples from around trees of all health statuses were primarily associated with the *Mortierella* (~5%) and *Leohumicola* (~3%, Figure B3D; Appendix B) genera.

The six most abundant bacterial phyla were present in soil samples taken around trees from all three health status groups (Figure 3.2A). Phyla below 1% mean relative abundance showed variable occurrence across the health status groups, whereby some bacterial phyla were observed at a higher occurrence with soil around dead trees, such as Latescibacterota and Sumerlaeota. Methylomirabilota were observed to have a higher occurrence in soils around healthy and dead trees; Cyanobacteria were observed more in soils around healthy and defoliated trees (Figure 3.2A).

Similarly, the top three most abundant taxa in the intermediate fungal dataset occurred in soil samples taken from around trees in all three health status groups (Figure 3.2B). Kickxellomycota occurred less in soils around dead trees, and Chytridiomycota occurred less in soil around healthy trees. Taxa of mean relative abundance below 0.1% were low in occurrence across soil samples from healthy, defoliated, and dead trees. However, Glomeromycota and Basidiobolomycota were slightly more occurrent in samples from around dead trees than defoliated or healthy trees (Figure 3.2B).

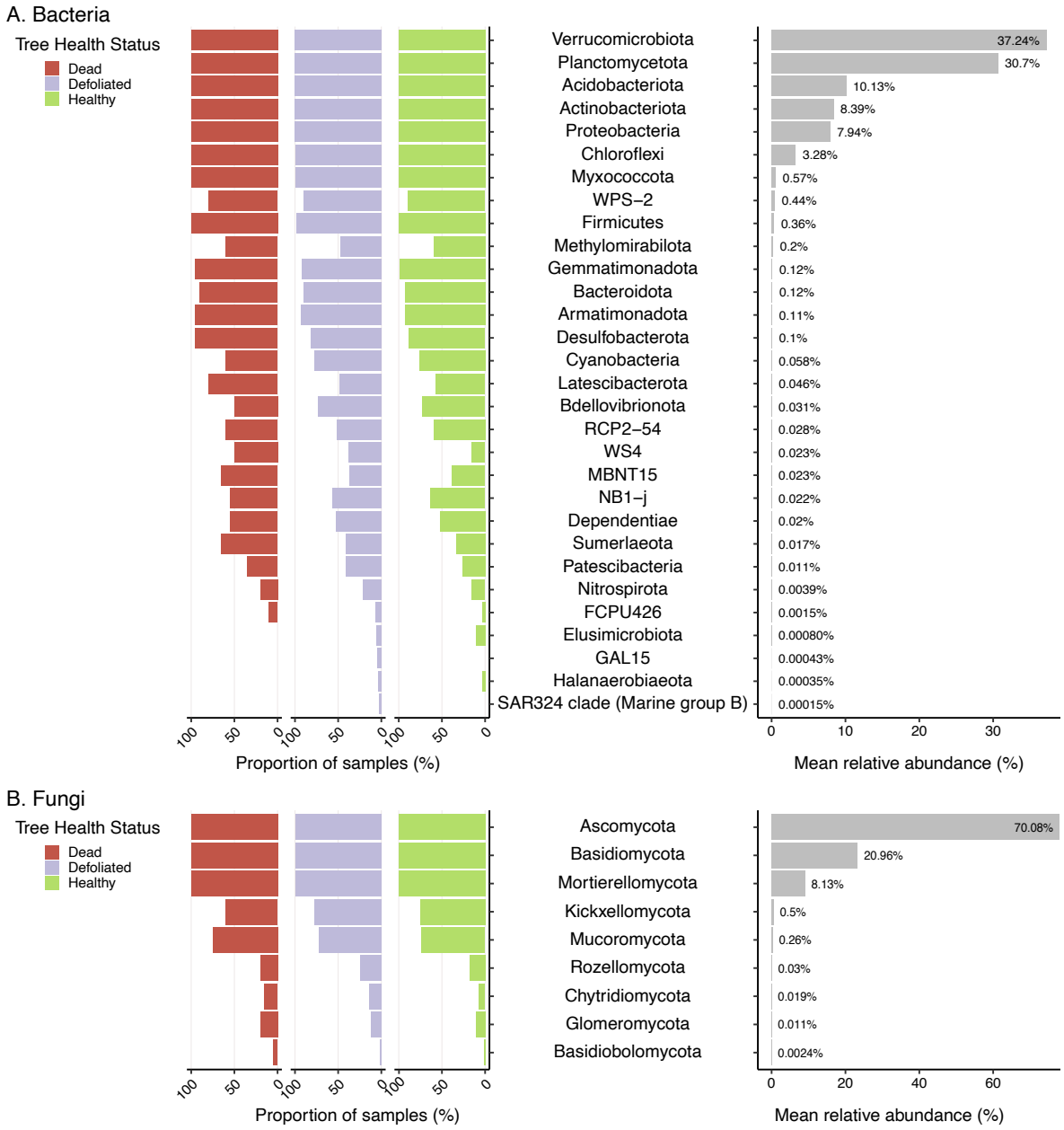

Figure 3.2: The representativeness of (A) bacterial and (B) fungal phyla detected in samples grouped by tree health status (dead: *n* = 20, healthy: *n* = 84, defoliated: bacterial dataset *n* = 276, fungal dataset *n* = 265). This figure is based on the intermediate taxa dataset (taxa in ≥1% and ≤90% of samples).

3.3.3.2 Soils around healthy and unhealthy trees showed similar level of alpha diversity

Similar bacterial alpha diversity, as estimated by Shannon index and observed richness (at ASV level), were found in soil microbial communities in the healthy and unhealthy groups (Wilcoxon, $P > 0.05$) (Figure B4A; Appendix B). On the other hand, the fungal communities showed significantly higher alpha diversity (observed richness: Wilcoxon, $P < 0.05$) in the unhealthy tree group compared to the healthy tree group (Figure B4B; Appendix B).

3.3.3.3 Microbial community composition differed significantly based on site but not tree health

Bacterial and fungal community composition did not differ significantly at the tree scale for samples taken around healthy or unhealthy trees (PERMANOVA, bacteria: $P = 0.56$, fungi: $P = 0.80$). However, bacterial and fungal community composition did differ significantly for samples taken from different sites (PERMANOVA, bacteria and fungi, both $P < 0.001$). Visualisation of community composition at the tree scale did not show any distinct groupings based on tree health status for either fungal or bacterial communities, with samples clustering more based on site and plot (Figure 3.3). The fungal community from soil surrounding dead trees showed two distinct groupings based on the site of the trees, with the two dead trees from plot 1 of the Piha site, and the three dead trees from plot 1 of the Cascades sites, no dead trees were sampled at the Huia site (Figure 3.3B).

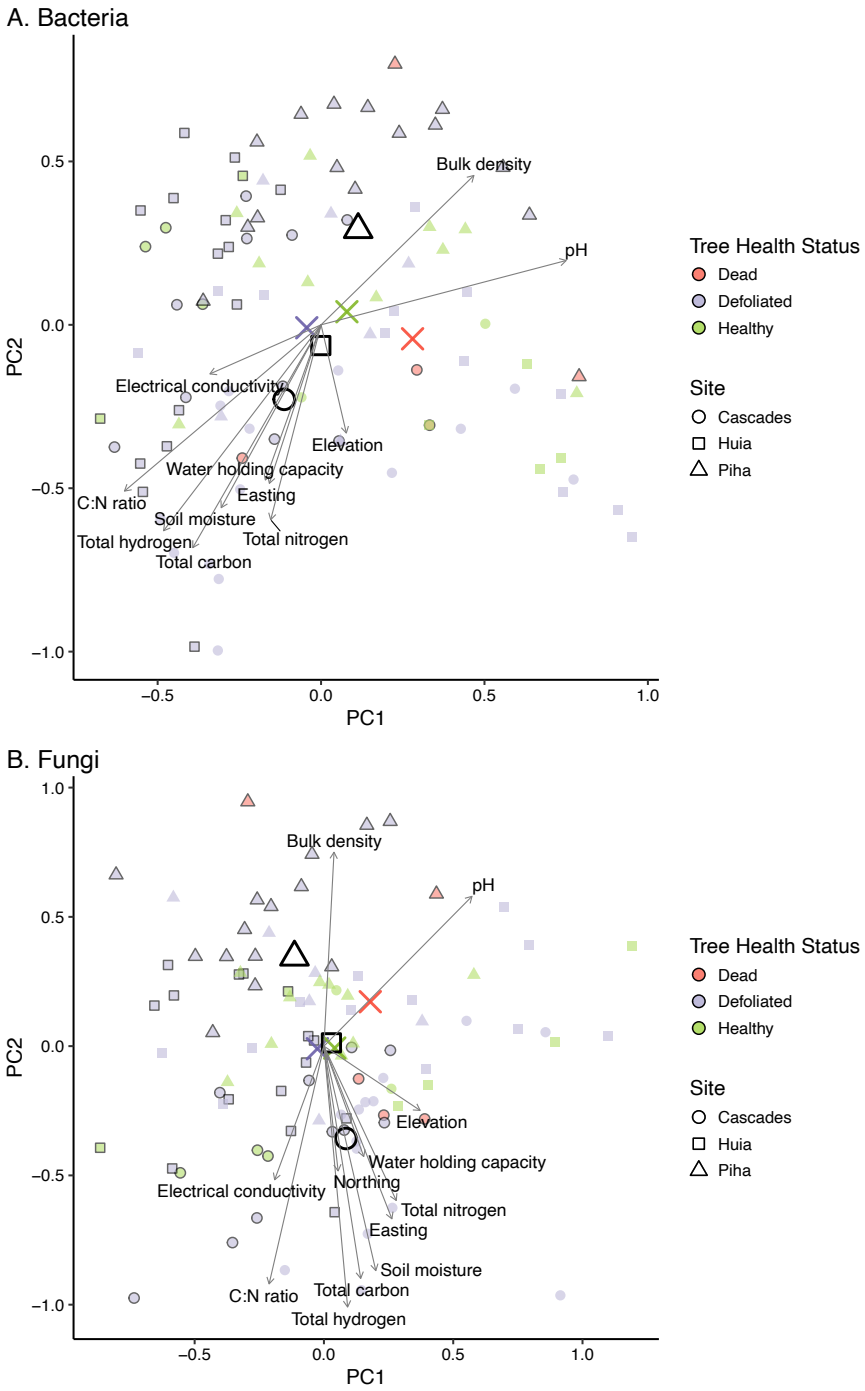

Figure 3.3: Robust Aitchison principal component analysis of (A) bacterial and (B) fungal community composition of the tree-scale robust Aitchison distance matrices of different tree health status groups, cardinal samples were combined per tree and ASV counts were averaged (dead: *n* = 5, healthy: *n* = 21, defoliated: *n* = 70). This figure is based on the intermediate taxa dataset (taxa in ≥1% and ≤90% of samples). Black borders indicate plot number, presence of black border = plot 1, no black border = plot 2. Larger shapes represent centroids of the sites. Large crosses indicate centroids of tree health status communities. Environmental variables were overlaid as vectors calculated using the *envfit* function via the vegan R package onto the ordination and only factors that were significantly correlated ($P < 0.05$) with ordination axes were included. Physicochemical data of soils were generated by (Mohini 2024).

3.3.3.4 Some taxa were notably associated with different tree health conditions

In total, 333 bacterial and 54 fungal ASVs were identified as differentially abundant among soil samples around trees classified as healthy or unhealthy (Figure B5; Appendix B). There were 185 bacterial ASVs and 21 fungal ASVs that were more abundant in soils surrounding healthy trees. The six bacterial ASVs with the greatest differential abundance (≥ 1.0 log fold change) surrounding unhealthy trees belonged to the Planctomycetota, Acidobacteriota, Proteobacteria and Verrucomicrobiota phyla (Figure 3.4A). Two bacterial ASVs had the largest differential abundance (≤ -1.0 log fold change) surrounding healthy trees, both belonging to the Verrucomicrobiota phylum. Of the three fungal ASVs that showed the largest differential abundance (≤ -1.0 log fold change) in healthy trees, they belonged to the Ascomycota, Basidiomycota, and unclassified phyla (Figure 3.4B). Four fungal ASVs showed high differential abundance (≥ 1.0 log fold change) in unhealthy trees, mostly belonging to the Ascomycota phylum.

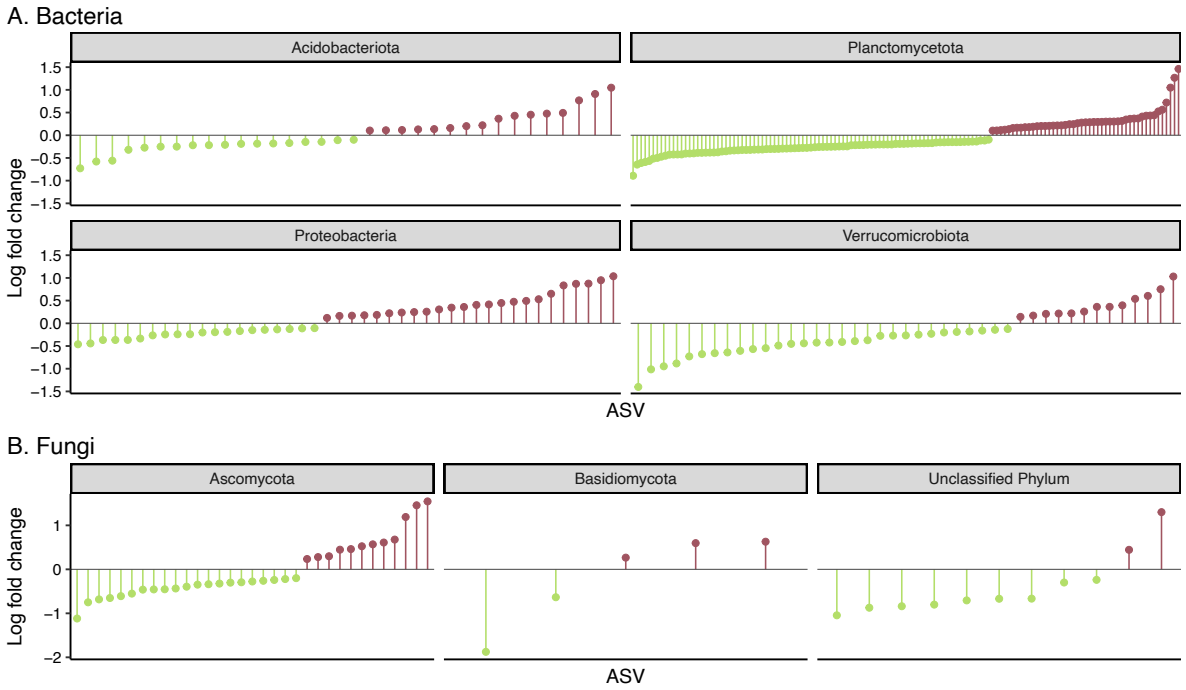

Figure 3.4: (A) Bacterial and (B) fungal ASVs, grouped at the phylum level, passing ANCOM-BC2 sensitivity scoring, showing the greatest differential abundance (|log fold change| > 1) between tree scale samples collected around healthy and unhealthy (combined defoliated and dead samples) trees. This analysis is based on the full dataset after ASVs present in less than 10% of samples were removed. Green data points indicate an increase in the abundance of ASVs in soils surrounding healthy trees, and red data points indicate an increase in the abundance of ASVs in soils surrounding unhealthy trees (defoliated and dead trees). All differentially abundant ASVs may be viewed in Figure B5.

3.3.4 Soil physicochemical properties were associated with bacterial and fungal community composition

Variance partitioning using db-RDA showed that soil physicochemical properties alone explained 36% and 25% of variance in the bacterial and fungal microbial communities, respectively, at the tree scale (Figure 3.5). The explained variance increased to 48% (bacteria) and 43% (fungi) with the inclusion of elevation and sites and plots. Independently, the spatial factor 'sites and plots' explained 23% and 21% of the variation in the community composition of bacteria and fungi, respectively (Figure 3.5). Environmental vector analysis showed that pH and electrical conductivity were strongly associated with the first principal component for bacterial composition; total nitrogen, elevation and water holding capacity were strongly associated with the second principal component (Figure 3.3A, Table B3; Appendix B). For fungal composition, elevation and pH were strongly associated with the first principal component (Figure 3.3B, Table B3; Appendix B). All environmental variables were associated with the second component. Sites differed markedly in soil moisture, electrical conductivity and elevation (Table B4; Appendix B).

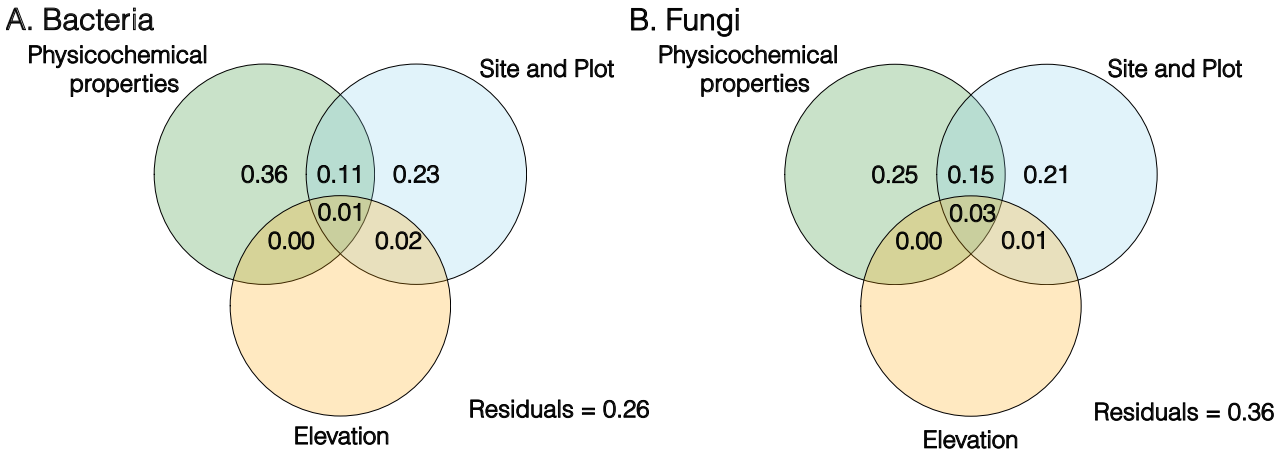

Figure 3.5: The amount of variation in (A) bacterial and (B) fungal community composition that could be explained by physicochemical properties (pH, total carbon, total nitrogen, total hydrogen, carbon to nitrogen (C:N) ratio, electrical conductivity, bulk density, and water holding capacity), site and plot, and elevation. Values less than 0 are not shown. This figure is based on the intermediate taxa dataset (taxa in ≥1% and ≤90% of samples).

3.4 Discussion

Our study shows that spatial variation in microbial community structure was greatest at the scale of tree-level, while variation between plots and sites was lower. Tree health status was not strongly associated with microbial community composition or diversity, with most taxa shared across soils from healthy, defoliated, and dead trees. However, some ASVs showed health-associated abundance patterns. Environmental variables, including soil moisture, pH, electrical conductivity,

and elevation, differed among sites and were strongly associated with differences in microbial community composition. By providing a comprehensive view of microbial community structure across spatial scales and diseased trees, these findings contribute to a deeper understanding of the ecological dynamics of soil microbiomes in forest ecosystems under threat from disease and environmental change.

3.4.1 Microbial community structure across spatial scales

Across the three spatial scales sampled, variation for both bacterial and fungal communities was highest among samples at the tree-level scale. Around individual trees (differences among samples taken at the four cardinal points around the same tree), bacterial and fungal communities varied in their composition and their diversity. It has been well established that the spatial scale of observations, both at the macro- and micro-scale, affect the perception of variation in soil microbial community composition (Averill et al. 2019; O'Brien et al. 2016; Zhang et al. 2020).

This result suggests that environmental factors that vary at a fine scale affect these communities' composition and diversity. These factors may include interactions with plant root systems and exudates (Adamczyk et al. 2021; Seitz et al. 2022) or the presence of a root-rotting plant pathogen (Gómez-Aparicio et al. 2022). Previous studies have shown that variations in localised environmental factors such as soil moisture, nutrient availability and pH are important drivers of microbial community structure (Fierer and Jackson 2006; Karimi et al. 2018).

In this study, some variation in microbial composition and diversity occurred at the among-plot and among-site scales, suggesting that factors varying at these larger spatial scales also influence microbial community structure. At these coarser spatial scales, fungal communities showed greater variation at the site level than the bacterial communities. This pattern is consistent with the idea that fungi are more tightly coupled to host plants and dominate decomposition of recalcitrant litter, making them more responsive to gradients in vegetation composition, litter quality, soil moisture, elevation, and temperature (Baldrian 2017; Liu et al. 2020a; Tedersoo et al. 2014; Urbanová et al. 2015; Yang et al. 2024). Studies indicate that fungi are more strongly filtered by spatial distances than bacteria (Liu et al. 2022; Zhang et al. 2020), and site-level differences in dominant tree species and litter inputs are associated with fungal community turnover (Marañón-Jiménez et al. 2021; Meng et al. 2024; Urbanová et al. 2015). These ecological strategies likely make fungal communities more sensitive to these coarser-scale biotic and abiotic gradients. Together,

these mechanisms may explain why fungal assemblages exhibited stronger site-level structuring than bacterial communities.

3.4.2 Tree health status and microbial community structure

Interestingly, tree health status was related to aspects of microbial community structure. Taken together, the results indicate that tree health is associated with subtle taxon-specific shifts against broad compositional stability at the community level. The stronger response in fungal richness relative to bacteria may be associated with increased litter fall and organic matter inputs, while the enrichment of certain taxa suggests a targeted reorganisation rather than distinct community turnover under declining tree health.

Such shifts in bacterial and fungal presence and abundance indicate that these communities may respond to changes in tree health. Prolonged infection by *P. agathidicida* leads to root rotting, canopy chlorosis and defoliation (Bellgard et al. 2013; Waipara et al. 2013). The woody and leaf litter deposited by kauri are acidic, tannin-rich and slow to decompose (Enright and Ogden 1987; Wyse and Burns 2013). Accumulation of this litter results in acidic mor humus formation under mature trees (Silvester 2000). As prolonged infection of kauri by *P. agathidicida* results in defoliation, the increased deposits of kauri leaf litter on the forest floor may contribute to the shifts in these microbial communities by altering available nutrients and pH. Soil environments are known to be influenced by their inhabiting plant communities due to their deposits onto the forest floor, including litterfall and their root exudates (Adamczyk et al. 2021; Veen et al. 2021). Previous experimental work has shown that the bacterial phylum Firmicutes and fungal phyla Mortierellomycota and Rozellomycota had significantly higher relative abundance in kauri seedling soils inoculated with *P. agathidicida* (Byers et al. 2021b). In contrast, previous field-based work showed an increased abundance of the bacterial phyla Firmicutes and Proteobacteria in soils surrounding asymptomatic soils (Byers et al. 2020b). Our results also showed an increase in the abundance of Firmicutes in soils around unhealthy trees. However, we also identified several other bacterial ASVs that showed significant increases in differential abundance belonging to the Verrucomicrobiota and Proteobacteria phyla. These bacterial phyla are involved in the successional stages of litter decomposition and may respond to the increased litter deposited on the forest floor under unhealthy trees (Buresova et al. 2019). Fungal phyla showing the greatest differences in abundance aligned with previous field-based work showing Ascomycota and Basidiomycota responding with variable abundance in soils surrounding both symptomatic and asymptomatic trees (Byers et al. 2020b).

Although overall community composition did not differ significantly among tree-health categories, bacterial alpha diversity tended to be highest in soils beneath healthy trees, whereas fungal richness was higher beneath unhealthy trees. This shift in diversity may be associated with declining tree health altering resource inputs and microenvironments in the surrounding soils. As tree health declines, root exudate flux and composition may be altered (Lamichhane et al. 2024; Rolfe et al. 2019), and litter inputs increased, shifting edaphic conditions and substrate quality (Tahovská et al. 2024; Veen et al. 2021). These changes may favour saprotrophic fungi, thereby increasing fungal diversity around unhealthy trees (Byers et al. 2020b; Gómez-Aparicio et al. 2022). Applying shotgun metagenomics would provide an additional analysis to evaluate these mechanistic shifts, allowing direct assessment of the functional potential of these communities to assess the metabolic shifts occurring under a gradient of tree health.

3.4.3 Association with environmental variables

The three sites differed in elevation and soil conditions, which reflected differences in bacterial and fungal community composition. In contrast, soil physicochemical properties overall did not vary significantly between different tree health groups, consistent with findings from other kauri forests systems (Byers et al. 2020b). More broadly, the observation that microbial communities differ among sites with contrasting soil conditions aligns with patterns reported in other soil microbiome studies (Hermans et al. 2020; Louisson et al. 2024; Mészárošová et al. 2024). Variation in microbial community structure was strongly associated with soil physicochemical factors. pH, electrical conductivity, and total nitrogen emerged as key drivers of both bacterial and fungal composition, explaining approximately 50% of the variation in bacterial communities and 44% in fungal communities. These results highlight the dominant role of edaphic conditions in shaping microbial assemblages, consistent with global studies showing soil chemistry as one of the strongest predictors of microbial diversity and composition (Bahram et al. 2018; Delgado-Baquerizo et al. 2017; Fierer and Jackson 2006). The prominence of pH in structuring soil microbiomes is well established in global datasets, whereas nutrient availability (e.g. nitrogen) and electrical conductivity drive additional, context-specific shifts in community composition (Fierer and Jackson 2006; Rath et al. 2018; Rousk et al. 2010; Wang et al. 2023b). Together, these findings reinforce the view that while pathogens and host health can influence microbial communities in targeted ways, the underlying soil conditions remain a dominant filter determining broad patterns of community structure.

3.4.4 Implications and considerations for future research

The observed shifts in microbial community composition associated with tree health decline have important ecological implications for kauri forests. As kauri dieback disease spreads, the resulting changes in soil microbial communities could alter nutrient cycling processes, decomposition rates, and plant-microbe interactions, potentially affecting forest regeneration and ecosystem resilience. Moreover, the differential abundance of certain microbial taxa in soils surrounding unhealthy trees raises questions about the potential roles of these microbes in either mitigating, exacerbating or predisposing tree decline. The low number of dead trees in the study was due to sampling within pre-established plots and sites. Future work should include more dead trees to fully quantify the distinct communities associated with these soils.

Future research should focus on a deeper identification of the differentially abundant taxa, as well as elucidating the functional roles of these taxa, particularly those associated with declining tree health. Investigating the interactions between pathogenic and beneficial microbes and their effects on tree physiology and soil processes will be key to understanding the mechanisms driving tree mortality in kauri forests. Additionally, exploring the potential for microbial-based interventions, such as biocontrol agents or soil amendments, could offer new strategies for managing kauri dieback and supporting forest health.

3.5 Conclusion

With the increasing stress that invasive pathogens impose on forest ecosystems, the role of the belowground microbial community remains a significant gap in our understanding of how ecosystems will respond to such a threat. This study begins to address the need for studies, particularly for systems outside of Europe and North America, on pathogen-driven tree decline and the effects of this on soil microbial communities. Here, we reveal variation in soil microbial communities in soils surrounding kauri trees of varying health status across different spatial scales. Differences in microbial abundance and fungal diversity but not microbial composition were associated with the health of kauri trees, suggesting that microbial communities may play a role in the ecological processes underpinning the soil-plant interactions altered by disease.

Chapter 4

Soil microbial functional potential in kauri forests is shaped by spatial and physicochemical gradients more than tree health decline

Author names

Zoe King [a], Hannah L. Buckley [a], Gavin Lear [b], Brent Seale [a], Kevin C. Lee [a], Donnabella Lacap-Bugler [a]

Author affiliations

[a] School of Science, Auckland University of Technology, Auckland CBD, Auckland, 1010, New Zealand

[b] School of Biological Sciences, University of Auckland, Auckland CBD, Auckland, 1010, New Zealand

Code availability

All code used in this chapter can be found in the following GitHub repository https://github.com/zoesking/kauri-soil-shotgun

Abstract

Soil microbial communities underpin key ecosystem processes such as decomposition and nutrient cycling, yet the influence of declining tree health on their functional potential remains poorly understood, particularly in Southern Hemisphere forests. Kauri (*Agathis australis*) tree dieback, caused by *Phytophthora agathidicida*, provides a case study for examining how declining tree health, together with spatial context and soil physicochemical conditions, is associated with variation of the functional potential of soil microbial communities. Soils were collected from 96 kauri trees across three sites in the Waitākere Ranges. Shotgun metagenomic sequencing was applied, generating over 11.3 billion high-quality reads and predicting over 11 million non-redundant genes. Functional annotation against eggNOG, CAZy, and NCyc databases revealed a broad representation of microbial functional potential, spanning core cellular processes, carbohydrate-active enzymes, and nitrogen cycling pathways. Multivariate analysis showed that the functional gene composition was significantly associated with soil physicochemical gradients, particularly total carbon, nitrogen, C:N ratio, and hydrogen, and by spatial context, with variation partitioning attributing 16% of functional gene compositional variation to edaphic factors and 10% to site and plot. Tree health had a smaller influence, manifesting as subtle compositional shifts rather than losses in overall functional potential. Soils around healthy trees were significantly enriched with genes associated with replication, cell wall biogenesis, energy production, carbohydrate degradation, nitrate reduction, and denitrification, as shown by differential abundance analysis. In contrast, soils around unhealthy trees contained fewer types of enriched genes, which were mainly associated with amino acid, coenzyme, and nucleotide metabolism. Despite elevated pools of total carbon and nitrogen beneath unhealthy trees, these soils showed reduced enrichment of decomposition and nitrogen-cycling genes, consistent with lowered nutrient turnover efficiency. Our findings indicate that kauri forest soil microbial functional potential is most strongly associated with spatially structured physicochemical gradients, while tree health shows a secondary, but detectable, association.

Key words: Soil microbial communities, shotgun metagenomics, functional potential, kauri dieback, tree health decline, soil physicochemical gradients, nutrient cycling

4.1 Introduction

Soil microbial communities are fundamental drivers of ecosystem processes, mediating the decomposition of organic matter, nutrient mineralisation, and the cycling of key elements such as carbon and nitrogen (Bani et al. 2018; van der Heijden et al. 2008). In forest systems, these communities help regulate carbon storage, influence greenhouse gas fluxes, and sustain nutrient availability for plant growth (Lladó et al. 2017; Singavarapu et al. 2023; Zhao et al. 2019). Disturbances to the forest soil microbiome, whether from vegetation change, land-use modification, climate change, or pathogen invasion, can disrupt microbial functions and potentially cause long-term shifts in ecosystem processes (Fichtner et al. 2014; Holden and Treseder 2013; Osburn et al. 2019; Osburn et al. 2023). At the same time, microbial functions are strongly influenced by soil physicochemical conditions, which act as filters determining the availability of resources and the efficiency of microbial metabolism (Cheng et al. 2021; Cline and Zak 2015; Sheng et al. 2025). The impacts of tree-borne diseases on the health and functioning of underlying soil microbial communities has been poorly studied to date, especially in Southern Hemisphere forests. Understanding how soil microbial communities respond to changing forest conditions is therefore critical for assessing potential impacts and ecosystem trajectories under disturbance.

Trees affected by biotic or abiotic stressors can alter surrounding microbial communities through changes in both the quality and quantity of organic inputs into the soil. Infected or declining trees often show increased litter fall, altered root exudation, and basal bleeding/gummosis, each of which introduce substrates and secondary metabolites into the soil that reshape nutrient availability and microbial metabolism (Glassman et al. 2018; Lamichhane et al. 2024; Van Tran et al. 2023; Yin et al. 2014). Across different disturbance contexts, these inputs have been linked to changes in soil moisture and chemistry, and the balance of carbon and nitrogen turnover (Custer et al. 2020; Mikkelson et al. 2016; Sapsford et al. 2021). Changes to these edaphic conditions between healthy and symptomatic trees has also been linked with changes in microbial community taxonomic composition (Gómez-Aparicio et al. 2022; Ruiz Gómez et al. 2019), and changes in the functional potential of the communities (Byers et al. 2020b; Qu et al. 2020). However, taxonomic change does not always translate into altered function. High microbial diversity is proposed to confer functional redundancy, whereby multiple taxa perform overlapping roles, buffering core ecosystem processes against compositional turnover (Allison and Martiny 2008; Louca et al. 2018). This functional redundancy has been observed in several forest systems after disturbance events (Lan et al. 2021; Mendes et al. 2015; Mikkelson et al. 2017). Therefore, determining when tree health decline leads

to functional shifts versus redundant reconfiguration is central to interpreting the potential long-term effects of forest disturbances.

Additionally, soil microbial and pathogen communities are not randomly distributed; they exhibit distinctive spatial clustering and track environmental gradients across both micro- and macro-spatial scales (O'Brien et al. 2016; Shen et al. 2020; Xia et al. 2020). Processes such as dispersal limitation, local drift, and environmental filtering by edaphic conditions generate background structure to these microbial communities that could mimic or mask apparent effects of tree health. Thus, spatial and edaphic factors constitute necessary controls in attributing variation to tree health effects.

In New Zealand, kauri (*Agathis australis*) is a foundation tree species that supports a unique forest ecosystem, characterised by the accumulation of acidic, tannin rich litter that is slow to decompose (Jongkind et al. 2007; Verkaik et al. 2006; Wyse et al. 2014). These forests are increasingly threatened by kauri dieback, a disease caused by the soil-borne oomycete *Phytophthora agathidicida*, which leads to root rot, canopy decline, basal bleeding/gummosis, and eventual tree death (Beever and Bellgard 2010; Bellgard et al. 2016a; Waipara et al. 2013; Weir et al. 2015). With limited studies conducted on the functional potential of microbial communities around kauri trees, questions still remain on how these soil microbial communities may respond to tree decline and whether shifts in microbial functions may feedback on ecosystem processes. This gap is particularly important given that altered litter inputs, soil chemistry, and microbial activity under declining trees could influence nutrient cycling and carbon storage.

Microbial functions in kauri soils have previously been characterised using GeoChip technology, a targeted microarray approach used to profile a defined set of environmentally relevant genes (Byers et al. 2020b; Lawrence et al. 2023). Only one study to date has compared the microbial functional potential between kauri trees affected by dieback (Byers et al. 2020b). This previous study focused on carbon and nitrogen cycling genes, finding significant differences in the composition and abundance of these genes between soils around symptomatic and asymptomatic kauri. Based on their findings, they suggest that there is an increase in carbon degradation rates in soils around symptomatic kauri but could not find any reasonable conclusions of the impact tree dieback may have on nitrogen cycling capabilities. Although this previous study has provided a first look into the functional response the soil microbial community may be having to kauri dieback, it was limited to

40 trees encompassing the extreme ends of tree health (i.e. trees at the late stages of disease expression) and only focused on a restricted set of carbon and nitrogen cycling genes.

To date, no studies have applied shotgun metagenomics to examine the broad functional potential of prokaryotic communities in soils around kauri trees affected by dieback or quantified the variation against spatial location and environmental conditions. The shotgun metagenomics approach offers an opportunity to assess microbial functional diversity at a greater breadth and resolution and allows us to explore the relationships between microbial functional potential, tree health, and environmental context.

Here, we characterise the prokaryotic functional potential in kauri forest soils using shotgun metagenomics and investigate the drivers of variation. Combining shotgun metagenomic profiling with soil physicochemical analyses across spatial scales, we aimed to answer the following questions: (1) How does the functional potential of soil microbial communities around kauri trees vary spatially? (2) Is the spatial variation in soil physicochemical properties related to that of the functional potential of soil microbial communities around kauri trees? (3) Does the functional potential of soil microbial communities vary significantly with tree health status? (4) Which functional processes and gene families are most strongly associated with soil physicochemical properties and tree health in kauri forest soils? By addressing these questions, we aim to increase understanding of the possible drivers of spatial variation in soil prokaryotic functional gene composition.

4.2 Methods

4.2.1 Field sampling

Soil was collected around kauri trees from the Waitākere Ranges (Te Wao Nui ā Tiriwa), Auckland, New Zealand. Trees were selected from three separate long term monitoring sites within the Waitākere Ranges, named for the proximity to the Cascades, Piha, and Huia (Figure C1; Appendix C). Within each of these sites are two permanent vegetation plots, established between 2012 and 2021. Each plot was 40 × 50 m, containing four, 10 × 50 m subplots with all kauri trees within the plots tagged at the plot's creation. Four kauri trees from each subplot were randomly selected for sampling (n = 96) and sampling was undertaken from June to August 2021. Soil was collected at four cardinal points around each tree (n = 384), 1 m from the trunk using a hand trowel to a depth of 10 cm after removing woody and leaf litter (Hill et al. 2017). Each cardinal soil sample was collected in

its own sterile Whirl-Pak (Madison, WI, USA) before being transferred to a -20 °C freezer and stored until processing. Canopy scores were recorded based off an established five-point scoring system (Horner et al. 2019b), with additional half-point increments to help differentiate later stages of infection (Froud et al. 2022). Trees were further grouped into three categories based on their canopy scores: 1-2 “healthy” (*n* = 21), 2.5 – 4.5 “defoliated” (*n* = 70), and 5 “dead” (*n* = 5).

4.2.2 Soil DNA extraction and metagenome shotgun sequencing

DNA was extracted from the 384 soil samples using a DNeasy PowerSoil Pro Kit (Qiagen, Germany), following the manufacturer’s instructions. Nuclease-free water was used as a negative control for each batch of extractions (*n* = 14). DNA concentration was determined fluorometrically using Qubit double-stranded DNA BR assay kit (Thermo Fisher Scientific, Massachusetts, USA).

DNA extractions were concentrated to 10 ng/µL before pooling 10 µL of each cardinal point sample (*n* = 4 per tree) into one sample per tree (*n* = 96). These then underwent library preparation and sequencing at Livestock Improvement Corporation (LIC; Hamilton, New Zealand). Libraries were constructed using an Illumina DNA Prep Kit (Illumina, California, USA) and indexed using IDT for Illumina DNA/RNA UD Indexes (IDT, Iowa, USA). Library preparation was performed using a PerkinElmer Applied Genomics Zephyr® G3 NGS Workstation. Samples were sequenced on an Illumina NovaSeq 6000 S4 2 x 150bp flowcell. One sample (UC-D2) failed sequencing and was excluded from further analysis.

4.2.3 Quality control

Raw and demultiplexed reads were quality checked using the FastQC (https://www.bioinformatics.babraham.ac.uk/projects/fastqc/) and MultiQC tools (Ewels et al. 2016). Based on these results, reads were trimmed using the BBDuk script via BBTools v.39.01 (Bushnell 2017) to remove adapters, poor quality sequences, and PhiX reads (qtrim=rl, trimq=25, k=25, hdist=1). Following trimming, nontarget DNA was removed. Initially, human DNA was removed using the BBMap script via BBtools v.39.01 using the masked human reference genome, hg19 RefSeq assembly: GCF_000001405.13 (minid=0.95, maxindel=3, bwr=0.16, bw=12, quickmatch, fast, minhits=2, qtrim=rl, trimq=10, untrim). Additionally, plant and animal DNA was removed using Kraken2 v2.1.2 (Wood et al. 2019). The refseq database for plants was downloaded using kraken2-build --download-library command. Eight custom databases were built to remove animalia DNA using taxonomy information downloaded from NCBI: annelida, arthropoda, chordata, mollusca, nematoda, platyhelminthes, tardigrada, and oomycota. Trimmed reads were filtered through each

database and reads matching the databases were removed using the KrakenTools v1.2 (Lu et al. 2022) extract_kraken_reads.py script using the --include-children and --exclude flags. After filtering, approximately 91% of reads remained in each sample (Appendix C3 Supplementary File 1).

4.2.4 Contig assembly, gene prediction, and gene annotation

Pre-processed reads underwent separate assemblies (one assembly per sample) using MEGAHIT v1.2.9 (Li et al. 2016) using default parameters and a minimum contig length of 1000 bp. Assembly statistics for each sample can be viewed in Appendix C3 Supplementary File 1. Prokaryotic genes were predicted using Prodigal v2.6.3 (Hyatt et al. 2010) using default parameters. Gene coding sequences were then clustered at 95% sequence identity using CD-HIT-EST v4.8.1 (Fu et al. 2012) (parameters: -aS 0.9, -G 0, -g 1, -d 0) to generate a non-redundant gene catalogue across all samples. Predicted genes were annotated against different databases to address changes in specific microbial functions. For a broad overview of functional genes, the non-redundant gene catalogue was annotated using eggNOG mapper v2.1.12 (Huerta-Cepas et al. 2019) with default settings and DIAMOND alignment against the eggNOG database v5.0. The eggNOG database was chosen for gene annotation as it minimises redundancy and offers a well-structured functional hierarchy (Zeller and Huson 2022). To assess more targeted changes in microbial functions associated with carbon degradation and nitrogen cycling, the non-redundant gene catalogue was aligned against the CAZy (Drula et al. 2022) and NCycDB (Tu et al. 2018) databases, two manually curated databases of specific carbohydrate-active enzymes and nitrogen cycling genes. Briefly, sequence data from each database was downloaded and formatted into a DIAMOND-compatible database before aligning predicted genes to these databases using DIAMOND v2.0.15 (Buchfink et al. 2021) with an e-value threshold of 10^{-5}. Raw reads were aligned to the non-redundant gene catalogue using Bowtie2 v2.4.5 (Langmead and Salzberg 2012), and gene coverage was calculated and normalised to transcripts per million (TPM), which normalises for both gene and contig length, using CoverM v0.7.0 (Aroney et al. 2025).

4.2.5 Soil physicochemical characteristics

Approximately 200 g of soil from each of the four cardinal point samples were manually homogenised to create one soil sample per tree. These samples were processed to determine soil pH, total carbon (%), total nitrogen (%), total hydrogen (%), carbon to nitrogen (C:N) ratio, electrical conductivity (µS/cm), bulk density (g/cm^3), soil moisture (%), and water holding capacity (%), as described by Manaaki Whenua Landcare Research (2021).

4.2.6 Statistical analysis

All statistical analyses and data visualisations were conducted in R v4.4.0 (R Core Team 2021). To aid interpretation, visualisations were prepared using three tree health categories (healthy, defoliated, and dead) to illustrate the full gradient of tree decline. However, for statistical analyses, defoliated and dead trees were combined into a single "unhealthy" category, resulting in two health groupings (healthy vs. unhealthy). This approach was necessary as only five dead trees were randomly selected for sampling, limiting the statistical power for comparisons if analysed separately. Due to this lack of power, only results for the two-level health grouping (healthy vs unhealthy) are presented where statistical significance testing was conducted, while still allowing visualisations to highlight patterns across the full three-level tree health gradient (healthy, defoliated, dead).

To assess soil physicochemical properties across spatial scales, these properties were first standardised to a mean of zero and a standard deviation of one. Euclidean distance matrices were calculated from the standardised data (Z-scores) to quantify dissimilarities between samples using the *prcomp* function. Principal component analysis (PCA) was performed to visualise variation in soil properties across samples. PCA biplots were constructed with arrows representing variable loadings; the arrow direction indicates the orientation of each soil property in ordination space, and arrow length is proportional to the magnitude of its correlation with the ordination axes. Differences in physicochemical properties across spatial scales (site and plot) were tested using a nested permutational multivariate analysis of variance (PERMANOVA) using the *adonis2* function from the 'vegan' package v2.7.1 (Oksanen et al. 2020). Due to the nested nature of our sampling design, consisting of three sites, each containing two plots, with 16 tree samples per plot, permutations were constrained. Specifically, permutations were blocked at the site level, allowing free shuffling of samples within each site but not between sites using the *how* function from the 'permute' package v0.9-8 (Simpson 2025). Pairwise PERMANOVA tests were conducted for significant groupings to identify specific differences between levels using the *pairwise.adonis* function from the 'pairwiseAdonis' package v0.4.1 (Martinez Arbizu 2020). Standard (i.e., non-nested) PERMANOVA was used to assess differences in soil physicochemical properties across trees of different health status (healthy vs unhealthy).

Dissimilarity matrices were generated using the Bray-Curtis method via the *vegdist* function from the 'vegan' package on the TPM normalised gene counts for each annotation dataset. For each annotation set, the read counts per sample were rescaled to relative proportions (dividing the abundance of each gene within a sample by the total abundance of all genes in that sample). To

assess concordance among annotation sets (eggNOG, NCyc, and CAZy) we compared inter-sample distance structures on the lower-triangle matrices from each Bray-Curtis distance matrix using Spearman rank correlations via the *cor.test* function from the 'stats' package.

Spatial variation in functional gene composition was assessed using nested PERMANOVA with site as the main factor and plot nested within site via the *adonis2* function. Pairwise PERMANOVA's were conducted to identify specific differences between spatial units using the *pairwise.adonis* function. Variation partitioning was performed to quantify the proportion of variation explained uniquely and jointly by tree health status, soil physicochemical properties, and spatial factors using the *varpart* function from the 'vegan' package. Constrained ordination (distance-based redundancy analysis) was used via the *capscale* function of the 'vegan' package to examine relationships between gene composition and spatial variables (site/plot), with environmental variables fitted using the *envfit* function from the 'vegan' package.

Gene presence-absence patterns across tree health groups (healthy, defoliated, and dead), were visualised using Venn diagrams via the 'ggvenn' package v0.1.10 in R (Linlin 2023). Gene richness (number of unique genes detected) was calculated for each sample using the *specnumber* function from the 'vegan' package, and differences between health groups (healthy vs unhealthy) was tested using a Wilcoxon rank-sum test.

Heatmaps of relative abundance were generated to visualise differences in functional gene profiles between health states across the three annotation databases (eggNOG, NCyc, and CAZy) using the 'ComplexHeatmap' package v2.21.2 (Gu 2022). To account for differences in sequencing depth per sample, TPM normalised counts were converted to relative abundances by dividing each gene's abundance by the total abundance per sample (column-wise normalisation). Subsequently, to emphasise the relative distribution of each gene across samples, values were row-normalised so that the abundances of each gene summed to 1 across all samples.

To determine differences in functional gene composition, the Bray-Curtis dissimilarity matrices were visualised using Principal Coordinate Analysis (PCoA) and differences in functional gene composition between health groups (healthy vs unhealthy) were tested using PERMANOVA via the *adonis2* function from the 'vegan' package.

Differential abundance analysis was performed using MaAsLin2 v1.7.3 (Mallick et al. 2021), with a prevalence filter retaining only genes present in at least 10% of samples. MaAsLin2 models

were used to test for associations between gene abundances and tree health states (healthy vs unhealthy). Results were reported as effect sizes (regression coefficient indicating the magnitude of change in relative abundance) and *q*-values (false discovery rate-adjusted *P*-values), with significance thresholds set at $q < 0.05$.

4.3 Results

4.3.1 Shotgun metagenome dataset overview

After quality control, 11,384,375,324 high-quality reads were obtained across the 95 soil samples. Assembly of reads into contigs produced a total of 21,571,945 contigs of 437,868,513 bp on average. Across all samples, 11,091,339 non-redundant genes were predicted from the contigs of which 8,422,475 could be annotated with the eggNOG database, 1,654,588 with the CAZy database, and 80,895 with the NCyc database.

4.3.2 Soil physicochemical properties vary across sites and plots but not tree health

Variation in soil physicochemical properties in kauri forests is primarily structured by spatial differences rather than tree health status. PCA (Figure 4.1A) did not show clear visual clustering by site, plot, or tree health; however, nested PERMANOVA showed that both site and plot had a significant influence on soil physicochemical properties ($P < 0.05$). Pairwise PERMANOVA revealed significant differences between all sites and plots (Table C1; Appendix C). No significant overall differences in soil physicochemical properties were detected between soils surrounding healthy vs. unhealthy trees (PERMANOVA, $P > 0.05$), although individual comparisons showed higher total carbon, total nitrogen, and soil moisture in soils from around unhealthy trees (Wilcoxon, $P < 0.05$; Figure 4.1B).

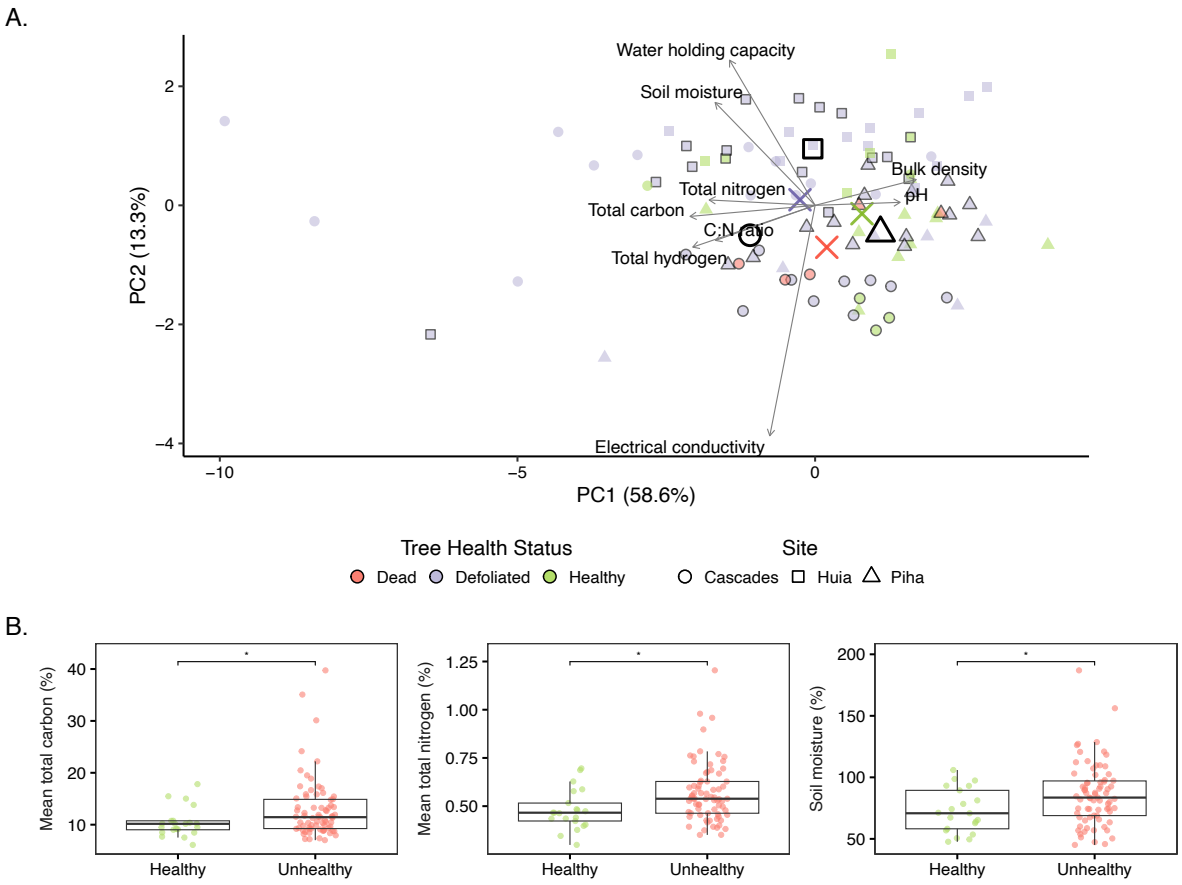

Figure 4.1: Soil physicochemical variation across kauri tree health states and locations. (A) Principal component analysis (PCA) of Euclidean distances of soil physicochemical properties of kauri trees of different health status (dead: *n* = 5, healthy: *n* = 21, defoliated: *n* = 69) across different sites (Cascades, Piha, Huia) and plots. Black borders indicate plot number, presence of black border = plot 1, no black border = plot 2. Larger shapes represent centroids of the sites. Large crosses indicate centroids of tree health status communities. (B) Boxplots of soil physicochemical properties that showed significant differences ($P < 0.05$) between tree health states in univariate analyses; other measured properties were not significant and can be viewed in Figure C2; Appendix C. Physicochemical data of soils were generated by Mohini (2024).

4.3.3 Gene composition reflects spatial structuring across sites and plots

Although eggNOG, NCyc, and CAZy annotations capture different subsets of microbial genes (broad functions, nitrogen cycling genes, and carbohydrate metabolism, respectively), all three annotation sets produced nearly identical inter-sample distance structures (Spearman ρ = 0.999). We therefore present the eggNOG results in the main text, with NCyc and CAZy producing similar results (Figure C3-Figure C6 and Table C2-Table C4; Appendix C).

Gene composition, based on Bray-Curtis dissimilarity of gene abundance counts, differed significantly among all sites and plots (pairwise PERMANOVA P <0.05, Table C2; Appendix C). Variation partitioning analysis using db-RDA revealed that the majority of explained variation in gene composition was attributed to soil physicochemical properties, accounting for 16% (Figure 4.2A)

while the spatial factor ‘sites and plots’ explained an additional 10% of the gene composition variation. Constrained ordination analysis (CAP/db-RDA), in which axes are explicitly constrained by site and plot to visualise group separation, improved the separation of samples by spatial grouping (Figure 4.2B) and explained 23.9% of the total variation in gene composition. However, tree health status remained distributed across the ordination space. Envfit analysis, overlaid as vectors on the constrained ordination, showed that this site-level variation was strongly associated with soil physicochemical properties, particularly total hydrogen (R^2 = 0.52), C:N ratio (R^2 = 0.46), and total carbon (R^2 = 0.39, Table C3; Appendix C).

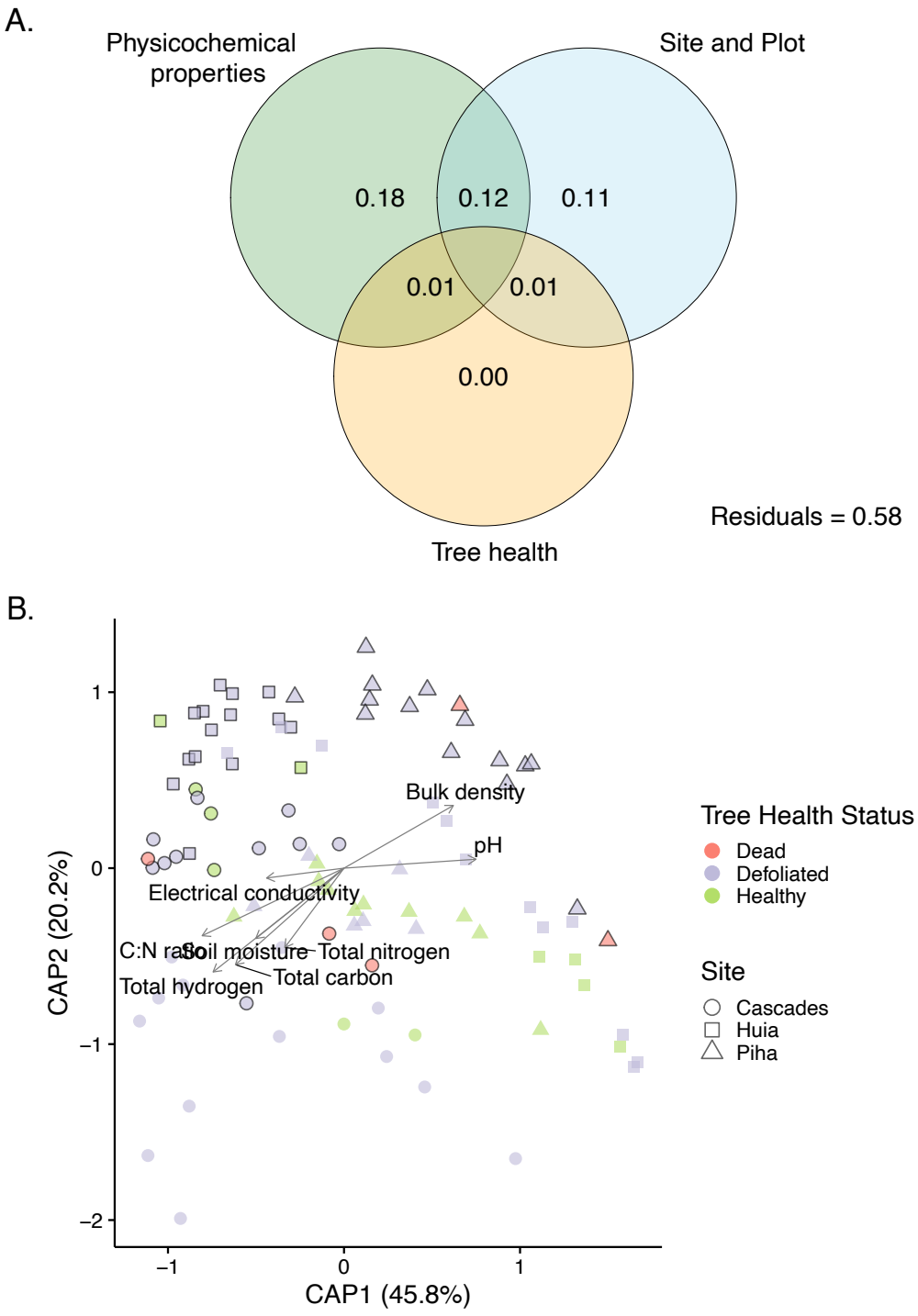

Figure 4.2: Drivers of variation in microbial functional gene composition annotated by the eggNOG database. (A) Variation partitioning analysis showing the proportion of variance in gene composition explained by physicochemical properties (pH, total carbon, total nitrogen, total hydrogen, carbon to nitrogen (C:N) ratio, electrical conductivity, bulk density, and water holding capacity), site and plot, and tree health (healthy and unhealthy). Values less than 0 are not shown. (B) Constrained ordination (db-RDA) of Bray-Curtis dissimilarities based on TPM-normalised gene abundance, constrained by site and nested plot (formula: site/plot) to account for spatial structure. Black borders indicate plot number, presence of black border = plot 1, no black border = plot 2. Overlaid vectors show significant soil physicochemical variables identified via the *envfit* function from the vegan R package that were significantly correlated (P <0.05) with ordination axes. Physicochemical data of soils were generated by Mohini (2024).

4.3.4 Gene presence, diversity, and composition across tree health groups

Functional gene profiles of the soil microbial communities showed high similarity across the tree health groups. Genes profiles were largely overlapping across tree health categories (Figure 4.3A), and overall gene diversity was similar between soils beneath healthy and unhealthy trees (Figure 4.3B; Wilcoxon $P > 0.05$). Heatmaps of gene abundances, grouped at broad functional categories (Figure C7-Figure C9; Appendix C) showed no distinct variations across tree health groupings (healthy, defoliated, dead), suggesting broad similarities in the relative abundance of functional genes. Nevertheless, multivariate analysis of Bray-Curtis dissimilarities detected significant compositional differences between healthy and unhealthy trees (Figure 4.3C; PERMANOVA $P < 0.05$, Table C4; Appendix C), indicating subtle shifts in individual gene composition even when broad functional profiles appear comparable.

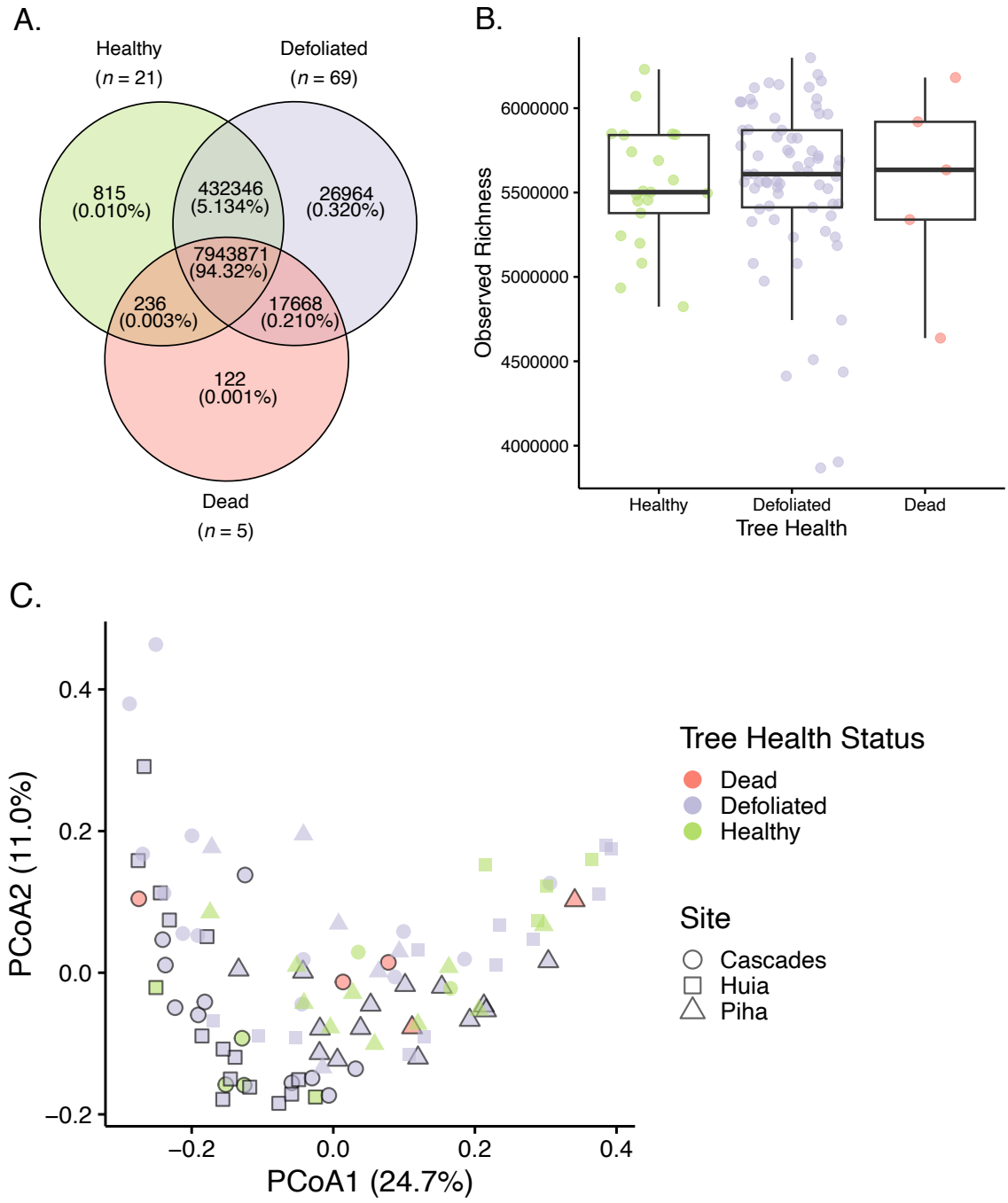

Figure 4.3: Gene diversity and composition of eggNOG annotated genes across kauri tree health states (healthy *n* = 21, defoliated *n* = 69, and dead *n* = 5). (A) Venn diagrams showing shared vs health-state-specific genes. (B) Box plots show gene diversity (richness; calculated as the number of annotated genes detected per sample). Each box represents the interquartile range of the data (IQR; 25th and 75th percentiles), whiskers show the largest and smallest values 1.5x the IQR and median values are represented by the bar within each box. (C) Gene composition differences visualised by Principal Coordinates Analysis of Bray-Curtis dissimilarities from TPM-normalised gene abundances. Black borders indicate plot number, presence of black border = plot 1, no black border = plot 2. Similar results were obtained for NCyc and CAZy annotations, which can be viewed in Figure C5 and Figure C6; Appendix C.

4.3.5 Differential abundance analysis

Differential abundance analysis of eggNOG-annotated orthologous groups (OGs) identified 278,721 as significantly differentially abundant between soils collected around healthy and unhealthy kauri trees (Figure 4.4A). A total of 3,691 unique COGs were identified as significantly differentially abundant, spanning all COG categories, suggesting that the differences between soils around healthy and unhealthy kauri comprise of a broad range of cellular and extracellular processes (Appendix C3 Supplementary File 2). Genes with higher abundance in soils around healthy kauri were more associated with the COG categories of replication, recombination and repair (L), cell wall/membrane/envelope biogenesis (M), energy production and conversion (C), signal transduction mechanisms (T), and unknown function (S). Genes showing the strongest enrichments in these soils included COG2826 (IS30 family transposase), COG1215 (glycosyltransferase), COG0043 (3-polyprenyl-4-hydroxybenzoate decarboxylase), and COG0006 (Xaa-Pro aminopeptidase) (Figure 4.4B). Fewer genes were significantly enriched in soils from around unhealthy trees, belonging to categories associated with amino acid metabolism (E), coenzyme transport and metabolism (H), and nucleotide transport and metabolism (F). The strongest enriched genes in these soils include COG2873 (O-acetylhomoserine/O-acetylserine sulfhydrylase), COG2107 (1,4-dihydroxy-6-naphtoate synthase), and COG0251 (enamine deaminase RidA/Endoribonuclease Rid7C) (Figure 4.4B).

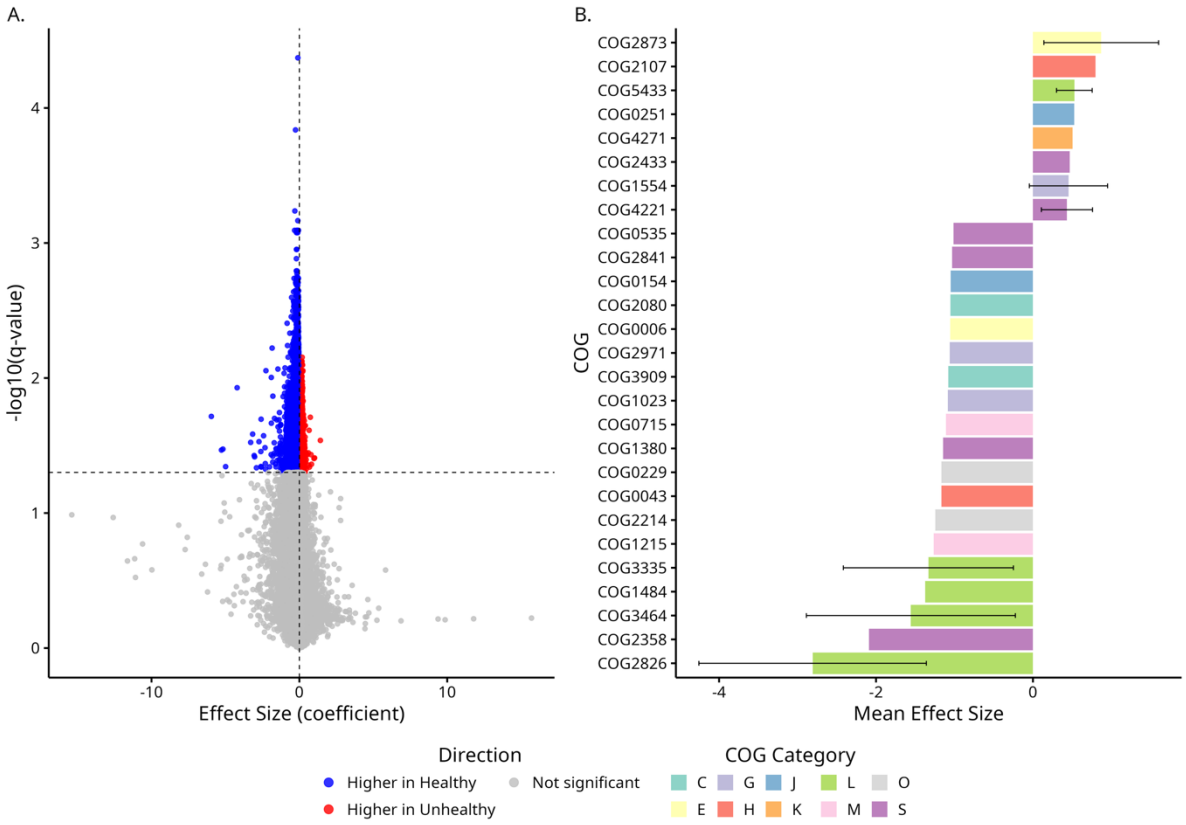

Figure 4.4: Differential abundance of eggNOG-annotated genes between soils from around healthy (*n* = 21) and unhealthy (*n* = 74) kauri trees. (A) Volcano plot shows the effect size (coefficient) and significance of predicted genes identified as differentially abundant by MaAsLin2. Negative coefficients indicate enrichments in soils around healthy kauri trees, while positive coefficients indicate enrichments in soils from around unhealthy kauri trees. (B) Bar plots depict the mean effect size ± standard error of the significantly differentially abundant genes with effect sizes > 0.4 and < -1, grouped by COG annotation. Error bars indicate the standard error of the mean effect size, calculated across genes sharing the same annotation; annotations represented by a single gene have no error bars. Bars are coloured by COG category, C = energy production and conversion, E = amino acid transport and metabolism, G = carbohydrate transport and metabolism, H = coenzyme metabolism, J = translation, ribosomal structure and biogenesis, K = transcription, L = DNA replication, recombination and repair, M = cell wall/membrane/envelope biogenesis, O = posttranslational modification, protein turnover, chaperones, S = function unknown. A full table of significantly differentially abundant genes and their eggNOG annotation is provided in Appendix C3 Supplementary File 2.

The analysis of NCyc-annotated genes detected 3,329 nitrogen cycling genes as significantly differentially abundant between soils associated with healthy and unhealthy kauri trees, with more genes significantly enriched in soils around healthy trees (Figure 4.5A; Appendix C3 Supplementary File 2). Genes involved in nitrate reduction, denitrification, nitrogen fixation, anammox, and organic nitrogen transformations were predominantly more significantly abundant in soils around healthy trees. Specifically, key genes such as *narG*, *nirK*, *nasA*, *narZ*, spanning both assimilatory and dissimilatory branches of the nitrogen cycle, showed increased abundance in soils around healthy trees (Figure 4.5B). In contrast, soils around unhealthy trees showed minimal enrichment, with only a small increase in abundance of genes involved in nitrification and nitrogen fixation (Figure 4.5B).

Overall, these results show that the microbial community in soils around healthy trees show an increased in abundance over a broader suite of nitrogen cycling functions compared to soils around unhealthy trees.

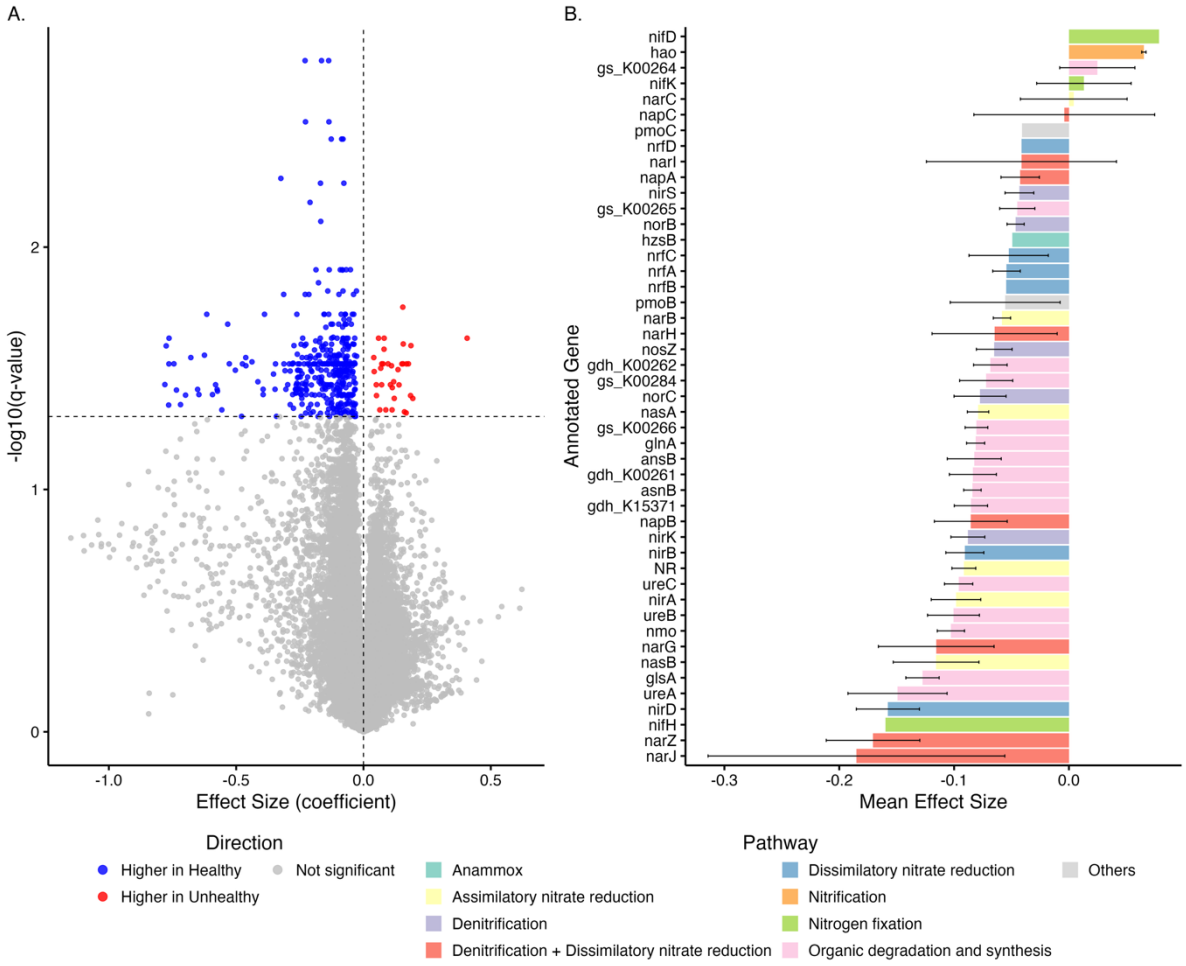

Figure 4.5: Differential abundance of NCyc-annotated genes between soils from around healthy (*n* = 21) and unhealthy (*n* = 74) kauri trees. (A) Volcano plot shows the effect size (coefficient) and significance of predicted genes identified as differentially abundant by MaAsLin2. Negative coefficients indicate enrichments in soils around healthy kauri trees, while positive coefficients indicate enrichments in soils from around unhealthy kauri trees. (B) Bar plots depict the mean effect size ± standard error of the differentially abundant genes, grouped by NCyc gene annotation and coloured by their pathway association. Error bars indicate the standard error of the mean effect size, calculated across genes sharing the same annotation; annotations represented by a single gene have no error bars.

Analysis of CAZy-annotated genes revealed 60,600 genes as significantly differentially abundant between soils associated with healthy and unhealthy kauri trees (Figure 4.6). Across all six CAZy enzyme families, the majority of genes showed increased abundance in soils around healthy trees (Appendix C3 Supplementary File 2). Within the glycoside hydrolase (GH) families, genes with the greatest differential abundance were involved in the activity of arabinofuranosidase (GH43_33;

involved with hemicellulose degradation), and α- glucosidases (GH31_8 and GH13_39; involved with starch degradation). Among the glycosyl transferase (GT) families, genes showing increased abundance in soils around healthy trees were involved with sialyltransferase (GT80), mannosyltransferase (GT15), or arabinofuranosyltransferases (GT95 and GT61). In contrast relatively few CAZy-annotated genes were more abundant in soils surrounding unhealthy kauri trees, including acetylgalactosaminidase (GH123_2), N-acetylglucosaminyltransferase (GT45; Appendix C3 Supplementary File 2), and alginate lyase (PL17_1; Appendix C3 Supplementary File 2).

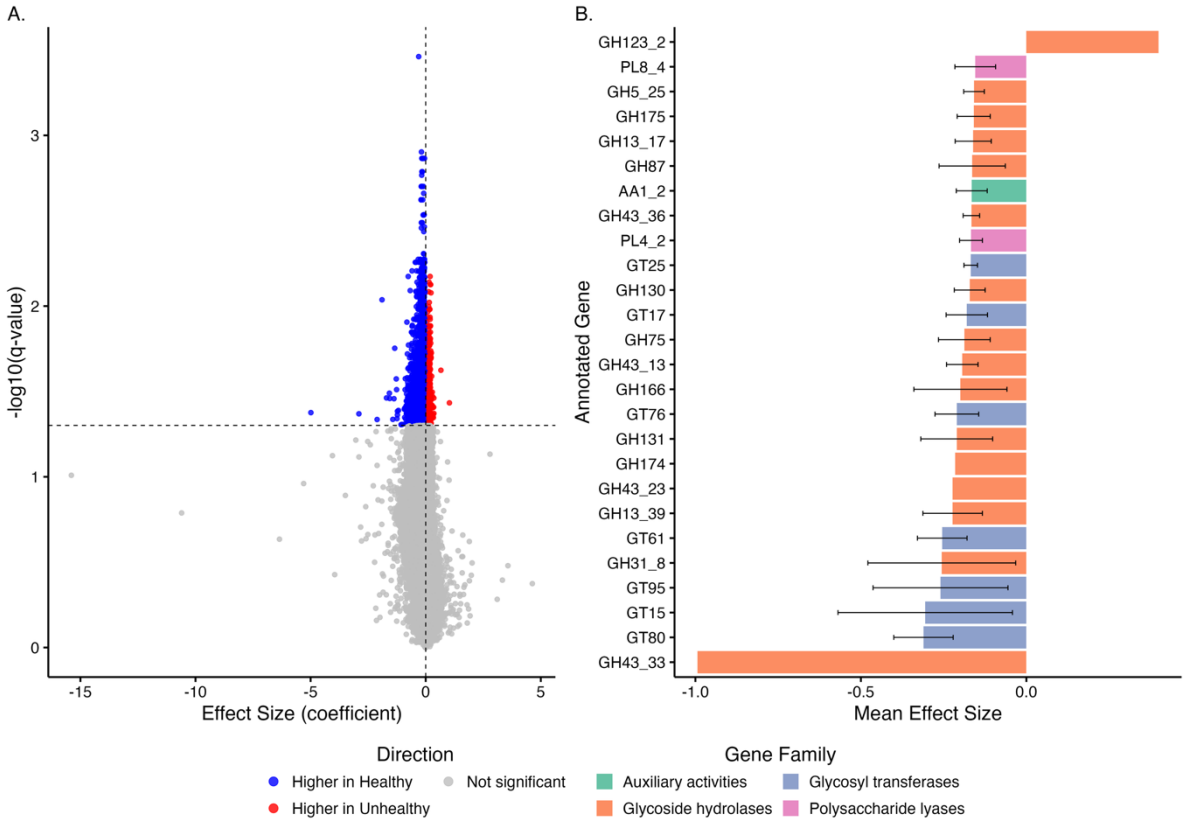

Figure 4.6: Differential abundance of CAZy-annotated genes between soils from around healthy (*n* = 21) and unhealthy (*n* = 74) kauri trees. (A) Volcano plot shows the effect size (coefficient) and significance of predicted genes identified as differentially abundant by MaAsLin2. Negative coefficients indicate enrichments in soils around healthy kauri trees, while positive coefficients indicate enrichments in soils from around unhealthy kauri trees. (B) Bar plots depict the mean effect size ± standard error of the significantly differentially abundant genes with an |effect size| > 0.15, grouped by their CAZy gene annotation and coloured by their associated enzyme class. Error bars indicate the standard error of the mean effect size, calculated across genes sharing the same annotation; annotations represented by a single gene have no error bars. A full table of significantly differentially abundant genes and their CAZy annotation is provided in Appendix C3 Supplementary File 2.

4.4 Discussion

4.4.1 Summary of key findings

This study aimed to assess the functional potential of soil microbial communities surrounding kauri trees in relation to soil physicochemical properties, spatial variation, and tree health. We found that while tree health status contributed to some variation in functional gene composition, the dominant drivers of microbial functional potential were soil physicochemical properties and spatial variation across sites and plots. These findings suggest that soil microbial functions in kauri forests are shaped more strongly by larger-scale environmental gradients than by the health condition of the individual kauri tree.

4.4.2 Spatial and environmental structuring of functional potential

Our analyses demonstrate that soil physicochemical properties are the primary drivers of microbial functional potential composition in kauri forests, while spatial heterogeneity provides an additional layer of structuring. Subtle shifts in edaphic conditions across spatial scales were associated with consistent differences in the soil environment, which corresponded with shifts in microbial community composition and function. The large influence attributed to spatial context for structuring the microbial functional potential likely reflects the environmental heterogeneity of soils across sites and plots.

Variation partitioning analysis confirmed that soil physicochemical properties explained the largest proportion of variation in functional gene composition across all annotation datasets (eggNOG, NCyc, and CAZy). These findings support the idea that microbial functional potential is modulated by environmental conditions (Chen et al. 2022b; Eslaminejad et al. 2020; Gartzia-Bengoetxea et al. 2016). While diverse microbial taxa may perform overlapping functions, the functional potential is constrained by bottom-up resource availability and soil chemistry (Dang et al. 2024; Raczka et al. 2021). In kauri forest soils, carbon and nitrogen availability, C:N ratios, and hydrogen content emerged as key factors associated with variation of functional gene composition. These properties are strongly linked to nutrient and energy fluxes and may influence the selective pressures that favour particular functional pathways over others (Khdhiri et al. 2017; Li et al. 2024; Wang et al. 2021b).

The additional variance explained by site and plot factors highlights the role of spatial context in structuring microbial functional potential. Across the three sites (Cascades, Piha, and Huia), kauri

were the most dominant species by basal area. However, due to the historical logging that occurred in Piha and Huia, these sites contained regenerating kauri stands with many smaller kauri trees compared to the Cascades site which had few but larger kauri trees (Elliott et al. 2025; Horner 2016). Additionally, the accompanying vegetation and ground cover varied among the sites and plots (Elliott et al. 2025). These site scale differences in vegetation cover, long-term soil development, and associated inputs of organic matter may be associated with the differences in the microbial functional potential seen across the sites, as seen in other forest systems (Fang et al. 2024; Gómez-Aparicio et al. 2022). At the finer plot scale, local processes such as litter inputs, root density, and microhabitat heterogeneity likely contribute to within-site differences (Štursová et al. 2016; Yang et al. 2018). These scale-dependent drivers underscore the complexity of belowground ecosystems, where microbial functional assemblages emerge from the interaction of broad-scale abiotic gradients and fine-scale heterogeneity.

These results align with findings from other soil microbiome studies that highlight that variation in microbial community and functional structure is primarily associated with soil edaphic changes, rather than host health status (Gazol et al. 2024; Scarlett et al. 2021). Collectively, this study highlights that forest soil microbial functional potential is primarily impacted by abiotic environmental conditions. Host-associated effects may influence these patterns locally, but they do not override the dominant role of spatially structured soil physicochemical properties.

4.4.3 Tree health effects on microbial functional potential

Although multivariate analysis detected no overall differences in soil physicochemical profiles between soils around healthy and unhealthy trees, univariate tests showed significantly higher total carbon, total nitrogen, and moisture in soils beneath unhealthy trees. At the same time, the overall richness and abundance of functional genes were comparable across health states, but gene composition differed, indicating that community structure, rather than total functional capacity differed between the health states. This pattern suggests a degree of functional redundancy in the soil microbiome where broad capabilities are maintained but are carried out by different taxa or gene assemblages (Louca et al. 2018). Such compositional shifts may alter the balance and efficiency of nutrient cycling and could be related to the elevated bulk carbon and nitrogen pools observed in the soils around unhealthy trees.

Similar findings have been reported in other forest systems affected by dieback, where broad microbial functions are largely conserved but compositional shifts emerge in association with tree

decline and altered soil physicochemical properties. In some forests, bark beetle-induced mortality has been linked to higher soil nitrogen and moisture due to increased litter inputs, reduced nutrient uptake, and reduced evapotranspiration, yet overall microbial diversity and functional gene abundance remained stable, consistent with functional redundancy in these communities (Ferrenberg et al. 2014; Kaňa et al. 2015). While infection of oak trees by *P. cinnamomi* led to increased total carbon around unhealthy trees, no association was found with the functional diversity and microbial biomass with tree dieback; however, lower microbial respiration was observed along with some alterations to carbon and nitrogen cycles depending on soil texture (Ávila et al. 2021). Together, these previous studies suggest that unhealthy trees alter soil environments in ways that result in nutrient accumulation and reorganise microbial functional composition without large-scale losses of diversity or abundance. In kauri forests, the higher total carbon, nitrogen, and moisture observed in soils around unhealthy trees are consistent with this pattern, pointing to functional redundancy that maintains broad metabolic capacity while subtle restructuring of functional composition may reduce nutrient turnover efficiency, allowing organic matter and nitrogen to accumulate despite apparent conservation of broad functional potential.

4.4.4 Functional processes and gene families associated with soil properties and tree health

Differential abundance analyses revealed that microbial communities in soils surrounding healthy kauri showed subtle enrichment of genes linked to core cellular processes, polysaccharide processing, carbohydrate biosynthesis and modification, and multiple nitrogen cycling pathways. In contrast, soils around unhealthy trees showed enrichment in a smaller set of genes linked to amino acid, coenzyme, and nucleotide metabolism. These functional differences align with our physicochemical results, where soils around unhealthy trees contained high concentrations of total carbon, total nitrogen, and moisture but did not show enrichment in the microbial functions that would facilitate their turnover. This suggests a decoupling of nutrient pools from microbial functional capacity under tree health decline, reflecting a reduced efficiency in nutrient cycling rather than a loss of microbial functional diversity.

Previous work using GeoChip 5S microarray in kauri forests reported contrasting results, with soils around symptomatic kauri showing more genes with a higher relative abundance involved in carbon and nitrogen cycling compared to asymptomatic trees (Byers et al. 2020b). This study also found elevated total carbon and total nitrogen concentrations in soils beneath symptomatic kauri, although these differences were not statistically significant, and suggested that carbon degradation processes may be enhanced under tree decline. However, no consistent patterns were observed

linking nitrogen cycling genes with kauri tree health. These contrasting results in enriched genes with the current study likely reflects differences in the scope of the methods used. GeoChip analysis targets a manually curated set of known genes involved in carbon-cycling, focussing primarily on degradation, fixation, and methane metabolism (Shi et al. 2019), providing a focused view of specific carbon-degrading pathways. Whereas, shotgun metagenomics with CAZy annotation reveals a broader overview of carbohydrate-active enzymes, encompassing both carbon degradation and transformation-related enzymes (Drula et al. 2022). These approaches therefore highlight complementary aspects of microbial functional potential where the microarray approach is well suited to tracking targeted carbon-degrading processes, while shotgun metagenomics reveals the wider enzymatic potential available to soil microbial communities. Taken together, these results suggest that microbial communities under healthy trees are enriched for a wider array of carbohydrate-related transformations, whereas a more focused view on degradation-associated genes reveals stronger enrichment in soils around symptomatic trees.

Our results both align and contrast with other forest dieback studies. In Mediterranean holm oak forests, Encinas-Valero et al. (2024) found that declining trees were associated with higher soil carbon and nitrogen pools as well as enrichment of genes linked to denitrification, nitrogen fixation, and phosphorus mineralisation, suggesting a functional shift towards nutrient mobilisation under tree health decline. Conversely, although unhealthy trees in kauri forests also showed higher bulk carbon and nitrogen, enrichment of genes related to their turnover was observed in soils around healthy trees, consistent with reduced microbial turnover efficiency, which could contribute to nutrient accumulation. Complementing both of these perspectives, Scarlett et al. (2021) showed that in temperate oak systems the overall nitrogen cycling potential was preserved across tree health gradients, with spatial and environmental context rather than tree health driving community composition. However, they also reported that *amoA* (involved in ammonia oxidation) abundance was greater around asymptomatic trees, which they attributed to higher soil pH, reinforcing the role of soil physicochemical properties in mediating tree health effects on microbial function. Together, these studies suggest that while tree decline consistently alters soil nutrient pools, microbial functional responses vary across ecosystems. In some cases, increasing the abundance of nutrient-mobilising genes, in others maintaining broad functional capacity with localised differences, and in kauri reducing microbial turnover efficiency despite nutrient accumulation.

One possible explanation for the reduced enrichment of decomposition-related genes in soils beneath unhealthy kauri is the distinctive chemistry of kauri litter. Kauri leaves are slow to

decompose due to high tannin and nitrogen-binding compounds, and increased litterfall under declining canopies may therefore contribute to the accumulation of recalcitrant organic matter in these soils (Jongkind et al. 2007; Verkaik et al. 2007; Wyse 2012). This would be consistent with our observations of elevated bulk carbon and nitrogen pools, but reduced enrichment of genes associated with carbohydrate degradation and nitrogen cycling. However, we did not measure the quantity or quality of litter inputs beneath trees in this study, and linking accumulated litter with microbial functional potential represents an important avenue for future research.

In summary, our differential abundance analysis indicates that kauri tree health influences the microbial functional potential of surrounding soils, but in ways that are subtle. While broad functional capacities were conserved across health states, soils beneath healthy trees were characterised by greater enrichment of genes linked to carbon degradation and nitrogen cycling, supporting more dynamic nutrient turnover. In contrast, soils beneath unhealthy trees showed reduced functional versatility despite accumulating higher carbon and nitrogen pools, a pattern that may reflect the slow decomposition of kauri litter and altered soil physicochemical properties. These findings underscore the complex interplay between tree health, soil physicochemical properties, and microbial community function, and highlight the need for further work linking litter inputs, soil chemistry, and microbial processes to understand feedback that may either stabilise or accelerate forest decline.

4.5 Conclusion

Our findings provide new insights into the redundancy and responsiveness of prokaryotic functions in kauri forest soils and highlights potential feedback between altered nutrient cycling and tree decline. Across the three kauri forest sites, soil physicochemical gradients and site/plot structure explained the most variation in prokaryotic functional potential, whereas tree health had a smaller effect that appeared as subtle compositional shifts rather than complete gains or losses of functional capacity. With elevated total carbon and total nitrogen but reduced enrichment of decomposition and nitrogen-cycling genes, this suggests a lower nutrient turnover efficiency beneath unhealthy trees. Future work should combine the differences in key nutrient cycling genes with targeted experiments to test whether reduced turnover efficiency under unhealthy trees translates into measurable functional deficiency.

Chapter 5

General discussion

Worldwide, forest ecosystems are facing increasing pressures from climate change, land-use change, and emerging pests and pathogens (Balla et al. 2021; Pascual et al. 2022; Smith et al. 2016). These stressors can affect the biodiversity, resilience, and health of these systems, highlighting the need to understand how these stressors can affect different aspects of the forest ecosystem. Soil microbial communities are an essential component of forest ecosystems that are central to nutrient cycling, facilitating plant growth, suppressing pathogen effects, while also harbouring disease-causing organisms (van der Heijden et al. 2008). However, the interactions between the soil microbial community, plant pathogens, and host trees are poorly understood, particularly in natural forest systems. In this thesis, kauri (*Agathis australis*), a culturally and ecologically significant foundation tree species, endemic to New Zealand, was used as a case study to explore these interactions. Threatened by the soil-borne oomycete *Phytophthora agathidicida*, kauri forests offer a case study for how soil microbial communities both shape and are shaped by pathogens, host decline, and the surrounding soil environment. However, these interactions do not occur in isolation but are embedded within a wider forest ecosystem shaped by climate, wildlife, vegetation, and soil conditions (Figure 5.1). Integrating amplicon sequencing, shotgun metagenomics, and soil physicochemical properties, the soil microbial community was profiled to provide insight into the associations among pathogen presence, tree health, spatial context, and edaphic gradients in structuring the soil microbial community composition and functional potential. Across the different analyses in this thesis, a consistent pattern emerged that soil microbial communities in kauri forests are spatially variable among sites and are primarily associated with soil physicochemical gradients, with pathogen presence and tree health status exerting a subtle but detectable influence. In this final chapter, connections among these findings are presented, along with their broader significance, followed by a discussion of potential avenues for future research.

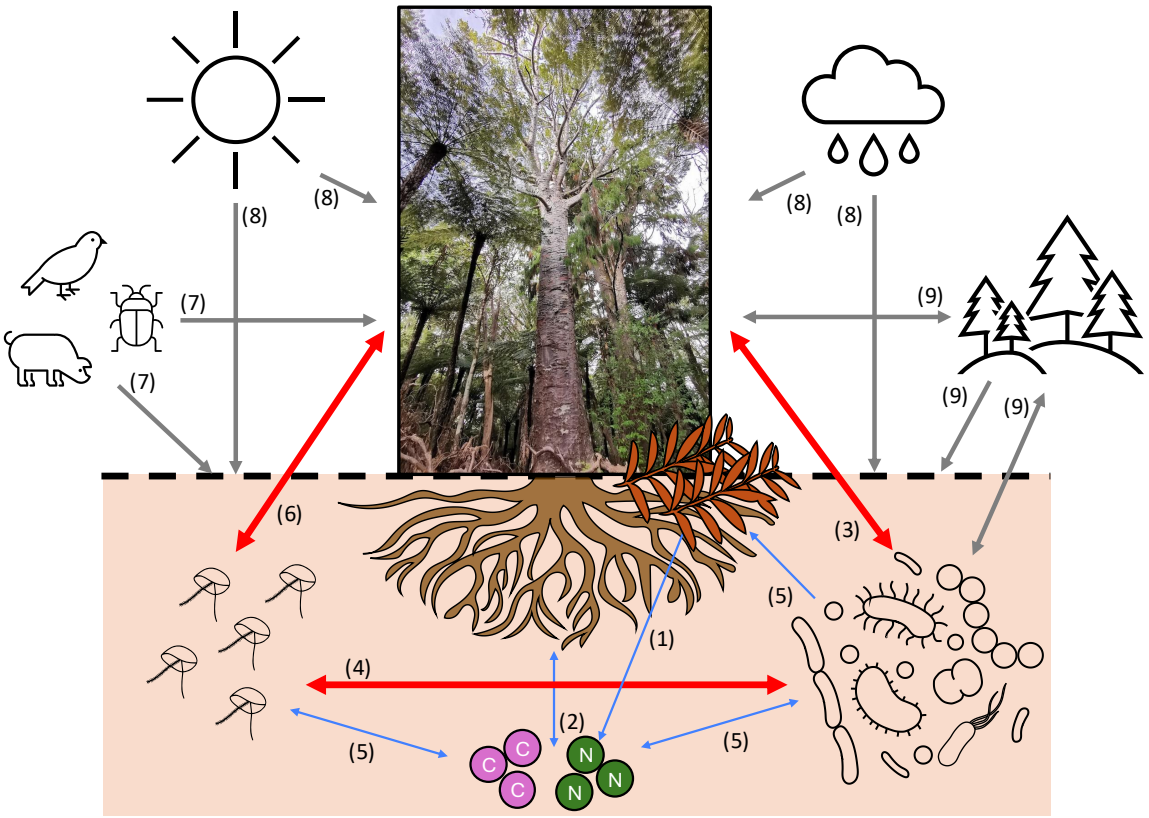

Figure 5.1: Conceptual diagram of the kauri forest system showing the multiple interacting components that shape tree health and soil microbial communities. The central kauri tree is placed within the wider ecological network that includes aboveground drivers such as sunlight, rainfall, wildlife, and other vegetation, and belowground processes involving soil physicochemical properties (purple (carbon) and green (nitrogen) circles), roots, microbes, and pathogens. Arrows represent flows of resources, influences, and interactions: Trees contribute (1) litter and (2) root exudates to soils. Soil microbes (3) support plant growth, can (4) influence pathogen dynamics, and (5) recycle nutrients while interacting with soil physicochemical properties that filter community composition and function. The pathogen (*P. agathidicida*) infects (6) tree roots, reducing tree health and contributing to canopy decline. (7) Wildlife, (8) climate, and (9) surrounding vegetation also shape both tree health and soil processes. The red coloured arrows represent the key interactions explored in this thesis, grey arrows indicate broader system drivers that are acknowledged but not directly studied, and blue arrows represent the influence of soil physicochemical properties which provide an essential backdrop for interpreting the tree-pathogen-microbe interactions.

5.1 Synthesis of findings

5.1.1 Weak direct, and stronger indirect, effects of *P. agathidicida* on soil microbial communities

Within kauri forests in the Waitākere Ranges, the confirmed presence (via LAMP analysis) of *P. agathidicida* was only weakly associated with microbial variation in community composition and functional potential (Chapter 2). A small subset of bacterial and fungal taxa was enriched in pathogen-detected soils, including some previously linked with disease suppression, but no

wholesale restructuring of the community was observed. These results suggest that direct effects of pathogen presence on microbial communities in the soil are limited. Instead, stronger signals emerged when canopy health was considered (Chapter 3 and Chapter 4). Soils beneath unhealthy trees were enriched in certain taxa, some of which are associated with later stages of litter decomposition, suggesting a potential link with the accumulation of litter under declining canopies. Taken together these findings suggest that the pathogen's impact on the soil microbial community is expressed indirectly, through host decline, which, in turn, alters soil nutrient inputs, rather than a direct effect between the pathogen and the microbes.

The notion that disturbance caused by *P. agathidicida* is likely mediated by tree health decline and associated shifts in litter and resource inputs aligns with previous work in kauri forests (Byers et al. 2020). Additionally, disease suppressive taxa have been observed to be enriched in soils with the pathogen present (Byers et al. 2021; Byers et al. 2020). However, these previous studies also reported significant differences in both fungal and bacterial community composition, as well as fungal diversity, between symptomatic and asymptomatic kauri. In contrast, this thesis found significant differences only in fungal diversity, with no major shifts in bacterial or fungal community composition between healthy and unhealthy trees. These differences likely reflect variation in disease stage, site heterogeneity, and analytical approach. Byers et al. (2020) focused on trees exhibiting extreme ends of tree health (asymptomatic vs advanced symptomatic, but not dead trees), selected within constrained and relatively uniform environments (mature trees >200 years old, similar canopy dominance, symptomatic/asymptomatic pairs within 200 m per site). By contrast, this thesis examined a broader gradient of decline across more heterogeneous sites, which revealed subtle patterns, rather than wholesale compositional turnover. Taken together, these findings suggest a range of microbial responses to kauri dieback, from clear restructuring under severe disease expression in relatively uniform environments, to subtler shifts in fungal diversity and abundance of certain taxa under more heterogeneous conditions.

5.1.2 Redundancy at broad scales, reorganisation at finer scales

The taxonomic and functional results from Chapter 3 and Chapter 4 show complementary patterns of soil microbial community structure in relation to tree health. Bacterial communities remained comparable in terms of diversity and composition across tree health states, while fungal communities showed changes in diversity but not broad-scale composition. Additionally, several taxa were differentially abundant between healthy and unhealthy trees, some of which are involved in successional stages of litter decomposition, which may be a response to increased litter deposits

under unhealthy kauri. The functional profiles of these communities show a similar pattern. Overall, functional richness did not differ significantly between trees of different health status, indicating high functional redundancy. Yet, gene composition did shift, with soils beneath healthy trees showing enrichment in genes associated with carbohydrate degradation, nitrate reduction, and denitrification, whereas soils around unhealthy trees showed enrichment in genes related to amino acid, coenzyme, and nucleotide metabolism. These shifts coincided with elevated pools of total carbon and nitrogen beneath the canopies of unhealthy trees, potentially from increased litterfall and slower nutrient turnover.

Together, these findings suggest that while microbial communities in kauri soils exhibit broad-scale functional redundancy, disturbances such as pathogen-driven tree decline can still reorganise the structure and abundance of certain functional pathways. These findings contribute to ongoing discussions suggesting that functional redundancy is not a complete buffer but rather a gradient, where broad ecosystem functions are maintained but the metabolic routes and efficiencies can shift (Fässler et al. 2025; Louca et al. 2018). Recent studies have shown that redundancy is lower for narrower, more specialised functions than for broad categories, emphasising the need to view functional redundancy as a spectrum rather than a guarantee of equivalence (Chen et al. 2022a; Eisenhauer et al. 2023). In this context, the kauri forest system suggests that microbial functional potential may remain broadly resilient to host decline, yet it can be subtly reorganised in ways that could influence decomposition and nutrient cycling.

5.1.3 Environmental filtering as the dominant structuring force

Across Chapter 3 and Chapter 4, soil physicochemical properties and spatial location explained more variation in microbial community structure and function than tree health. Microbial communities showed pronounced heterogeneity at fine scales around individual trees, a pattern widely reported in forest soils and often attributed to the influence of root exudation, litter inputs, and fine-scale variation in soil conditions within the rhizosphere (Feng et al. 2022; Haichar et al. 2008; Štursová et al. 2014). Significant differences were also observed among plots and sites, reflecting broader environmental gradients (such as vegetation type, soil development, and elevation) that are well known to shape microbial community composition and structure (Nielsen et al. 2010; Onet et al. 2025; Zhang et al. 2022a). Soil chemistry, particularly total carbon, nitrogen, C:N ratio, pH, and moisture, emerged as consistent correlates of both microbial taxonomic and functional composition. This finding not only aligns with global evidence that edaphic factors are the dominant filters of soil microbial communities, constraining both who is there and what functional potential is represented,

but this in turn sets the baseline for decomposition and nutrient cycling in forests (Cheng et al. 2021; Delgado-Baquerizo et al. 2017; Docherty et al. 2015). Within this context, it suggests that pathogen and tree-health effects are best understood as secondary influences operating against strong environmental constraints.

5.1.4 Complementary molecular approaches for ecological insight and monitoring

In Chapter 2, the strengths and limitations of molecular methods for detecting pathogens and profiling microbial communities were also evaluated. LAMP assays provided high sensitivity for *P. agathidicida* but required enrichment before successful detection. Shotgun metagenomics delivered high sequencing depth, revealing subtle reorganisation of functional gene composition, while amplicon sequencing with functional inference offered a lower-cost alternative for capturing broad-scale patterns across large sample sets. Together, these approaches showed that no single method can capture the full complexity of pathogen presence and soil microbial communities, but each provides context-dependent insights into particular components of the system. Importantly, applying them side-by-side revealed that pathogen presence had only weak direct effects on community structure and function, highlighting the value of a complementary tiered strategy: LAMP for targeted pathogen detection, amplicon sequencing for scalable monitoring, and deep shotgun metagenomic sequencing for fine-scale resolution. The balance between depth and scalability is particularly important for threatened forest systems like kauri, where both detailed ecological understanding and ongoing surveillance are required.

5.2 Novelty of the research

This thesis increases our understanding of the effects of biotic disturbances in forest ecosystems. It provides a comprehensive analysis of soil microbiomes in a Southern Hemisphere forest under threat from a plant pathogen, contributing a wider geographic framework for understanding disease effects in natural forest systems. By applying shotgun metagenomics and complementary molecular approaches across almost 100 kauri trees across a health gradient that included dead trees, results suggest that the subtle effects associated with the pathogen are primarily mediated through indirect pathways of host decline, while environmental filtering and functional redundancy dominate at broader scales. Additionally, by integrating tree health, pathogen presence, soil microbial communities, and soil properties, this work not only fills geographic and methodological gaps it also helps the global understanding of how soil microbial communities respond to forest disturbance events.

5.3 Limitations and future research directions

While this thesis provides novel insights into the pathogen-tree-microbe interactions in kauri forest soils, several limitations should be acknowledged. First, although the results suggest that tree health exerts only a subtle influence on soil microbial communities, it remains possible that the variation associated with the declining health of the tree was not fully captured by the datasets analysed. Microbial responses to host decline may be patchy, non-linear, or expressed at scales that were not resolved in this study (Štursová et al. 2016; Wang et al. 2015). Therefore, the conclusion that tree health has a limited influence should be interpreted carefully, recognising that more intensive sampling and alternative approaches may reveal stronger signals. Extending the geographic scope to encompass other major kauri forest areas such as Waipoua, Punaruku, and Aotea/Great Barrier Island, alongside repeated sampling of the same trees over time, would help disentangle geographic variability and temporal dynamics. In particular, extending sampling across seasons would provide a clearer view of microbial responses, especially since other *Phytophthora* species are known to be shaped by seasonal factors such as rainfall and temperature (Kozanitas et al. 2024; Serrano et al. 2022).

Second, Chapter 4 only used DNA-based approaches that characterise functional potential rather than realised function of these communities. Shotgun metagenomics provided comprehensive profiles of genes present, while amplicon sequencing with functional inference captured broad-scale patterns (Chapter 2). However, neither approach establishes whether genes are expressed or active and are limited in the reference databases used for annotation (Douglas et al. 2020; Sharpton 2014; Sun et al. 2020). As such, these results allow for inference and hypothesis generation, but not direct measurements of microbial processes or causality. For example, although shifts in functional profiles and taxonomic composition are consistent with suspected changes in litter inputs and root exudation under declining trees, these drivers were not directly measured in the field. Future work should incorporate metatranscriptomics and metaproteomics, together with enzyme assays, and nutrient flux measurements to link functional potential to realised activity (Alexander et al. 2025; Auer et al. 2024; Pan et al. 2024; Peng et al. 2023; Zeng et al. 2023). Direct measurements of litter inputs, root exudates, and more refined soil chemistry analysis (e.g. micronutrients, secondary metabolites, partitioning of carbon and nitrogen into more meaningful fractions) would also help connect observed microbial shifts to host resource dynamics (Feng et al. 2024a; Habtewold et al. 2020; Peng et al. 2022; Yingtao et al. 2025; Yuan et al. 2018).

Third, the profiling methods used here only allow for relative abundance estimations of the microbial community. The relative abundance data only describes proportional differences and not absolute counts of features. This limits the ability to determine whether observed shifts reflect true increases or decreases in abundance or if these are changes in community balance which may mask the ecological roles of microbial communities (Morton et al. 2019; Tkacz et al. 2018). Combining amplicon profiling with absolute abundance measurements, such as quantitative PCR or digital droplet PCR, can help resolve the absolute abundance of microbial members and strengthen interpretations (Kokkoris et al. 2021; Zhang et al. 2022b). Additionally, the functional analysis in Chapter 4 focused solely on prokaryotic genes, leaving the functional potential of fungi unexplored. As fungal communities have shown greater sensitivity to tree health at the taxonomic level (Byers et al. 2020b; Chen et al. 2022c; Gómez-Aparicio et al. 2022), extending shotgun analyses to capture fungal functional genes, as well as exploring viral communities and assembling bacterial MAGs, would provide a more complete picture of soil functional diversity under canopy decline.

In summary, this thesis demonstrates that direct effects of *P. agathidicida* on soil microbial communities appear weak, while indirect effects mediated through canopy health and resource inputs may be more important. Building on these findings will require linking potential to realised functions, expanding spatial and temporal scope, measuring currently unaccounted drivers, and situating microbial responses within the broader ecosystem rather than a pathogen-centred frame. Addressing these limitations will not only advance our understanding of the wider impacts of kauri dieback but also contribute to broader theories of how soil microbial communities respond to biotic disturbance events in forest ecosystems.

5.4 Concluding remarks

Overall, this thesis shows that soil microbial communities in kauri forests in the Waitākere Ranges are primarily structured by edaphic and spatial filters, with tree health and pathogen presence exerting subtler, indirect influences. Bacterial communities remained broadly stable, whereas fungal communities were more sensitive, suggesting that while broad functional capacities are maintained, microbial assemblages can reorganise at finer taxonomic and functional levels. By integrating complementary molecular approaches with measurements of soil physicochemical properties and spatial location, this work advances our understanding of how soil microbial communities respond to biotic disturbance events in natural forest systems, using kauri dieback as a case study. It also highlights practical tools for long-term monitoring in the face of the ongoing kauri dieback threat.

More broadly, the findings underscore the importance of soil microbial communities in mediating forest responses to disturbances and points to future efforts that combine molecular, ecological, and management perspectives as vital for protecting kauri and other foundation tree species worldwide.

References

Abad ZG, Burgess TI, Redford AJ, Bienapfl JC, Srivastava S, Mathew R, Jennings K. 2023. IDphy: An international online resource for molecular and morphological identification of *Phytophthora*. Plant Dis. 107(4):987-998 10.1094/pdis-02-22-0448-fe.

Abarenkov K, Nilsson RH, Larsson K-H, Taylor Andy FS, May Tom W, Frøslev TG, Pawlowska J, Lindahl B, Põldmaa K, Truong C et al. 2023. The UNITE database for molecular identification and taxonomic communication of fungi and other eukaryotes: sequences, taxa and classifications reconsidered. Nucleic Acids Res. 52(D1):D791-D797 10.1093/nar/gkad1039.

Abbas A, Duan J, Abdoulaye AH, Fu Y, Lin Y, Xie J, Cheng J, Jiang D. 2022. Deciphering bacterial community of the fallow and paddy soil focusing on possible biocontrol agents. Agronomy. 12(2):431, https://www.mdpi.com/2073-4395/12/2/431

Adamczyk M, Rüthi J, Frey B. 2021. Root exudates increase soil respiration and alter microbial community structure in alpine permafrost and active layer soils. Environ Microbiol. 23(4):2152-2168 https://doi.org/10.1111/1462-2920.15383.

Ahmed M, Ogden J. 1987. Population dynamics of the emergent conifer *Agathis australis* (D. Don) Lindl. (Kauri) in New Zealand I. Population structures and tree growth rates in mature stands. N Z J Bot. 25(2):217-229 10.1080/0028825X.1987.10410068.

Ahmed M, Ogden J. 1991. Descriptions of some mature kauri forests of New Zealand. Tane. 33:89-112,

Akinola SA, Ayangbenro AS, Babalola OO. 2021. The immense functional attributes of maize rhizosphere microbiome: A shotgun sequencing approach. Agriculture. 11(2):118, https://www.mdpi.com/2077-0472/11/2/118

Akrofi AY, Appiah AA, Opoku IY. 2003. Management of *Phytophthora* pod rot disease on cocoa farms in Ghana. Crop Protection. 22(3):469-477 https://doi.org/10.1016/S0261-2194(02)00193-X.

Alexander NR, Brown RS, Duwadi S, Womble SG, Ludwig DW, Moe KC, Murdock JN, Phillips JL, Veach AM, Walker DM. 2025. Leveraging fine-scale variation and heterogeneity of the wetland soil microbiome to predict nutrient flux on the landscape. Microb Ecol. 88(1):22 10.1007/s00248-025-02516-1.

Aley J, MacDonald E. 2018. Mark II prototype cleaning station – compliance research report. Department of Conservation.

Allison SD, Martiny JBH. 2008. Resistance, resilience, and redundancy in microbial communities. PNAS. 105(supplement_1):11512-11519 10.1073/pnas.0801925105.

Anderegg WRL, Trugman AT, Badgley G, Anderson CM, Bartuska A, Ciais P, Cullenward D, Field CB, Freeman J, Goetz SJ et al. 2020. Climate-driven risks to the climate mitigation potential of forests. Science. 368(6497):eaaz7005 10.1126/science.aaz7005.

Andersen KS, Kirkegaard RH, Karst SM, Albertsen M. 2018. ampvis2: an R package to analyse and visualise 16S rRNA amplicon data. bioRxiv. https://doi.org/10.1101/299537.

Anthony MA, Crowther TW, van der Linde S, Suz LM, Bidartondo MI, Cox F, Schaub M, Rautio P, Ferretti M, Vesterdal L et al. 2022. Forest tree growth is linked to mycorrhizal fungal composition and function across Europe. ISME J. 16(5):1327-1336 10.1038/s41396-021-01159-7.

Anthony WE, Allison SD, Broderick CM, Chavez Rodriguez L, Clum A, Cross H, Eloe-Fadrosh E, Evans S, Fairbanks D, Gallery R et al. 2024. From soil to sequence: Filling the critical gap in genome-resolved metagenomics is essential to the future of soil microbial ecology. Environ Microbiome. 19(1):56 10.1186/s40793-024-00599-w.

Aroney STN, Newell RJP, Nissen JN, Camargo AP, Tyson GW, Woodcroft BJ. 2025. CoverM: Read alignment statistics for metagenomics. Bioinformatics. 41(4) https://doi.org/10.1093/bioinformatics/btaf147.

Auer L, Buée M, Fauchery L, Lombard V, Barry KW, Clum A, Copeland A, Daum C, Foster B, LaButti K et al. 2024. Metatranscriptomics sheds light on the links between the functional traits of fungal guilds and ecological processes in forest soil ecosystems. New Phytologist. 242(4):1676-1690 https://doi.org/10.1111/nph.19471.

Averill C, Cates LL, Dietze MC, Bhatnagar JM. 2019. Spatial vs. temporal controls over soil fungal community similarity at continental and global scales. ISME J. 13(8):2082-2093 10.1038/s41396-019-0420-1.

Averill C, Fortunel C, Maynard DS, van den Hoogen J, Dietze MC, Bhatnagar JM, Crowther TW. 2022. Alternative stable states of the forest mycobiome are maintained through positive feedbacks. Nat Ecol Evol. 6(4):375-382 10.1038/s41559-022-01663-9.

Avershina E, Qureshi AI, Winther-Larsen HC, Rounge TB. 2025. Challenges in capturing the mycobiome from shotgun metagenome data: lack of software and databases. Microbiome. 13(1):66 10.1186/s40168-025-02048-3.

Avila JM, Gallardo A, Ibáñez B, Gómez-Aparicio L. 2016. *Quercus suber* dieback alters soil respiration and nutrient availability in Mediterranean forests. J Ecol. 104(5):1441-1452 https://doi.org/10.1111/1365-2745.12618.

Ávila JM, Gallardo A, Ibáñez B, Gómez-Aparicio L. 2021. Pathogen-induced tree mortality modifies key components of the C and N cycles with no changes on microbial functional diversity. Ecosystems. 24(2):451-466 10.1007/s10021-020-00528-1.

Babadoost M, Pavon C. 2013. Survival of oospores of *Phytophthora capsici* in soil. Plant Dis. 97(11):1478-1483 10.1094/PDIS-12-12-1123-RE.

Bader MKF, Leuzinger S. 2019. Hydraulic coupling of a leafless kauri tree remnant to conspecific hosts. iScience. 19:1238-1247 https://doi.org/10.1016/j.isci.2019.05.009.

Bahram M, Hildebrand F, Forslund SK, Anderson JL, Soudzilovskaia NA, Bodegom PM, Bengtsson-Palme J, Anslan S, Coelho LP, Harend H et al. 2018. Structure and function of the global topsoil microbiome. Nature. 560(7717):233-237 10.1038/s41586-018-0386-6.

Baldrian P. 2017. Forest microbiome: diversity, complexity and dynamics. FEMS Microbiol Rev. 41(2):109-130 10.1093/femsre/fuw040.

Balla A, Silini A, Cherif-Silini H, Chenari Bouket A, Moser WK, Nowakowska JA, Oszako T, Benia F, Belbahri L. 2021. The threat of pests and pathogens and the potential for biological control in forest ecosystems. Forests. 12(11):1579, https://www.mdpi.com/1999-4907/12/11/1579

Bani A, Pioli S, Ventura M, Panzacchi P, Borruso L, Tognetti R, Tonon G, Brusetti L. 2018. The role of microbial community in the decomposition of leaf litter and deadwood. Appl Soil Ecol. 126:75-84 https://doi.org/10.1016/j.apsoil.2018.02.017.

Barati AA, Zhoolideh M, Azadi H, Lee J-H, Scheffran J. 2023. Interactions of land-use cover and climate change at global level: How to mitigate the environmental risks and warming effects. Ecol Indicators. 146:109829 https://doi.org/10.1016/j.ecolind.2022.109829.

Bardgett RD, van der Putten WH. 2014. Belowground biodiversity and ecosystem functioning. Nature. 515(7528):505-511 10.1038/nature13855.

Bassett IE, Auckland Council Biosecurity. 2016. Progress report: kauri dieback detector dog training.

Bassett IE, Horner IJ, Hough EG, Wolber FM, Egeter B, Stanley MC, Krull CR. 2017. Ingestion of infected roots by feral pigs provides a minor vector pathway for kauri dieback disease *Phytophthora agathidicida*. Forestry. 90(5):640-648 10.1093/forestry/cpx019.

Batista BD, Wang J, Liu H, Kaur S, Macdonald CA, Qiu Z, Trivedi P, Delgado-Baquerizo M, Xiong C, Liang J et al. 2024. Biotic and abiotic responses to soilborne pathogens and environmental predictors of soil health. Soil Biol Biochem. 189:109246 https://doi.org/10.1016/j.soilbio.2023.109246.

Beachman J. 2017. The introduction and spread of kauri dieback disease in New Zealand. Did historic forestry operations play a role? MPI Technical Paper 2017/52.

Beakes GW, Glockling SL, Sekimoto S. 2012. The evolutionary phylogeny of the oomycete “fungi”. Protoplasma. 249(1):3-19 10.1007/s00709-011-0269-2.

Beever RE, Bellgard SE. 2010. Detection of *Phytophthora* taxon Agathis (PTA). Wellington, New Zealand: Ministry for Agriculture & Forestry, Biosecurity New Zealand.

Beever RE, Waipara NW, Ramsfield TD, Dick MA, Horner IJ. 2009. Kauri (*Agathis australis*) under threat from *Phytophthora*? Proceedings of the Fourth Meeting of IUFRO Working Party S07.02.09: U.S. Department of Agriculture, Forest Service, Albany. No. General Technical report PSW-GTR-211.

Bell J. 2021. First dogs trained to sniff out kauri dieback fungi. [accessed November 16 2021]https://www.rnz.co.nz/news/national/434562/first-dogs-trained-to-sniff-out-kauri-dieback-fungi.

Bellgard SE, Padamsee M, Probst CM, Lebel T, Williams SE. 2016a. Visualizing the early infection of *Agathis australis* by *Phytophthora agathidicida*, using microscopy and fluorescent *in situ* hybridization. For Pathol. 46(6):622-631 https://doi.org/10.1111/efp.12280.

Bellgard SE, Paderes EP, Beever RE. 2010. Comparative efficacy of disinfectants against *Phytophthora* Taxon *Agathis* (PTA). Paper presented at 5th IUFRO Conference *Phytophthora* in Forests and Natural Ecosystems: *Phytophthora* diseases in forest trees and natural ecosystems, Rotorua, New Zealand, 7–12 March 2010.

Bellgard SE, Pennycook SR, Weir BS, Waipara NW. 2016b. *Phytophthora agathidicida*. For Phytophthoras. 6(1) 10.5399/osu/fp.5.1.3748.

Bellgard SE, Weir BS, Pennycook SR, Paderes EP, Winks C, Beever RE, Than DJ, Hill L, Williams SE. 2013. Specialist *Phytophthora* research: Biology, pathology, ecology and detection of PTA. Ministry for Primary Industries.

Berendsen RL, Vismans G, Yu K, Song Y, de Jonge R, Burgman WP, Burmølle M, Herschend J, Bakker PAHM, Pieterse CMJ. 2018. Disease-induced assemblage of a plant-beneficial bacterial consortium. ISME J. 12(6):1496-1507 10.1038/s41396-018-0093-1.

Bergin DO, Steward GA. 2004. Kauri: ecology, establishment, growth, and management. Forest Research.

Bharti R, Grimm DG. 2021. Current challenges and best-practice protocols for microbiome analysis. Brief Bioinform. 22(1):178-193 10.1093/bib/bbz155.

Bilański P, Kowalski T. 2022. Fungal endophytes in *Fraxinus excelsior* petioles and their *in vitro* antagonistic potential against the ash dieback pathogen *Hymenoscyphus fraxineus*. Microbiol Res. 257:126961 https://doi.org/10.1016/j.micres.2022.126961.

Bolyen E, Rideout JR, Dillon MR, Bokulich NA, Abnet CC, Al-Ghalith GA, Alexander H, Alm EJ, Arumugam M, Asnicar F et al. 2019. Reproducible, interactive, scalable and extensible microbiome data science using QIIME 2. Nat Biotechnol. 37(8):852-857 10.1038/s41587-019-0209-9.

Bonfante P, Anca I-A. 2009. Plants, mycorrhizal fungi, and bacteria: A network of interactions. Annu Rev Microbiol. 63(63):363-383 https://doi.org/10.1146/annurev.micro.091208.073504.

Borcard D, Legendre P, Drapeau P. 1992. Partialling out the spatial component of ecological variation. Ecology. 73(3):1045-1055 10.2307/1940179.

Bradshaw RE, Bellgard SE, Black A, Burns BR, Gerth ML, McDougal RL, Scott PM, Waipara NW, Weir BS, Williams NM et al. 2020. *Phytophthora agathidicida*: Research progress, cultural perspectives and knowledge gaps in the control and management of kauri dieback in New Zealand. Plant Pathol. 69(1):3-16 https://doi.org/10.1111/ppa.13104.

Brasier C, Scanu B, Cooke D, Jung T. 2022. *Phytophthora*: an ancient, historic, biologically and structurally cohesive and evolutionarily successful generic concept in need of preservation. IMA Fungus. 13(1):12 10.1186/s43008-022-00097-z.

Brevik EC, Cerdà A, Mataix-Solera J, Pereg L, Quinton JN, Six J, Van Oost K. 2015. The interdisciplinary nature of SOIL. SOIL. 1(1):117-129 10.5194/soil-1-117-2015.

Brumfield KD, Huq A, Colwell RR, Olds JL, Leddy MB. 2020. Microbial resolution of whole genome shotgun and 16S amplicon metagenomic sequencing using publicly available NEON data. PLOS One. 15(2):e0228899 10.1371/journal.pone.0228899.

Buchfink B, Reuter K, Drost H-G. 2021. Sensitive protein alignments at tree-of-life scale using DIAMOND. Nat Methods. 18(4):366-368 10.1038/s41592-021-01101-x.

Buresova A, Kopecky J, Hrdinkova V, Kamenik Z, Omelka M, Sagova-Mareckova M. 2019. Succession of microbial decomposers is determined by litter type, but site conditions drive decomposition rates. Appl Environ Microbiol. 85(24):e01760-01719 10.1128/AEM.01760-19.

Burgess TI, López-Villamor A, Paap T, Williams B, Belhaj R, Crone M, Dunstan W, Howard K, Hardy GESJ. 2021. Towards a best practice methodology for the detection of *Phytophthora* species in soils. Plant Pathol. 70(3):604-614 https://doi.org/10.1111/ppa.13312.

Buscardo E, Geml J, Nagy L. 2024. Seasonal dependence of deterministic versus stochastic processes influencing soil fungal community composition in a lowland Amazonian rain forest. Commun Earth Environ. 5(1):334 10.1038/s43247-024-01273-2.

Bushnell B. 2017. BBTools Software Package. https://sourceforge.net/projects/bbmap/.

Byers A-K, Condron L, Callaghan M, Waipara N, Black A. 2021a. Identification of *Burkholderia* and *Penicillium* isolates from kauri (*Agathis australis*) soils that inhibit the mycelial growth of *Phytophthora agathidicida*. N Z Plant Prot. 74(1):42-54 10.30843/nzpp.2021.74.11736.

Byers A-K, Condron L, Donavan T, O'Callaghan M, Patuawa T, Waipara N, Black A. 2020a. Soil microbial diversity in adjacent forest systems – contrasting native, old growth kauri (*Agathis australis*) forest with exotic pine (*Pinus radiata*) plantation forest. FEMS Microbiol Ecol. 96(5) 10.1093/femsec/fiaa047.

Byers A-K, Condron L, O'Callaghan M, Waipara N, Black A. 2021b. The response of soil microbial communities to the infection of kauri (*Agathis australis*) seedlings with *Phytophthora agathidicida*. For Pathol. 51(4):e12708 https://doi.org/10.1111/efp.12708.

Byers A-K, Condron LM, O'Callaghan M, Waipara NW, Black A. 2020b. Soil microbial community restructuring and functional changes in ancient kauri (*Agathis australis*) forests impacted by the invasive pathogen *Phytophthora agathidicida*. Soil Biol Biochem. 150:108016 https://doi.org/10.1016/j.soilbio.2020.108016.

Cahill DM, Hardham AR. 1994. A dipstick immunoassay for the specific detection of *Phytophthora cinnamomi* in soils. Phytopathology. 84(11):1284-1292,

Callahan BJ, McMurdie PJ, Holmes SP. 2017. Exact sequence variants should replace operational taxonomic units in marker-gene data analysis. ISME J. 11(12):2639-2643 10.1038/ismej.2017.119.

Callahan BJ, McMurdie PJ, Rosen MJ, Han AW, Johnson AJA, Holmes SP. 2016. DADA2: High-resolution sample inference from Illumina amplicon data. Nat Methods. 13(7):581-583 10.1038/nmeth.3869.

Callahan BJ, Wong J, Heiner C, Oh S, Theriot CM, Gulati AS, McGill SK, Dougherty MK. 2019. High-throughput amplicon sequencing of the full-length 16S rRNA gene with single-nucleotide resolution. Nucleic Acids Res. 47(18):e103-e103 10.1093/nar/gkz569.

Camacho C, Coulouris G, Avagyan V, Ma N, Papadopoulos J, Bealer K, Madden TL. 2009. BLAST+: Architecture and applications. BMC Bioinform. 10(1):421 10.1186/1471-2105-10-421.

Canelles Q, Aquilué N, James PMA, Lawler J, Brotons L. 2021. Global review on interactions between insect pests and other forest disturbances. Landscape Ecol. 36(4):945-972 10.1007/s10980-021-01209-7.

Carrell AA, Frank AC. 2014. *Pinus flexilis* and *Picea engelmannii* share a simple and consistent needle endophyte microbiota with a potential role in nitrogen fixation. Front Microbiol. 5 10.3389/fmicb.2014.00333.

Carrell AA, Hicks BB, Sidelinger E, Johnston ER, Jawdy SS, Clark MM, Klingeman DM, Cregger MA. 2023. Nitrogen addition alters soil fungal communities, but root fungal communities are resistant to change. Front Microbiol. 13 10.3389/fmicb.2022.1033631.

Chemeltorit PP, Mutaqin KH, Widodo W. 2017. Combining *Trichoderma hamatum* THSW13 and *Pseudomonas aeruginosa* BJ10–86: A synergistic chili pepper seed treatment for *Phytophthora capsici* infested soil. Eur J Plant Pathol. 147(1):157-166 10.1007/s10658-016-0988-5.

Chen H, Ma K, Huang Y, Fu Q, Qiu Y, Lin J, Schadt CW, Chen H. 2022a. Lower functional redundancy in “narrow” than “broad” functions in global soil metagenomics. SOIL. 8(1):297-308 10.5194/soil-8-297-2022.

Chen H, Ma K, Lu C, Fu Q, Qiu Y, Zhao J, Huang Y, Yang Y, Schadt CW, Chen H. 2022b. Functional redundancy in soil microbial community based on metagenomics across the globe. Front Microbiol. 13 10.3389/fmicb.2022.878978.

Chen Y, Wang J, Yang N, Wen Z, Sun X, Chai Y, Ma Z. 2018. Wheat microbiome bacteria can reduce virulence of a plant pathogenic fungus by altering histone acetylation. Nat Commun. 9(1):3429 10.1038/s41467-018-05683-7.

Chen Y, Xi J, Xiao M, Wang S, Chen W, Liu F, Shao Y, Yuan Z. 2022c. Soil fungal communities show more specificity than bacteria for plant species composition in a temperate forest in China. BMC Microbiol. 22(1):208 10.1186/s12866-022-02591-1.

Cheng J, Han Z, Cong J, Yu J, Zhou J, Zhao M, Zhang Y. 2021. Edaphic variables are better indicators of soil microbial functional structure than plant-related ones in subtropical broad-leaved forests. Sci Total Environ. 773:145630 https://doi.org/10.1016/j.scitotenv.2021.145630.

Chetham J, Shortland T. 2013. Kauri cultural health indicators - monitoring framework. Repo Consultancy Ltd Report prepared for the Kauri Dieback Joint Agency Response, Tangata Whenua Roopu.

Choudhary DK, Prakash A, Johri BN. 2007. Induced systemic resistance (ISR) in plants: Mechanism of action. Indian J Microbiol. 47(4):289-297 10.1007/s12088-007-0054-2.

Cleveland CC, Townsend AR, Schimel DS, Fisher H, Howarth RW, Hedin LO, Perakis SS, Latty EF, Von Fischer JC, Elseroad A et al. 1999. Global patterns of terrestrial biological nitrogen (N2) fixation in natural ecosystems. Glob Biogeochem Cycles. 13(2):623-645 https://doi.org/10.1029/1999GB900014.

Cline LC, Zak DR. 2015. Soil microbial communities are shaped by plant-driven changes in resource availability during secondary succession. Ecology. 96(12):3374-3385 https://doi.org/10.1890/15-0184.1.

Compant S, Reiter B, Sessitsch A, Nowak J, Clément C, Barka EA. 2005. Endophytic colonization of *Vitis vinifera* L. by plant growth-promoting bacterium *Burkholderia* sp. strain PsJN. Appl Environ Microbiol. 71(4):1685-1693 10.1128/AEM.71.4.1685-1693.2005.

Conrad R. 1996. Soil microorganisms as controllers of atmospheric trace gases (H2, CO, CH4, OCS, N2O, and NO). Microbiol Rev. 60(4):609-640 10.1128/mr.60.4.609-640.1996.

Constancias F, Saby NPA, Terrat S, Dequiedt S, Horrigue W, Nowak V, Guillemin J-P, Biju-Duval L, Chemidlin Prévost-Bouré N, Ranjard L. 2015. Contrasting spatial patterns and ecological attributes of soil bacterial and archaeal taxa across a landscape. Microbiologyopen. 4(3):518-531 https://doi.org/10.1002/mbo3.256.

Cooke DEL, Drenth A, Duncan JM, Wagels G, Brasier CM. 2000. A molecular phylogeny of *Phytophthora* and related oomycetes. Fungal Genet Biol. 30(1):17-32 https://doi.org/10.1006/fgbi.2000.1202.

Cooke DEL, Schena L, Cacciola SO. 2007. Tools to detect, identify and monitor *Phytophthora* species in natural ecosystems. J Plant Pathol. 89(1):13-28, http://www.jstor.org/stable/41998353

Crone M, McComb JA, O'Brien PA, Hardy GESJ. 2013. Survival of *Phytophthora cinnamomi* as oospores, stromata, and thick-walled chlamydospores in roots of symptomatic and asymptomatic annual and herbaceous perennial plant species. Fungal Biol. 117(2):112-123 https://doi.org/10.1016/j.funbio.2012.12.004.

Crowther TW, Glick HB, Covey KR, Bettigole C, Maynard DS, Thomas SM, Smith JR, Hintler G, Duguid MC, Amatulli G et al. 2015. Mapping tree density at a global scale. Nature. 525(7568):201-205 10.1038/nature14967.

Curtis TP, Sloan WT, Scannell JW. 2002. Estimating prokaryotic diversity and its limits. PNAS. 99(16):10494-10499 10.1073/pnas.142680199.

Custer GF, Diepen LTAv, Stump WL. 2020. Structural and functional dynamics of soil microbes following spruce beetle infestation. Appl Environ Microbiol. 86(3):e01984-01919 10.1128/AEM.01984-19.

Dang R, Liu J, Lichtfouse E, Zhou L, Zhou M, Xiao L. 2024. Soil microbial carbon use efficiency and the constraints. Ann Microbiol. 74(1):37 10.1186/s13213-024-01780-9.

Daniel R. 2005. The metagenomics of soil. Nat Rev Microbiol. 3(6):470-478 10.1038/nrmicro1160.

Davis NM, Proctor DM, Holmes SP, Relman DA, Callahan BJ. 2018. Simple statistical identification and removal of contaminant sequences in marker-gene and metagenomics data. Microbiome. 6(1):226 10.1186/s40168-018-0605-2.

de Lange PJ, Rolfe JR, Barkla JW, Courtney SP, Champion PD, Perrie LR, Beadel SM, Ford KA, Breitwieser I, Schönberger I et al. 2018. Conservation status of New Zealand indigenous vascular plants, 2017. Wellington, New Zealand: Department of Conservation. https://www.doc.govt.nz/documents/science-and-technical/nztcs22entire.pdf.

de Muinck EJ, Trosvik P, Gilfillan GD, Hov JR, Sundaram AYM. 2017. A novel ultra high-throughput 16S rRNA gene amplicon sequencing library preparation method for the Illumina HiSeq platform. Microbiome. 5(1):68 10.1186/s40168-017-0279-1.

Delgado-Baquerizo M, Guerra CA, Cano-Díaz C, Egidi E, Wang J-T, Eisenhauer N, Singh BK, Maestre FT. 2020. The proportion of soil-borne pathogens increases with warming at the global scale. Nat Clim Change. 10(6):550-554 10.1038/s41558-020-0759-3.

Delgado-Baquerizo M, Maestre FT, Eldridge DJ, Singh BK. 2016. Microsite differentiation drives the abundance of soil ammonia oxidizing bacteria along aridity gradients. Front Microbiol. 7 10.3389/fmicb.2016.00505.

Delgado-Baquerizo M, Reich PB, Khachane AN, Campbell CD, Thomas N, Freitag TE, Abu Al-Soud W, Sørensen S, Bardgett RD, Singh BK. 2017. It is elemental: soil nutrient stoichiometry drives bacterial diversity. Environ Microbiol. 19(3):1176-1188 https://doi.org/10.1111/1462-2920.13642.

Department of Conservation. 2019. DOC track upgrades in Auckland to prevent kauri dieback spread. Department of Conservation; [accessed 2025 23 January]. https://www.doc.govt.nz/news/media-releases/2019/doc-track-upgrades-in-auckland-to-prevent-kauri-dieback-spread/.

Department of Conservation. n.d. Tāne Mahuta Walk. Department of Conservation; [accessed 2021 May 6]. https://www.doc.govt.nz/parks-and-recreation/places-to-go/northland/places/waipoua-forest/things-to-do/tane-mahuta-walk/.

Dick MA, Bellgard SE. 2010. Preliminary survey for *Phytophthora* taxon Agathis.

Dick MA, Kimberley M. 2013. Deactivation of oospores of *Phytophthora* taxon Agathis. Scion Client report prepared for Ministry of Primary Industries, February 2013. MPI 15775.

Diez-Hermano S, Poveda J, Benito Á, Peix Á, Martín-Pinto P, Diez JJ. 2024. Soil mycobiome and forest endophytic fungi: Is there a relationship between them? For Ecol Manage. 562:121924 https://doi.org/10.1016/j.foreco.2024.121924.

Diez-Hermano S, Poveda J, Niño-Sanchez J, Bocos-Asenjo IT, Peix Á, Martín-Pinto P, Diez JJ. 2023. Rhizosphere mycobiome diversity in four declining Mediterranean tree species. Front For Glob Change. 6 10.3389/ffgc.2023.1215701.

Docherty KM, Borton HM, Espinosa N, Gebhardt M, Gil-Loaiza J, Gutknecht JLM, Maes PW, Mott BM, Parnell JJ, Purdy G et al. 2015. Key edaphic properties largely explain temporal and geographic variation in soil microbial communities across four biomes. PLOS One. 10(11):e0135352 10.1371/journal.pone.0135352.

Dominati E, Patterson M, Mackay A. 2010. A framework for classifying and quantifying the natural capital and ecosystem services of soils. Ecol Econ. 69(9):1858-1868 https://doi.org/10.1016/j.ecolecon.2010.05.002.

Douglas GM, Maffei VJ, Zaneveld JR, Yurgel SN, Brown JR, Taylor CM, Huttenhower C, Langille MGI. 2020. PICRUSt2 for prediction of metagenome functions. Nat Biotechnol. 38(6):685-688 10.1038/s41587-020-0548-6.

Drula E, Garron M-L, Dogan S, Lombard V, Henrissat B, Terrapon N. 2022. The carbohydrate-active enzyme database: functions and literature. Nucleic Acids Res. 50(D1):D571-D577 10.1093/nar/gkab1045.

Ecroyd CE. 1982. Biological flora of New Zealand 8. *Agathis australis* (D. Don) Lindl. (Araucariaceae) Kauri. N Z J Bot. 20(1):17-36 10.1080/0028825X.1982.10426402.

Eisenhauer N, Hines J, Maestre FT, Rillig MC. 2023. Reconsidering functional redundancy in biodiversity research. NPJ Biodivers. 2(1):9 10.1038/s44185-023-00015-5.

Elliott TAW, Bellingham PJ, Perry GLW, Burns BR. 2025. A virulent soil pathogen alters temperate rain forest understorey sapling population dynamics and successional trajectories. J Veg Sci. 36(2):e70014 https://doi.org/10.1111/jvs.70014.

Encinas-Valero M, Esteban R, Hereş A-M, Vivas M, Solla A, Moreno G, Corcobado T, Odriozola I, Garbisu C, Epelde L et al. 2024. Alteration of the tree–soil microbial system triggers a feedback loop that boosts holm oak decline. Funct Ecol. 38(2):374-390 https://doi.org/10.1111/1365-2435.14473.

Enright NJ, Ogden J. 1987. Decomposition of litter from common woody species of kauri (*Agathis australis* Salisb.) forest in northern New Zealand. Aust J Ecol. 12(2):109-124 https://doi.org/10.1111/j.1442-9993.1987.tb00933.x.

Enright NJ, Ogden J, Rigg LS. 1999. Dynamics of forests with *Araucariaceae* in the Western Pacific. J Veg Sci. 10(6):793-804 10.2307/3237304.

Erwin DC, Ribeiro OK. 1996. *Phytophthora* diseases worldwide. American Phytopathological Society.

Eslaminejad P, Heydari M, Kakhki FV, Mirab-balou M, Omidipour R, Muñoz-Rojas M, Lucas-Borja ME. 2020. Plant species and season influence soil physicochemical properties and microbial function in a semi-arid woodland ecosystem. Plant Soil. 456(1/2):43-59, https://doi.org/10.1007/s11104-020-04691-1

Ewels P, Magnusson M, Lundin S, Käller M. 2016. MultiQC: Summarize analysis results for multiple tools and samples in a single report. Bioinformatics. 32(19):3047-3048 10.1093/bioinformatics/btw354.

Falkowski PG, Fenchel T, Delong EF. 2008. The microbial engines that drive Earth's biogeochemical cycles. Science. 320(5879):1034-1039 10.1126/science.1153213.

Fang Y, He X, Xie Q, Li D. 2024. Increasing tree phylogenetic diversity stimulates microbial functional potential in a subtropical forest. J Plant Ecol. 17(6) 10.1093/jpe/rtae096.

Fasolo A, Deb S, Stevanato P, Concheri G, Squartini A. 2024. ASV vs OTUs clustering: Effects on alpha, beta, and gamma diversities in microbiome metabarcoding studies. PLOS One. 19(10):e0309065 10.1371/journal.pone.0309065.

Fässler D, Heinken A, Hertel J. 2025. Characterising functional redundancy in microbiome communities via relative entropy. Comput Struct Biotechnol. 27:1482-1497 https://doi.org/10.1016/j.csbj.2025.03.012.

Feng J, He K, Zhang Q, Han M, Zhu B. 2022. Changes in plant inputs alter soil carbon and microbial communities in forest ecosystems. Global Change Biol. 28(10):3426-3440 https://doi.org/10.1111/gcb.16107.

Feng J, Wang L, Zhai C, Jiang L, Yang Y, Huang X, Ru J, Song J, Zhang L, Wan S. 2024a. Root carbon inputs outweigh litter in shaping grassland soil microbiomes and ecosystem multifunctionality. NPJ Biofilms Microbiomes. 10(1):150 10.1038/s41522-024-00616-3.

Feng Z, Liang Q, Yao Q, Bai Y, Zhu H. 2024b. The role of the rhizobiome recruited by root exudates in plant disease resistance: Current status and future directions. Environ Microbiome. 19(1):91 10.1186/s40793-024-00638-6.

Fernández-Pavía SP, Grünwald NJ, Díaz-Valasis M, Cadena-Hinojosa M, Fry WE. 2004. Soilborne oospores of *Phytophthora infestans* in Central Mexico survive winter fallow and infect potato plants in the field. Plant Dis. 88(1):29-33 10.1094/PDIS.2004.88.1.29.

Ferrenberg S, Knelman JE, Jones JM, Beals SC, Bowman WD, Nemergut DR. 2014. Soil bacterial community structure remains stable over a 5-year chronosequence of insect-induced tree mortality. Front Microbiol. 5 10.3389/fmicb.2014.00681.

Fichtner A, von Oheimb G, Härdtle W, Wilken C, Gutknecht JLM. 2014. Effects of anthropogenic disturbances on soil microbial communities in oak forests persist for more than 100 years. Soil Biol Biochem. 70:79-87 https://doi.org/10.1016/j.soilbio.2013.12.015.

Fierer N, Jackson RB. 2006. The diversity and biogeography of soil bacterial communities. PNAS. 103(3):626-631 10.1073/pnas.0507535103.

Finzi AC, Abramoff RZ, Spiller KS, Brzostek ER, Darby BA, Kramer MA, Phillips RP. 2015. Rhizosphere processes are quantitatively important components of terrestrial carbon and nutrient cycles. Global Change Biol. 21(5):2082-2094 https://doi.org/10.1111/gcb.12816.

Flint ML, Dreistadt SH. 1998. Natural enemies handbook: The illustrated guide to biological pest control. Univ of California Press.

Franzosa EA, Hsu T, Sirota-Madi A, Shafquat A, Abu-Ali G, Morgan XC, Huttenhower C. 2015. Sequencing and beyond: Integrating molecular 'omics' for microbial community profiling. Nat Rev Microbiol. 13(6):360-372 10.1038/nrmicro3451.

Froud K. 2020. Kauri Dieback Building Knowledge. Biosecurity Research.

Froud K, Chew YC, Kean J, Jane M, Killick S, Ashby E, Taua-Gordon R, Jamieson A, Tolich L. 2022. 2021 Waitākere Ranges kauri population health monitoring survey.

Froud K, Chew YC, Kean JM, Meiforth J, Geddes H, Jamieson A, Manukau E, Moni MT, Maxwell-Butler Z, Anderson G et al. 2025. Te Ngāherehere o Kohukohunui / Hūnua Ranges kauri population health monitoring survey. Auckland Council, Environmental Services.

Fu L, Niu B, Zhu Z, Wu S, Li W. 2012. CD-HIT: Accelerated for clustering the next-generation sequencing data. Bioinformatics. 28(23):3150-3152 10.1093/bioinformatics/bts565.

Fukuda K, Ogawa M, Taniguchi H, Saito M. 2016. Molecular approaches to studying microbial communities: Targeting the 16S ribosomal RNA gene. J UOEH. 38(3):223-232 10.7888/juoeh.38.223.

Gadgil PD. 1974. *Phytophthora heveae*, a pathogen of kauri. New Zealand Forest Service.

Galletti S, Paris R, Cianchetta S. 2020. Selected isolates of *Trichoderma gamsii* induce different pathways of systemic resistance in maize upon *Fusarium verticillioides* challenge. Microbiol Res. 233:126406 https://doi.org/10.1016/j.micres.2019.126406.

Gao C-H, Chen C, Akyol T, Dusa A, Yu G, Cao B, Cai P. 2024. ggVennDiagram: Intuitive Venn diagram software extended. iMeta. 3(1):e177 https://doi.org/10.1002/imt2.177.

Gao M, Xiong C, Gao C, Tsui CKM, Wang M-M, Zhou X, Zhang A-M, Cai L. 2021. Disease-induced changes in plant microbiome assembly and functional adaptation. Microbiome. 9(1):187 10.1186/s40168-021-01138-2.

Gardes M, Bruns TD. 1993. ITS primers with enhanced specificity for basidiomycetes - application to the identification of mycorrhizae and rusts. Mol Ecol. 2(2):113-118 https://doi.org/10.1111/j.1365-294X.1993.tb00005.x.

Garrastatxu J, Odriozola I, Esteban R, Encinas-Valero M, Morais DK, Větrovský T, Yuste JC. 2024. Fungal symbionts associate with holm oak tree health in declining oak savannas of the southwest of the Iberian Peninsula. Appl Soil Ecol. 195:105210 https://doi.org/10.1016/j.apsoil.2023.105210.

Gartzia-Bengoetxea N, Kandeler E, Martínez de Arano I, Arias-González A. 2016. Soil microbial functional activity is governed by a combination of tree species composition and soil properties in temperate forests. Appl Soil Ecol. 100:57-64 https://doi.org/10.1016/j.apsoil.2015.11.013.

Gazol A, González de Andrés E, Valverde Á, Igual JM, Serrano A, Camarero JJ. 2024. The strong seasonality of soil microbial community structure in declining Mediterranean pine forests depends more on soil conditions than on tree vitality. Sci Total Environ. 957:177560 https://doi.org/10.1016/j.scitotenv.2024.177560.

Geyer KM, Altrichter AE, Takacs-Vesbach CD, Van Horn DJ, Gooseff MN, Barrett JE. 2014. Bacterial community composition of divergent soil habitats in a polar desert. FEMS Microbiol Ecol. 89(2):490-494 https://doi.org/10.1111/1574-6941.12306.

Ghimire SR, Richardson PA, Kong P, Hu J, Lea-Cox JD, Ross DS, Moorman GW, Hong C. 2011. Distribution and diversity of *Phytophthora* species in nursery irrigation reservoir adopting water recycling system during winter months. J Phytopathol. 159(11-12):713-719 https://doi.org/10.1111/j.1439-0434.2011.01831.x.

Glassman SI, Weihe C, Li J, Albright MBN, Looby CI, Martiny AC, Treseder KK, Allison SD, Martiny JBH. 2018. Decomposition responses to climate depend on microbial community composition. PNAS. 115(47):11994-11999 10.1073/pnas.1811269115.

Gómez-Alpizar L, Carbone I, Ristaino JB. 2007. An Andean origin of *Phytophthora infestans* inferred from mitochondrial and nuclear gene genealogies. PNAS. 104(9):3306-3311 10.1073/pnas.0611479104.

Gómez-Aparicio L, Domínguez-Begines J, Villa-Sanabria E, García LV, Muñoz-Pajares AJ. 2022. Tree decline and mortality following pathogen invasion alters the diversity, composition and network structure of the soil microbiome. Soil Biol Biochem. 166:108560 https://doi.org/10.1016/j.soilbio.2022.108560.

Griffin EA, Carson WP. 2018. Tropical tree endophytes: Cryptic drivers of tropical forest diversity. In: Pirttilä AM, Frank AC, editors. Endophytes of Forest Trees: Biology and Applications. Cham: Springer International Publishing. p. 63-103.

Gu S, Wei Z, Shao Z, Friman V-P, Cao K, Yang T, Kramer J, Wang X, Li M, Mei X et al. 2020. Competition for iron drives phytopathogen control by natural rhizosphere microbiomes. Nat Microbiol. 5(8):1002-1010 10.1038/s41564-020-0719-8.

Gu Z. 2022. Complex heatmap visualization. iMeta. 1(3):e43 https://doi.org/10.1002/imt2.43.

Guo J, Gong X, Yu S, Wei B, Chu L, Liu J, He X, Yu M. 2023. Responses of soil microbial diversity to forest management practices after pine wilt disease infection. Forests. 14(5):862, https://www.mdpi.com/1999-4907/14/5/862

Habtewold JZ, Helgason BL, Yanni SF, Janzen HH, Ellert BH, Gregorich EG. 2020. Litter composition has stronger influence on the structure of soil fungal than bacterial communities. Eur J Soil Biol. 98:103190 https://doi.org/10.1016/j.ejsobi.2020.103190.

Hackl E, Pfeffer M, Donat C, Bachmann G, Zechmeister-Boltenstern S. 2005. Composition of the microbial communities in the mineral soil under different types of natural forest. Soil Biol Biochem. 37(4):661-671 https://doi.org/10.1016/j.soilbio.2004.08.023.

Hackwell K, Bertram G. 1999. Pests & weeds: The cost of restoring an indigenous dawn chorus: A blueprint for action against the impacts of introduced pest organisms on the New Zealand environment. New Zealand Conservation Authority.

Haichar FeZ, Marol C, Berge O, Rangel-Castro JI, Prosser JI, Balesdent J, Heulin T, Achouak W. 2008. Plant host habitat and root exudates shape soil bacterial community structure. ISME J. 2(12):1221-1230 10.1038/ismej.2008.80.

Halkett J. 1983. A basis for the management of New Zealand kauri (*Agathis Australis* (D. Don) Lindl.) forest. N Z J For. 28(1):15-23,

Halkett J, Sale EV. 1986. The world of the kauri. Auckland N.Z: Reed Methuen.

Handelsman J. 2004. Metagenomics: Application of genomics to uncultured microorganisms. Microbiol Mol Biol Rev. 68(4):669-685 10.1128/mmbr.68.4.669-685.2004.

Handelsman J, Rondon MR, Brady SF, Clardy J, Goodman RM. 1998. Molecular biological access to the chemistry of unknown soil microbes: A new frontier for natural products. Chemistry & Biology. 5(10):R245-R249 https://doi.org/10.1016/S1074-5521(98)90108-9.

Hardoim PR, Overbeek LSv, Berg G, Pirttilä AM, Compant S, Campisano A, Döring M, Sessitsch A. 2015. The hidden world within plants: Ecological and evolutionary considerations for defining

functioning of microbial endophytes. Microbiol Mol Biol Rev. 79(3):293-320 10.1128/mmbr.00050-14.

Hargreaves AJ, Duncan JM. 1978. Detection of *Phytophthora* species in field soils by simple baiting procedures. Soil Biol Biochem. 10(4):343-345 https://doi.org/10.1016/0038-0717(78)90034-2.

Hartmann M, Niklaus PA, Zimmermann S, Schmutz S, Kremer J, Abarenkov K, Lüscher P, Widmer F, Frey B. 2013. Resistance and resilience of the forest soil microbiome to logging-associated compaction. ISME J. 8(1):226-244 10.1038/ismej.2013.141.

Hermans SM, Buckley HL, Case BS, Curran-Cournane F, Taylor M, Lear G. 2017. Bacteria as emerging indicators of soil condition. Appl Environ Microbiol. 83(1):e02826-02816 10.1128/AEM.02826-16.

Hermans SM, Buckley HL, Case BS, Curran-Cournane F, Taylor M, Lear G. 2020. Using soil bacterial communities to predict physico-chemical variables and soil quality. Microbiome. 8(1):79 10.1186/s40168-020-00858-1.

Hill L, Waipara NW, Stanley R, Hammon C. 2017. Kauri dieback report 2017: An investigation into the distribution of kauri dieback, and implications for its future management, within the Waitākere Ranges Regional Park. Auckland Council.

Ho HH. 2018. The taxonomy and biology of *Phytophthora* and *Pythium*. JBMOA. 6(1):40-45 10.15406/jbmoa.2018.06.00174.

Hobbie JE, Hobbie EA. 2006. 15N in symbiotic fungi and plants estimates nitrogen and carbon flux rates in arctic tundra. Ecology. 87(4):816-822 https://doi.org/10.1890/0012-9658(2006)87[816:NISFAP]2.0.CO;2.

Högberg MN, Högberg P, Myrold DD. 2007. Is microbial community composition in boreal forest soils determined by pH, C-to-N ratio, the trees, or all three? Oecologia. 150(4):590-601 https://doi.org/10.1007/s00442-006-0562-5.

Holden SR, Treseder KK. 2013. A meta-analysis of soil microbial biomass responses to forest disturbances. Front Microbiol. 4 10.3389/fmicb.2013.00163.

Horner I. 2016. Phosphite barriers for kauri dieback–scoping exercise. A confidential report prepared for the Ministry for Primary Industries by Plant & Food Research.

Horner IJ, Arnet MJ. 2020. Phosphite large tree treatment trials: Brief report April 2020. Plant & Food Research report prepared for: Ministry for Primary Industries, April 2020. Milestone No. 66676. Contract No. 33523. Job code: P/345160/04. SPTS No. 18008.

Horner IJ, Arnet MJ, Bellgard SE, Probst CM, Paynter Q, Claydon J. 2019a. 17748 Temperature treatment protocol for deactivating oospores of *Phytophthora agathidicida*. Biosecurity New Zealand Technical Paper No: 2020/06, Prepared for Planning and Intelligence, Kauri Dieback Programme, October 2019. ISBN No: 978-1-99-002582-2 (online).

Horner IJ, Arnet MJ, Carroll E, Hedderley M, Horner MB. 2024. Phosphite trials for control of *Phytophthora agathidicida* in kauri – re-evaluation after 10 years. Plant & Food Research.

Horner IJ, Hough EG. 2011. Phosphorous acid for controlling *Phytophthora* taxon agathis in kauri. Plant & Food Research Client report prepared for MAF Biosecurity, July 2011. PFR SPTS No. 5802. .

Horner IJ, Hough EG. 2013. Phosphorous acid for controlling *Phytophthora* taxon Agathis in kauri glasshouse trials. N Z Plant Prot. 66(0):242-248 10.30843/nzpp.2013.66.5673.

Horner IJ, Hough EG. 2014. Pathogenicity of four *Phytophthora* species on kauri in vitro and glasshouse trials. N Z Plant Prot. 67(0):54-59 10.30843/nzpp.2014.67.5722.

Horner IJ, Hough EG. 2015. Assay of stored soils for presence of *Phytophthora agathidicida*. Plant & Food Research Client report prepared for Ministry of Primary Industries, June 2015. PFR SPTS No. 11718.

Horner IJ, Hough EG, Horner MB. 2015. Forest efficacy trials on phosphite for control of kauri dieback. N Z Plant Prot. 68(0):7-12 10.30843/nzpp.2015.68.5791.

Horner IJ, Hough EG, Horner MB. 2017. Trunk sprays and lower phosphite injection rates for kauri dieback control. Plant & Food Research Client report prepared for Ministy of Primary Industries, March 2017. PFR SPTS No. 14471.

Horner IJ, Jesson L, Hill L, Barton M. 2019b. Kauri Rescue™: A citizen science programme evaluating kauri dieback controls.

Huckvale E, Moseley HNB. 2023. kegg_pull: A software package for the RESTful access and pulling from the Kyoto Encyclopedia of Gene and Genomes. BMC Bioinform. 24(1):78 10.1186/s12859-023-05208-0.

Huerta-Cepas J, Szklarczyk D, Heller D, Hernández-Plaza A, Forslund SK, Cook H, Mende DR, Letunic I, Rattei T, Jensen Lars J et al. 2019. eggNOG 5.0: A hierarchical, functionally and phylogenetically annotated orthology resource based on 5090 organisms and 2502 viruses. Nucleic Acids Res. 47(D1):D309-D314 10.1093/nar/gky1085.

Hunter S, Horner I, Hosking J, Carroll E, Newland J, Arnet M, Waipara N, Burns B, Scott P, Williams N. 2024. *Phytophthora* communities associated with *Agathis australis* (kauri) in Te Wao Nui o

Tiriwa/Waitākere Ranges, New Zealand. Forests. 15(5):735, https://www.mdpi.com/1999-4907/15/5/735

Huttenhower C, Gevers D, Knight R, Abubucker S, Badger JH, Chinwalla AT, Creasy HH, Earl AM, FitzGerald MG, Fulton RS et al. 2012. Structure, function and diversity of the healthy human microbiome. Nature. 486(7402):207-214 10.1038/nature11234.

Hyatt D, Chen G-L, LoCascio PF, Land ML, Larimer FW, Hauser LJ. 2010. Prodigal: prokaryotic gene recognition and translation initiation site identification. BMC Bioinform. 11(1):119 10.1186/1471-2105-11-119.

Irwin G, Johns D, Flay RGJ, Munaro F, Sung Y, Mackrell T. 2017. A Review of Archaeological Māori Canoes (Waka) Reveals Changes in Sailing Technology and Maritime Communications in Aotearoa/New Zealand, AD 1300–1800. JPA. 8(2):31-43, https://pacificarchaeology.org/index.php/journal/article/view/235

Islam W, Noman A, Naveed H, Huang Z, Chen HYH. 2020. Role of environmental factors in shaping the soil microbiome. Environ Sci Pollut Res. 27(33):41225-41247 10.1007/s11356-020-10471-2.

Jamieson A, Bassett IE, Hill LMW, Hill S, Davis A, Waipara NW, Hough EG, Horner IJ. 2014. Aerial surveillance to detect kauri dieback in New Zealand. N Z Plant Prot. 67(0):60-65 10.30843/nzpp.2014.67.5723.

Jeffers S, Martin S. 1986. Comparison of two media selective for *Phytophthora* and *Pythium* species. Plant Dis. 70(11):1038-1043 10.1094/PD-70-1038.

Jiang G, Wang N, Zhang Y, Wang Z, Zhang Y, Yu J, Zhang Y, Wei Z, Xu Y, Geisen S et al. 2021. The relative importance of soil moisture in predicting bacterial wilt disease occurrence. Soil Ecol Lett. 3(4):356-366 10.1007/s42832-021-0086-2.

Jones W, Hill K, Allen J. 1995. *Wollemia nobilis*, a new living Australian genus and species in the *Araucariaceae*. Telopea. 6:173-176 10.7751/TELOPEA19953014.

Jongkind AG, Velthorst E, Buurman P. 2007. Soil chemical properties under kauri (*Agathis australis*) in The Waitākere Ranges, New Zealand. Geoderma. 141(3):320-331 https://doi.org/10.1016/j.geoderma.2007.06.014.

Jung T, Colquhoun IJ, Hardy GESJ. 2013. New insights into the survival strategy of the invasive soilborne pathogen *Phytophthora cinnamomi* in different natural ecosystems in Western Australia. For Pathol. 43(4):266-288 https://doi.org/10.1111/efp.12025.

Jung T, Pérez-Sierra A, Durán A, Horta Jung M, Balci Y, Scanu B. 2018. Canker and decline diseases caused by soil- and airborne *Phytophthora* species in forests and woodlands. Persoonia. 40:182-220 10.3767/persoonia.2018.40.08.

Kaňa J, Tahovská K, Kopáček J, Šantrůčková H. 2015. Excess of organic carbon in mountain spruce forest soils after bark beetle outbreak altered microbial N transformations and mitigated N-saturation. PLOS One. 10(7):e0134165 10.1371/journal.pone.0134165.

Karimi B, Terrat S, Dequiedt S, Saby NPA, Horrigue W, Lelièvre M, Nowak V, Jolivet C, Arrouays D, Wincker P et al. 2018. Biogeography of soil bacteria and archaea across France. Sci Adv. 4(7):eaat1808 10.1126/sciadv.aat1808.

Kauri Dieback Programme. n.d. Programme Partners. Kauri Dieback Programme; [accessed 2021 May 25]. https://www.kauriprotection.co.nz/programme-partners/.

Keenan RJ, Reams GA, Achard F, de Freitas JV, Grainger A, Lindquist E. 2015. Dynamics of global forest area: Results from the FAO Global Forest Resources Assessment 2015. For Ecol Manage. 352:9-20 https://doi.org/10.1016/j.foreco.2015.06.014.

Keith H, Mackey BG, Lindenmayer DB. 2009. Re-evaluation of forest biomass carbon stocks and lessons from the world's most carbon-dense forests. PNAS. 106(28):11635-11640 10.1073/pnas.0901970106.

Ketehouli T, Pasche J, Buttrós VH, Goss EM, Martins SJ. 2024. The underground world of plant disease: Rhizosphere dysbiosis reduces above-ground plant resistance to bacterial leaf spot and alters plant transcriptome. Environ Microbiol. 26(7):e16676 https://doi.org/10.1111/1462-2920.16676.

Khare E, Mishra J, Arora NK. 2018. Multifaceted interactions between endophytes and plant: Developments and prospects. Front Microbiol. 9 10.3389/fmicb.2018.02732.

Khdhiri M, Piché-Choquette S, Tremblay J, Tringe SG, Constant P. 2017. The tale of a neglected energy source: Elevated hydrogen exposure affects both microbial diversity and function in soil. Appl Environ Microbiol. 83(11):e00275-00217 doi:10.1128/AEM.00275-17.

Kiesewalter HT, Lozano-Andrade CN, Wibowo M, Strube ML, Maróti G, Snyder D, Jørgensen TS, Larsen TO, Cooper VS, Weber T et al. 2021. Genomic and chemical diversity of *Bacillus subtilis* secondary metabolites against plant pathogenic fungi. mSystems. 6(1):10.1128/msystems.00770-00720 10.1128/msystems.00770-20.

Köhl J, Kolnaar R, Ravensberg WJ. 2019. Mode of action of microbial biological control agents against plant diseases: Relevance beyond efficacy. Front Plant Sci. Volume 10 10.3389/fpls.2019.00845.

Kokkoris V, Vukicevich E, Richards A, Thomsen C, Hart MM. 2021. Challenges using droplet digital PCR for environmental samples. Appl Microbiol. 1(1):74-88, https://www.mdpi.com/2673-8007/1/1/7

Kozanitas M, Knaus BJ, Tabima JF, Grünwald NJ, Garbelotto M. 2024. Climatic variability, spatial heterogeneity and the presence of multiple hosts drive the population structure of the pathogen *Phytophthora ramorum* and the epidemiology of Sudden Oak Death. Ecography. 2024(10):e07012 https://doi.org/10.1111/ecog.07012.

Kroon LPNM, Brouwer H, de Cock AWAM, Govers F. 2012. The genus *Phytophthora* anno 2012. Phytopathology. 102(4):348-364 10.1094/phyto-01-11-0025.

Krull CR, Waipara NW, Choquenot D, Burns BR, Gormley AM, Stanley MC. 2013. Absence of evidence is not evidence of absence: Feral pigs as vectors of soil-borne pathogens. Austral Ecol. 38(5):534-542 https://doi.org/10.1111/j.1442-9993.2012.02444.x.

Kurz WA, Stinson G, Rampley GJ, Dymond CC, Neilson ET. 2008. Risk of natural disturbances makes future contribution of Canada's forests to the global carbon cycle highly uncertain. PNAS. 105(5):1551-1555 10.1073/pnas.0708133105.

Kuzyakov Y, Blagodatskaya E. 2015. Microbial hotspots and hot moments in soil: Concept & review. Soil Biol Biochem. 83:184-199 https://doi.org/10.1016/j.soilbio.2015.01.025.

Lacey RF, Sullivan-Hill BA, Deslippe JR, Keyzers RA, Gerth ML. 2021. The Fatty Acid Methyl Ester (FAME) profile of *Phytophthora agathidicida* and its potential use as diagnostic tool. FEMS Microbiol Lett. 368(17) 10.1093/femsle/fnab113.

Lambert S, Waipara NW, Black A, Mark-Shadbolt M, Wood W. 2018. Indigenous biosecurity: Māori responses to kauri dieback and myrtle rust in Aotearoa New Zealand. In: Urquhart J, Marzano M, Potter C, editors. The Human Dimensions of Forest and Tree Health: Global Perspectives. Cham: Springer International Publishing. p. 109-137.

Lamichhane JR, Barbetti MJ, Chilvers MI, Pandey AK, Steinberg C. 2024. Exploiting root exudates to manage soil-borne disease complexes in a changing climate. Trends Microbiol. 32(1):27-37 https://doi.org/10.1016/j.tim.2023.07.011.

Lan G, Wu Z, Yang C, Sun R, Chen B, Zhang X. 2021. Forest conversion alters the structure and functional processes of tropical forest soil microbial communities. Land Degradation & Development. 32(2):613-627 https://doi.org/10.1002/ldr.3757.

Langille MGI, Zaneveld J, Caporaso JG, McDonald D, Knights D, Reyes JA, Clemente JC, Burkepile DE, Vega Thurber RL, Knight R et al. 2013. Predictive functional profiling of microbial

communities using 16S rRNA marker gene sequences. Nat Biotechnol. 31(9):814-821 10.1038/nbt.2676.

Langmaier M, Lapin K. 2020. A systematic review of the impact of invasive alien plants on forest regeneration in European temperate forests. Front Plant Sci. 11 10.3389/fpls.2020.524969.

Langmead B, Salzberg SL. 2012. Fast gapped-read alignment with Bowtie 2. Nat Methods. 9(4):357-359 10.1038/nmeth.1923.

Lauber CL, Hamady M, Knight R, Fierer N. 2009. Pyrosequencing-based assessment of soil pH as a predictor of soil bacterial community structure at the continental scale. Appl Environ Microbiol. 75(15):5111-5120 10.1128/AEM.00335-09.

Lawrence P, Jackson L, Padamsee M, Lee K, Lacap-Bugler D. 2024. Screening of *Agathis australis* endophytes as biological control agents against kauri dieback pathogen *Phytophthora agathidicida*. J Plant Pathol. 107:39–51 10.1007/s42161-023-01569-w.

Lawrence P, Padamsee M, Lee K, Lacap-Bugler DC. 2023. Soil microbial functional gene dataset associated with *Agathis australis*. Data Br. 51:109791 https://doi.org/10.1016/j.dib.2023.109791.

Lawrence SA, Armstrong CB, Patrick WM, Gerth ML. 2017. High-throughput chemical screening identifies compounds that inhibit different stages of the *Phytophthora agathidicida* and *Phytophthora cinnamomi* life cycles. Front Microbiol. 8:1340-1340 10.3389/fmicb.2017.01340.

Leake J, Johnson D, Donnelly D, Muckle G, Boddy L, Read D. 2004. Networks of power and influence: The role of mycorrhizal mycelium in controlling plant communities and agroecosystem functioning. Canad J Bot. 82(8):1016-1045 10.1139/b04-060.

Lee M. 2022. bit: aAmultipurpose collection of bioinformatics tools. F1000Research. 11(122) 10.12688/f1000research.79530.1.

Lee S-J, Rose JKC. 2010. Mediation of the transition from biotrophy to necrotrophy in hemibiotrophic plant pathogens by secreted effector proteins. Plant Signal Behav. 5(6):769-772 10.4161/psb.5.6.11778.

Lee S-M, Kong HG, Song GC, Ryu C-M. 2020. Disruption of Firmicutes and Actinobacteria abundance in tomato rhizosphere causes the incidence of bacterial wilt disease. ISME J. 15(1):330-347 10.1038/s41396-020-00785-x.

Legeay J, Husson C, Cordier T, Vacher C, Marcais B, Buée M. 2019. Comparison and validation of Oomycetes metabarcoding primers for *Phytophthora* high throughput sequencing. J Plant Pathol. 101(3):743-748 10.1007/s42161-019-00276-9.

Lewis K. 2018. Characterising the growth response and pathogenicity of *Phytophthora agathidicida* in soils from contrasting land-uses. Lincoln University https://hdl.handle.net/10182/9593.

Lewis KSJ, Black A, Condron LM, Waipara NW, Scott PM, Williams NM, O'Callaghan M. 2019. Land-use changes influence the sporulation and survival of *Phytophthora agathidicida*, a lethal pathogen of New Zealand kauri (*Agathis australis*). For Pathol. 49(2):e12502 https://doi.org/10.1111/efp.12502.

Li D, Luo R, Liu C-M, Leung C-M, Ting H-F, Sadakane K, Yamashita H, Lam T-W. 2016. MEGAHIT v1.0: A fast and scalable metagenome assembler driven by advanced methodologies and community practices. Methods. 102:3-11 https://doi.org/10.1016/j.ymeth.2016.02.020.

Li K, Lin H, Han M, Yang L. 2024. Soil metagenomics reveals the effect of nitrogen on soil microbial communities and nitrogen-cycle functional genes in the rhizosphere of *Panax ginseng*. Front Plant Sci. 15 10.3389/fpls.2024.1411073.

Li Y, Ge Y, Wang J, Shen C, Wang J, Liu Y-J. 2021. Functional redundancy and specific taxa modulate the contribution of prokaryotic diversity and composition to multifunctionality. Mol Ecol. 30(12):2915-2930 https://doi.org/10.1111/mec.15935.

Lin H, Peddada SD. 2024. Multigroup analysis of compositions of microbiomes with covariate adjustments and repeated measures. Nat Methods. 21(1):83-91 10.1038/s41592-023-02092-7.

Linlin Y. 2023. ggvenn: Draw Venn Diagram by 'ggplot2'. https://github.com/yanlinlin82/ggvenn.

Liu H, Li J, Carvalhais LC, Percy CD, Prakash Verma J, Schenk PM, Singh BK. 2021. Evidence for the plant recruitment of beneficial microbes to suppress soil-borne pathogens. New Phytologist. 229(5):2873-2885 https://doi.org/10.1111/nph.17057.

Liu J, Wang Q, Ku Y, Zhang W, Zhu H, Zhao Z. 2022. Precipitation and soil pH drive the soil microbial spatial patterns in the *Robinia pseudoacacia* forests at the regional scale. CATENA. 212:106120 https://doi.org/10.1016/j.catena.2022.106120.

Liu S, Wang H, Tian P, Yao X, Sun H, Wang Q, Delgado-Baquerizo M. 2020a. Decoupled diversity patterns in bacteria and fungi across continental forest ecosystems. Soil Biol Biochem. 144:107763 https://doi.org/10.1016/j.soilbio.2020.107763.

Liu Y-X, Qin Y, Chen T, Lu M, Qian X, Guo X, Bai Y. 2020b. A practical guide to amplicon and metagenomic analysis of microbiome data. Protein Cell. 12(5):315-330 10.1007/s13238-020-00724-8.

Lladó S, López-Mondéjar R, Baldrian P. 2017. Forest soil bacteria: Diversity, involvement in ecosystem processes, and response to global change. Microbiol Mol Biol Rev. 81(2) 10.1128/mmbr.00063-16.

Lladó S, López-Mondéjar R, Baldrian P. 2018. Drivers of microbial community structure in forest soils. Appl Microbiol Biotechnol. 102(10):4331-4338 10.1007/s00253-018-8950-4.

Lorrey AM, Boswijk G, Hogg A, Palmer JG, Turney CSM, Fowler AM, Ogden J, Woolley J-M. 2018. The scientific value and potential of New Zealand swamp kauri. Quat Sci Rev. 183:124-139 https://doi.org/10.1016/j.quascirev.2017.12.019.

Louca S, Polz MF, Mazel F, Albright MBN, Huber JA, O'Connor MI, Ackermann M, Hahn AS, Srivastava DS, Crowe SA et al. 2018. Function and functional redundancy in microbial systems. Nat Ecol Evol. 2(6):936-943 10.1038/s41559-018-0519-1.

Louisson Z, Gutiérrez-Ginés MJ, Taylor M, Buckley HL, Hermans SM, Lear G. 2024. Soil conditions are a more important determinant of microbial community composition and functional potential than neighboring plant diversity. iScience. 27(6) 10.1016/j.isci.2024.110056.

Loyd AL, Benson DM, Ivors KL. 2014. *Phytophthora* populations in nursery irrigation water in relationship to pathogenicity and infection frequency of *Rhododendron* and *Pieris*. Plant Dis. 98(9):1213-1220 10.1094/PDIS-11-13-1157-RE.

Lozano-Tovar MD, Garrido-Jurado I, Quesada-Moraga E, Raya-Ortega MC, Trapero-Casas A. 2017. *Metarhizium brunneum* and *Beauveria bassiana* release secondary metabolites with antagonistic activity against *Verticillium dahliae* and *Phytophthora megasperma* olive pathogens. Crop Protection. 100:186-195 https://doi.org/10.1016/j.cropro.2017.06.026.

Lozano-Tovar MD, Ortiz-Urquiza A, Garrido-Jurado I, Trapero-Casas A, Quesada-Moraga E. 2013. Assessment of entomopathogenic fungi and their extracts against a soil-dwelling pest and soil-borne pathogens of olive. Biol Control. 67(3):409-420 https://doi.org/10.1016/j.biocontrol.2013.09.006.

Lu J, Breitwieser FP, Thielen P, Salzberg SL. 2017. Bracken: estimating species abundance in metagenomics data. PeerJ Comput Sci. 3:e104 10.7717/peerj-cs.104.

Lu J, Rincon N, Wood DE, Breitwieser FP, Pockrandt C, Langmead B, Salzberg SL, Steinegger M. 2022. Metagenome analysis using the Kraken software suite. Nat Protoc. 17(12):2815-2839 10.1038/s41596-022-00738-y.

Macinnis-Ng C, Schwendenmann L. 2015. Litterfall, carbon and nitrogen cycling in a southern hemisphere conifer forest dominated by kauri (*Agathis australis*) during drought. Plant Ecol. 216(2):247-262 https://doi.org/10.1007/s11258-014-0432-x.

Macinnis-Ng C, Wyse SV, Webb T, Taylor D, Schwendenmann L. 2017. Sustained carbon uptake in a mixed age southern conifer forest. Trees. 31(3):967-980 10.1007/s00468-017-1521-y.

Madison JD, LaBumbard BC, Woodhams DC. 2023. Shotgun metagenomics captures more microbial diversity than targeted 16S rRNA gene sequencing for field specimens and preserved museum specimens. PLOS One. 18(9):e0291540 10.1371/journal.pone.0291540.

Maestre FT, Delgado-Baquerizo M, Jeffries TC, Eldridge DJ, Ochoa V, Gozalo B, Quero JL, García-Gómez M, Gallardo A, Ulrich W et al. 2015. Increasing aridity reduces soil microbial diversity and abundance in global drylands. PNAS. 112(51):15684-15689 10.1073/pnas.1516684112.

Maheshwari M, Abulreesh HH, Khan MS, Ahmad I, Pichtel J. 2017. Horizontal gene transfer in soil and the rhizosphere: Impact on ecological fitness of bacteria. In: Meena VS, Mishra PK, Bisht JK, Pattanayak A, editors. Agriculturally Important Microbes for Sustainable Agriculture : Volume I: Plant-soil-microbe nexus. Singapore: Springer Singapore. p. 111-130.

Maitra P, Hrynkiewicz K, Szuba A, Jagodziński AM, Al-Rashid J, Mandal D, Mucha J. 2024. Metabolic niches in the rhizosphere microbiome: dependence on soil horizons, root traits and climate variables in forest ecosystems. Front Plant Sci. 15 10.3389/fpls.2024.1344205.

Mallick H, Rahnavard A, McIver LJ, Ma S, Zhang Y, Nguyen LH, Tickle TL, Weingart G, Ren B, Schwager EH et al. 2021. Multivariable association discovery in population-scale meta-omics studies. PLoS Comp Biol. 17(11):e1009442 10.1371/journal.pcbi.1009442.

Manaaki Whenua Landcare Research. 2021. Soil testing. [accessed 2021 1 September]. https://www.landcareresearch.co.nz/partner-with-us/laboratories-and-diagnostics/environmental-chemistry-laboratory/soil-testing/.

Marañón-Jiménez S, Radujković D, Verbruggen E, Grau O, Cuntz M, Peñuelas J, Richter A, Schrumpf M, Rebmann C. 2021. Shifts in the abundances of saprotrophic and ectomycorrhizal fungi with Altered leaf litter inputs. Front Plant Sci. 12 10.3389/fpls.2021.682142.

Martin M. 2011. Cutadapt removes adapter sequences from high-throughput sequencing reads. EMBnetjournal. 17(1):10-12 10.14806/ej.17.1.200.

Martinez Arbizu P. 2020. pairwiseAdonis: Pairwise multilevel comparison using adonis. https://github.com/pmartinezarbizu/pairwiseAdonis.

Martino C, Morton JT, Marotz CA, Thompson LR, Tripathi A, Knight R, Zengler K. 2019. A novel sparse compositional technique reveals microbial perturbations. mSystems. 4(1):10.1128/msystems.00016-00019 10.1128/msystems.00016-19.

Mascher F, Hase C, Bouffaud M-L, Défago G, Moënne-Loccoz Y. 2014. Cell culturability of *Pseudomonas protegens* CHA0 depends on soil pH. FEMS Microbiol Ecol. 87(2):441-450 10.1111/1574-6941.12234.

McKenzie EHC, Buchanan PK, Johnston PR. 2002. Checklist of fungi on kauri (*Agathis australis*) in New Zealand. N Z J Bot. 40(2):269-296 10.1080/0028825X.2002.9512788.

McMurdie PJ, Holmes S. 2013. phyloseq: An R package for reproducible interactive analysis and graphics of microbiome census data. PLOS One. 8(4):e61217 10.1371/journal.pone.0061217.

Meiforth JJ, Buddenbaum H, Hill J, Norton DA, Shepherd J. 2019. Detection of New Zealand kauri trees with AISA aerial hyperspectral data for use in multispectral monitoring. Remote Sens. 11(23) 10.3390/rs11232865.

Mélida H, Sandoval-Sierra JV, Diéguez-Uribeondo J, Bulone V. 2013. Analyses of extracellular carbohydrates in oomycetes unveil the existence of three different cell wall types. Eukaryotic Cell. 12(2):194-203 10.1128/ec.00288-12.

Mendes LW, Tsai SM, Navarrete A, xe, cio A, de Hollander M, van Veen JA, Kuramae EE. 2015. Soil-borne microbiome: Linking diversity to function. Microb Ecol. 70(1):255-265 https://doi.org/10.1007/s00248-014-0559-2.

Meng W, Chang L, Qu Z, Liu B, Liu K, Zhang Y, Huang L, Sun H. 2024. Dominant tree species and litter quality govern fungal community dynamics during litter decomposition. Journal of Fungi 10(10) 10.3390/jof10100690.

Mészárošová L, Kuťáková E, Kohout P, Münzbergová Z, Baldrian P. 2024. Plant effects on microbiome composition are constrained by environmental conditions in a successional grassland. Environ Microbiome. 19(1):8 10.1186/s40793-024-00550-z.

Mikkelson KM, Brouillard BM, Bokman CM, Sharp JO. 2017. Ecosystem resilience and limitations revealed by soil bacterial community dynamics in a bark beetle-impacted forest. mBio. 8(6):10.1128/mbio.01305-01317 10.1128/mbio.01305-17.

Mikkelson KM, Lozupone CA, Sharp JO. 2016. Altered edaphic parameters couple to shifts in terrestrial bacterial community structure associated with insect-induced tree mortality. Soil Biol Biochem. 95:19-29 https://doi.org/10.1016/j.soilbio.2015.12.001.

Mohini T. 2024. Physicochemical characterisation of soil from dieback kauri forest. [Auckland, New Zealand]: Auckland University of Technology http://hdl.handle.net/10292/17335.

Morales-Rodríguez C, Martín-García J, Ruiz-Gómez FJ, Poveda J, Diez JJ. 2024. Relationships between rhizosphere microbiota and forest health conditions in *Pinus pinaster* stands at the Iberian Peninsula. Appl Soil Ecol. 193:105142 https://doi.org/10.1016/j.apsoil.2023.105142.

Morgan XC, Huttenhower C. 2012. Chapter 12: Human microbiome analysis. PLoS Comp Biol. 8(12):e1002808 10.1371/journal.pcbi.1002808.

Morrison EW, Frey SD, Sadowsky JJ, van Diepen LTA, Thomas WK, Pringle A. 2016. Chronic nitrogen additions fundamentally restructure the soil fungal community in a temperate forest. Fungal Ecol. 23:48-57 https://doi.org/10.1016/j.funeco.2016.05.011.

Morrison TM, English DA. 1967. The significance of mycorrhizal nodules of *Agathis australis*. New Phytologist. 66(2):245-250 https://doi.org/10.1111/j.1469-8137.1967.tb06002.x.

Morton JT, Marotz C, Washburne A, Silverman J, Zaramela LS, Edlund A, Zengler K, Knight R. 2019. Establishing microbial composition measurement standards with reference frames. Nat Commun. 10(1):2719 10.1038/s41467-019-10656-5.

Muñoz-Ramírez ZY, González-Escobedo R, Avila-Quezada GD, Ramírez-Sánchez O, Higareda-Alvear VM, Zapata-Chávez E, Borrego-Loya A, Muñoz-Castellanos LN. 2024. Exploring microbial rhizosphere communities in asymptomatic and symptomatic apple trees using amplicon sequencing and shotgun metagenomics. Agronomy. 14(2):357, https://www.mdpi.com/2073-4395/14/2/357

Nannipieri P, Ascher J, Ceccherini MT, Landi L, Pietramellara G, Renella G. 2017. Microbial diversity and soil functions. Eur J Soil Sci. 68(1):12-26 https://doi.org/10.1111/ejss.4_12398.

Nelkner J, Henke C, Lin TW, Pätzold W, Hassa J, Jaenicke S, Grosch R, Pühler A, Sczyrba A, Schlüter A. 2019. Effect of long-term farming practices on agricultural soil microbiome members represented by metagenomically assembled genomes (MAGs) and their predicted plant-beneficial genes. Genes. 10(6):424, https://www.mdpi.com/2073-4425/10/6/424

New Zealand Herald. 2005. Kauri to be Northland tourism icon. [accessed May 28 2021]https://www.nzherald.co.nz/nz/kauri-to-be-northland-tourism-icon/2B4QBJR4EZPECEXHIVVB2KGEA4/.

Nielsen UN, Osler GHR, Campbell CD, Burslem DFRP, van der Wal R. 2010. The influence of vegetation type, soil properties and precipitation on the composition of soil mite and microbial communities at the landscape scale. J Biogeogr. 37(7):1317-1328 https://doi.org/10.1111/j.1365-2699.2010.02281.x.

O'Brien SL, Gibbons SM, Owens SM, Hampton-Marcell J, Johnston ER, Jastrow JD, Gilbert JA, Meyer F, Antonopoulos DA. 2016. Spatial scale drives patterns in soil bacterial diversity. Environ Microbiol. 18(6):2039-2051 https://doi.org/10.1111/1462-2920.13231.

Oksanen J, Blanchet FG, Friendly M, Kindt R, Legendre P, McGlinn D, Minchin PR, O'Hara RB, Simpson GL, Solymos P et al. 2020. vegan: Community ecology package.

Onet A, Grenni P, Onet C, Stoian V, Crisan V. 2025. Forest soil microbiomes: A review of key research from 2003 to 2023. Forests. 16(1):148, https://www.mdpi.com/1999-4907/16/1/148

Orwin J. 2004. Kauri: witness to a nation's history. Auckland, N.Z.: New Holland.

Osburn ED, McBride SG, Aylward FO, Badgley BD, Strahm BD, Knoepp JD, Barrett JE. 2019. Soil bacterial and fungal communities exhibit distinct long-term responses to disturbance in temperate forests. Front Microbiol. 10 10.3389/fmicb.2019.02872.

Osburn ED, Moon C, Stephenson T, Kittipalawattanapol K, Jones M, Strickland MS, Lynch LM. 2023. Disturbance of eucalypt forests alters the composition, function, and assembly of soil microbial communities. FEMS Microbiol Ecol. 99(9) 10.1093/femsec/fiad085.

Owens JN, Catalano GL, Aitken-Christie J. 1997. The reproductive biology of kauri (*Agathis australis*). IV. Late embryogeny, histochemistry, cone and seed morphology. Int J Plant Sci. 158(4):395-407 https://doi.org/10.1086/297449.

Owens JN, Catalano GL, Morris SJ, Aitken-Christie J. 1995. The reproductive biology of kauri (*Agathis australis*). I. Pollination and prefertilization development. Int J Plant Sci. 156(3):257-269 10.1086/297248.

Pachoute J, dos Santos GR, de Souza DJ. 2024. Antagonistic effects of *Beauveria bassiana* on seed-borne fungi of cowpea (*Vigna unguiculata*). Biologia. 79(5):1487-1495 10.1007/s11756-024-01615-7.

Padamsee M, Johansen RB, Stuckey SA, Williams SE, Hooker JE, Burns BR, Bellgard SE. 2016. The arbuscular mycorrhizal fungi colonising roots and root nodules of New Zealand kauri *Agathis australis*. Fungal Biol. 120(5):807-817 https://doi.org/10.1016/j.funbio.2016.01.015.

Palmer JTT, Vink JNA, Castro LM, Craig OJS, Davison EE, Gerth ML. 2025. Improved isolation and PCR detection of *Phytophthora agathidicida* oospores from soils. Microbiol Spectr. 13(5):e00135-00125 10.1128/spectrum.00135-25.

Palozzi JE, Lindo Z. 2018. Are leaf litter and microbes team players? Interpreting home-field advantage decomposition dynamics. Soil Biol Biochem. 124:189-198 https://doi.org/10.1016/j.soilbio.2018.06.018.

Pan H, Wattiez R, Gillan D. 2024. Soil metaproteomics for microbial community profiling: Methodologies and challenges. Curr Microbiol. 81(8):257 10.1007/s00284-024-03781-y.

Pantigoso HA, Newberger D, Vivanco JM. 2022. The rhizosphere microbiome: Plant–microbial interactions for resource acquisition. J Appl Microbiol. 133(5):2864-2876 10.1111/jam.15686.

Pascual LS, Segarra-Medina C, Gómez-Cadenas A, López-Climent MF, Vives-Peris V, Zandalinas SI. 2022. Climate change-associated multifactorial stress combination: A present challenge for our ecosystems. J Plant Physiol. 276:153764 https://doi.org/10.1016/j.jplph.2022.153764.

Pau'uvale A, Dewan C, Mora H, Waipara NW, Bellgard SE. 2011. Kauri killer on the loose?—Study of human vectors and PTA hygiene treatments.

Paulson J, Olson N, Braccia D, Wagner J, Talukder H, Pop M, Bravo H. 2013a. metagenomeSeq: Statistical analysis for sparse high-throughput sequncing. Bioconductor package.

Paulson J, Stine OC, Bravo HC, Pop M. 2013b. Differential abundance analysis for microbial marker-gene surveys. Nat Methods. 10(12):1200-1202 10.1038/nmeth.2658.

Pauvert C, Buée M, Laval V, Edel-Hermann V, Fauchery L, Gautier A, Lesur I, Vallance J, Vacher C. 2019. Bioinformatics matters: The accuracy of plant and soil fungal community data is highly dependent on the metabarcoding pipeline. Fungal Ecol. 41:23-33 https://doi.org/10.1016/j.funeco.2019.03.005.

Peng J, Zhou X, Rensing C, Liesack W, Zhu Y-G. 2023. Soil microbial ecology through the lens of metatranscriptomics. Soil Ecol Lett. 6(3):230217 10.1007/s42832-023-0217-z.

Peng Z, Liang C, Gao M, Qiu Y, Pan Y, Gao H, Liu Y, Li X, Wei G, Jiao S. 2022. The neglected role of micronutrients in predicting soil microbial structure. NPJ Biofilms Microbiomes. 8(1):103 10.1038/s41522-022-00363-3.

Philippot L, Raaijmakers JM, Lemanceau P, van der Putten WH. 2013. Going back to the roots: the microbial ecology of the rhizosphere. Nat Rev Microbiol. 11(11):789-799 10.1038/nrmicro3109.

Phillips RP, Finzi AC, Bernhardt ES. 2011. Enhanced root exudation induces microbial feedbacks to N cycling in a pine forest under long-term CO2 fumigation. Ecol Lett. 14(2):187-194 https://doi.org/10.1111/j.1461-0248.2010.01570.x.

Pinho D, Barroso C, Froufe H, Brown N, Vanguelova E, Egas C, Denman S. 2020. Linking tree health, rhizosphere physicochemical properties, and microbiome in acute oak decline. Forests. 11(11):1153, https://www.mdpi.com/1999-4907/11/11/1153

Plassart P, Prévost-Bouré NC, Uroz S, Dequiedt S, Stone D, Creamer R, Griffiths RI, Bailey MJ, Ranjard L, Lemanceau P. 2019. Soil parameters, land use, and geographical distance drive soil bacterial communities along a European transect. Sci Rep. 9(1):605 10.1038/s41598-018-36867-2.

Podger FD, Newhook FJ. 1971. *Phytophthora cinnamomi* in indigenous plant communities in New Zealand. N Z J Bot. 9(4):625-638 10.1080/0028825X.1971.10430225.

Qu Z-L, Liu B, Ma Y, Xu J, Sun H. 2020. The response of the soil bacterial community and function to forest succession caused by forest disease. Funct Ecol. 34(12):2548-2559 https://doi.org/10.1111/1365-2435.13665.

Quast C, Pruesse E, Yilmaz P, Gerken J, Schweer T, Yarza P, Peplies J, Glöckner FO. 2012. The SILVA ribosomal RNA gene database project: improved data processing and web-based tools. Nucleic Acids Res. 41(D1):D590-D596 10.1093/nar/gks1219.

R Core Team. 2021. R: A language and environment for statistical computing. Vienna, Austria: R Foundation for Statistical Computing.

Rabiey M, Hailey LE, Roy SR, Grenz K, Al-Zadjali MAS, Barrett GA, Jackson RW. 2019. Endophytes vs tree pathogens and pests: can they be used as biological control agents to improve tree health? Eur J Plant Pathol. 155(3):711-729 10.1007/s10658-019-01814-y.

Raczka NC, Piñeiro J, Tfaily MM, Chu RK, Lipton MS, Pasa-Tolic L, Morrissey E, Brzostek E. 2021. Interactions between microbial diversity and substrate chemistry determine the fate of carbon in soil. Sci Rep. 11(1):19320 10.1038/s41598-021-97942-9.

Rajala T, Velmala SM, Tuomivirta T, Haapanen M, Müller M, Pennanen T. 2013. Endophyte communities vary in the needles of Norway spruce clones. Fungal Biol. 117(3):182-190 https://doi.org/10.1016/j.funbio.2013.01.006.

Ramakodi MP. 2021. A comprehensive evaluation of single-end sequencing data analyses for environmental microbiome research. Arch Microbiol. 203(10):6295-6302 10.1007/s00203-021-02597-9.

Ranadive K, Belsare M, Deokule SS, Jagtap-Ranadive N, Jadhav H, Vaidya J. 2013. Glimpses of antimicrobial activity of fungi from World. JNBR. 2:142-162,

Rao Y, Zeng L, Jiang H, Mei L, Wang Y. 2022. *Trichoderma atroviride* LZ42 releases volatile organic compounds promoting plant growth and suppressing Fusarium wilt disease in tomato seedlings. BMC Microbiol. 22(1):88 10.1186/s12866-022-02511-3.

Rath KM, Fierer N, Murphy DV, Rousk J. 2018. Linking bacterial community composition to soil salinity along environmental gradients. ISME J. 13(3):836-846 10.1038/s41396-018-0313-8.

Rausch P, Rühlemann M, Hermes BM, Doms S, Dagan T, Dierking K, Domin H, Fraune S, von Frieling J, Hentschel U et al. 2019. Comparative analysis of amplicon and metagenomic sequencing methods reveals key features in the evolution of animal metaorganisms. Microbiome. 7(1):133 10.1186/s40168-019-0743-1.

Reis TA, Oliveira TD, Zorzete P, Faria P, Corrêa B. 2020. A non-toxigenic *Aspergillus flavus* strain prevents the spreading of *Fusarium verticillioides* and fumonisins in maize. Toxicon. 181:6-8 https://doi.org/10.1016/j.toxicon.2020.04.091.

Reverchon F, García-Meléndez M, Guevara-Avendaño E, Mora-Chávez O, Solís-García IA, Dáttilo W, Guererro-Analco JA, Méndez-Bravo A, Monribot-Villanueva JL, Patiño-Conde V et al. 2023. Shifts in the rhizosphere microbiome and exudation profile of avocado (*Persea americana Mill.*) during infection by *Phytophthora cinnamomi* and in presence of a biocontrol bacterial strain. CABI Agric Biosci. 4(1):23 10.1186/s43170-023-00167-1.

Ridout M, Newcombe G. 2015. The frequency of modification of *Dothistroma* pine needle blight severity by fungi within the native range. For Ecol Manage. 337:153-160 https://doi.org/10.1016/j.foreco.2014.11.010.

Riesenfeld CS, Schloss PD, Handelsman J. 2004. Metagenomics: Genomic analysis of microbial communities. Annu Rev Genet. 38(1):525-552 10.1146/annurev.genet.38.072902.091216.

Roesch LFW, Fulthorpe RR, Riva A, Casella G, Hadwin AKM, Kent AD, Daroub SH, Camargo FAO, Farmerie WG, Triplett EW. 2007. Pyrosequencing enumerates and contrasts soil microbial diversity. ISME J. 1(4):283-290 10.1038/ismej.2007.53.

Rolfe SA, Griffiths J, Ton J. 2019. Crying out for help with root exudates: Adaptive mechanisms by which stressed plants assemble health-promoting soil microbiomes. Curr Opin Microbiol. 49:73-82 https://doi.org/10.1016/j.mib.2019.10.003.

Romero F, Cazzato S, Walder F, Vogelgsang S, Bender SF, van der Heijden MGA. 2022. Humidity and high temperature are important for predicting fungal disease outbreaks worldwide. New Phytologist. 234(5):1553-1556 https://doi.org/10.1111/nph.17340.

Rousk J, Bååth E, Brookes PC, Lauber CL, Lozupone C, Caporaso JG, Knight R, Fierer N. 2010. Soil bacterial and fungal communities across a pH gradient in an arable soil. ISME J. 4(10):1340-1351 10.1038/ismej.2010.58.

Roy BA, Alexander HM, Davidson J, Campbell FT, Burdon JJ, Sniezko R, Brasier C. 2014. Increasing forest loss worldwide from invasive pests requires new trade regulations. Front Ecol Environ. 12(8):457-465 https://doi.org/10.1890/130240.

Ruiz Gómez FJ, Navarro-Cerrillo RM, Pérez-de-Luque A, Oβwald W, Vannini A, Morales-Rodríguez C. 2019. Assessment of functional and structural changes of soil fungal and oomycete communities in holm oak declined *dehesas* through metabarcoding analysis. Sci Rep. 9(1):5315 10.1038/s41598-019-41804-y.

Saatchi S, Longo M, Xu L, Yang Y, Abe H, André M, Aukema JE, Carvalhais N, Cadillo-Quiroz H, Cerbu GA et al. 2021. Detecting vulnerability of humid tropical forests to multiple stressors. Onearth. 4(7):988-1003 10.1016/j.oneear.2021.06.002.

Sale EV. 1978. Quest for the kauri: forest giants and where to find them. Wellington N.Z.: A.H. & A.W. Reed.

Sanson J. 2016. Independent review of the state of kauri dieback knowledge. Bio-Protection.

Santoyo G, Moreno-Hagelsieb G, del Carmen Orozco-Mosqueda M, Glick BR. 2016. Plant growth-promoting bacterial endophytes. Microbiol Res. 183:92-99 https://doi.org/10.1016/j.micres.2015.11.008.

Sapkota R, Nicolaisen M. 2015. An improved high throughput sequencing method for studying oomycete communities. J Microbiol Methods. 110:33-39 https://doi.org/10.1016/j.mimet.2015.01.013.

Sapsford SJ, Paap T, Hardy GESJ, Burgess TI. 2021. Anthropogenic disturbance impacts mycorrhizal communities and abiotic soil properties: Implications for an endemic forest dsease. Front For Glob Change. 3 10.3389/ffgc.2020.593243.

Sasse J, Martinoia E, Northen T. 2018. Feed your friends: Do plant exudates shape the root microbiome? Trends Plant Sci. 23(1):25-41 10.1016/j.tplants.2017.09.003.

Scarlett K, Denman S, Clark DR, Forster J, Vanguelova E, Brown N, Whitby C. 2021. Relationships between nitrogen cycling microbial community abundance and composition reveal the indirect effect of soil pH on oak decline. ISME J. 15(3):623-635 10.1038/s41396-020-00801-0.

Schoch CL, Seifert KA, Huhndorf S, Robert V, Spouge JL, Levesque CA, Chen W, Consortium FB, List FBCA, Bolchacova E et al. 2012. Nuclear ribosomal internal transcribed spacer (ITS) region as a universal DNA barcode marker for *Fungi*. PNAS. 109(16):6241-6246 10.1073/pnas.1117018109.

Schulz B, Boyle C. 2006. What are endophytes? Microbial root endophytes. Springer. p. 1-13.

Schulz-Bohm K, Gerards S, Hundscheid M, Melenhorst J, de Boer W, Garbeva P. 2018. Calling from distance: Attraction of soil bacteria by plant root volatiles. ISME J. 12(5):1252-1262 10.1038/s41396-017-0035-3.

Seitz VA, McGivern BB, Daly RA, Chaparro JM, Borton MA, Sheflin AM, Kresovich S, Shields L, Schipanski ME, Wrighton KC et al. 2022. Variation in root exudate composition influences soil microbiome membership and function. Appl Environ Microbiol. 88(11):e00226-00222 10.1128/aem.00226-22.

Serna-Chavez HM, Fierer N, van Bodegom PM. 2013. Global drivers and patterns of microbial abundance in soil. Global Ecol Biogeogr. 22(10):1162-1172 https://doi.org/10.1111/geb.12070.

Serrano MS, Romero MÁ, Homet P, Gómez-Aparicio L. 2022. Climate change impact on the population dynamics of exotic pathogens: The case of the worldwide pathogen *Phytophthora cinnamomi*. Agric For Meteorol. 322:109002 https://doi.org/10.1016/j.agrformet.2022.109002.

Sharpton TJ. 2014. An introduction to the analysis of shotgun metagenomic data. Front Plant Sci. 5(209) 10.3389/fpls.2014.00209.

Shen C, Gunina A, Luo Y, Wang J, He J-Z, Kuzyakov Y, Hemp A, Classen AT, Ge Y. 2020. Contrasting patterns and drivers of soil bacterial and fungal diversity across a mountain gradient. Environ Microbiol. 22(8):3287-3301 https://doi.org/10.1111/1462-2920.15090.

Shen C, Xiong J, Zhang H, Feng Y, Lin X, Li X, Liang W, Chu H. 2013. Soil pH drives the spatial distribution of bacterial communities along elevation on Changbai Mountain. Soil Biol Biochem. 57:204-211 https://doi.org/10.1016/j.soilbio.2012.07.013.

Shen W, Ren H. 2021. TaxonKit: A practical and efficient NCBI taxonomy toolkit. J Genet Genom. 48(9):844-850 https://doi.org/10.1016/j.jgg.2021.03.006.

Shen W, Sipos B, Zhao L. 2024. SeqKit2: A Swiss army knife for sequence and alignment processing. iMeta. 3(3):e191 https://doi.org/10.1002/imt2.191.

Sheng X, Pan D, Yang X, Cao G, Lu Z, Wen H, Fan Z, Song Q, Liu H, Wei H et al. 2025. Climatic and edaphic controls on soil microbial diversity and composition across tropical to cold temperate forests. Plant Soil. 10.1007/s11104-025-07606-0.

Shi Z, Yin H, Van Nostrand JD, Voordeckers JW, Tu Q, Deng Y, Yuan M, Zhou A, Zhang P, Xiao N et al. 2019. Functional gene array-based ultrasensitive and quantitative detection of microbial populations in complex communities. mSystems. 4(4) https://doi.org/10.1128/msystems.00296-19.

Shortland T. 2011. Cultural indicators for kauri ngahere. Repo Consultancy Ltd Report prepared for the Kauri Dieback Tangata Whenua Roopu.

Shortland T. 2017a. Kauri dieback cultural health indicator pilot project report. He Puna Marama Trust, Report prepared for the Minisintry of Primary Industries, Contract No. 17874

Shortland T. 2017b. Rongoā (traditional medicine practices) improving the health of kauri forests. Nga Tirairaka o Ngati Hine.

Siegel-Hertz K, Edel-Hermann V, Chapelle E, Terrat S, Raaijmakers JM, Steinberg C. 2018. Comparative microbiome analysis of a *Fusarium* wilt suppressive soil and a *Fusarium* wilt conducive soil from the Châteaurenard region. Front Microbiol. 9 10.3389/fmicb.2018.00568.

Silvester WB. 2000. The biology of kauri (*Agathis australis*) in New Zealand 11. Nitrogen cycling in four kauri forest remnants. N Z J Bot. 38(2):205-220 10.1080/0028825X.2000.9512678.

Silvester WB, Orchard TA. 1999. The biology of kauri (*Agathis australis*) in New Zealand. Production, biomass, carbon storage, and litter fall in four forest remnants. N Z J Bot. 37(3):553-571 10.1080/0028825X.1999.9512653.

Simpson GL. 2025. permute: Functions for generating restricted permutations of data. https://github.com/gavinsimpson/permute.

Singavarapu B, Du J, Beugnon R, Cesarz S, Eisenhauer N, Xue K, Wang Y, Bruelheide H, Wubet T. 2023. Functional potential of soil microbial communities and their subcommunities varies with tree mycorrhizal type and tree diversity. Microbiol Spectr. 11(2):e04578-04522 10.1128/spectrum.04578-22.

Singh BK, Delgado-Baquerizo M, Egidi E, Guirado E, Leach JE, Liu H, Trivedi P. 2023. Climate change impacts on plant pathogens, food security and paths forward. Nat Rev Microbiol. 21(10):640-656 10.1038/s41579-023-00900-7.

Singh J, Curran-Cournane F, Waipara NW, Schwendenmann L, Lear G. 2017. Comparison of methods used to detect the organism responsible for kauri dieback, *Phytophthora agathidicida*, from soil samples. Auckland Council.

Singh VP. 2006. Gymnosperm (naked seeds plant): structure and development. Sarup & Sons.

Singleton CM, Petriglieri F, Kristensen JM, Kirkegaard RH, Michaelsen TY, Andersen MH, Kondrotaite Z, Karst SM, Dueholm MS, Nielsen PH et al. 2021. Connecting structure to function with the recovery of over 1000 high-quality metagenome-assembled genomes from activated sludge using long-read sequencing. Nat Commun. 12(1):2009 10.1038/s41467-021-22203-2.

Sivaprakasam N, Vaithiyanathan S, Gandhi K, Narayanan S, Kavitha PS, Rajasekaran R, Muthurajan R. 2024. Metagenomics approaches in unveiling the dynamics of Plant Growth-Promoting Microorganisms (PGPM) vis-à-vis *Phytophthora* sp. suppression in various crop ecological systems. Res Microbiol. 175(7):104217 https://doi.org/10.1016/j.resmic.2024.104217.

Smith P, House JI, Bustamante M, Sobocká J, Harper R, Pan G, West PC, Clark JM, Adhya T, Rumpel C et al. 2016. Global change pressures on soils from land use and management. Global Change Biol. 22(3):1008-1028 https://doi.org/10.1111/gcb.13068.

Steward GA, Beveridge AE. 2010. A review of New Zealand kauri (*Agathis australis* (D.Don) Lindl.): its ecology, history, growth and potential for management for timber. N Z J For Sci. 40:33-59, https://www.scionresearch.com/__data/assets/pdf_file/0007/58885/NZJFS40201033-59_STEWARD.pdf

Stewart JE, Kim M-S, Lalande B, Klopfenstein NB. 2021. Pathobiome and microbial communities associated with forest tree root diseases. In: Asiegbu FO, Kovalchuk A, editors. Forest Microbiology. Academic Press. p. 277-292.

Stockey RA. 1982. The *Araucariaceae*: An evolutionary perspective. Rev Palaeobot Palynol. 37(1):133-154 https://doi.org/10.1016/0034-6667(82)90041-0.

Stockey RA. 1994. Mesozoic *Araucariaceae*: Morphology and systematic relationships. J Plant Res. 107(4):493-502 10.1007/BF02344070.

Stoeck T, Bass D, Nebel M, Christen R, Jones MDM, Breiner H-W, Richards TA. 2010. Multiple marker parallel tag environmental DNA sequencing reveals a highly complex eukaryotic community in marine anoxic water. Mol Ecol. 19(s1):21-31 https://doi.org/10.1111/j.1365-294X.2009.04480.x.

Struijk M, Stavert JR, Le Grice RJ, Schwendenmann L, Romera PJ, Mitchell G, Sünnemann M, Yang J, Hjelm F, Barnes AD. 2024. The threat of a major tree pathogen to forest soil mesofauna food webs and ecosystem functioning. Front Ecol Evol. 12 10.3389/fevo.2024.1338109.

Štursová M, Bárta J, Šantrůčková H, Baldrian P. 2016. Small-scale spatial heterogeneity of ecosystem properties, microbial community composition and microbial activities in a temperate mountain forest soil. FEMS Microbiol Ecol. 92(12) 10.1093/femsec/fiw185.

Štursová M, Šnajdr J, Cajthaml T, Bárta J, Šantrůčková H, Baldrian P. 2014. When the forest dies: The response of forest soil fungi to a bark beetle-induced tree dieback. ISME J. 8(9):1920-1931 10.1038/ismej.2014.37.

Sun S, Jones RB, Fodor AA. 2020. Inference-based accuracy of metagenome prediction tools varies across sample types and functional categories. Microbiome. 8(1):46 10.1186/s40168-020-00815-y.

Tahovská K, Choma M, Čapek P, Kaštovská E, Kaňa J, Kopáček J. 2024. Increased saprotrophic activity and phosphate leaching following forest soil decomposition without root access. Forests. 15(8):1378, https://www.mdpi.com/1999-4907/15/8/1378

Tarnocai C, Canadell JG, Schuur EAG, Kuhry P, Mazhitova G, Zimov S. 2009. Soil organic carbon pools in the northern circumpolar permafrost region. Glob Biogeochem Cycles. 23(2) https://doi.org/10.1029/2008GB003327.

Te Kawerau ā Maki. 2017. Waitākere Rāhui [accessed 2021 September 27]. http://tekawerau.iwi.nz/node/13.

Tedersoo L, Albertsen M, Anslan S, Callahan B. 2021. Perspectives and benefits of high-throughput long-read sequencing in microbial ecology. Appl Environ Microbiol. 87(17):e00626-00621 10.1128/AEM.00626-21.

Tedersoo L, Bahram M, Põlme S, Kõljalg U, Yorou NS, Wijesundera R, Ruiz LV, Vasco-Palacios AM, Thu PQ, Suija A et al. 2014. Global diversity and geography of soil fungi. Science. 346(6213):1256688 10.1126/science.1256688.

Tellenbach C, Sumarah MW, Grünig CR, Miller JD. 2013. Inhibition of *Phytophthora* species by secondary metabolites produced by the dark septate endophyte *Phialocephala europaea*. Fungal Ecol. 6(1):12-18 https://doi.org/10.1016/j.funeco.2012.10.003.

Terhonen E, Blumenstein K, Kovalchuk A, Asiegbu FO. 2019. Forest tree microbiomes and associated fungal endophytes: Functional roles and impact on forest health. Forests. 10(1):42, https://www.mdpi.com/1999-4907/10/1/42

Than DJ, Hughes KJD, Boonhan N, Tomlinson JA, Woodhall JW, Bellgard SE. 2013. A TaqMan real-time PCR assay for the detection of *Phytophthora* 'taxon Agathis' in soil, pathogen of Kauri in New Zealand. For Pathol. 43(4):324-330 https://doi.org/10.1111/efp.12034.

The Gymnosperm Database. n.d. *Agathis australis*. [accessed 2024 December 4]. https://www.conifers.org/ar/Agathis_australis.php.

Tkacz A, Hortala M, Poole PS. 2018. Absolute quantitation of microbiota abundance in environmental samples. Microbiome. 6(1):110 10.1186/s40168-018-0491-7.

Tong Y, Zheng X, Hu Y, Wu J, Liu H, Deng Y, Lv W, Yao H, Chen J, Ge T. 2024. Root exudate-mediated plant–microbiome interactions determine plant health during disease infection. Agric, Ecosyst Environ. 370:109056 https://doi.org/10.1016/j.agee.2024.109056.

Toole DR, Zhao J, Martens-Habbena W, Strauss SL. 2021. Bacterial functional prediction tools detect but underestimate metabolic diversity compared to shotgun metagenomics in southwest Florida soils. Appl Soil Ecol. 168:104129 https://doi.org/10.1016/j.apsoil.2021.104129.

Tremblay ÉD, Duceppe M-O, Bérubé JA, Kimoto T, Lemieux C, Bilodeau GJ. 2018. Screening for exotic forest pathogens to increase survey capacity using metagenomics. Phytopathology. 108(12):1509-1521 10.1094/PHYTO-02-18-0028-R.

Trevors JT. 2009. One gram of soil: a microbial biochemical gene library. Antonie Van Leeuwenhoek. 97(2):99 10.1007/s10482-009-9397-5.

Tringe SG, von Mering C, Kobayashi A, Salamov AA, Chen K, Chang HW, Podar M, Short JM, Mathur EJ, Detter JC et al. 2005. Comparative metagenomics of microbial communities. Science. 308(5721):554-557 10.1126/science.1107851.

Tu Q, Lin L, Cheng L, Deng Y, He Z. 2018. NCycDB: a curated integrative database for fast and accurate metagenomic profiling of nitrogen cycling genes. Bioinformatics. 35(6):1040-1048 10.1093/bioinformatics/bty741.

Tuite J. 1969. Plant pathological methods. Fungi and bacteria. Minneapolis, Minn: Burgess Pub. Co.

Turner RS. 2005. After the famine: Plant pathology, *Phytophthora infestans*, and the late blight of potatoes, 1845–1960. Hist Stud Phys Biol. 35(2):341-370 10.1525/hsps.2005.35.2.341.

Tyler BM. 2002. Molecular basis of recognition between *Phytophthora* pathogens and their hosts. Annu Rev Phytopathol. 40(1):137-167 10.1146/annurev.phyto.40.120601.125310.

Urbanová M, Šnajdr J, Baldrian P. 2015. Composition of fungal and bacterial communities in forest litter and soil is largely determined by dominant trees. Soil Biol Biochem. 84:53-64 https://doi.org/10.1016/j.soilbio.2015.02.011.

van der Heijden MGA, Bardgett RD, Van Straalen NM. 2008. The unseen majority: Soil microbes as drivers of plant diversity and productivity in terrestrial ecosystems. Ecol Lett. 11(3):296-310 https://doi.org/10.1111/j.1461-0248.2007.01139.x.

van der Heijden MGA, Martin FM, Selosse M-A, Sanders IR. 2015. Mycorrhizal ecology and evolution: The past, the present, and the future. New Phytologist. 205(4):1406-1423 https://doi.org/10.1111/nph.13288.

van der Heijden MGA, Streitwolf-Engel R, Riedl R, Siegrist S, Neudecker A, Ineichen K, Boller T, Wiemken A, Sanders IR. 2006. The mycorrhizal contribution to plant productivity, plant nutrition and soil structure in experimental grassland. New Phytologist. 172(4):739-752 https://doi.org/10.1111/j.1469-8137.2006.01862.x.

Van Tran Q, Ha CV, Vvedensky VV, Linh Le TT, Han V-C. 2023. Pathogenicity and fungicide sensitivity of *Phytophthora parvispora*, a new pathogen causing gummosis and root rot disease on citrus trees. Microb Pathog. 175:105986 https://doi.org/10.1016/j.micpath.2023.105986.

Vartoukian SR, Palmer RM, Wade WG. 2010. Strategies for culture of 'unculturable' bacteria. FEMS Microbiol Lett. 309(1):1-7 10.1111/j.1574-6968.2010.02000.x.

Veen GF, ten Hooven FC, Weser C, Hannula SE. 2021. Steering the soil microbiome by repeated litter addition. J Ecol. 109(6):2499-2513 https://doi.org/10.1111/1365-2745.13662.

Velásquez AC, Castroverde CDM, He SY. 2018. Plant–Pathogen warfare under changing climate conditions. Curr Biol. 28(10):R619-R634 https://doi.org/10.1016/j.cub.2018.03.054.

Venice F, Vizzini A, Frascella A, Emiliani G, Danti R, Della Rocca G, Mello A. 2021. Localized reshaping of the fungal community in response to a forest fungal pathogen reveals resilience of Mediterranean mycobiota. Sci Total Environ. 800:149582 https://doi.org/10.1016/j.scitotenv.2021.149582.

Verkaik E, Berendse F, Gardner RO. 2007. Low soil water and nutrient availability below New Zealand kauri (*Agathis australis* (D. Don) Lindl.) trees increase the relative fitness of kauri seedlings. Plant Ecol. 191(2):163-170 10.1007/s11258-006-9234-0.

Verkaik E, Jongkind AG, Berendse F. 2006. Short-term and long-term effects of tannins on nitrogen mineralisation and litter decomposition in kauri (*Agathis australis* (D. Don) Lindl.) forests. Plant Soil. 287(1/2):337-345 https://doi.org/10.1007/s11104-006-9081-8.

Vos M, Wolf AB, Jennings SJ, Kowalchuk GA. 2013. Micro-scale determinants of bacterial diversity in soil. FEMS Microbiol Rev. 37(6):936-954 10.1111/1574-6976.12023.

Waipara NW, Hill S, Hill LMW, Hough EG, Horner IJ. 2013. Surveillance methods to determine tree health distribution of kauri dieback disease and associated pathogens. N Z Plant Prot. 66(0):235-241 10.30843/nzpp.2013.66.5671.

Walters DR, Ratsep J, Havis ND. 2013. Controlling crop diseases using induced resistance: challenges for the future. J Exp Bot. 64(5):1263-1280 10.1093/jxb/ert026.

Wang H, Liu R, You MP, Barbetti MJ, Chen Y. 2021a. Pathogen biocontrol using plant growth-promoting bacteria (PGPR): Role of bacterial diversity. Microorganisms. 9(9):1988, https://www.mdpi.com/2076-2607/9/9/1988

Wang L, Sun Y, Li J, Tigabu M, Xu Q, Ma X, Li M. 2023a. Rhizosphere soil nutrients and bacterial community diversity of four broad-leaved trees planted under Chinese fir stands with different stocking density levels. Front For Glob Change. 6 10.3389/ffgc.2023.1135692.

Wang Q, Garrity GM, Tiedje JM, Cole JR. 2007. Naïve bayesian classifier for rapid assignment of rRNA sequences into the new bacterial taxonomy. Appl Environ Microbiol. 73(16):5261-5267 10.1128/AEM.00062-07.

Wang X, Feng J, Ao G, Qin W, Han M, Shen Y, Liu M, Chen Y, Zhu B. 2023b. Globally nitrogen addition alters soil microbial community structure, but has minor effects on soil microbial diversity and richness. Soil Biol Biochem. 179:108982 https://doi.org/10.1016/j.soilbio.2023.108982.

Wang X, Van Nostrand JD, Deng Y, Lü X, Wang C, Zhou J, Han X. 2015. Scale-dependent effects of climate and geographic distance on bacterial diversity patterns across northern China's grasslands. FEMS Microbiol Ecol. 91(12) 10.1093/femsec/fiv133.

Wang Y, Chen L, Xiang W, Ouyang S, Zhang T, Zhang X, Zeng Y, Hu Y, Luo G, Kuzyakov Y. 2021b. Forest conversion to plantations: A meta-analysis of consequences for soil and microbial properties and functions. Global Change Biol. 27(21):5643-5656 https://doi.org/10.1111/gcb.15835.

Wei Y, Quan F, Lan G, Wu Z, Yang C. 2022. Space rather than seasonal changes explained more of the spatiotemporal variation of tropical soil microbial communities. Microbiol Spectr. 10(6):e01846-01822 10.1128/spectrum.01846-22.

Weir BS, Paderes EP, Anand N, Uchida JY, Pennycook SR, Bellgard SE, Beever RE. 2015. A taxonomic revision of *Phytophthora* Clade 5 including two new species, *Phytophthora agathidicida* and *P. cocois*. Phytotaxa. 205(1):21-38 http://dx.doi.org/10.11646/phytotaxa.205.1.2.

Wen T, Ding Z, Thomashow LS, Hale L, Yang S, Xie P, Liu X, Wang H, Shen Q, Yuan J. 2023. Deciphering the mechanism of fungal pathogen-induced disease-suppressive soil. New Phytologist. 238(6):2634-2650 https://doi.org/10.1111/nph.18886.

White M. 2019 May 28 2021. Too many tourists? North & South.

White TJ, Bruns T, Lee S, Taylor J. 1990. Amplification and direct sequencing of fungal ribosomal RNA genes for phylogenetics. In: Innis MA, Gelfand DH, Sninsky JJ, TJ W, editors. PCR protocols, a guide to methods and applications. San Diego, California: Academic Press. p. 315-322.

Whitman WB, Coleman DC, Wiebe WJ. 1998. Prokaryotes: The unseen majority. PNAS. 95(12):6578-6583 10.1073/pnas.95.12.6578.

Whitmore TC. 1977. A first look at *Agathis*. Commenwealth Forestry Institute, University of Oxford.

Wilson VR, Gould KS, Lovel PH, Aitken-Christie J. 1998. Branch morphology and abscission in kauri, *Agathis australis* (Araucariaceae). N Z J Bot. 36(1):135-140 10.1080/0028825X.1998.9512552.

Win TT, Bo B, Malec P, Khan S, Fu P. 2021. Newly isolated strain of *Trichoderma asperellum* from disease suppressive soil is a potential bio-control agent to suppress *Fusarium* soil borne fungal phytopathogens. J Plant Pathol. 103(2):549-561 https://doi.org/10.1007/s42161-021-00780-x.

Winkworth RC, Bellgard SE, McLenachan PA, Lockhart PJ. 2021. The mitogenome of *Phytophthora agathidicida*: Evidence for a not so recent arrival of the “kauri killing” *Phytophthora* in New Zealand. PLOS One. 16(5):e0250422 10.1371/journal.pone.0250422.

Winkworth RC, Nelson BCW, Bellgard SE, Probst CM, McLenachan PA, Lockhart PJ. 2020. A LAMP at the end of the tunnel: A rapid, field deployable assay for the kauri dieback pathogen, *Phytophthora agathidicida*. PLOS One. 15(1):e0224007 10.1371/journal.pone.0224007.

Wood DE, Lu J, Langmead B. 2019. Improved metagenomic analysis with Kraken 2. Genome Biol. 20(1):257 10.1186/s13059-019-1891-0.

Woodcroft BJ, Aroney STN, Zhao R, Cunningham M, Mitchell JAM, Nurdiansyah R, Blackall L, Tyson GW. 2025. Comprehensive taxonomic identification of microbial species in metagenomic data using SingleM and Sandpiper. Nat Biotechnol. 10.1038/s41587-025-02738-1.

Wright ES, Vetsigian KH. 2016. Quality filtering of Illumina index reads mitigates sample cross-talk. BMC Genomics. 17(1):876 10.1186/s12864-016-3217-x.

Wright PJ, Frampton RA, Anderson C, Hedderley D. 2022. Factors associated with soils suppressive to black scurf of potato caused by *Rhizoctonia solani*. N Z Plant Prot. 75:31-49 10.30843/nzpp.2022.75.11761.

Wyse SV. 2012. Growth responses of five forest plant species to the soils formed beneath New Zealand kauri (*Agathis australis*). N Z J Bot. 50(4):411-421 10.1080/0028825X.2012.724428.

Wyse SV, Burns BR. 2011. Do host bark traits influence trunk epiphyte communities? N Z J Ecol. 35(3):296-301, http://www.jstor.org/stable/24060742

Wyse SV, Burns BR. 2013. Effects of *Agathis australis* (New Zealand kauri) leaf litter on germination and seedling growth differs among plant species. N Z J Ecol. 37(2):178-183, http://www.jstor.org/stable/24060779

Wyse SV, Burns BR, Wright SD. 2014. Distinctive vegetation communities are associated with the long-lived conifer *Agathis australis* (New Zealand kauri, Araucariaceae) in New Zealand rainforests. Austral Ecol. 39(4):388-400 https://doi.org/10.1111/aec.12089.

Xia Q, Rufty T, Shi W. 2020. Soil microbial diversity and composition: Links to soil texture and associated properties. Soil Biol Biochem. 149:107953 https://doi.org/10.1016/j.soilbio.2020.107953.

Xu J, Zhang Y, Zhang P, Trivedi P, Riera N, Wang Y, Liu X, Fan G, Tang J, Coletta-Filho HD et al. 2018. The structure and function of the global citrus rhizosphere microbiome. Nat Commun. 9(1):4894 10.1038/s41467-018-07343-2.

Yang B, Yang Z, He K, Zhou W, Feng W. 2024. Soil fungal community diversity, co-occurrence networks, and assembly processes under diverse forest ecosystems. Microorganisms. 12(9):1915 10.3390/microorganisms12091915.

Yang F, Tian J, Fang H, Gao Y, Zhang X, Yu G, Kuzyakov Y. 2018. Spatial heterogeneity of microbial community and enzyme activities in a broad-leaved Korean pine mixed forest. Eur J Soil Biol. 88:65-72 https://doi.org/10.1016/j.ejsobi.2018.07.001.

Yang K, Fu R, Feng H, Jiang G, Finkel O, Sun T, Liu M, Huang B, Li S, Wang X et al. 2023. RIN enhances plant disease resistance via root exudate-mediated assembly of disease-suppressive rhizosphere microbiota. Mol Plant. 16(9):1379-1395 10.1016/j.molp.2023.08.004.

Yang X, Tyler BM, Hong C. 2017. An expanded phylogeny for the genus *Phytophthora*. IMA Fungus. 8(2):355-384 10.5598/imafungus.2017.08.02.09.

Yin H, Wheeler E, Phillips RP. 2014. Root-induced changes in nutrient cycling in forests depend on exudation rates. Soil Biol Biochem. 78:213-221 https://doi.org/10.1016/j.soilbio.2014.07.022.

Yingtao L, Qiaofeng L, Lijuan W, Shuyun Q, Zhou J, Wenping Z, Aili Z. 2025. Integrated analysis of transcriptomics and metabolomics and high-throughput amplicon sequencing reveals the synergistic effects of secondary metabolites and rhizosphere microbiota on root rot resistance in *Psammosilene tunicoides*. Front Microbiol. 16 10.3389/fmicb.2025.1554406.

Yoshida K, Schuenemann VJ, Cano LM, Pais M, Mishra B, Sharma R, Lanz C, Martin FN, Kamoun S, Krause J et al. 2013. The rise and fall of the *Phytophthora infestans* lineage that triggered the Irish potato famine. Elife. 2:e00731 10.7554/eLife.00731.

Yu L, Zi H, Zhu H, Liao Y, Xu X, Li X. 2022. Rhizosphere microbiome of forest trees is connected to their resistance to soil-borne pathogens. Plant Soil. 479(1):143-158 10.1007/s11104-022-05505-2.

Yuan J, Zhao J, Wen T, Zhao M, Li R, Goossens P, Huang Q, Bai Y, Vivanco JM, Kowalchuk GA et al. 2018. Root exudates drive the soil-borne legacy of aboveground pathogen infection. Microbiome. 6(1):156 10.1186/s40168-018-0537-x.

Yuste JC, Barba J, Fernandez-Gonzalez AJ, Fernandez-Lopez M, Mattana S, Martinez-Vilalta J, Nolis P, Lloret F. 2012. Changes in soil bacterial community triggered by drought-induced gap succession preceded changes in soil C stocks and quality. Ecol Evol. 2(12):3016-3031 10.1002/ece3.409.

Zeller M, Huson DH. 2022. Comparison of functional classification systems. NAR Genom Bioinform. 4(4):lqac090 10.1093/nargab/lqac090.

Zeng L, Xiao W, Liu C, Lei L, Jian Z, Shen Y, Li M-H. 2023. Effects of thinning and understorey removal on soil extracellular enzyme activity vary over time during forest recovery after treatment. Plant Soil. 492(1):457-469 10.1007/s11104-023-06187-0.

Zhang J, Xu M, Zou X, Chen J. 2022a. Structural and functional characteristics of soil microbial community in a *Pinus massoniana* forest at different elevations. PeerJ. 10:e13504 10.7717/peerj.13504.

Zhang K, Delgado-Baquerizo M, Zhu Y-G, Chu H. 2020. Space is more important than season when shaping soil microbial communities at a large spatial scale. mSystems. 5(3):10.1128/msystems.00783-00719 10.1128/msystems.00783-19.

Zhang K, Maltais-Landry G, James M, Mendez V, Wright D, George S, Liao H-L. 2022b. Absolute microbiome profiling highlights the links among microbial stability, soil health, and crop productivity under long-term sod-based rotation. Biol Fertility Soils. 58(8):883-901 10.1007/s00374-022-01675-4.

Zhao J-F, Peng S-S, Chen M-P, Wang G-Z, Cui Y-B, Liao L-G, Feng J-G, Zhu B, Liu W-J, Yang L-Y et al. 2019. Tropical forest soils serve as substantial and persistent methane sinks. Sci Rep. 9(1):16799 10.1038/s41598-019-51515-z.

Appendix A

A.1 Supplementary figures

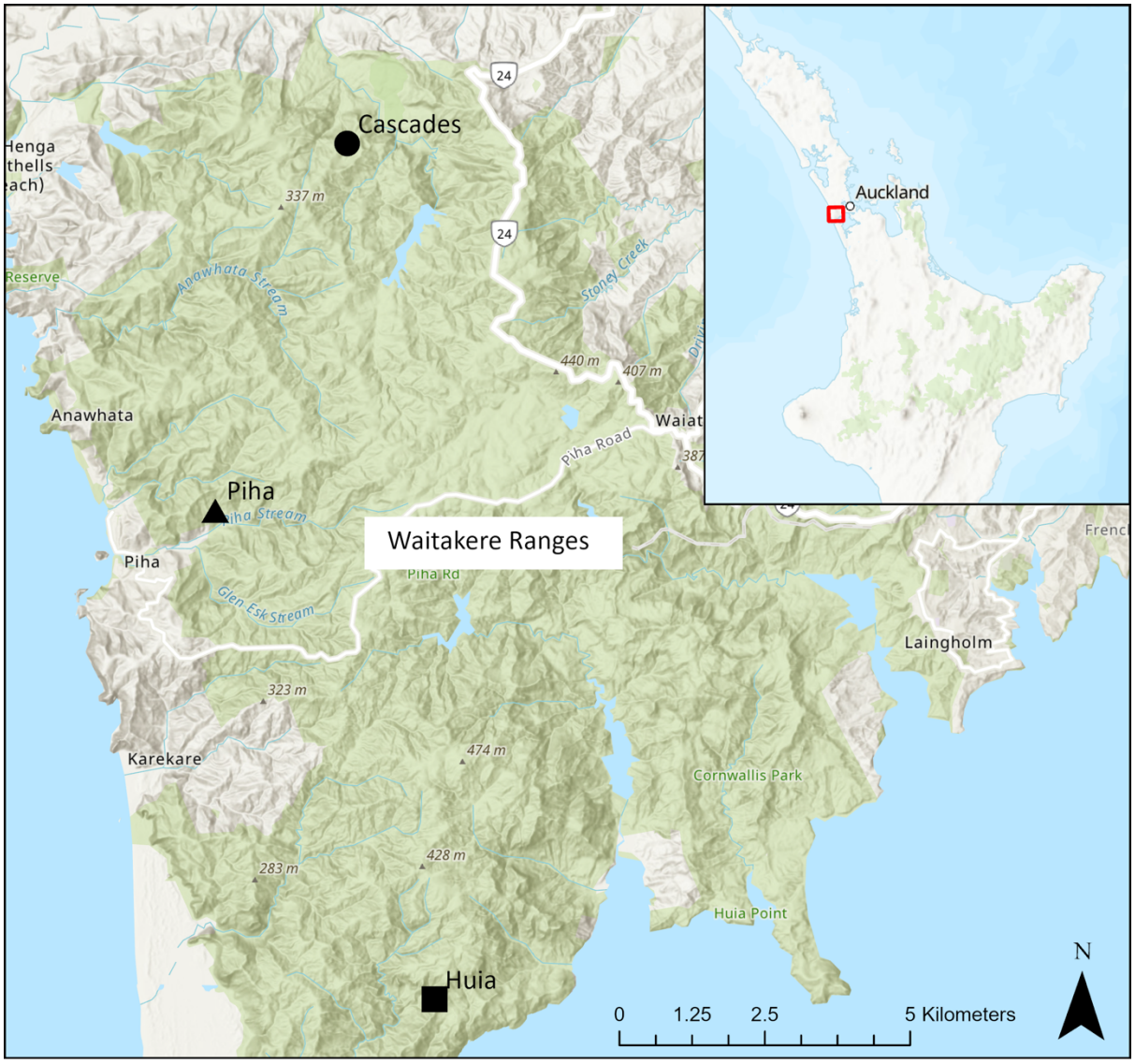

Figure A1: Map of the three sampling sites (Cascades, Piha, Huia) in the North Island, New Zealand, that each contain two plots (*n* = 6) where 16 kauri trees, per plot, were selected for soil sampling (*n* = 96).

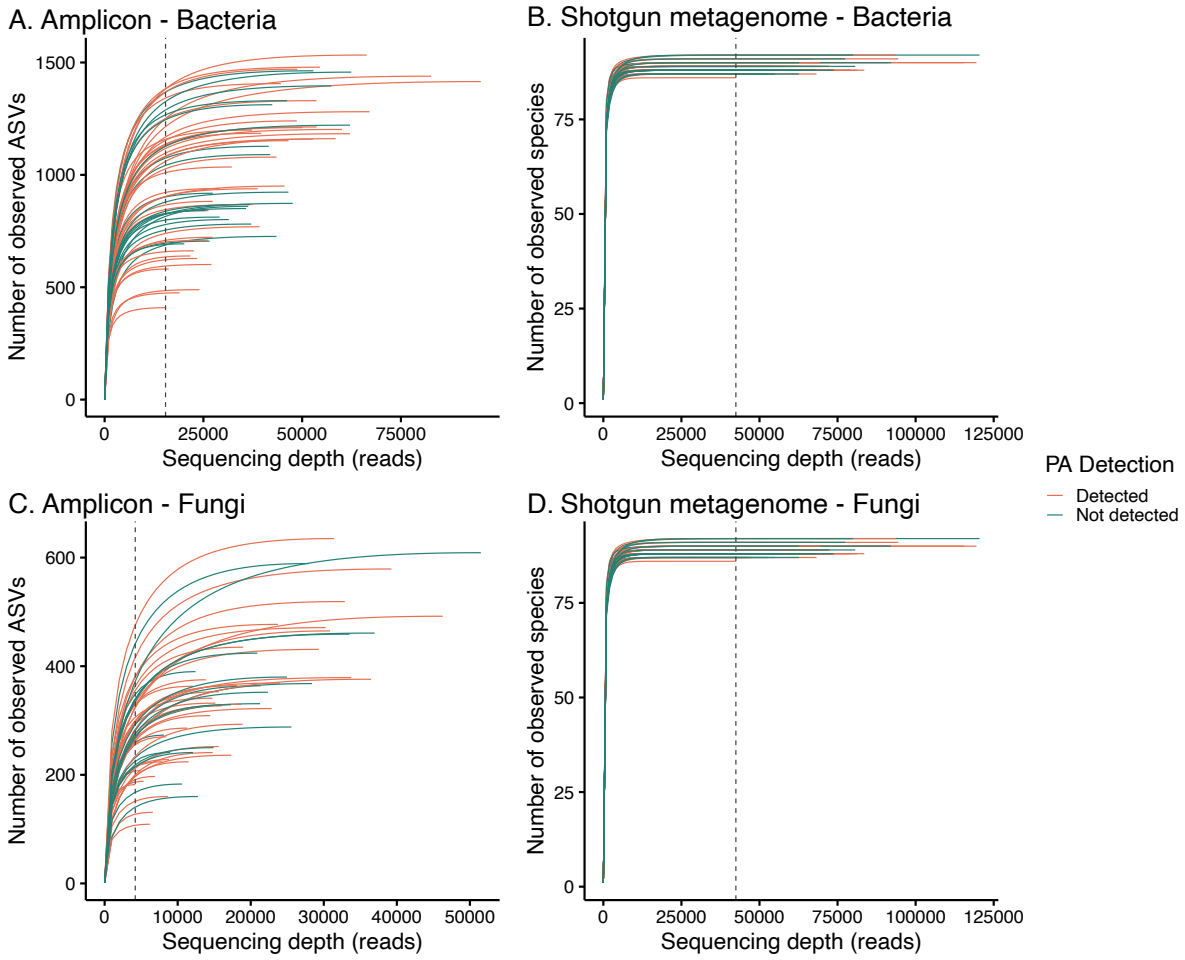

Figure A2: Rarefaction curves showing observed microbial richness in amplicon and shotgun metagenome datasets. Figures A and B show rarefaction curves for (A) bacterial and (C) fungal ASVs from amplicon sequencing, while figures B and D show rarefaction curves for (B) bacterial and (D) fungal species identified from shotgun metagenome data. Each curve represents an individual soil samples collected from around kauri trees, coloured by *P. agathidicida* (PA) detection status based on LAMP analysis. The dotted line indicates the minimum sequencing depth to with each dataset was rarefied to.

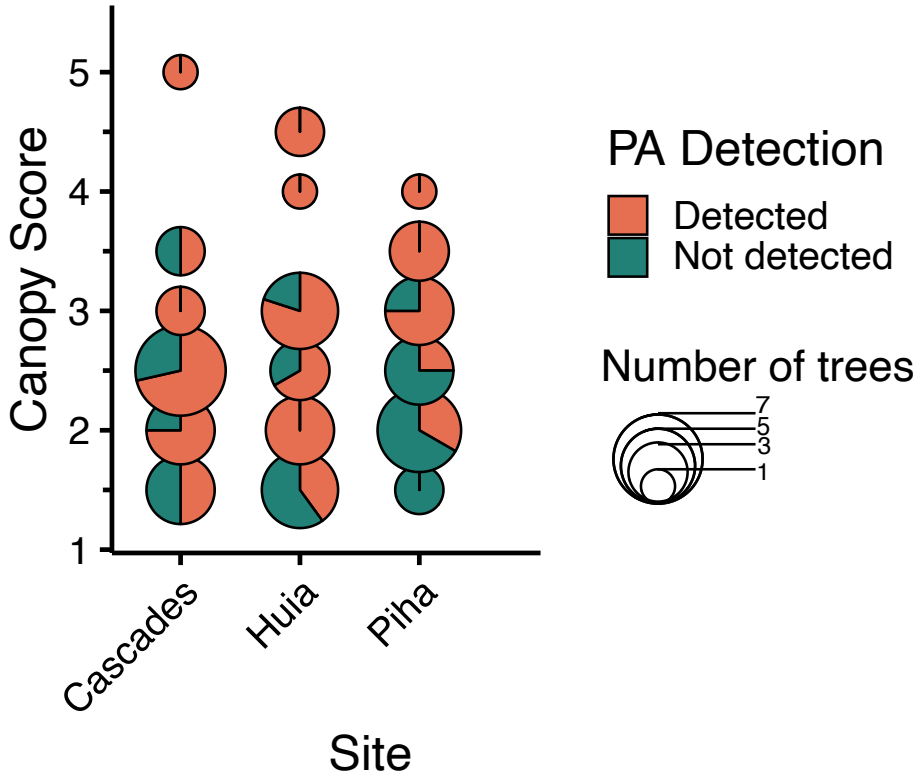

Figure A3: Canopy healthy scores of kauri trees across sites (Cascades, Huia, and Piha, within the Waitākere Ranges, Auckland, New Zealand), with point size proportional to the number of trees at each site-score combination. Each point is displayed as a pie chart showing the proportion of trees testing positive or negative for *P. agathidicida* by LAMP analysis.

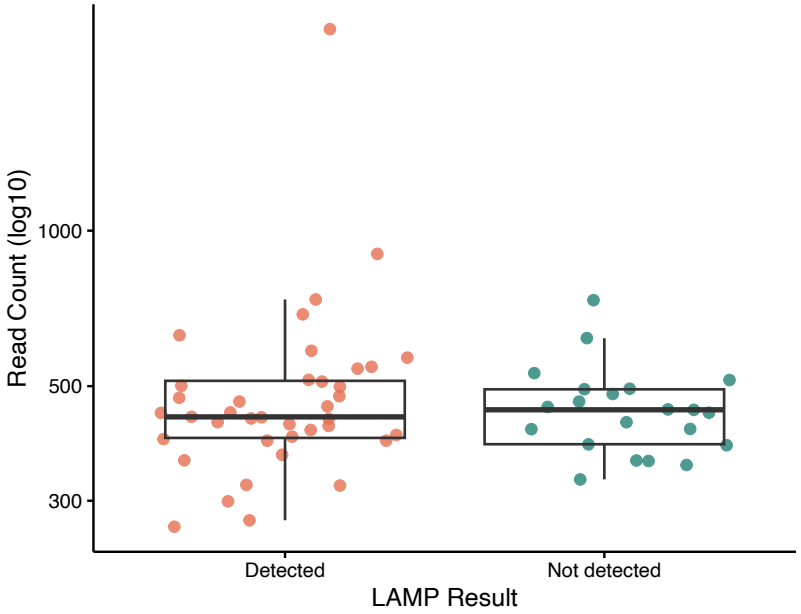

Figure A4: Read count of *P. agathidicida*-associated DNA per sample against detection status inferred by LAMP analysis (detected n = 39, not detected n = 21). Boxes represent the interquartile range of the data (25th and 75th percentiles), whiskers show the largest and smallest values 1.5x the IQR and median values are represented by the bar within each box.

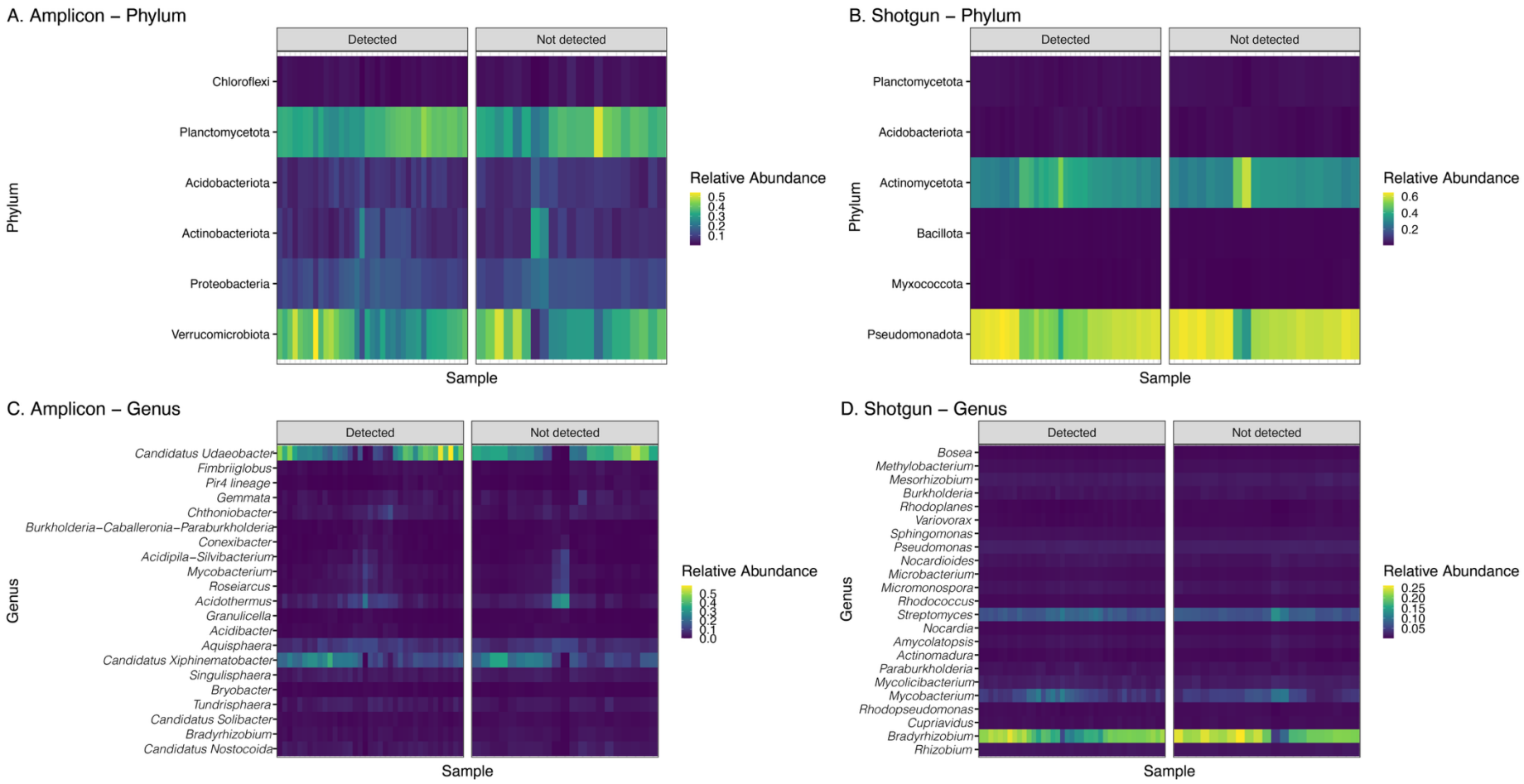

Figure A5: Heatmap of the relative abundance of the top bacterial phyla (>1% MRA), and genera (>0.5% MRA) identified using amplicon and shotgun metagenomic sequencing. Detection of *P. agathidicida* was determined by LAMP analysis (detected *n* = 37 (amplicon), 39 (shotgun), or not detected (*n* = 21)). The heatmap uses NMDS ordination to order the samples (columns) arranging them based on their similarity in microbial community composition as captured by the first ordination axis.

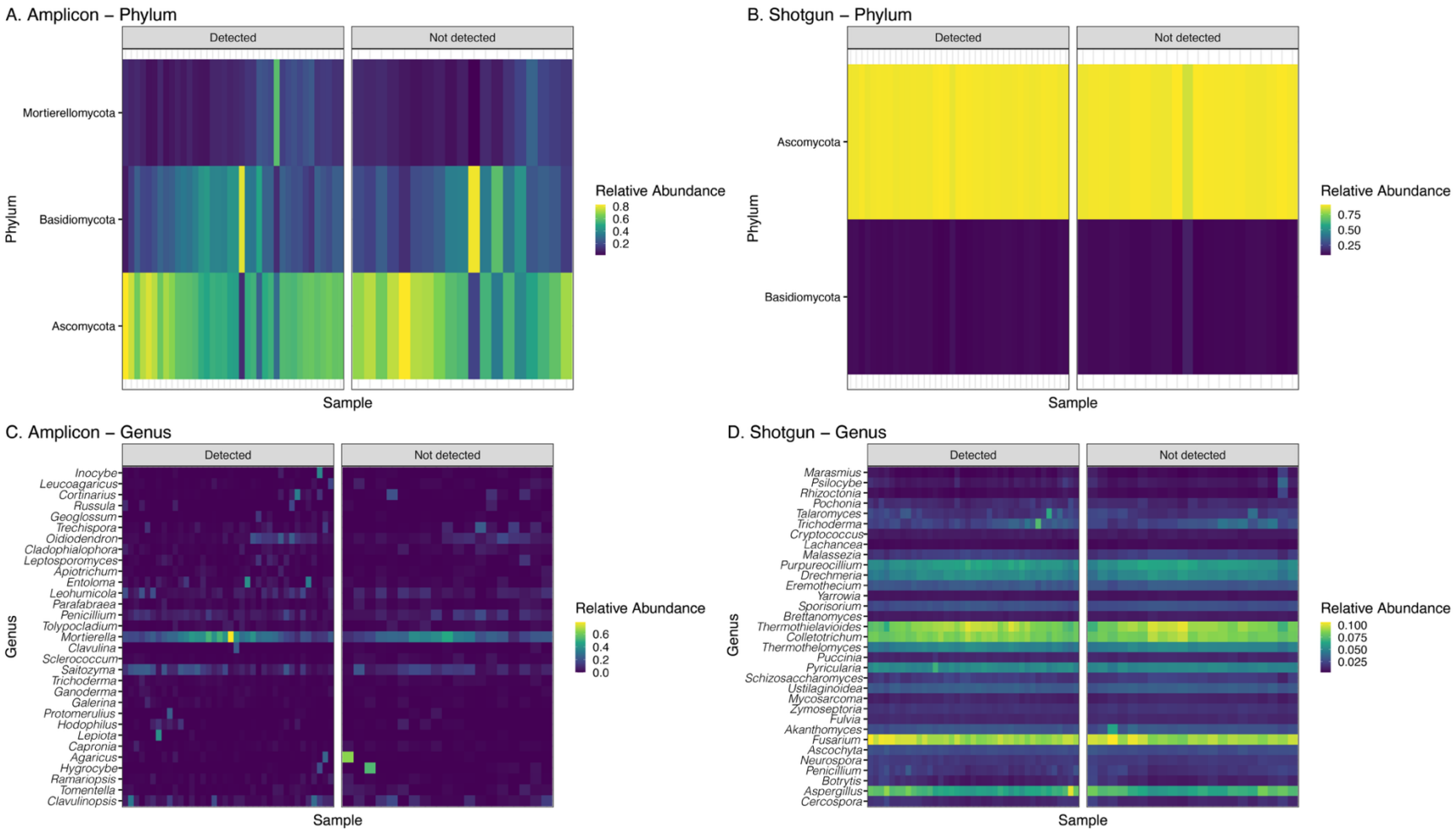

Figure A6: Heatmap of the relative abundance of the top fungal phyla (>1% MRA), and genera (>0.5% MRA) identified using amplicon and shotgun metagenomic sequencing. Detection of *P. agathidicida* was determined by LAMP analysis (detected *n* = 38 (amplicon), 39 (shotgun), or not detected *n* = 19 (amplicon), 21 (shotgun)). The heatmap uses NMDS ordination to order the samples (columns) arranging them based on their similarity in microbial community composition as captured by the first ordination axis.

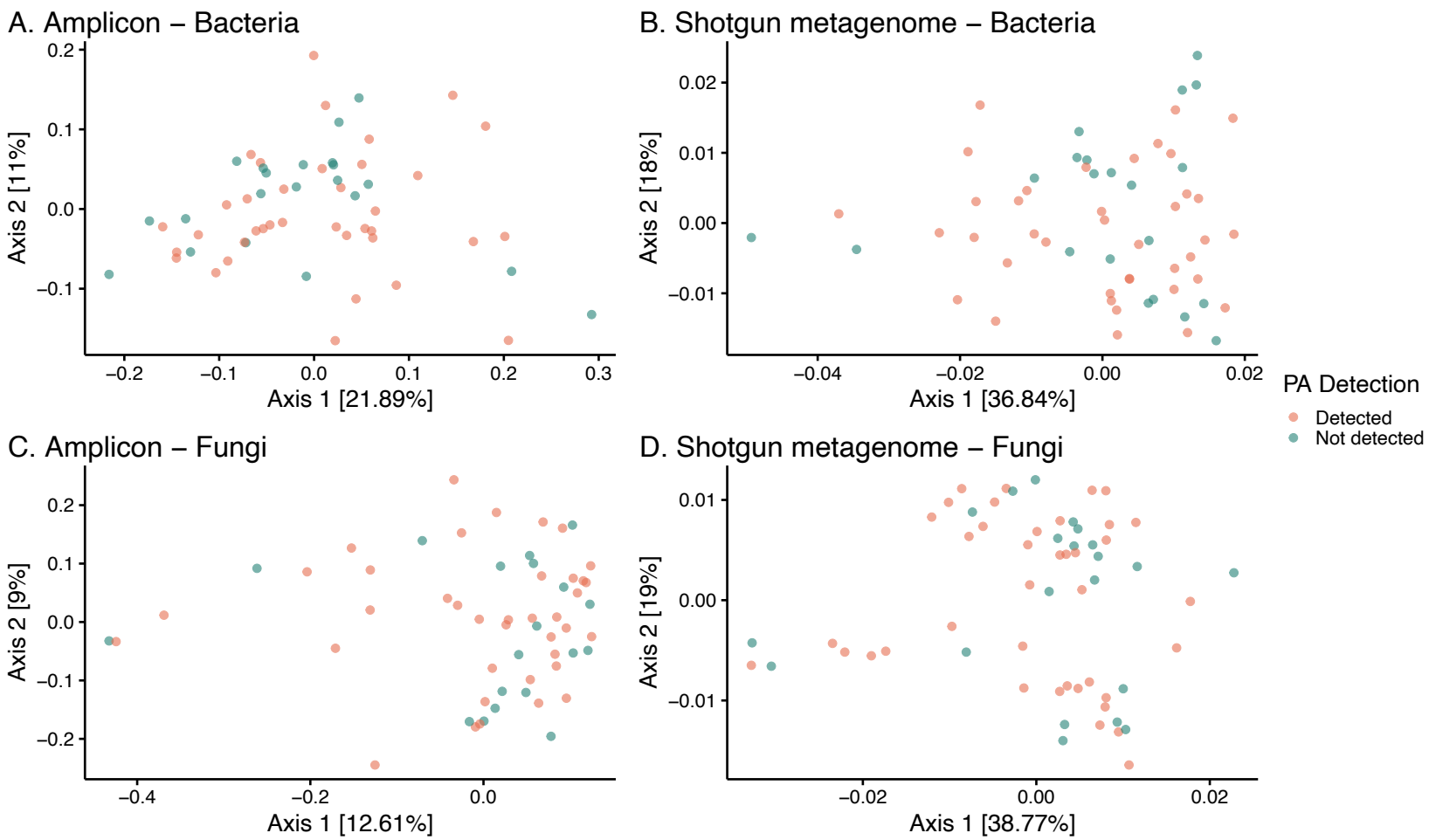

Figure A7: Principal Coordinates Analysis (PCoA) of (A and B) bacterial and (C and D) fungal genus-level community composition of Bray-Curtis distance matrices from amplicon and shotgun metagenome datasets. Samples were normalised by cumulative-sum scaling. Points are coloured based on LAMP detection of *P. agathidicida* (Bacterial dataset: detected *n* = 37 (amplicon), 39 (shotgun) and not detected *n* = 21 (amplicon and shotgun). Fungal dataset: detected *n* = 38 (amplicon), 39 (shotgun), or not detected *n* = 19 (amplicon), 21 (shotgun).

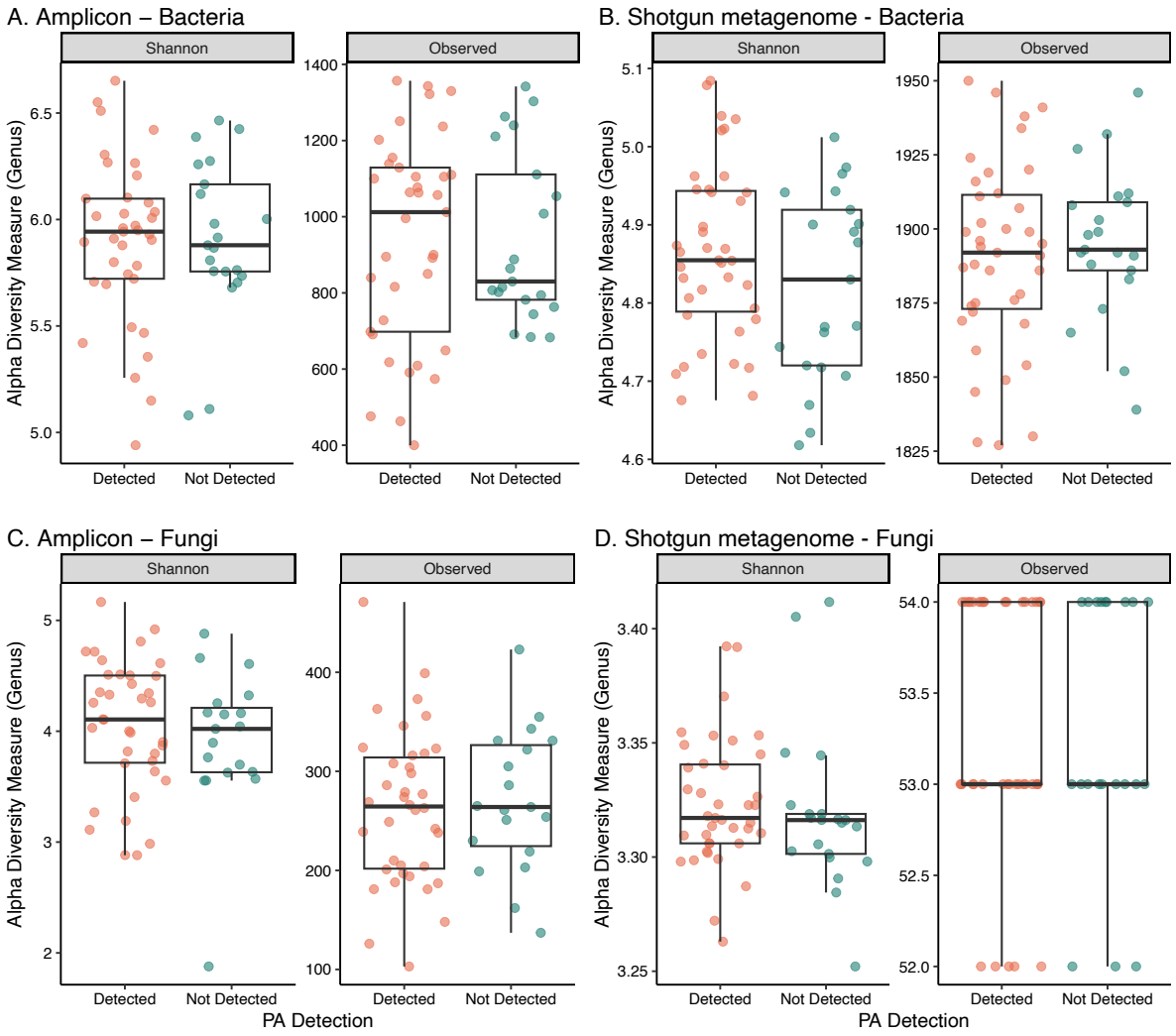

Figure A8: Measures of (A and B) bacterial and (C and D) fungal taxonomic alpha diversity at the genus level estimated by Shannon diversity and observed richness from amplicon and shotgun metagenome datasets. Samples are grouped based on the LAMP detection of *P. agathidicida* (Bacterial dataset: detected *n* = 37 (amplicon), 39 (shotgun) and not detected *n* = 21 (amplicon and shotgun). Fungal dataset: detected *n* = 38 (amplicon), 39 (shotgun), or not detected *n* = 19 (amplicon), 21 (shotgun)). Samples were rarefied to an even depth (Reads per sample: amplicon 16S: 15,420, amplicon ITS: 4,192, shotgun bacteria: 9,963,524, shotgun fungi: 42,440). Boxes represent the interquartile range of the data (25th and 75th percentiles), whiskers show the largest and smallest values 1.5x the IQR and median values are represented by the bar within each box.

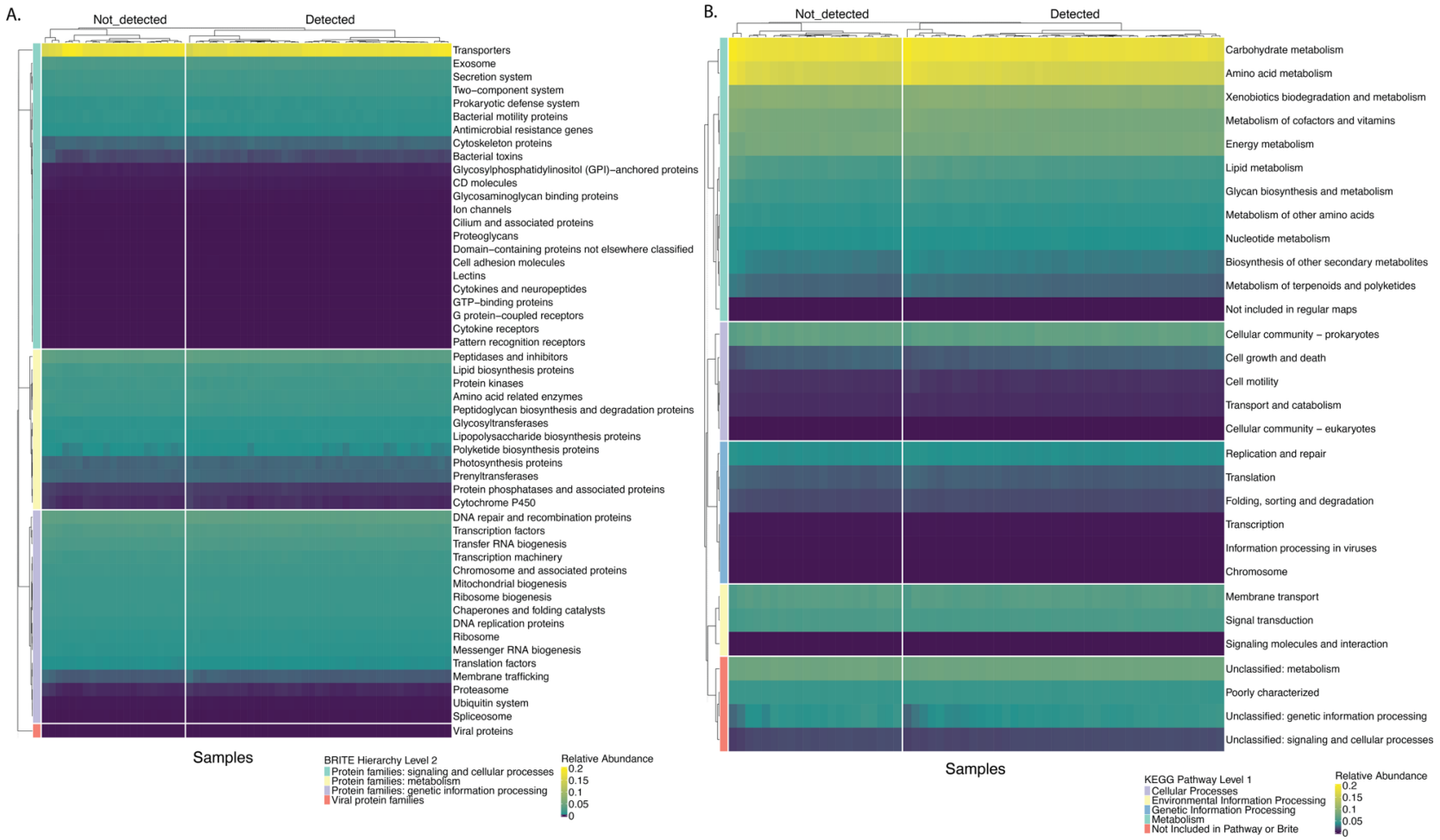

Figure A9: Heatmaps showing the relative abundance of KOs identified through shotgun metagenome sequencing and eggNOG annotation, grouped by KEGG functional classifications and LAMP detection of *P. agathidicida* (detected *n* = 39, not detected *n* = 21). (A) KOs grouped according to KEGG BRITE hierarchies at level 2 and level 3, (B) KOs grouped by KEGG pathway levels 1 and level 2. Samples are clustered based on default Euclidian clustering from the ComplexHeatmap R package. Pathways associated with Organismal systems and Human disease were removed from the dataset.

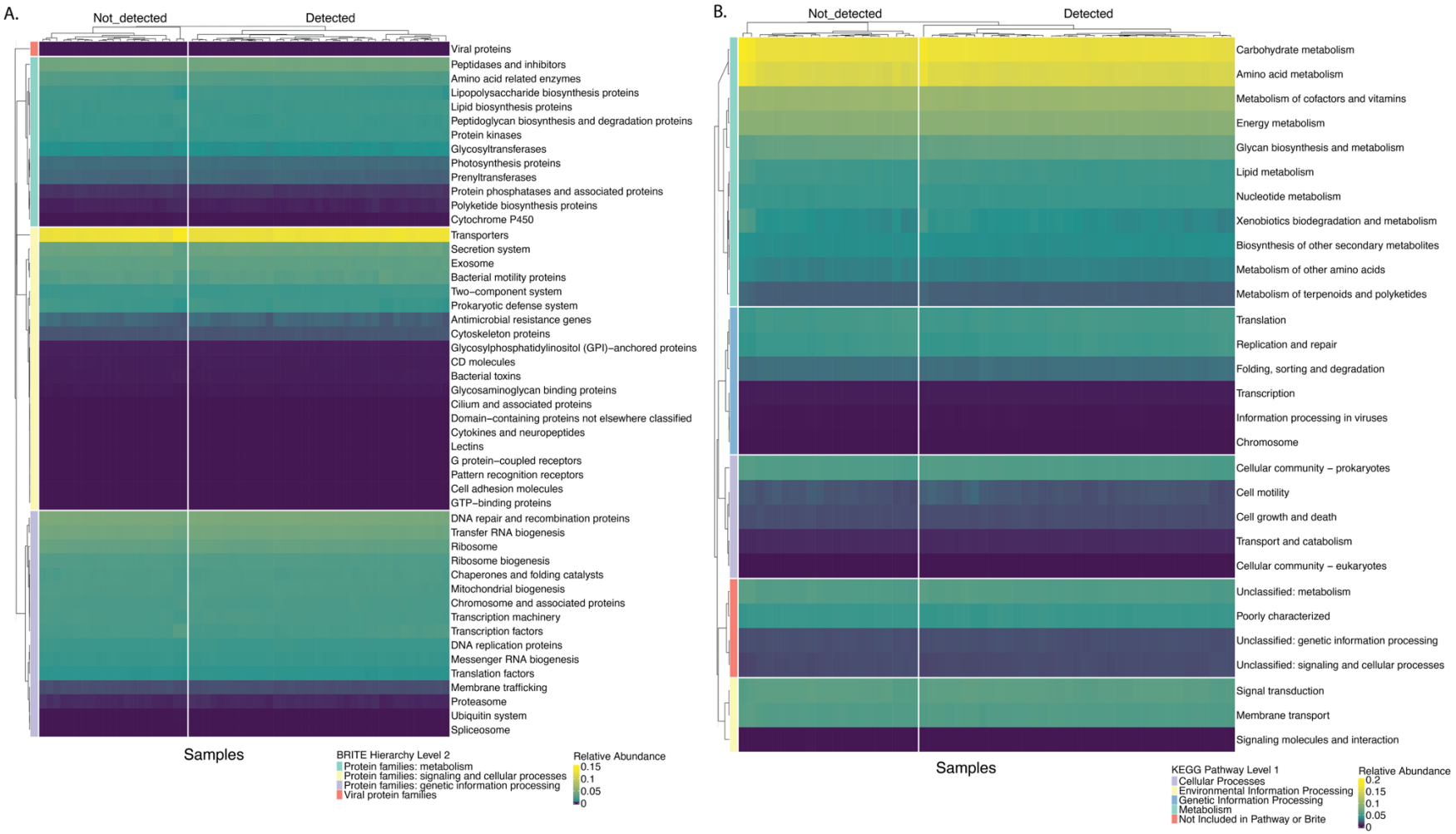

Figure A10: Heatmaps showing the relative abundance of KOs identified through functional inference by PICRUSt2 of ASVs from amplicon sequencing, grouped by KEGG functional classifications and LAMP detection of *P. agathidicida* (detected *n* = 37, not detected *n* = 21). (A) KOs grouped according to KEGG BRITE hierarchies at level 2 and level 3, (B) KOs grouped by KEGG pathway levels 1 and level 2. Samples are clustered based on default Euclidian clustering from the ComplexHeatmap R package. Pathways associated with Organismal systems and Human disease were removed from the dataset.

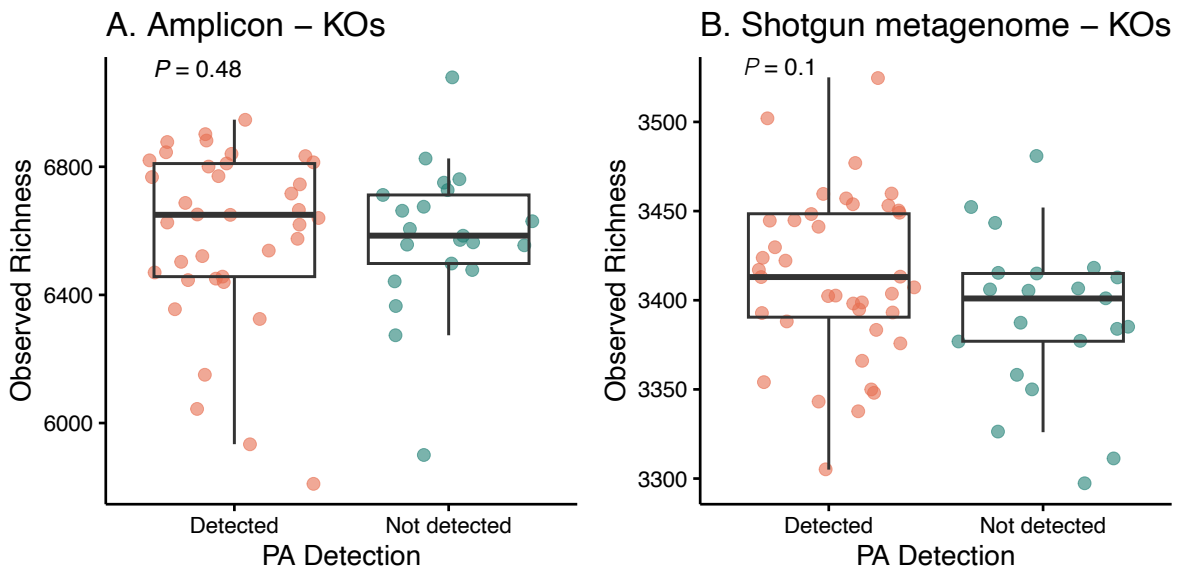

Figure A11: Boxplots showing estimated alpha diversity of microbial functional potential based on KO profiles from (A) amplicon sequencing (via PICRUSt2) and (B) shotgun metagenome sequencing (via eggNOG annotation). Samples were grouped by LAMP detection of *P. agathidicida* (detected *n* = 37 (amplicon), 39 (shotgun), not detected *n* = 21 (amplicon), 21 (shotgun)). Boxes represent the interquartile range of the data (25th and 75th percentiles), whiskers show the largest and smallest values 1.5x the IQR and median values are represented by the bar within each box.

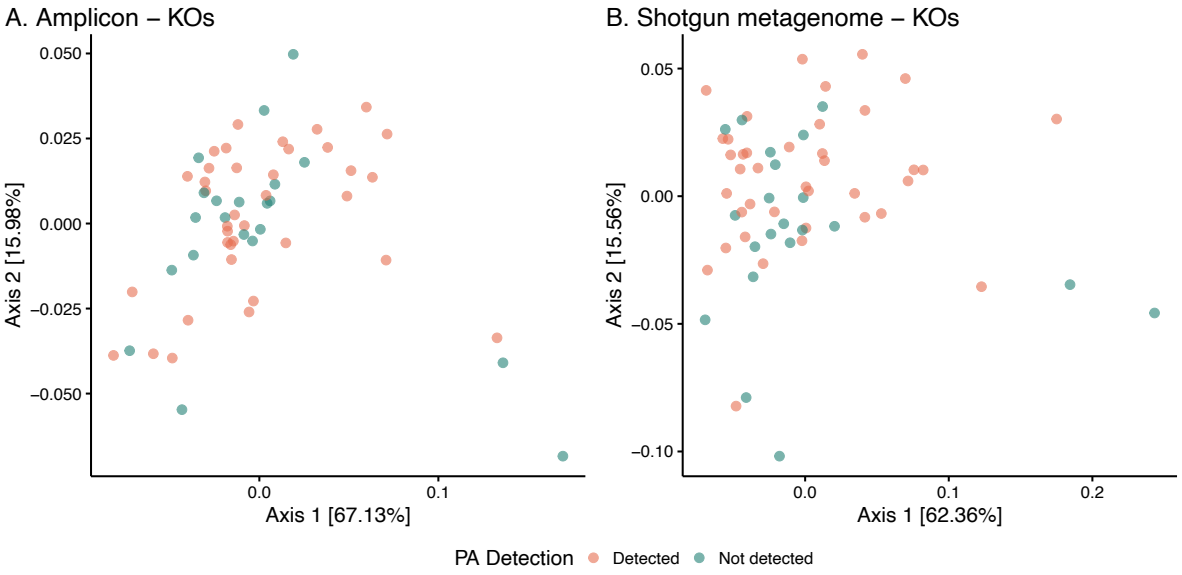

Figure A12: Principal Coordinates Analysis (PCoA) of amplicon-based inference (PICRUSt2) and shotgun metagenome sequencing (eggNOG annotation) of KOs based on Bray-Curtis distance matrices. Samples were normalised by CSS. Points are coloured based on LAMP detection of *P. agathidicida* (detected *n* = 37 (amplicon), 39 (shotgun), not detected *n* = 21 (amplicon), 21 (shotgun)).

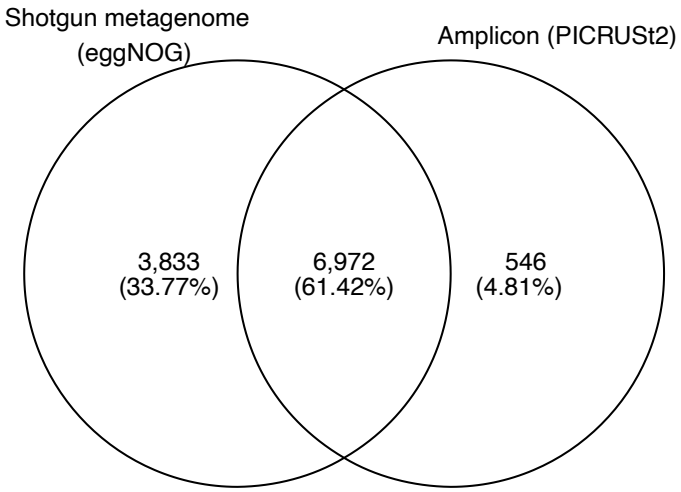

Figure A13: Venn diagram showing the overlap of KOs identified from shotgun metagenome sequencing (eggNOG annotation) and amplicon-based functional inference (PICRUSt2).

A.2 Supplementary tables

Table A1: Amplicon samples with <1000 reads that were removed prior to statistical analyses.

16S samples	**ITS samples**
NRT-PI-K4-16S	NRT-CI-D26-ITS
NRT-HI-K1-16S	NRT-HI-K4-ITS
	NRT-PU-D124-ITS

Codes H, P, C = Sampling site (Huia, Piha, Cascades). Codes I and U = Sampling plot (I = Plot 1, U = Plot 2).

A.3 Supplementary files

Raw read statistics of shotgun metagenomic reads before and after quality control can be viewed in Appendix_A3_Supplementary_File_1.tsv.

Appendix B

B.1 Supplementary figures

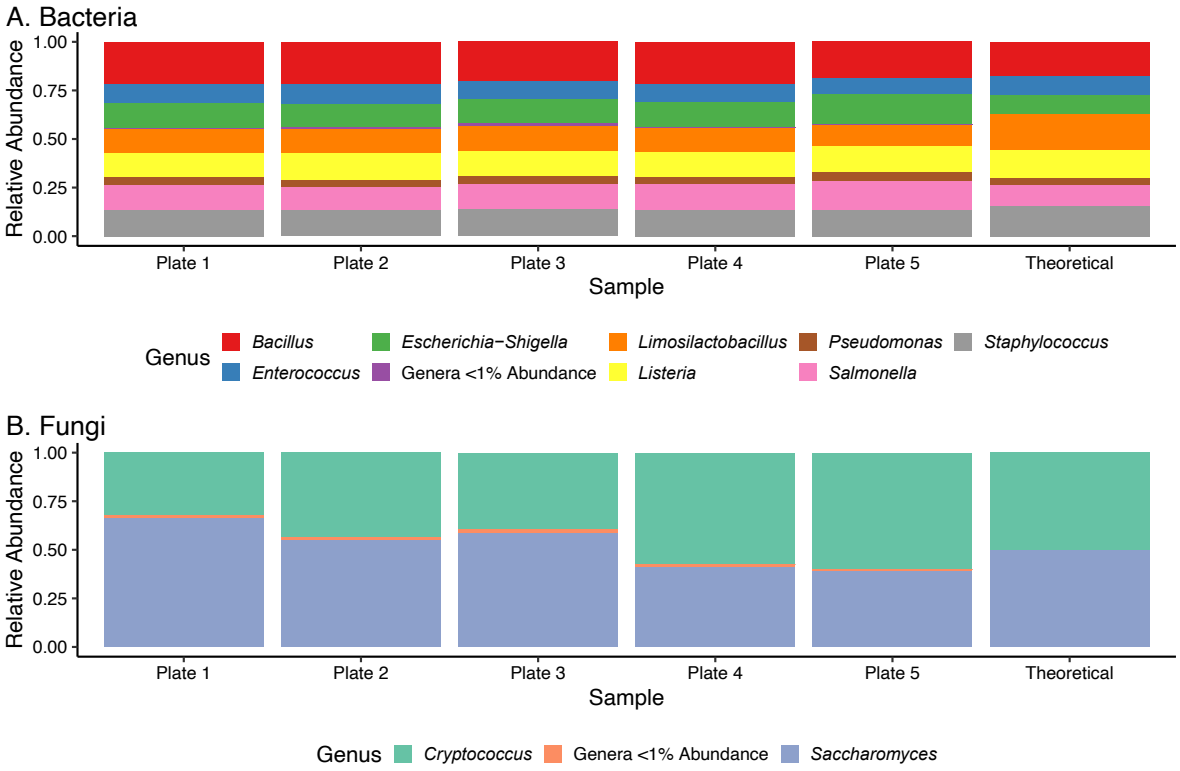

Figure B1: Relative abundances of genera identified in (A) bacterial and (B) fungal mock microbial community controls. The theoretical sample provides the expected abundances of taxa within the ZymoBIOMICS Microbial Community DNA standard (mock community DNA standard).

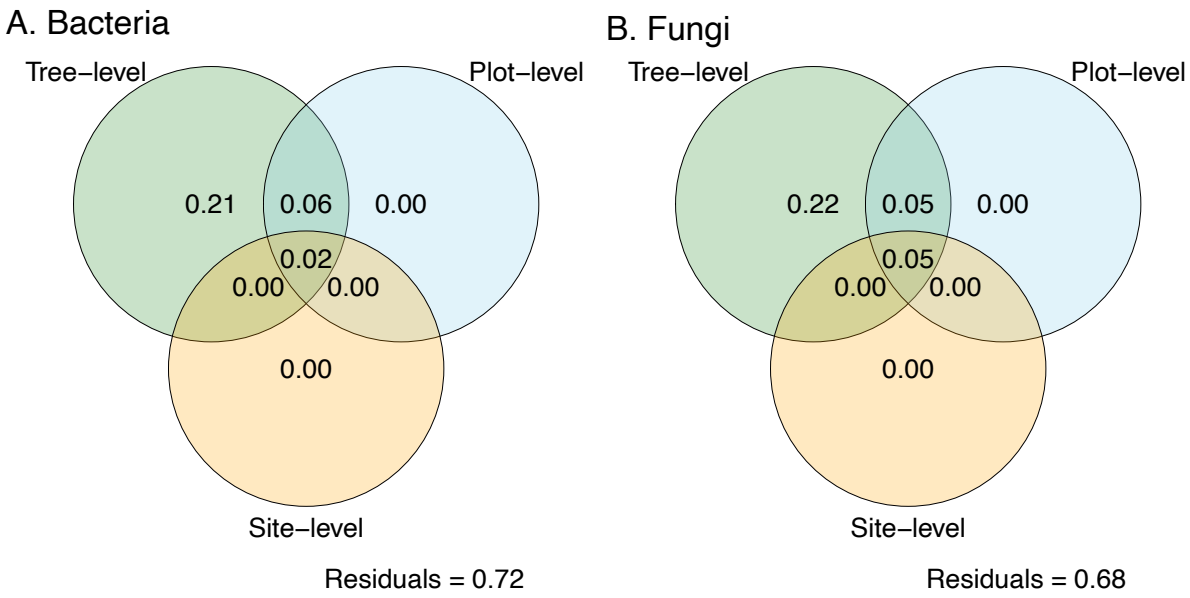

Figure B2: The amount of variation in (A) bacterial and (B) fungal community diversity across three spatial scales: site-level (*n* = 3), plot-level (*n* = 6), and tree-level (*n* = 96) determined by variation partitioning analysis using db-RDA on the Euclidean distance matrix of observed richness counts. This figure is based on the full taxa dataset.

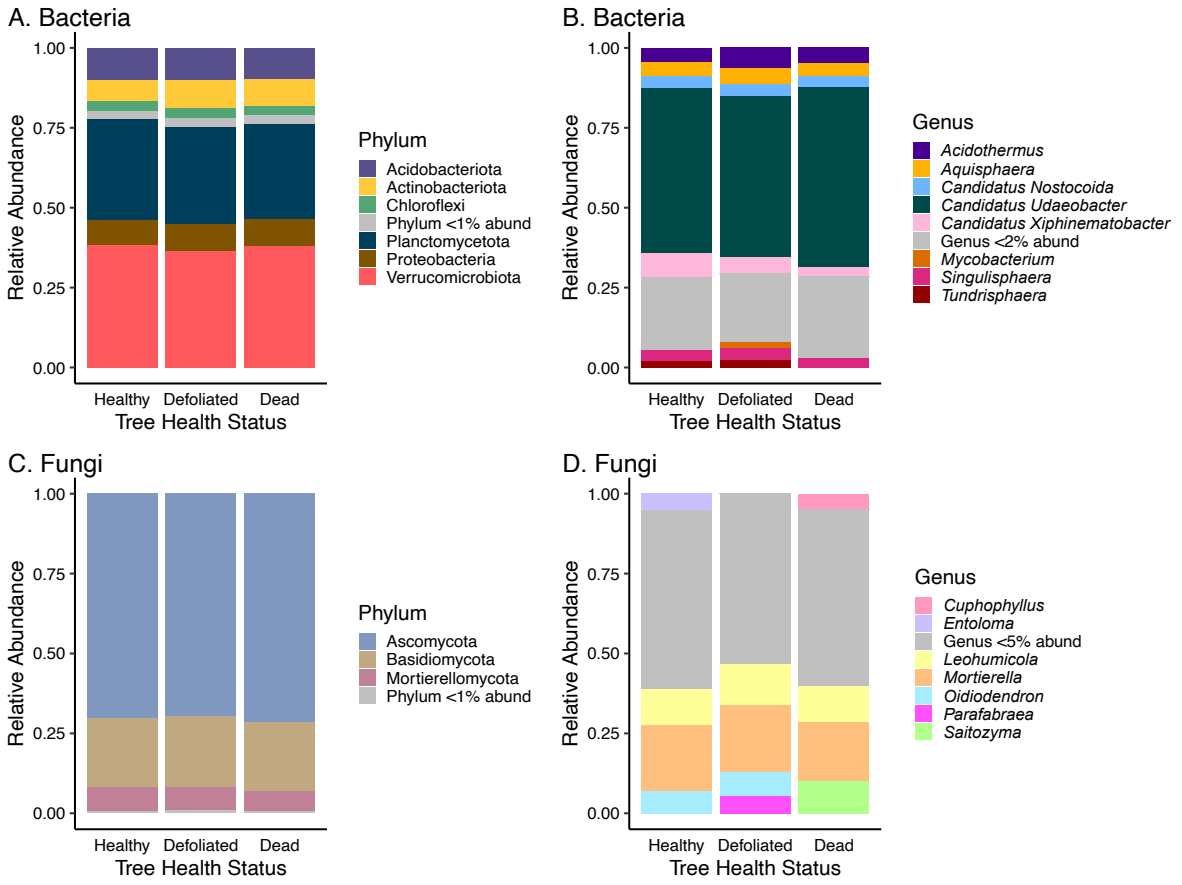

Figure B3: Stacked bar plots of relative abundance. Proportional relative abundance of bacterial (A) phyla and (B) genera and fungal (C) phyla and (D) genera from soil surrounding kauri trees of three health status groupings. This figure is based on the intermediate taxa dataset. Samples within respective health status groupings were collapsed together. Un-collapsed relative abundance data of phyla (dead: *n* = 20, healthy: *n* = 84, defoliated: bacterial dataset *n* = 276, fungal dataset: *n* = 265) can be viewed in Figure B10.

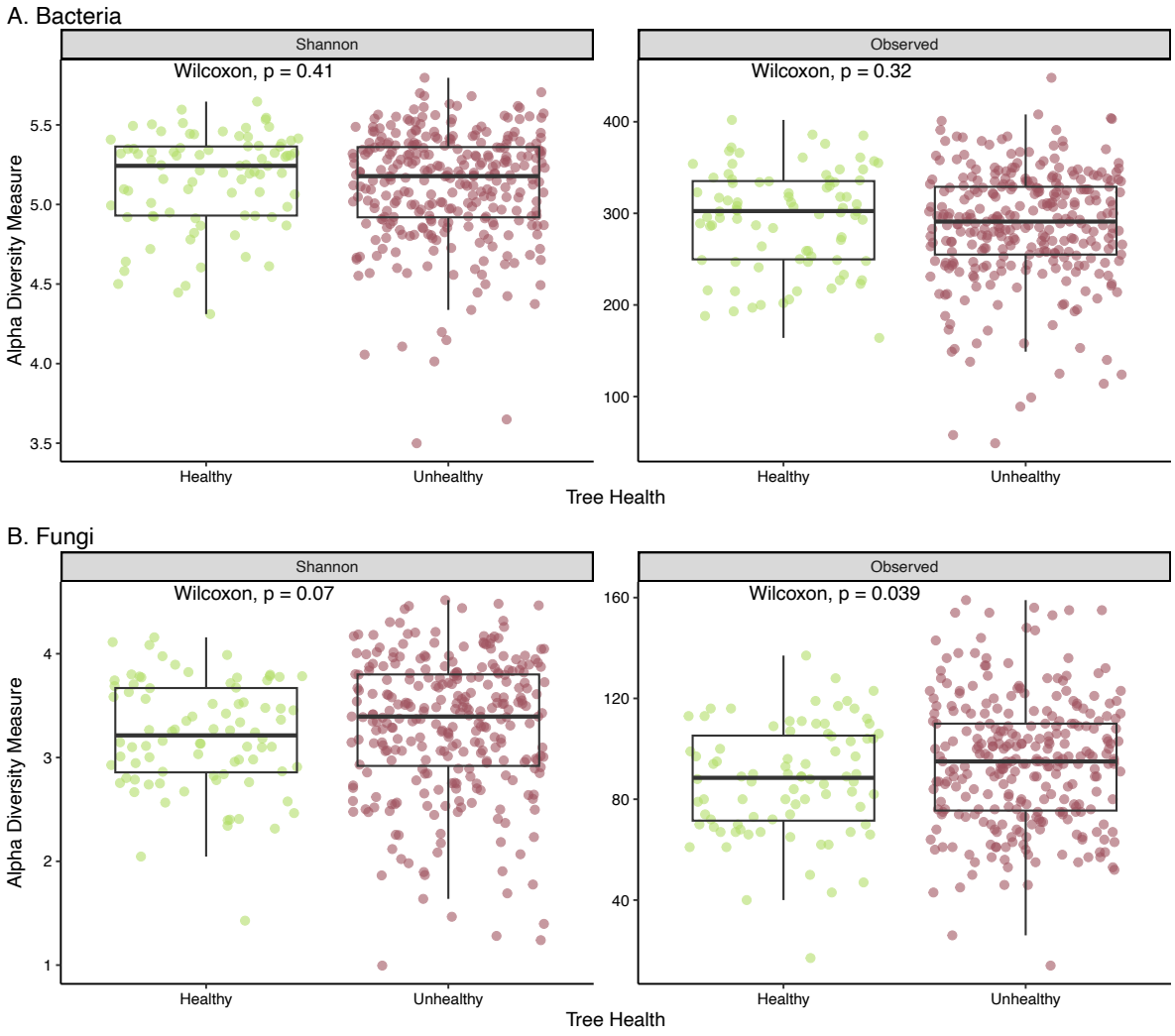

Figure B4: Measures of (A) bacterial and (B) fungal alpha diversity estimated by Shannon diversity and observed richness between tree health status groups (healthy: *n* = 84, unhealthy (defoliated and dead trees): bacterial dataset *n* = 296, fungal dataset: *n* = 285). This figure is based on the intermediate taxa dataset (9,331 bacteria ASVs, 3,733 fungal ASVs). Samples were rarefied to an even depth (775 and 596 reads for bacteria and fungi, respectively). Boxes represent the interquartile range of the data (25th and 75th percentiles), whiskers show the largest and smallest values 1.5x the IQR and median values are represented by the bar within each box. Coloured points represent cardinal point samples.

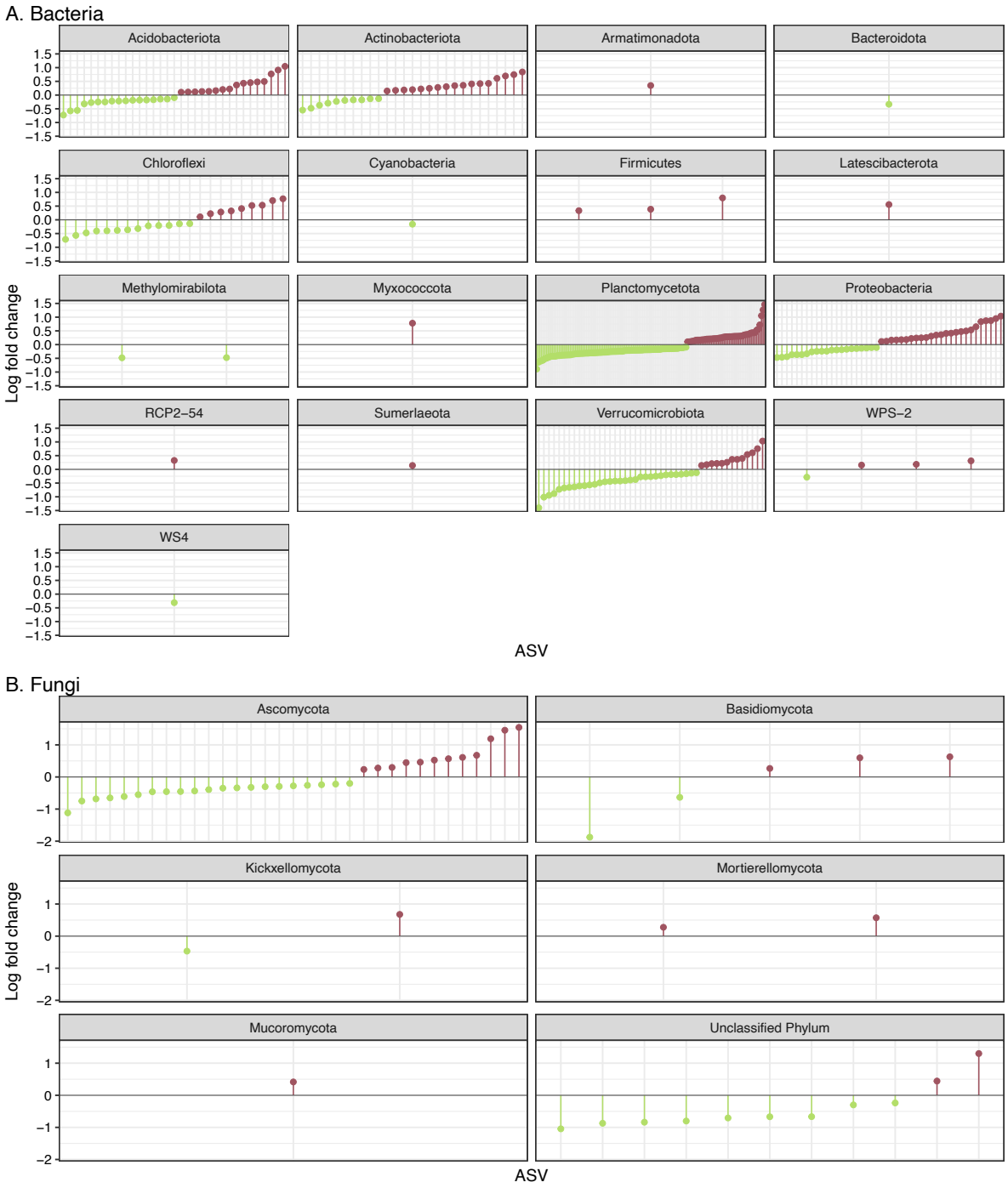

Figure B5: Log fold change of differential abundance. (A) Bacterial and (B) fungal ASVs, grouped at the phylum level, passing ANCOM-BC2 sensitivity scoring, showing differential abundance between tree scale samples collected around healthy and unhealthy (combined defoliated and dead samples) trees. This analysis is based on the full dataset. Green data points indicate an increase in the abundance of ASVs in soils surrounding healthy trees, and red data points indicate an increase in the abundance of ASVs in soils surrounding unhealthy tree.

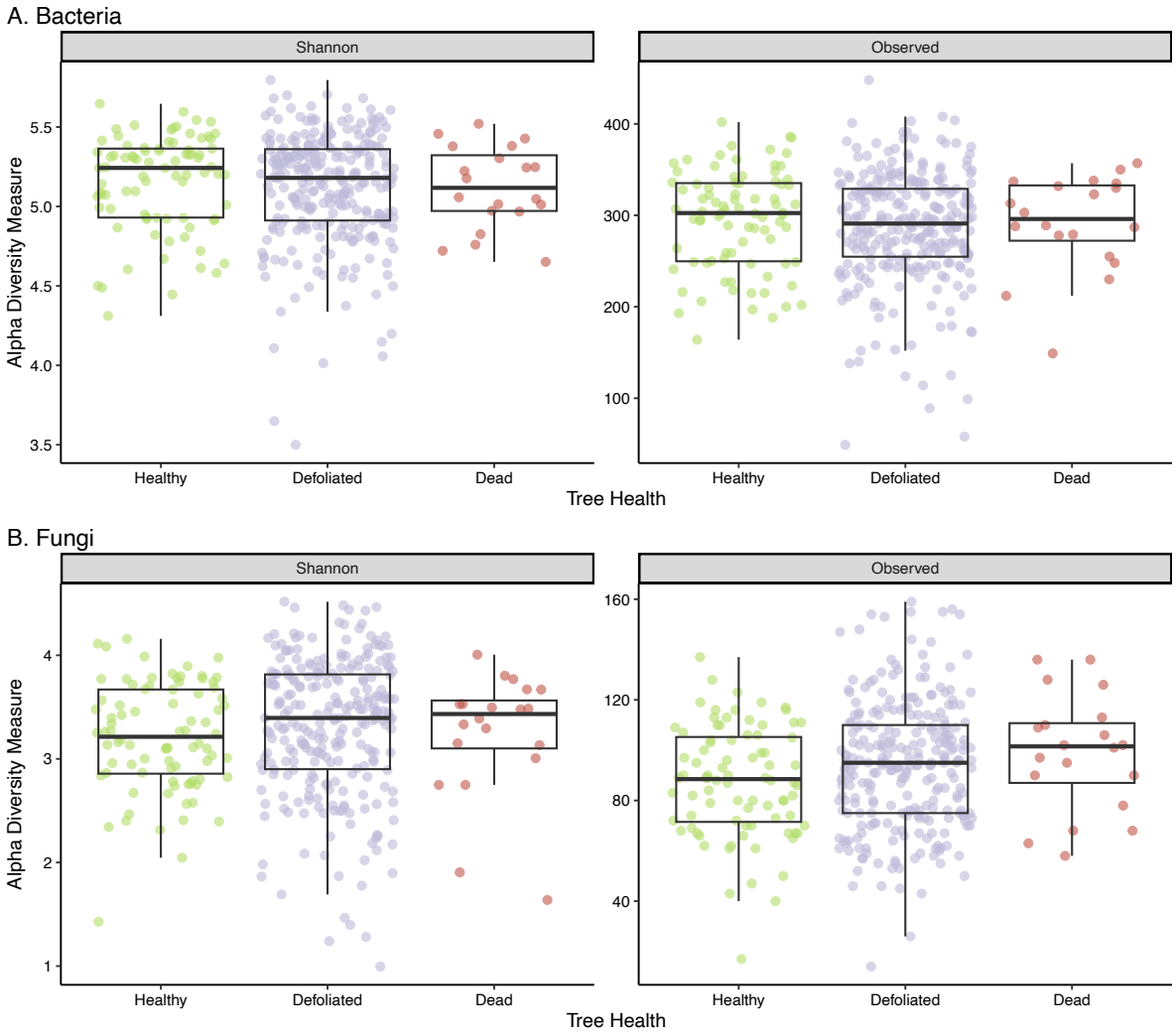

Figure B6: Measures of (A) bacterial and (B) fungal alpha diversity estimated by Shannon diversity and observed richness between tree health status groups (healthy: *n* = 84, dead: *n* = 20, defoliated: bacterial dataset *n* = 276, fungal dataset: *n* = 265). This figure is based on the full taxa dataset. Samples were rarefied to an even depth (1499 and 997 reads for bacteria and fungi, respectively). Boxes represent the interquartile range of the data (25th and 75th percentiles), whiskers show the largest and smallest values 1.5x the IQR and median values are represented by the bar within each box. Coloured points represent cardinal point samples.

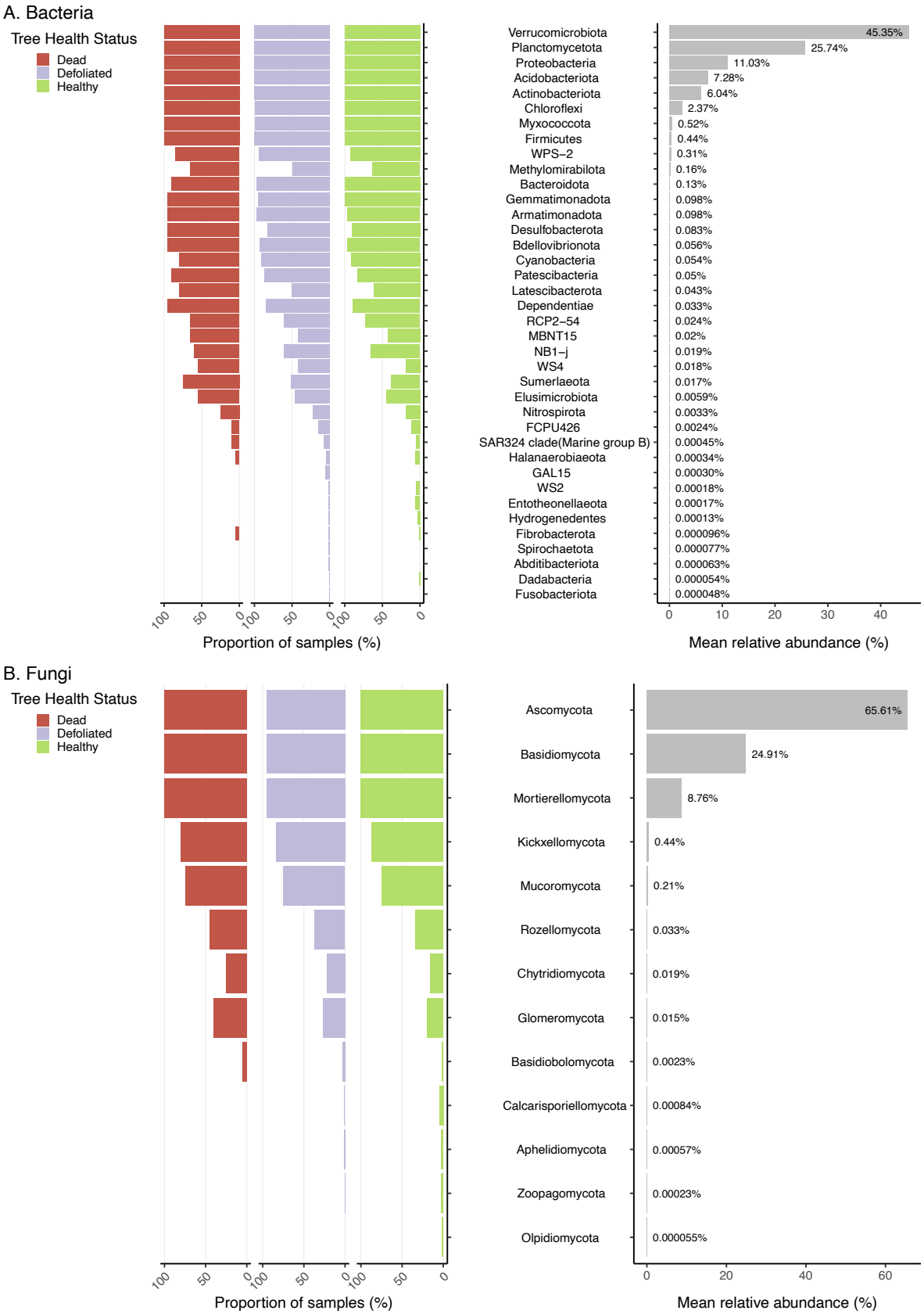

Figure B7: The representativeness of (A) bacterial and (B) fungal phyla detected in samples grouped by tree health status (dead: *n* = 20, healthy: *n* = 84, defoliated: bacterial dataset *n* = 276, fungal dataset *n* = 265). This figure is based on the full taxa dataset.

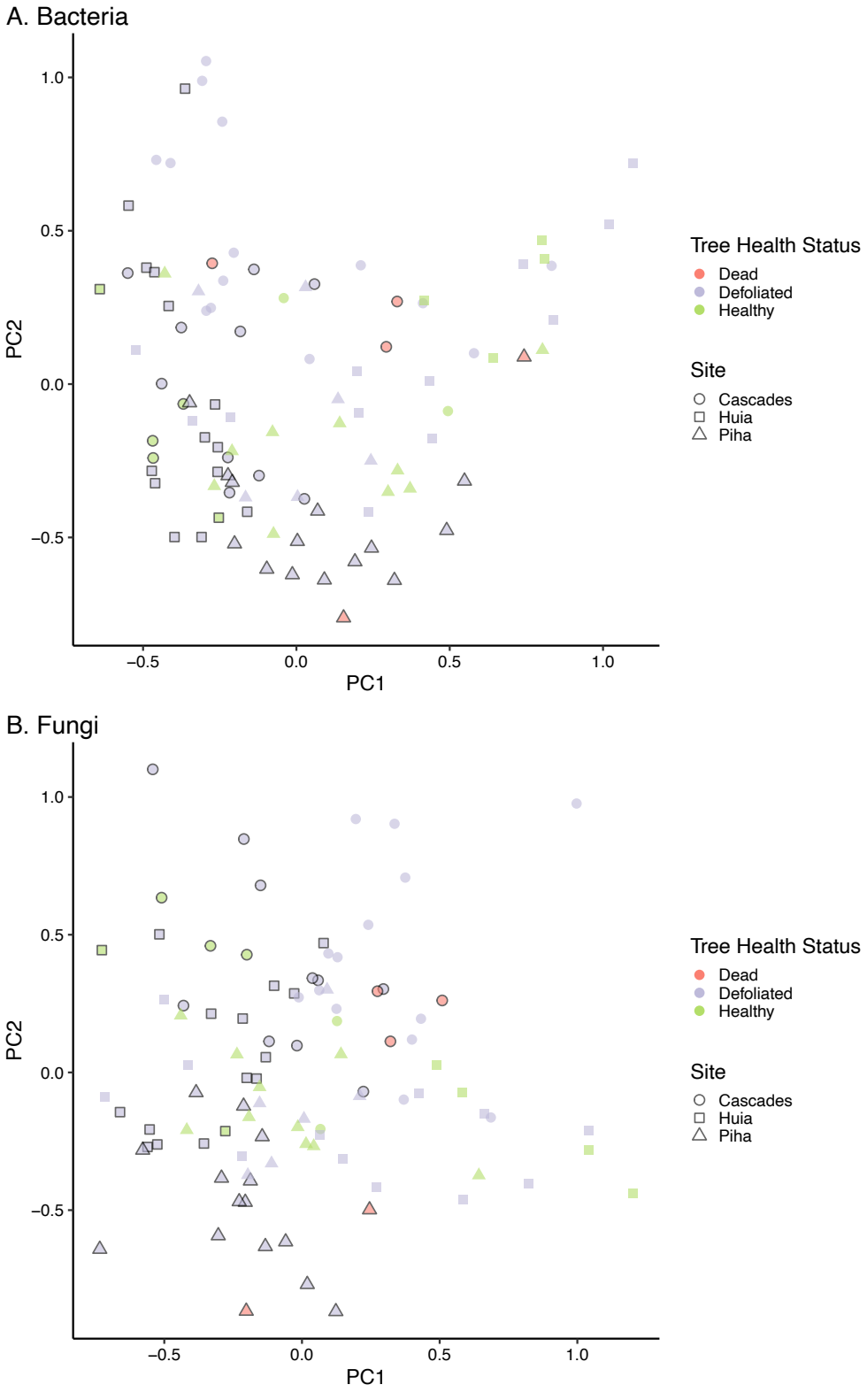

Figure B8: Robust Aitchison principal component analysis of (A) bacterial and (B) fungal community composition of Robust Aitchison distance matrices of different tree health status groups, cardinal samples were combined per tree and ASV counts were averaged (dead: *n* = 5, healthy: *n* = 21, defoliated: *n* = 70). This figure is based on the full taxa dataset. Black borders indicate plot number, presence of black border = plot 1, no black border = plot 2.

A. Bacteria

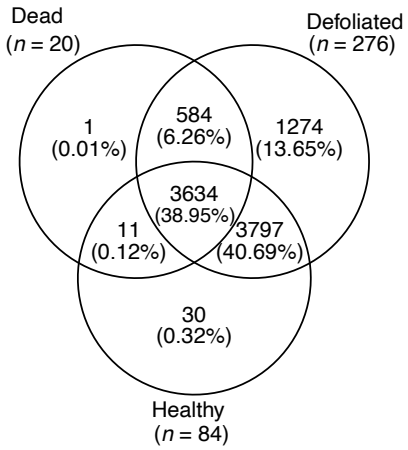

B. Fungi

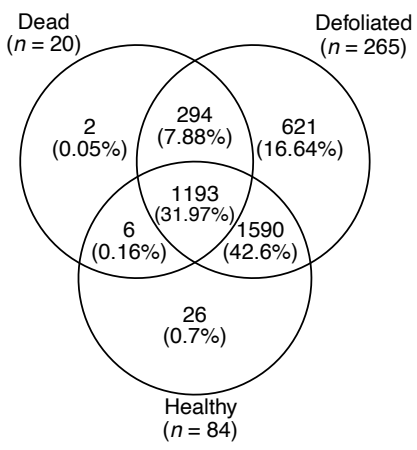

Figure B9: (A) Bacterial and (B) fungal ASVs shared amongst tree health status groupings. This figure is based on the intermediate taxa dataset.

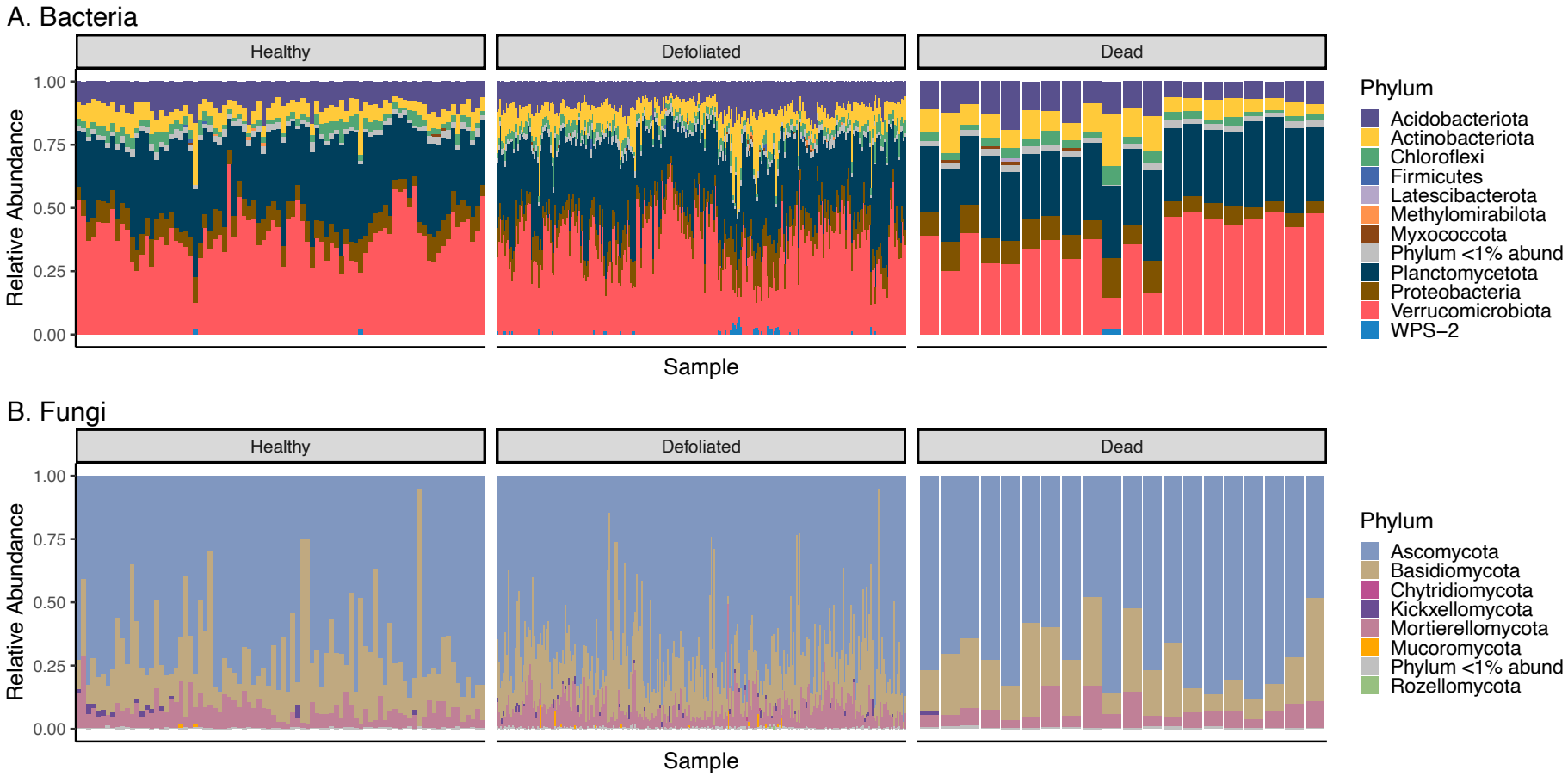

Figure B10: Relative abundance of (A) bacterial and (B) fungal phyla surrounding kauri trees of three health status groupings (dead: *n* = 20, healthy: *n* = 84, defoliated: bacterial dataset *n* = 276, fungal dataset: *n* = 265). This figure is based on the intermediate taxa dataset.

B.2 Supplementary tables

Table B1: Samples with <1000 reads, removed during quality control of amplicon data.

16S samples	**ITS samples**
IC-B126-W-16S	IC-A172-S-ITS
IH-A39-W-16S	IH-C114-N-ITS
IP-A26-W-16S	IP-B10-S-ITS
UC-D29-N-16S	UC-A43-E-ITS
	UC-A43-W-ITS
	UC-A94-W-ITS
	UC-B128-E-ITS
	UC-B128-S-ITS
	UC-B128-W-ITS
	UH-A2-N-ITS
	UH-A2-S-ITS
	UH-C4-N-ITS
	UH-C4-S-ITS
	UH-D17-N-ITS
	UP-A282-N-ITS
	UP-A282-S-ITS
	UP-B171-W-ITS

Table B2: Allocation of ASVs and sequences across the three different subcommunities of the dataset. Percentage value is representative of the full dataset.

	Category	ASV number	Sequence number	Relative abundance
Bacteria	Full dataset	52,759 (100%)	15,690,282 (100%)	100%
	Prevalent taxa	28 (0.05%)	4,351,500 (27.73%)	28%
	Intermediate taxa	9,331 (17.69%)	10,856,270 (69.19%)	69%
	Rare taxa	43,400 (82.26%)	482,512 (3.08%)	3%
Fungi	Full dataset	18,201 (100%)	7,014,423 (100%)	100%
	Prevalent taxa	5 (0.03%)	1,281,977 (18.28%)	18%
	Intermediate taxa	3,733 (20.51%)	5,080,943 (72.43%)	73%
	Rare taxa	14,463 (79.46%)	651,503 (9.29%)	9%

Table B3: Environmental variables associated with soil bacterial and fungal community composition. Factors that were significantly correlated with ordination axes are denoted by *, where $P \leq 0.05$ is *, $P \leq 0.01$ is **, and $P \leq 0.001$ is ***.

	Bacteria			Fungi		
Environmental variable	**PC1**	**PC2**	**R^2**	**PC1**	**PC2**	**R^2**
Total hydrogen	-0.607	-0.794	0.479***	0.090	-0.996	0.434***
Total carbon	-0.499	-0.867	0.472***	0.156	-0.988	0.350***
C:N ratio	-0.764	-0.646	0.473***	-0.225	-0.974	0.377***
pH	0.967	0.254	0.458***	0.703	0.711	0.281***
Bulk density	0.715	0.699	0.326***	0.052	0.999	0.238***
Soil moisture	-0.479	-0.878	0.310***	0.225	-0.974	0.336***
Total nitrogen	-0.250	-0.968	0.289***	0.424	-0.906	0.184***
Water holding capacity	-0.338	-0.941	0.194***	0.339	-0.941	0.087*
Easting	-0.310	-0.951	0.198***	0.366	-0.931	0.218***
Electrical Conductivity	-0.915	-0.404	0.105**	-0.346	-0.938	0.128***
Elevation	0.227	-0.974	0.088*	0.831	-0.556	0.085*
Northing	-0.636	-0.771	0.022	0.113	-0.994	0.100**

Table B4: Environmental variables of sites (mean ± standard deviation).

	Site		
Environmental variable	**Cascades**	**Piha**	**Huia**
Total hydrogen (%)	2.74 ± 0.57	2.22 ± 0.12	2.31 ± 0.12
Total carbon (%)	14.77 ± 7.12	10.35 ± 3.00	12.08 ± 4.46
C:N ratio	23.08 ± 4.12	20.87 ± 4.64	22.53 ± 3.57
pH	5.30 ± 0.64	5.26 ± 0.31	5.32 ± 0.61
Bulk density (g/cm^3)	0.31 ± 0.08	0.41 ± 0.08	0.37 ± 0.08
Soil moisture (%)	93.98 ± 25.74	60.44 ± 10.59	94.76 ± 15.65
Total nitrogen (%)	0.62 ± 0.17	0.51 ± 0.12	0.53 ± 0.12
Water holding capacity (%)	59.51 ± 6.07	57.93 ± 5.08	63.59 ± 3.62
Easting	1734765 ± 105.11	1732486 ± 438.45	1736284 ± 54.16
Electrical Conductivity (µS/cm)	124.93 ± 38.83	110.7 ± 28.70	84.80 ± 32.21
Elevation	188.56 ± 29.77	116.52 ± 54.38	242.02 ± 23.24
Northing	5916343 ± 113.11	5910072 ± 129.14	5901602 ± 17.44

Appendix C

C.1 Supplementary figures

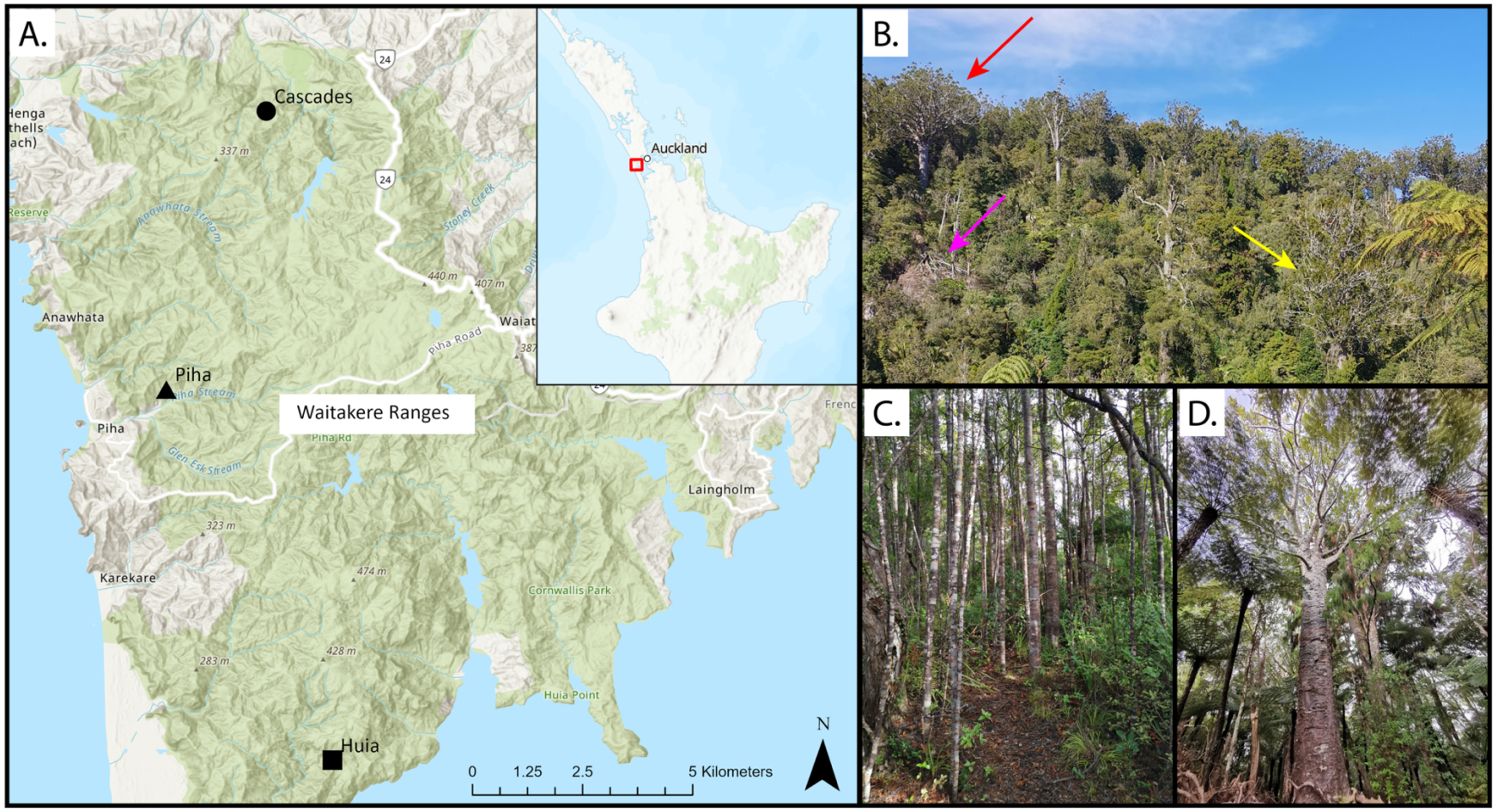

Figure C1: Study area and representative images of kauri forest. (A) Map of the Waitākere Ranges in the Auckland region of the North Island, New Zealand (inset), showing the three study sites where soils samples were collected. Each site contained two plots, and 16 trees per plot were sampled. (B) Kauri forest within the Waitākere Ranges, showing a mature healthy kauri canopy (red arrow), declining kauri canopy (yellow arrow), and a fallen dead kauri (pink arrow). (C) Regenerating stand of young kauri trees. (D) Mature kauri tree representing the intact forest canopy structure.

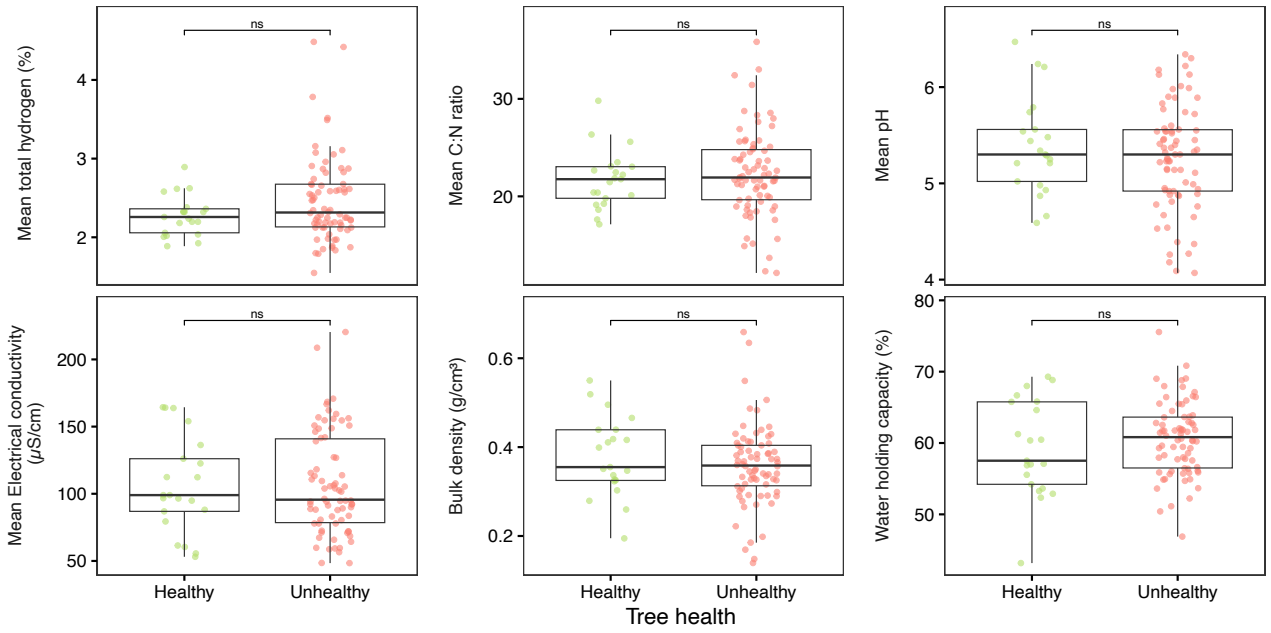

Figure C2: Boxplots showing the distribution of soil physicochemical properties across healthy (n = 21) and unhealthy (n = 74) kauri tree groups. Each panel represents one physicochemical property, with differences between groups tested using the Wilcoxon rank-sum test. Asterisks (*) indicate statistically significant differences ($P < 0.05$). Each box represents the interquartile range of the data (25th and 75th percentiles), whiskers show the largest and smallest values 1.5x the IQR and median values are represented by the bar within each box. Physicochemical data of soils were generated by Mohini (2024).

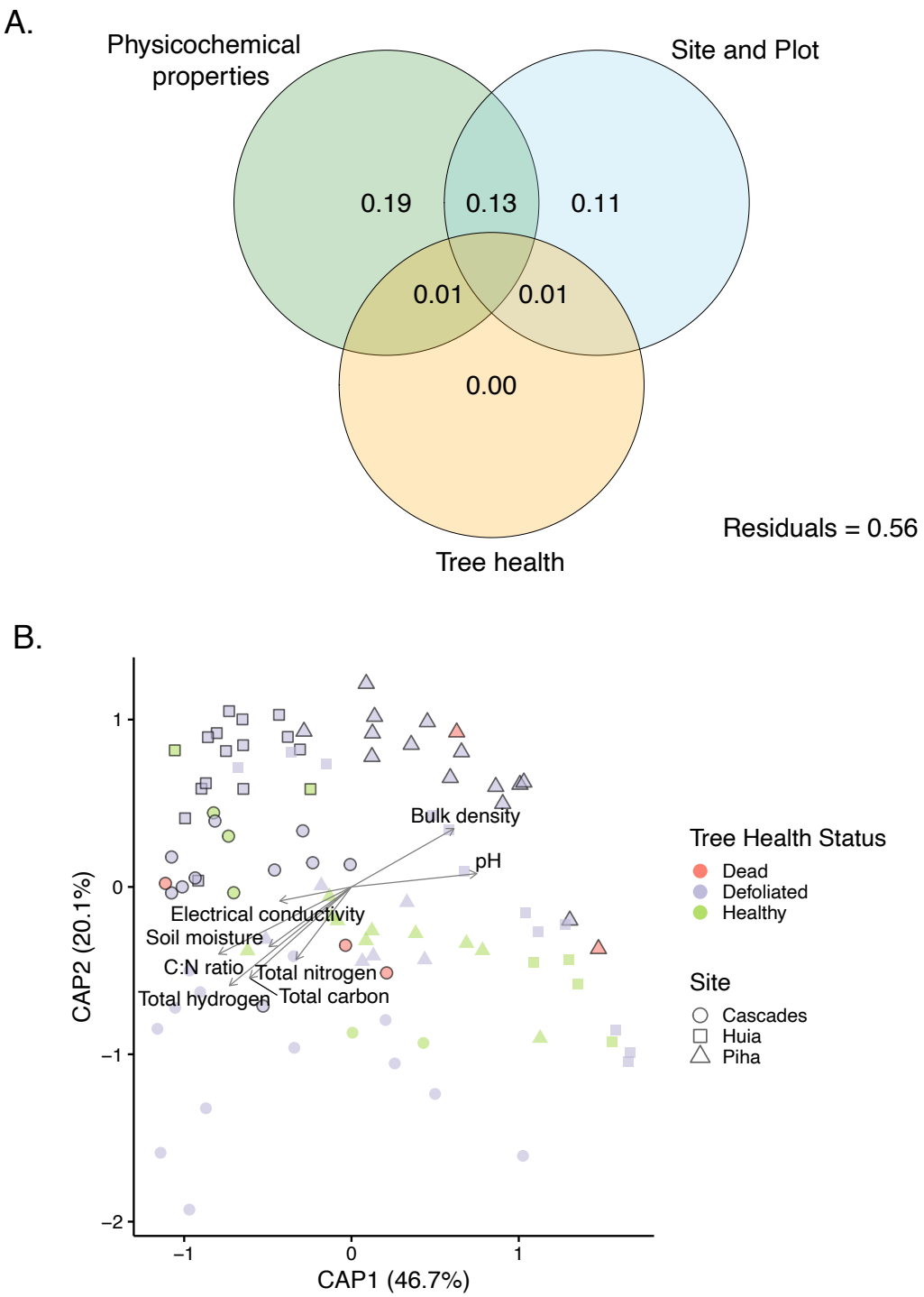

Figure C3: Drivers of variation in microbial functional gene composition annotated by the NCyc database. (A) Variation partitioning analysis showing the proportion of variance in gene composition explained by physicochemical properties (pH, total carbon, total nitrogen, total hydrogen, carbon to nitrogen (C:N) ratio, electrical conductivity, bulk density, and water holding capacity), site and plot, and tree health (healthy and unhealthy). Values less than 0 are not shown. (B) Constrained ordination (db-RDA) of Bray-Curtis dissimilarities based on TPM-normalised gene abundance, constrained by site and nested plot (formula: site/plot) to account for spatial structure. Black borders indicate plot number, presence of black border = plot 1, no black border = plot 2. Overlaid vectors show significant soil physicochemical variables identified via the *envfit* function from the vegan R package that were significantly correlated (P <0.05) with ordination axes. Physicochemical data of soils were generated by Mohini (2024).

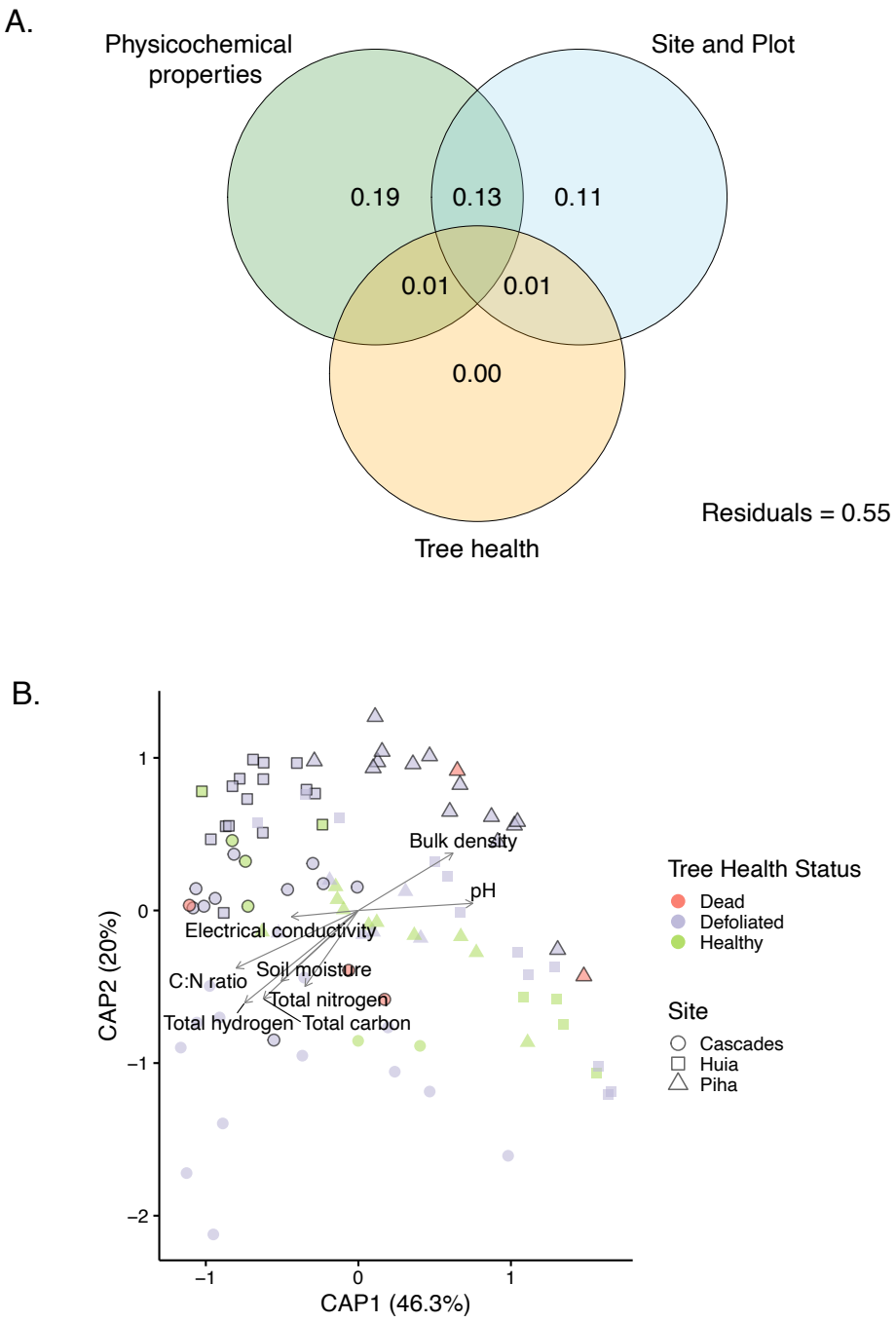

Figure C4: Drivers of variation in microbial functional gene composition annotated by the CAZy database. (A) Variation partitioning analysis showing the proportion of variance in gene composition explained by physicochemical properties (pH, total carbon, total nitrogen, total hydrogen, carbon to nitrogen (C:N) ratio, electrical conductivity, bulk density, and water holding capacity), site and plot, and tree health (healthy and unhealthy). Values less than 0 are not shown. (B) Constrained ordination (db-RDA) of Bray-Curtis dissimilarities based on TPM-normalised gene abundance, constrained by site and nested plot (formula: site/plot) to account for spatial structure. Black borders indicate plot number, presence of black border = plot 1, no black border = plot 2. Overlaid vectors show significant soil physicochemical variables identified via the *envfit* function from the vegan R package that were significantly correlated (*P* <0.05) with ordination axes. Physicochemical data of soils were generated by Mohini (2024).

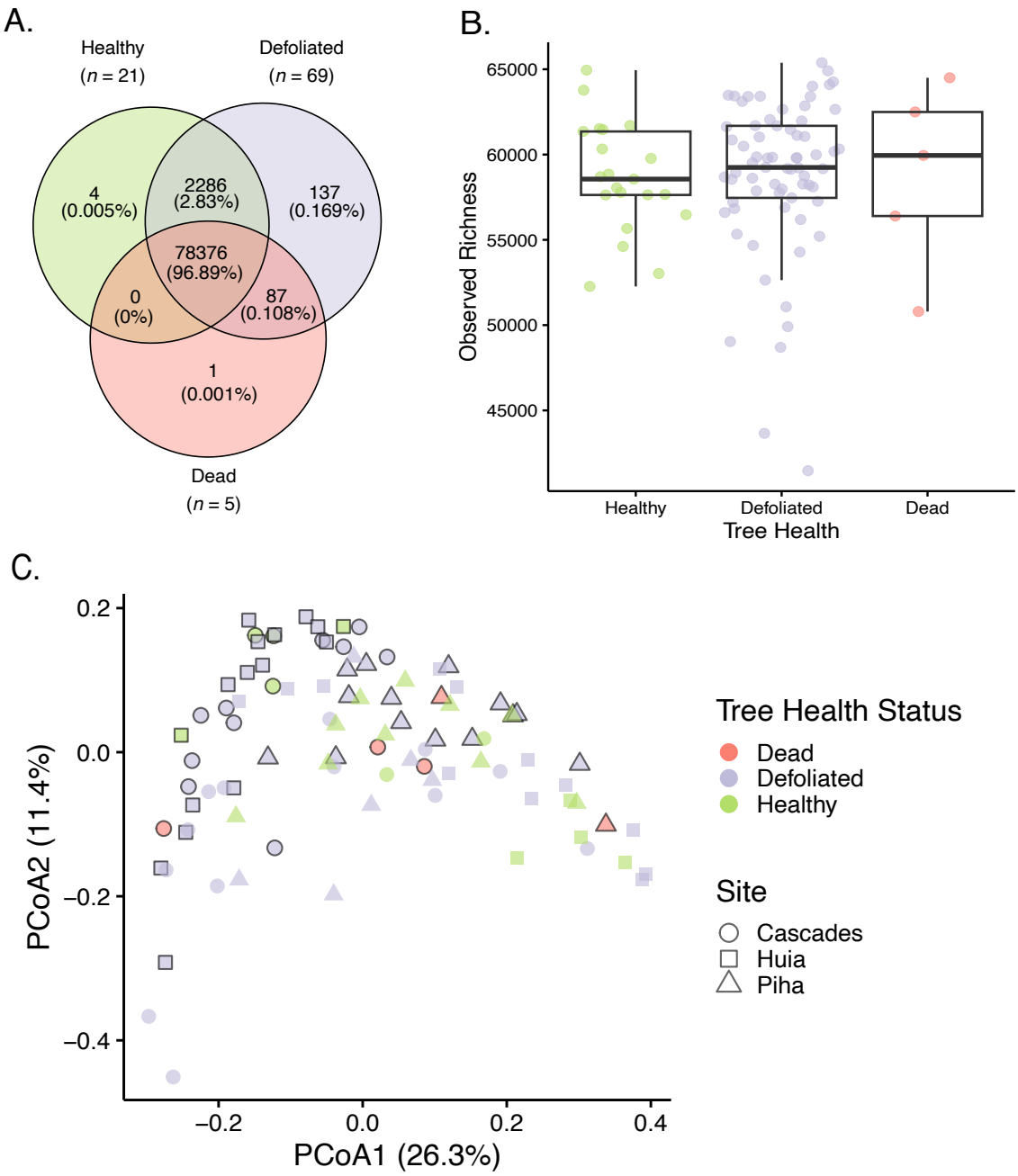

Figure C5: Gene diversity and composition of NCyc annotated genes across kauri tree health states (healthy *n* = 21, defoliated *n* = 69, and dead *n* = 5). (A) Venn diagrams showing shared vs health-state-specific genes. (B) Box plots show gene diversity (richness; calculated as the number of annotated genes detected per sample). Each box represents the interquartile range of the data (IQR; 25th and 75th percentiles), whiskers show the largest and smallest values 1.5x the IQR and median values are represented by the bar within each box. (C) Gene composition differences visualised using PCoA of Bray-Curtis dissimilarities from TPM-normalised gene abundances. Black borders indicate plot number, presence of black border = plot 1, no black border = plot 2.

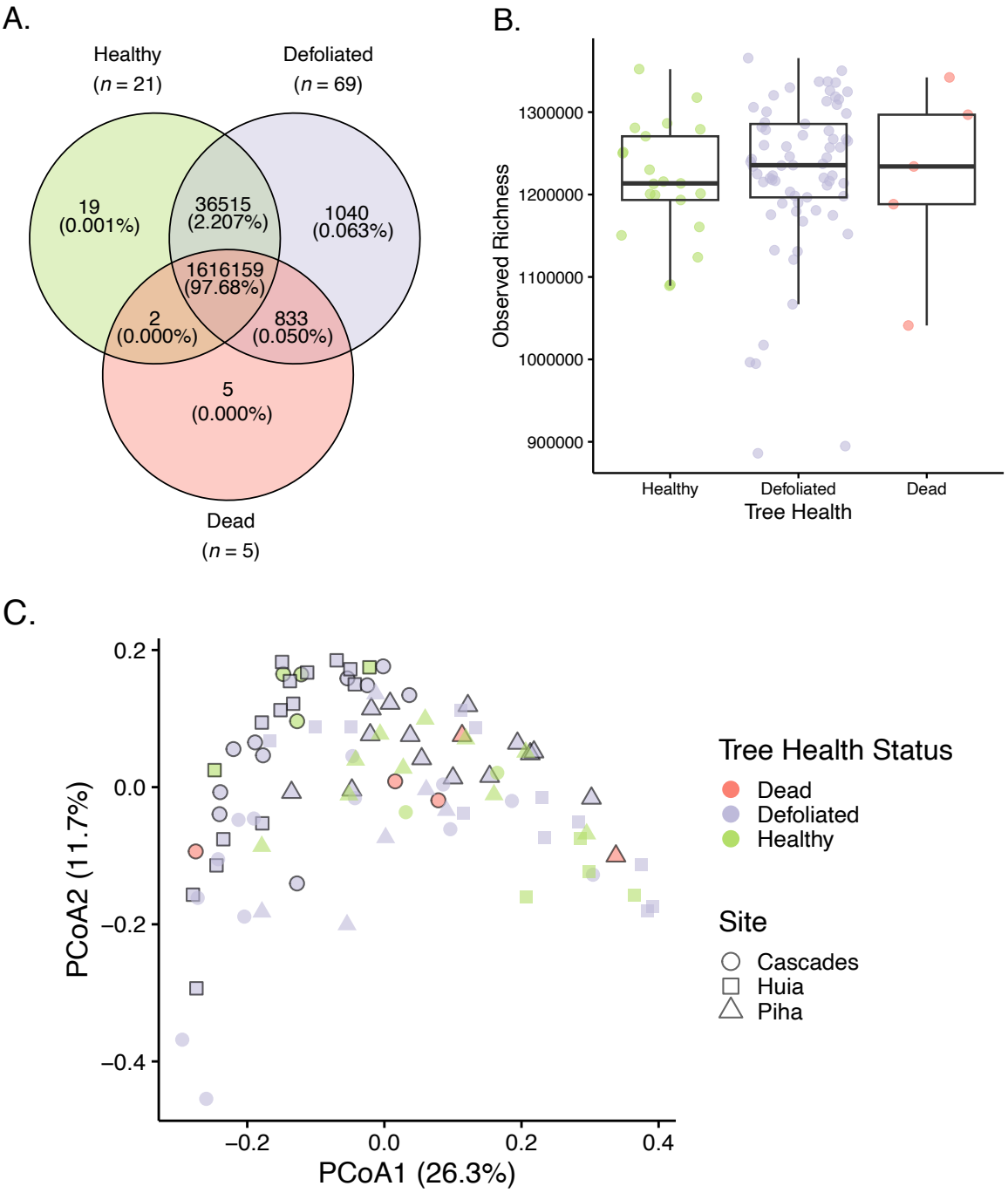

Figure C6: Gene diversity and composition of CAZy annotated genes across kauri tree health states (healthy *n* = 21, defoliated *n* = 69, and dead *n* = 5). (A) Venn diagrams showing shared vs health-state-specific genes. (B) Box plots show gene diversity (richness; calculated as the number of annotated genes detected per sample). Each box represents the interquartile range of the data (IQR; 25th and 75th percentiles), whiskers show the largest and smallest values 1.5x the IQR and median values are represented by the bar within each box. (C) Gene composition differences visualised using PCoA of Bray-Curtis dissimilarities from TPM-normalised gene abundances. Black borders indicate plot number, presence of black border = plot 1, no black border = plot 2.

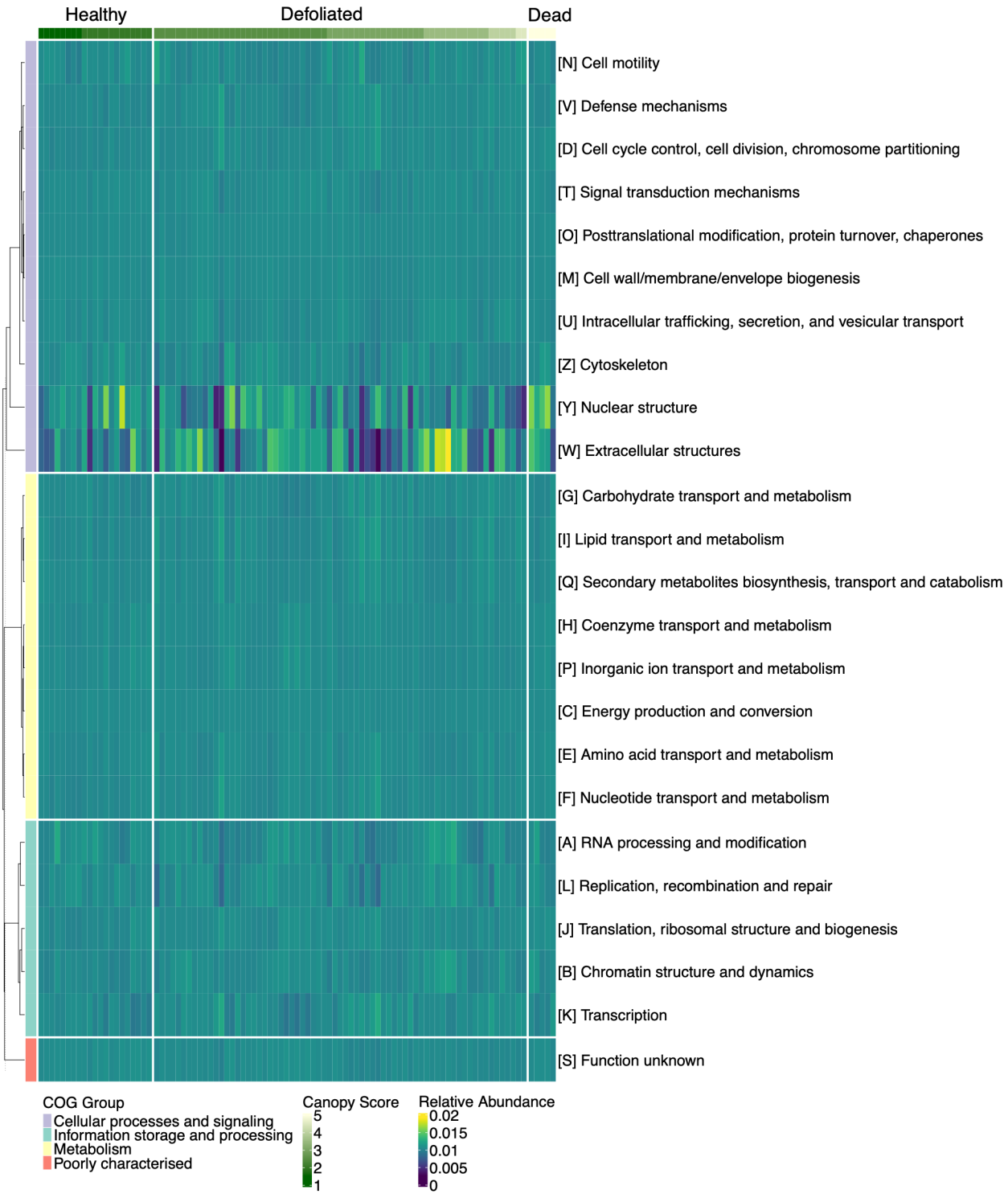

Figure C7: Heatmap of functional gene composition based on eggNOG annotations. For each gene, TPM counts were first normalised within samples (per-column normalisation), and then scaled so that values summed to 1 across all samples (per-row normalisation). Colours represent the relative distribution of each gene across samples. Columns represent individual samples, ordered and grouped by canopy score, while rows are organised by higher-level COG functional groupings. The heatmap was generated using ComplexHeatmap v. 2.21.2 (Gu 2022).

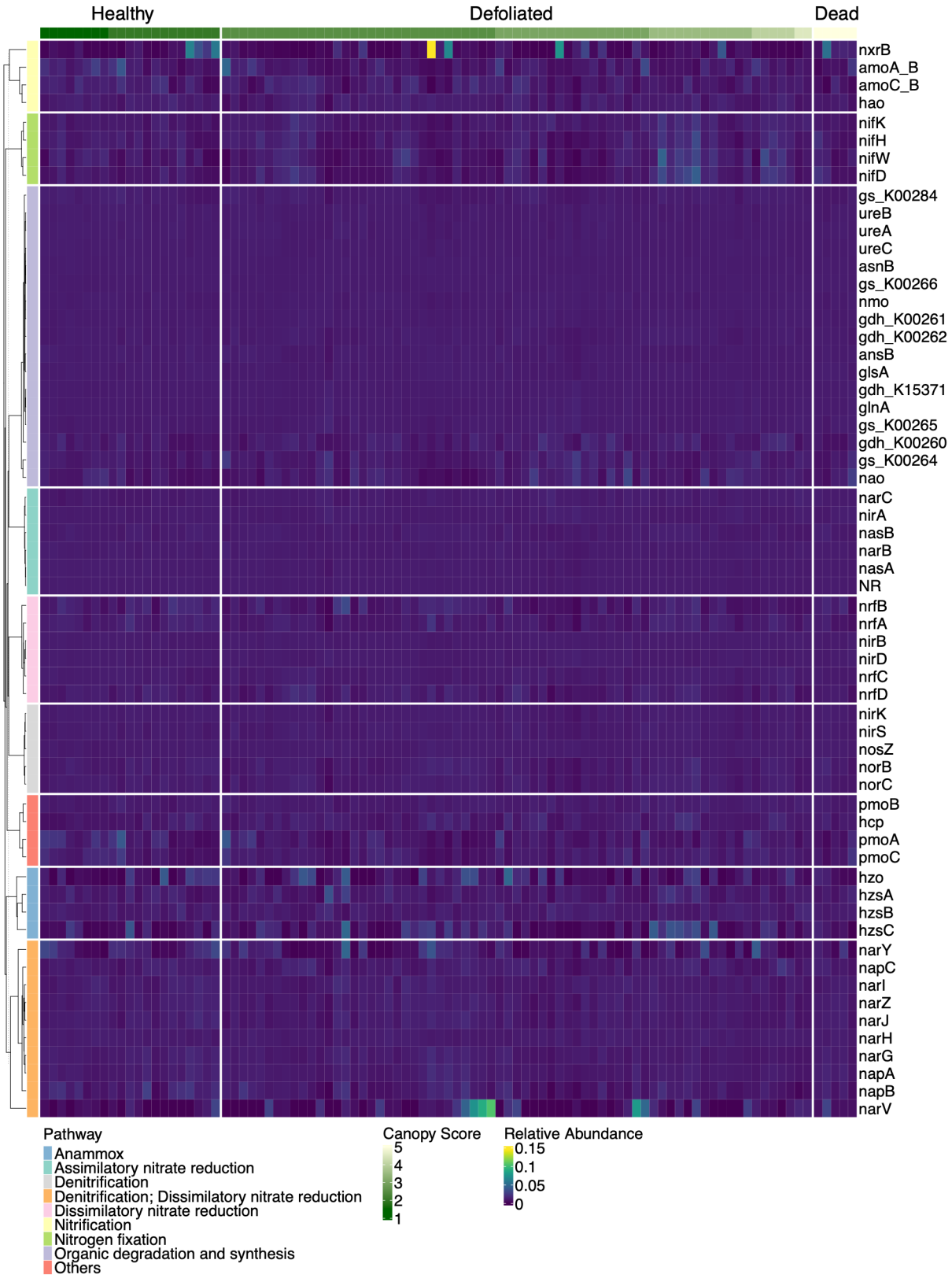

Figure C8: Heatmap of functional gene composition based on NCyc annotations. For each gene, TPM counts were first normalised within samples (per-column normalisation), and then scaled so that values summed to 1 across all samples (per-row normalisation). Colours represent the relative distribution of each gene across samples. Columns represent individual samples, ordered and grouped by canopy score, while rows are organised by the pathway the genes are involved in. The heatmap was generated using ComplexHeatmap v. 2.21.2 (Gu 2022).

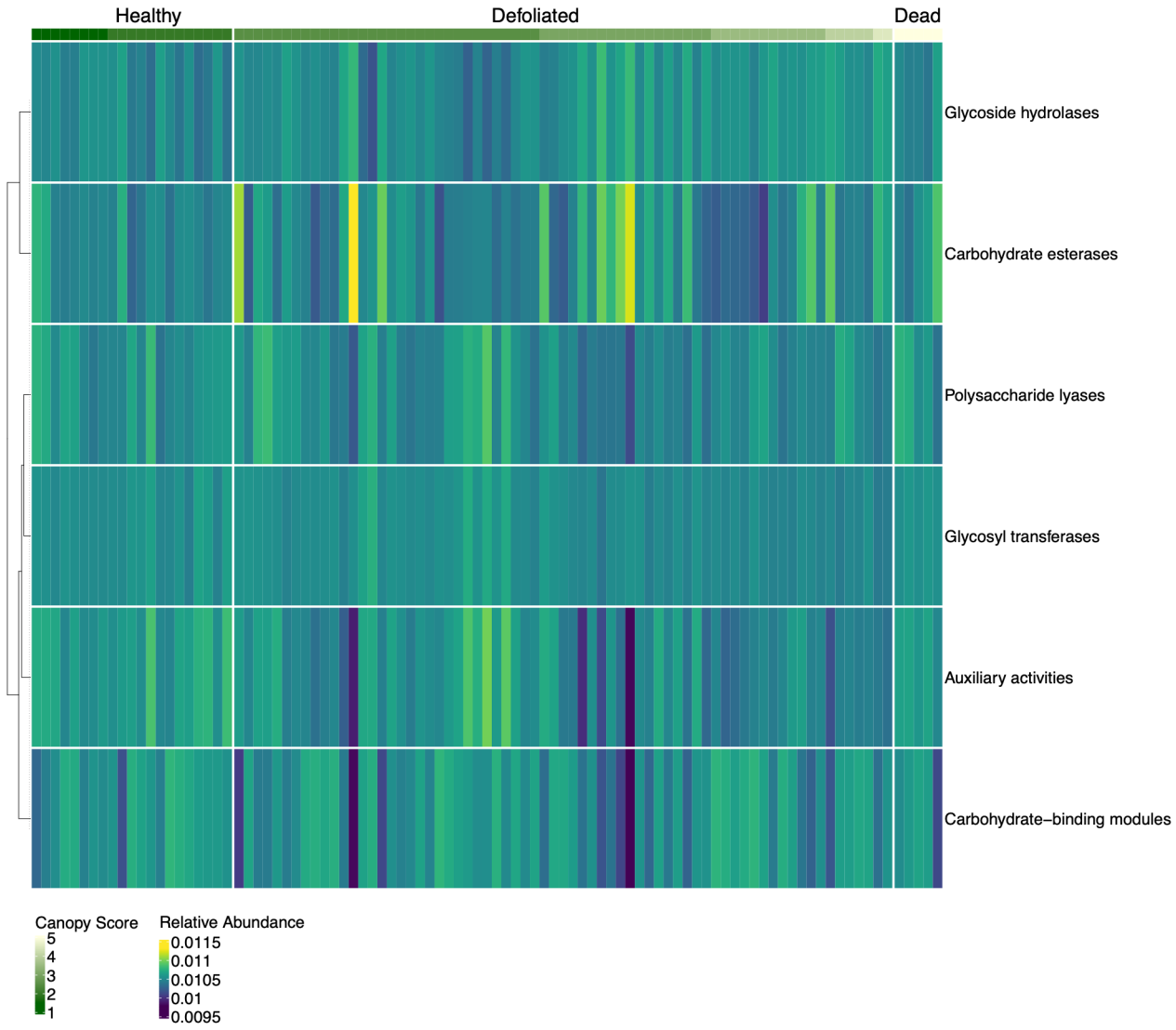

Figure C9: Heatmap of functional gene composition based on CAZy annotations. For each gene, TPM counts were first normalised within samples (per-column normalisation) before grouping by CAZy enzyme family. Counts per family were then scaled so that values summed to 1 across all samples (per-row normalisation). Colours represent the relative distribution of each enzyme family across samples. Columns represent individual samples, ordered and grouped by canopy score. The heatmap was generated using ComplexHeatmap v. 2.21.2 (Gu 2022).

C.2 Supplementary tables

Table C1: Pairwise PERMANOVA results comparing soil physicochemical properties between sites and between plots within sites. Analyses were based on Euclidean distance matrices generated from standardised soil variables. Pairwise comparisons between plots were nested within sites to account for the hierarchical sampling design. *P*-values were adjusted using Holm correction.

Pairs	Degrees of freedom	Sum of Squares	R^2	Adjusted *P*-value
Site comparisons				
Piha vs Huia	1	63.4	0.15	0.003 (*)
Piha vs Cascades	1	95.6	0.16	0.003 (*)
Huia vs Cascades	1	60.0	0.10	0.003 (*)
Plot comparisons				
Plot 2-Piha vs Plot 1-Piha	1	29.5	0.18	0.002 (*)
Plot 1-Huia vs Plot 2-Huia	1	30.9	0.15	0.002 (*)
Plot 2-Cascades vs Plot 1-Cascades	1	93.9	0.28	0.001 (*)

Table C2: Pairwise PERMANOVA results comparing gene composition between sites and between plots within sites. Analyses were based on Bray-Curtis distance matrices generated from TPM normalised gene coverage. Pairwise comparisons between plots were nested within sites to account for the hierarchical sampling design. *P*-values were adjusted using Holm correction.

Pairs	Degrees of freedom	Sum of Squares	R^2	Adjusted *P*-value
eggNOG site comparisons				
Piha vs Huia	1	0.56	0.07	0.003 (*)
Piha vs Cascades	1	0.99	0.12	0.003 (*)
Huia vs Cascades	1	0.65	0.07	0.003 (*)
eggNOG plot comparisons				
Plot 2-Piha vs Plot 1-Piha	1	0.56	0.16	0.001 (**)
Plot 1-Huia vs Plot 2-Huia	1	1.20	0.28	0.001 (**)
Plot 2-Cascades vs Plot 1-Cascades	1	0.43	0.11	0.002 (*)
NCyc site comparisons				
Piha vs Huia	1	0.53	0.07	0.003 (*)
Piha vs Cascades	1	0.97	0.12	0.003 (*)
Huia vs Cascades	1	0.62	0.07	0.003 (*)
NCyc plot comparisons				
Plot 2-Piha vs Plot 1-Piha	1	0.53	0.16	0.001 (**)
Plot 1-Huia vs Plot 2-Huia	1	1.2	0.29	0.001 (**)
Plot 2-Cascades vs Plot 1-Cascades	1	0.41	0.11	0.001 (**)
CAZy site comparisons				
Piha vs Huia	1	0.53	0.07	0.003 (*)
Piha vs Cascades	1	0.98	0.13	0.003 (*)
Huia vs Cascades	1	0.62	0.08	0.003 (*)
CAZy plot comparisons				
Plot 2-Piha vs Plot 1-Piha	1	0.54	0.16	0.001 (**)
Plot 1-Huia vs Plot 2-Huia	1	1.18	0.29	0.001 (**)

Plot 2-Cascades vs Plot 1-Cascades	1	0.41	0.12	0.001 (**)

Table C3: Results of *envfit* analysis showing correlations between soil physicochemical properties and microbial functional potential across three functional annotation datasets (eggNOG, NCyc, and CAZy).

	CAP1	**CAP2**	**R^2**	***P*-value**
			eggNOG	
pH	1.0	0.07	0.32	0.001 (***)
Electrical conductivity	-1.0	-0.13	0.11	0.005 (**)
Total carbon	-0.75	-0.66	0.39	0.001 (***)
Total hydrogen	-0.78	-0.62	0.52	0.001 (***)
Total nitrogen	-0.60	-0.80	0.18	0.001 (***)
C:N ratio	-0.90	-0.43	0.46	0.001 (***)
Bulk density	0.87	0.50	0.29	0.001 (***)
Soil moisture	-0.78	-0.62	0.24	0.001 (***)
Water holding capacity	-0.63	-0.78	0.02	0.339
			NCyc	
pH	0.99	0.11	0.34	0.001 (***)
Electrical conductivity	-0.98	-0.19	0.11	0.006 (**)
Total carbon	-0.75	-0.67	0.40	0.001 (***)
Total hydrogen	-0.78	-0.63	0.52	0.001 (***)
Total nitrogen	-0.61	-0.79	0.18	0.001 (***)
C:N ratio	-0.89	-0.45	0.47	0.001 (***)
Bulk density	0.87	0.49	0.29	0.001 (***)
Soil moisture	-0.81	-0.59	0.22	0.001 (***)
Water holding capacity	-0.72	-0.70	0.02	0.375
			CAZy	
pH	0.75	0.05	0.32	0.001 (***)
Electrical conductivity	-0.44	-0.06	0.11	0.005 (**)
Total carbon	-0.62	-0.55	0.39	0.001 (***)

Total hydrogen	-0.74	-0.59	0.52	0.001 (***)
Total nitrogen	-0.34	-0.45	0.18	0.001 (***)
C:N ratio	-0.81	-0.38	0.46	0.001 (***)
Bulk density	0.62	0.36	0.29	0.001 (***)
Soil moisture	-0.50	-0.40	0.24	0.001 (***)
Water holding capacity	-0.55	-0.83	0.04	0.149

Table C4: PERMOANOVA results testing differences in gene composition between healthy (*n* = 21) and unhealthy (*n* = 74) kauri trees based on Bray-Curtis dissimilarities. Analyses were conducted separately for the three functional gene annotation databases (eggNOG, NCyc, and CAZy). Gene composition was derived from TPM normalised gene abundance profiles.

	Degrees of freedom	**Sum of Squares**	**R^2**	**pseudo-F**	***P*-value**
			eggNOG PERMANOVA		
Tree health status	1	0.30	0.02	2.17	0.022 (*)
Residual	93	12.7	0.98		
			CAZy PERMANOVA		
Tree health status	1	0.28	0.02	2.20	0.023 (*)
Residual	93	11.9	0.98		
			NCyc PERMANOVA		
Tree health status	1	0.29	0.02	2.25	0.021 (*)
Residual	93	12.1	0.98		

C.3 Supplementary files

Raw read (before and after quality control) and assembly statistics of shotgun metagenome data (per sample) can be viewed in Appendix_C3_Supplementary_File_1.xlsx.

MaAsLin2 results from eggNOG, NCyc, and CAZy analyses, grouped by gene annotation can be viewed in Appendix_C3_Supplementary_File_2.xlsx.